DESIGN OF A NON-VITIATED HEATER GROUND TEST FACILITY FOR SUPERSONIC COMBUSTION

By

ADRIAN BLOT

A THESIS PRESENTED TO THE GRADUATE SCHOOL
OF THE UNIVERSITY OF FLORIDA IN PARTIAL FULFILLMENT
OF THE REQUIREMENTS FOR THE DEGREE OF
MASTER OF SCIENCE

UNIVERSITY OF FLORIDA

2009

To Alysen and my Family

ACKNOWLEDGMENTS

I thank Dr. Corin Segal for his guidance and for this educational and research opportunity. I thank my family for all their loving support and I thank my colleagues in the lab who assisted me in this research.

TABLE OF CONTENTS

LIST OF TABLES

LIST OF FIGURES

Abstract of Thesis Presented to the Graduate School
of the University of Florida in Partial Fulfillment of the
Requirements for the Degree of Master of Science

DESIGN OF A NON-VITIATED HEATER GROUND TEST FACILITY FOR SUPERSONIC COMBUSTION

By

Adrian Blot

August 2009

Chair: Corin Segal
Major: Aerospace Engineering

To date, few ground-based experimental facilities for hypersonic flight simulation have the capacity of performing non-vitiated testing. Vitiated facilities introduce species that affect chemical reactions during testing. The goal of this work was to investigate the performance of a design for a new non-vitiated heater ground test facility for supersonic combustion.

The non-vitiated heater has been designed to simulate flight Mach numbers up to Mach 5. This work shows the feasibility and design of this ground test facility as well as the design of an optional second stage heater which will allow back-to-back experiments under vitiated and non-vitiated conditions as well as produce larger Mach numbers. Insulation was designed to improve the performance of the heater as well as provide structural support and safety.

A scaled down prototype, of the non-vitiated heater, was tested to determine the performance of the design. Reynolds numbers, based on the inlet air conditions and the stainless steel tube inner diameter, from 19,000 to 130,000 were tested and the desired stagnation temperature of 1300K was achieved at a Reynolds number of 42,000. The efficiency of this heater was found to be dependent on the Reynolds number and the exit stagnation temperature of the heated air. The efficiency has a maximum value of 90% at a Reynolds number of 85,000 and decreases linearly at a rate of 4% per 100K of increasing exit air stagnation temperature. The

efficiency's rate of change also depends on the Reynolds number and decreases with increasing Reynolds number. Further it was found the system heats and cools quickly where temperature changes of 19K per second was experienced allowing experiments which require fast transients.

A vitiated second stage heater was also designed to simulate Mach numbers up to 6 for a mass flow rate of 250g/s. This heater uses hydrogen as the working fuel and requires oxygen replenishment to provide accurate air composition at the test section. This heater is to be installed downstream of the non-vitiated heater and may be operated independently or simultaneously with the non-vitiating heater. Hydrogen fuel rates up to 6.0g/s are required to raise the stagnation temperature of the air to 1800K, the value required to simulate Mach 6 flight conditions. A bellmouth has also been designed to couple the test section to either heater.

CHAPTER 1
SUPERSONIC WINDTUNNEL GROUND TEST FACILITIES

Introduction

The purpose of this work is to present and evaluate a non-vitiated ground test facility for supersonic combustion to simulate flight condition up to Mach 5. Few wind tunnel testing facilities are capable of non-vitiated supersonic combustion and achieving high flight enthalpies. The importance of test facilities is broad, ranging from fundamental research to commercial and military uses for performance improvements and cost reduction of aerodynamic systems.[1] They are also required to provide data in cases where current analytical models are insufficient or existing models must be validated.[2] As an example, validation is needed for flight Mach numbers from 3 to 6, which encompasses the flight transition from ramjet to scramjet operation.[3]

Ground test facilities are specialized to operate within a limited window of test conditions due to manufacturing difficulties. At high Mach numbers especially above Mach 8, the following shortcomings arise: adequate test flow uniformity and fluid property equilibrium over a wide range of conditions cannot be maintained, surface conditions are not identical to models, flow contamination from surface erosion or vitiation of a pre-combusted gas, and insufficient test times.[2]

Operating test times can be used to classify test facilities. The following sections discuss the different types of supersonic ground test facilities that are currently in use and their primary purposes outlining some of advantages and disadvantages. Figure 1-1 shows the equivalent flight conditions that general types of facilities today are able to simulate and features a few specific facilities. Shown in the figure is the range of optimized scramjet operation designated by the area between the two dynamic pressures, q=1atm and q=0.25atm. An overview of main operational characteristics of several types of facilities follows.

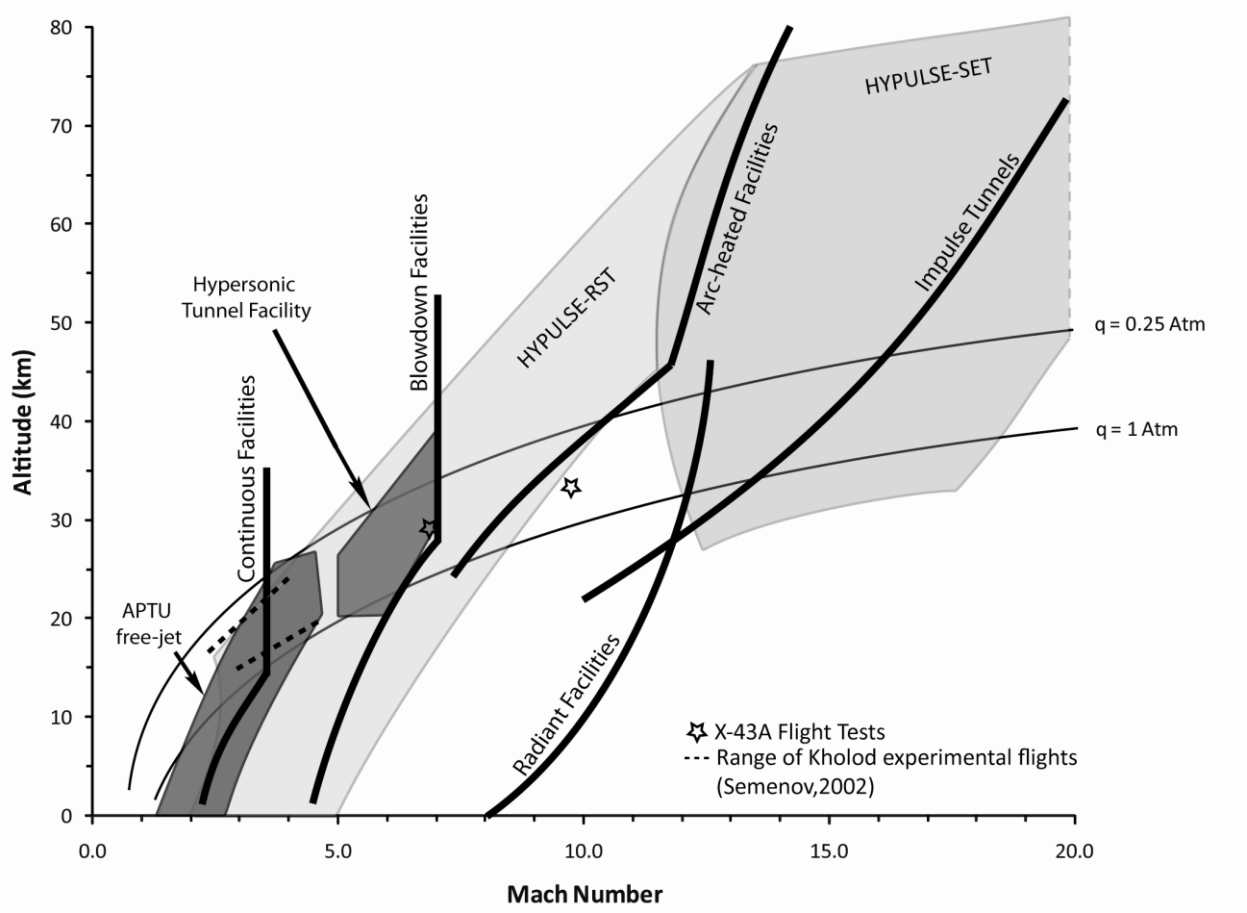

Figure 1-1. Supersonic wind tunnel ground test facilities flight envelopes. Shows the flight Mach number limits of general types of facilities. The region between the dynamic pressures q=0.25atm and q=1atm bounds the range of optimized scramjet operation. Also shown are the experimental scramjet flight tests of the X-43 and Kholod.[2 4 5 6 7]

Long Duration Facilities

Long duration facilities typically have run times on the order of minutes or longer. Facilities used to simulate supersonic flow include electric, arc, or combustion heated facilities, of which two categories exist, continuous and blow-down facilities. Continuous facilities have test times that are only limited by the experiment requirements; however test conditions are limited by the available mass flow rate.[2] Blow-down facilities have test times on the order of seconds to minutes. They are driven by a high pressure vessel of stored gas which produces a high pressure differential enabling tests in a high pressure high Reynolds number environment. The size of this vessel is the limiting factor on the amount of time experiments can be run.[2] Many continuous and blow-down facilities exist today; however discussion is limited to those capable of simulating flight conditions pertaining to supersonic combustion, specifically heated facilities.

Arc Heated Facilities

Electric arc heaters were first used for aeronautical research in the late 1950's. These facilities are used to simulate conditions of high enthalpy such as earth reentry heating or high Mach number testing. Typical arc heaters produce a high temperature gas stream using radiative, conductive, and convective heat transfer from a high voltage DC electric arc discharge. This stream is passed into a cooled plenum and is then expanded through a nozzle to the test section. Arc heaters are classified by the method used to stabilize the arc discharge, and include vortex-stabilized, magnetically stabilized, and segmented arcs.[8]

Vortex stabilized arc heaters are examples of the simplest configuration. The working fluid is injected tangentially into a swirl chamber at the electrode interface, generating a vortex spiral that can be augmented further with magnetic coils as the fluid passes through the anode and cathode. This vortex generation ensures a high heat flux generation zone at the arc-electrode

contact site and minimizes contact wear on the cathode by distribution over a relatively large surface area. Vortex stabilized facilities are inexpensive, easily maintained, reliable, and is capable of very long run times of minutes to hours. Drawbacks to this approach include issues of flow quality and reduced efficiency which arise from an uncontrolled arc length and a fixed voltage differential. Due to the fixed voltage differential a greater magnitude of current is required to increase the overall power, however this results in greater electrode erosion. Magnetic stabilized heaters use a center-axis anode discharging to the outer wall. The stability of the arc column is maintained through the use of external magnetic coils placed around the heater plenum.[8]

Segmented arcs form the modern high performance arc heater, essentially a hybrid of the vortex and magnetic stabilized arc heaters with the addition of a segmented construction which efficiently produces clean high temperature gas. Only segmented arc heaters are able to provide the combination of total pressure, enthalpy, and run times required for many endoatmospheric aerothermal simulations. The use of this type of arc-heater has the following performance advantages: high efficiency by the optimization of heat transfer from arc column to working gas, arc stability at high pressures, high voltage operations resulting in lower required currents and reduced electrode erosion, and repeatability of the flow field with respect to total enthalpy. The disadvantages of this heater are related to initial and maintenance costs as well as the relative complexity of such a system.[8] The SCIROCCO facility in Italy is a segmented arc facility which is capable of producing stagnation temperatures from 2,000 to 10,000K producing test conditions up to Mach 12. The main purpose of this facility is to duplicate aerothemodynamic conditions encountered by space vehicles for Earth reentry. The facility requires 70MW power and processes air over a pressure range of 1-17 bar.[4] Figure 1-2 shows the configurations of these three types.

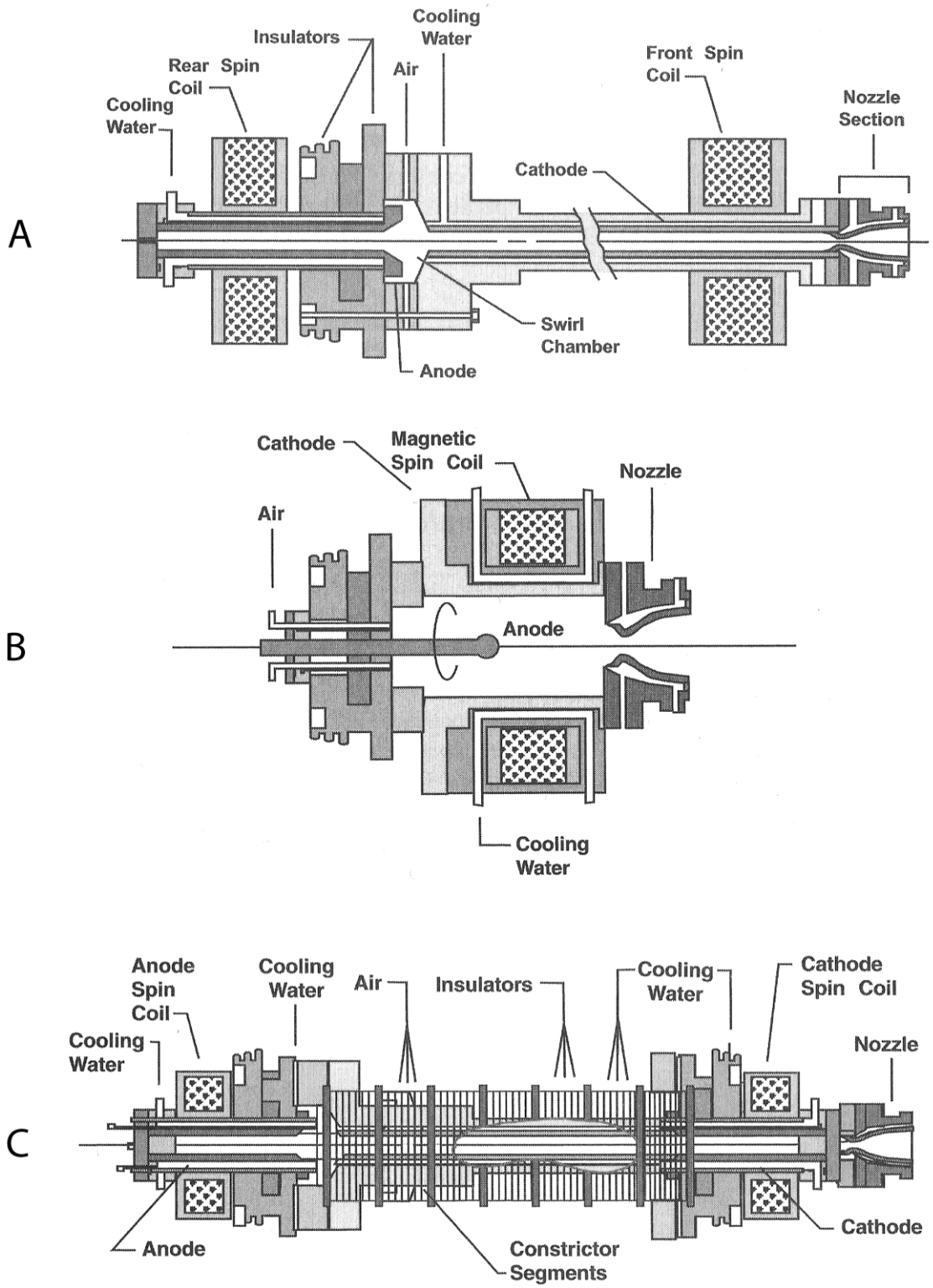

Figure 1-2. Arc facility configurations. A is a vortex stabilized arc B is the magnetic stabilized arc and C is the segmented arc configuration. (Smith, Felderman, and Shope)[8]

In general, arc heated facilities have several drawbacks with respect to supersonic combustion. They are limited in the pressures they are able to achieve due to the volume flow rate of fluid that can be passed through the arc to achieve the desired temperatures.[2] The arc of plasma used to heat the fluid creates contaminants in the flow from the dissociation of molecules in the gas mixture. This results in different flow characteristics which can affect results in combustion facilities due to the addition of free radicals. These radicals can influence flame ignition and stability.

Combustion Heaters

Combustion heaters use fuels mixed into the test flow where they are combusted to increase the temperature of the fluid. The total temperature of the fluid that can be achieved in these heaters is directly dependent on the fuel being used. For hydrocarbons this limit corresponds to stagnation temperatures required for Mach 7 while the use of hydrogen allows for even higher Mach numbers.[2]

This method of heating produces a number of undesired effects. The process of combustion introduces combustion products, unburned fuel, and alters the oxygen content of the test air. Oxygen enrichment and replenishment is required to provide the correct oxygen mole fraction for the test section and ensure proper fuel combustion.[5] This creates the need to control and monitor the oxygen content of the test fluid to ensure proper amounts of oxygen exist in the test flow to properly simulate atmospheric conditions that will be used in combustion tests. The Aerodynamic and Propulsion Test Unit (APTU) facility uses Butane fuel in the combustor to increase the stagnation temperature of the working fluid to 1100K for test time up to 12 minutes. Figure 1-3 is a current schematic of the APTU facility and Figure 1-4 details the High Temperature Tunnel (HTT) facility's combustor which uses methane fuel to increase the stagnation temperature of the working fluid to 2200K with pressures from 4.1 to 27.6MPa. After

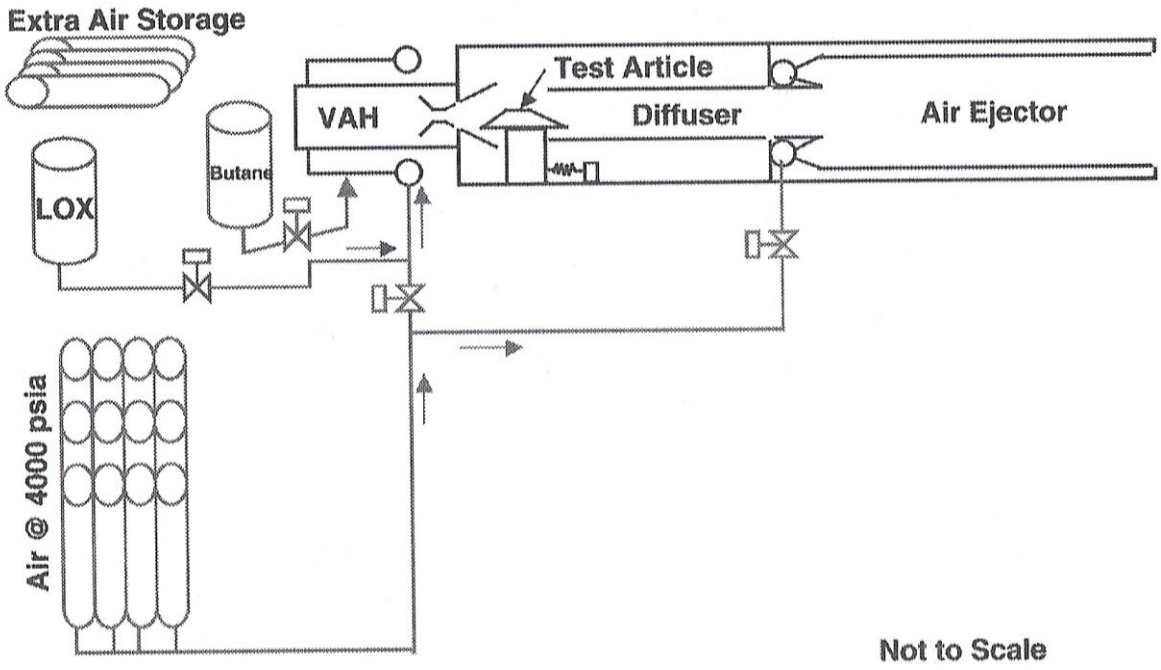

Figure 1-3. Layout of the APTU vitiated heater facility. Butane and oxygen are mixed in the vitiated air heater where the fuel is combusted. The air is then expanded through the nozzle to the test section and ejected. (Rigney and Garrard)[5]

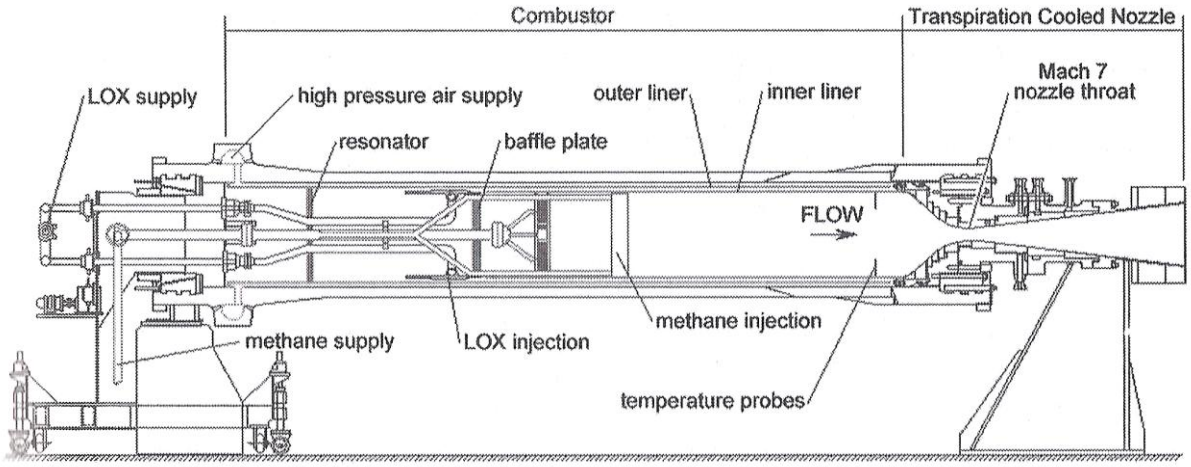

Figure 1-4. The HTT facility's vitiated heater combustor. Details components and shows fuel, air, and oxidizer supply. (Hodge and Harvin)[9]

combustion the test gas is expanded through a nozzle providing Mach numbers up to 7 and then is exhausted to a 26ft diameter spherical test chamber with test times up to 2 minutes.[9]

Non-Vitiated Heaters

Heaters of this type introduce no flow contaminants into the test flow. Methods used to achieve this involve electric resistance heating and other specialized heat transfer devices or methods. One method of electric resistance heating involves passing air over a heating element. Alternatively, storage heating can be used as done is by the High Temperature Facility (HTF) facility at the NASA Glenn Research center.

Storage heaters transfer heat to the working fluid after preheating. Preheating can be done by combustion or electrical heating. The HTF passes nitrogen through an induction heated graphite core where oxygen is later added and mixed to obtain proper nitrogen to oxygen concentrations to match that of air. The graphite core is heated via induction from a current that is passed through its shell[6] (Figure 1-5). The core is 12.2 m tall and weighs 27,000 kg and is heated at a maximum rate of 28K per hour to minimize thermal stresses, resulting in 100 plus hours to reach a temperature of 2800K. This facility has a domed test chamber with a diameter of 7.6m with a thrust stand that can handle a test article up to 7300kg.[6]

Short Duration Facilities

These facilities are shock tunnels and have run times on the order of milliseconds to a few seconds. Test gas conditions are achieved through a compression process resulting from a shock wave propagating through the tunnel at the local speed of sound of the test gas. Run times are highly dependent on the fluid temperature, which determines the local speed of sound, and physical length of the tube. This relation of the speed of sound to temperature determines the velocity of the shock and expansion waves and the length of the tube determines the duration of the test by the time it takes for the shock wave to travel the length of the tube.

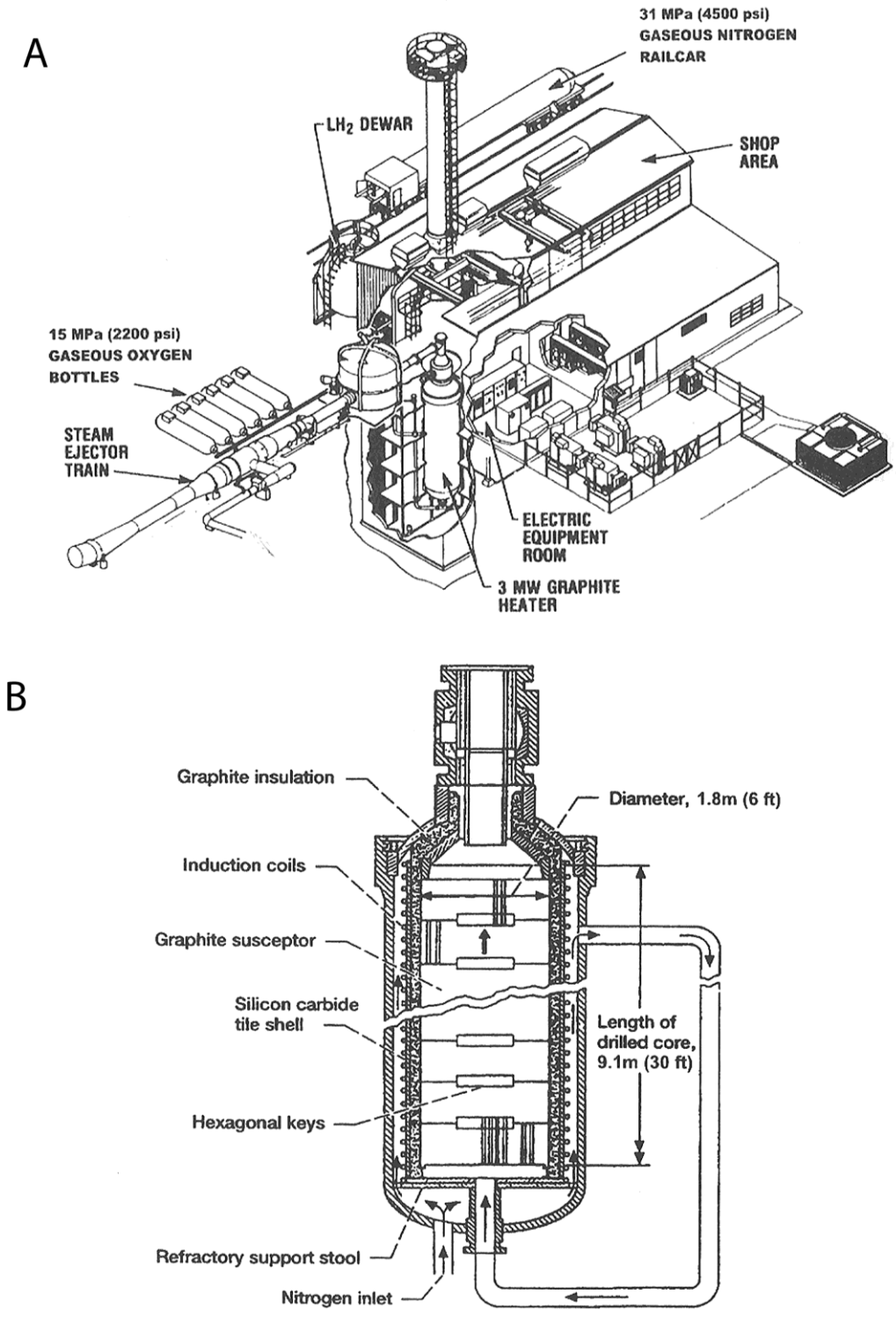

Figure 1-5. The HTF non-vitiating facility layout. A shows the scale of the facility. B details the graphite core storage heater. (Woike and Willis)[6]

There are a number of arc facilities because of the need to simulate Mach numbers up to 20, simulate vehicle reentry, rocket performance simulations, and other high temperature high pressure testing requirements.[2,7] Shock tunnels are categorized by the driver method used to create the shock; these methods are gas-driven, piston driven, and detonation driven.[10]

Gas Driven Shock Tunnels

Gas driver shock tunnels typically use light gases that are heated and pressurized to specified conditions. Once the proper pressure and temperature is achieved, a diaphragm which initially separates the driver gas from the driven gas bursts to create a shock wave. To achieve the proper temperature the driver gas can be heated electrically or via deflagration combustion. In the electric heated systems the gas can be heated internally or externally up to a temperature of 500K.[7]

Deflagration combustion heating typically uses stoichiometric mixtures of hydrogen and oxygen in helium driver gas. Combustion stability is a serious issue because of the difficulty in maintaining deflagration burning at high pressures which is limited to 40MPa. Due to the possibility of detonation from such a setup such systems must be designed to withstand detonation combustion, where pressures produced are up to five times greater than deflagration combustion.[7]

Detonation Driven Shock Tunnels

This operational mode has similarities to those of the gas driven shock tunnel, specifically deflagration combustion, the difference being in the type of combustion that occurs. Detonation driven shock tunnels use the detonation of a gaseous reactive mixture to heat and compress the driving gas.[10] The difference between detonation and deflagration relates to the speed of the combustion wave, detonation waves having the highest propagation speeds. The wave produced by the detonation is known as the Chapman-Jouguet wave.[7] Detonation driven shock tunnels

were first used in 1957, however testing was stopped due to high mechanical loading of the shock tube from the intersection of the reflected and incident shocks. This method was reintroduced in 1989 when Yu[10] used a buffer tube that reduced the high mechanical loads. Combination of detonation driver and expansion tubes achieve extremely high enthalpy conditions. The Hypulse facility run by NASA is one such facility having the capacity to simulate Mach numbers up to 25. This tunnel can be operated as a reflected shock or shock expansion tunnel.[7]

Two modes have been developed known as forward and backward driver modes. The backward mode results in uniform and steady flow condition for a relatively long period of time and more closely resembles the process of the classical shock tube. This mode uses detonation between the driver and the driven section where the detonation wave propagates backward into the driver section leaving behind a quasi-steady flow with constant properties from which the primary shock is driven into the low pressure section.[10]

The forward mode creates a detonation wave at the upstream end of the driver section. The detonation wave ruptures the main diaphragm between the driver and driven section and the high pressure and temperature behind this wave drives the incident shock, which runs along the driven section. An issue that occurs under normal operation is the Taylor expansion wave behind the detonation wave overcomes and attenuates the incident shockwave resulting in unsteady flow ahead of the nozzle. Several methods have been developed to reduce this phenomenon; however none have been able to eliminate it. There is a performance gain using the forward mode detonation driver for today's existing shock tunnels; however is it does not achieve the performance, with respect to reservoir pressure and enthalpy, of free- piston shock tunnels. This is due to the limitation on the temperature of the driver gas from the detonation process. Despite this the forward detonation mode is used as opposed to piston driven facilities because of the

lower initial investment, relative simplicity, and minimal required maintenance.[10] Figure 1-6 shows the physical schematics of the two different modes with corresponding wave diagrams. The wave diagrams show the series of wave propagation and reflections that occur during the detonation processes.

Piston Driven

This method uses a piston to compress the driver gas until the diaphragm separating the driver gas from the driven gas ruptures creating the shockwave. The stagnation conditions of the test gas results after the shock has reflected from the end of the shock tube, and are dependent on the compression ratio, driver gas composition, diaphragm rupture pressure, and initial pressure of the driven gas. Due to the small volume of driver gas that results after compression the driver gas pressure drops rapidly resulting in a rapid decay of shock tube performance. The tuned operation method was developed to address this issue.[11] The result is the piston is accelerated to nearly sonic speeds to compress the driving gas[10], and remains in motion from its momentum as the diaphragm bursts maintaining the pressure for a longer duration. The piston is decelerated to a stop at the compression end of the tube by the remaining driver gas after the test period.[11]

The High Enthalpy Shock Tunnel (HEG) facility (Figure 1-7) is operated as a reflected shock tunnel and has an overall length of 60m. A piston is accelerated to 1000km/hr to compress the driver gas and rupture the diaphragm. A shock is generated which travels through the tunnel and upon reflection ruptures a secondary diaphragm beginning the test. This process creates stagnation temperatures and pressures up to 9900K and 85MPa respectively.[13]

A difficulty in the use of heavy pistons lies in their inability to produce stagnation temperature greater than 2000K. A solution was developed and is the multi-cascade compression (MCC) method which allows for stagnation temperatures up to 4000K for diatomic gases with test duration of 50 to 1000ms more than other shock tube methods for similar conditions.[12]

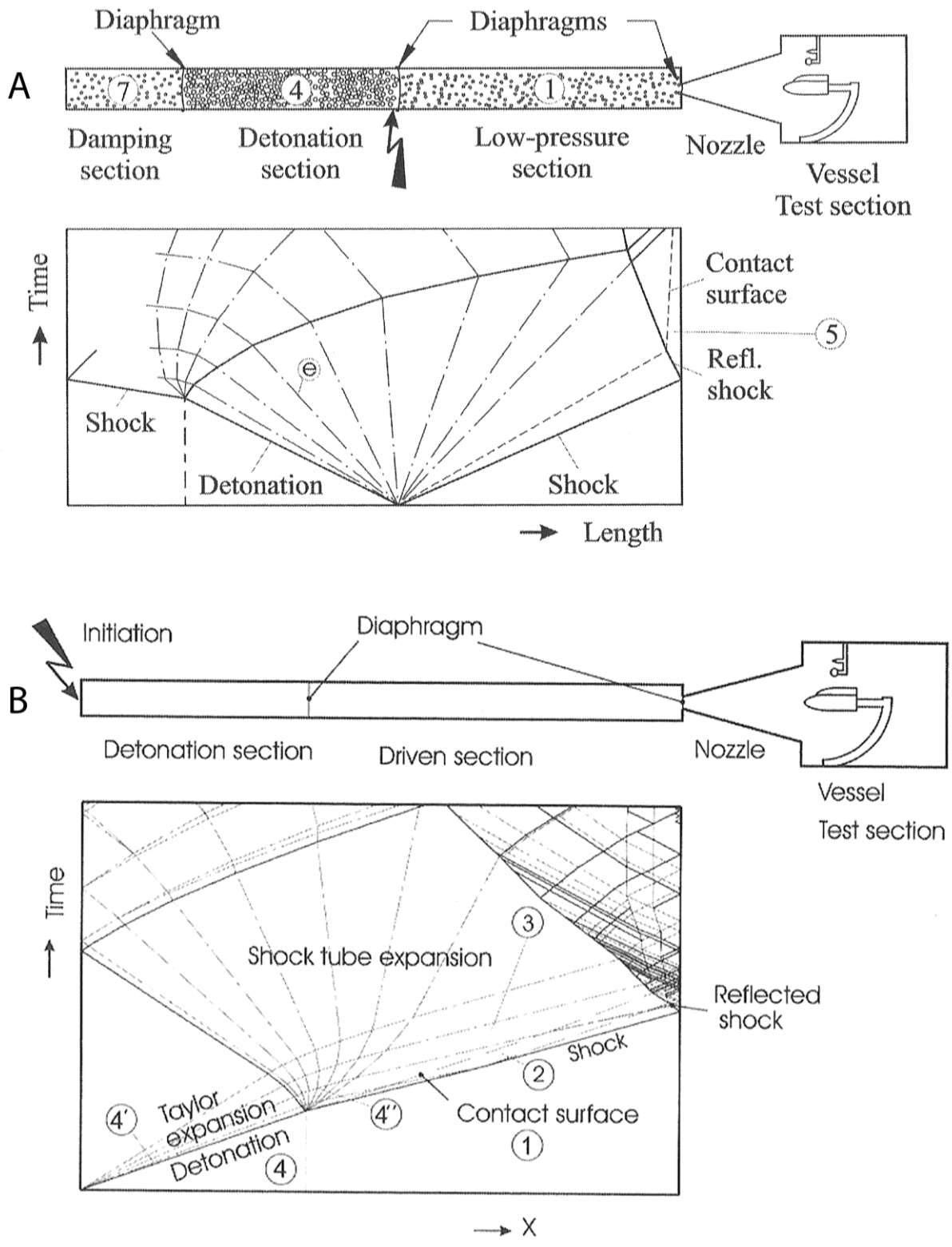

Figure 1-6. Backward and forward operating modes of detonation driven shock tunnels with corresponding wave diagrams. A shows the forward or downstream detonation mode detonation shock tunnel. B shows the backward or upstream detonation mode. (Olivier et al)[10]

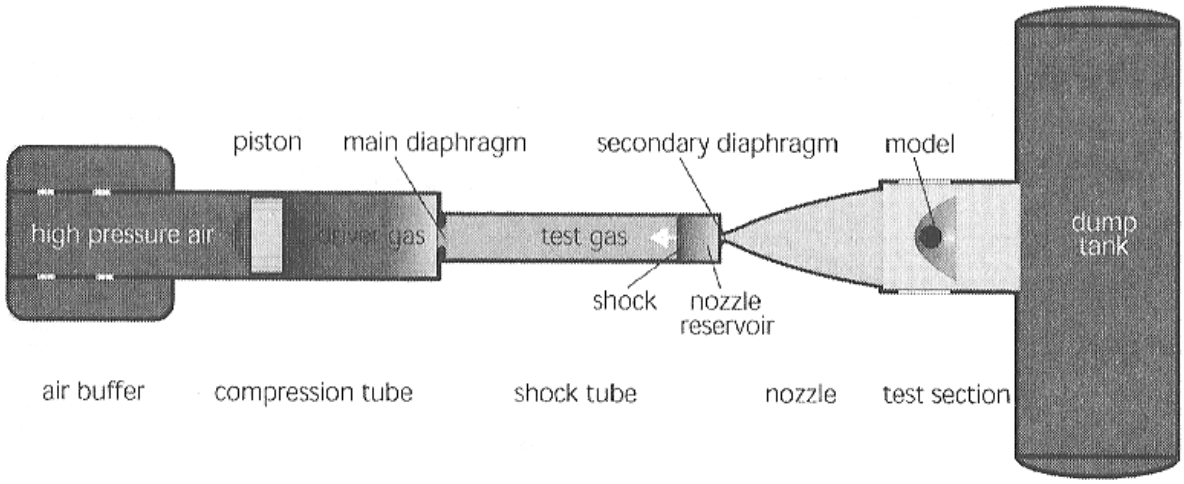

Figure 1-7. The HEG piston driven shock tube facility operated as a reflected shock tunnel. The piston compresses the driver gas which ruptures the main diaphragm creating a shock wave that propagates through the test gas and reflects off and rupturing the secondary diaphragm. The test gas is then expanded through the nozzle to the test section and exhausted into the dump tank. (Hannemann and Beck)[13]

CHAPTER 2
NON-VITIATED HEATER DESIGN

Design Parameters

The design requirement of this heater was to achieve high stagnation temperatures for air to simulate conditions of flight for Mach numbers up to Mach 5, specifically supersonic combustion. This design condition requires heating a mass flow rate of air of 250 g/s to 1300K which provides a flight Mach number of 5 at an atmospheric temperature of 297K at an altitude of 230kft. Hence air heating by non-vitiating methods is required for accurate atmospheric flight simulation.

This can be done by electric heating. The system designed here, modeled after a facility at the Central Institute for Aviation Motors (CIAM) in Moscow, uses stainless steel tubing as the resistance heater with the air passing through the core. In order to process the required quantity of air a series of these tubes are operated in parallel. The facility will require 800kW at max power. The facility layout (Figure 2-1) includes the addition of an optional second stage heater that requires a supply of hydrogen and oxygen.

Material Selection

Several materials, listed in Table 2-1, were investigated for use in the heater. It can be seen there are differences in electrical conductivity and maximum operating temperatures. These properties, as well as cost, and availability were used as the selection criteria. Inconel and Monel were removed from selection due to cost, and availability. Nickel and Fecralloy were eliminated due to their unavailability in tube stock and other required sizes. Finally stainless steel 310 has the highest operating temperature which was the reason it was chosen for this design. It has the lowest cost, availability in tube stock and other forms that are required, good corrosive resistance, and an acceptable electrical resistance.

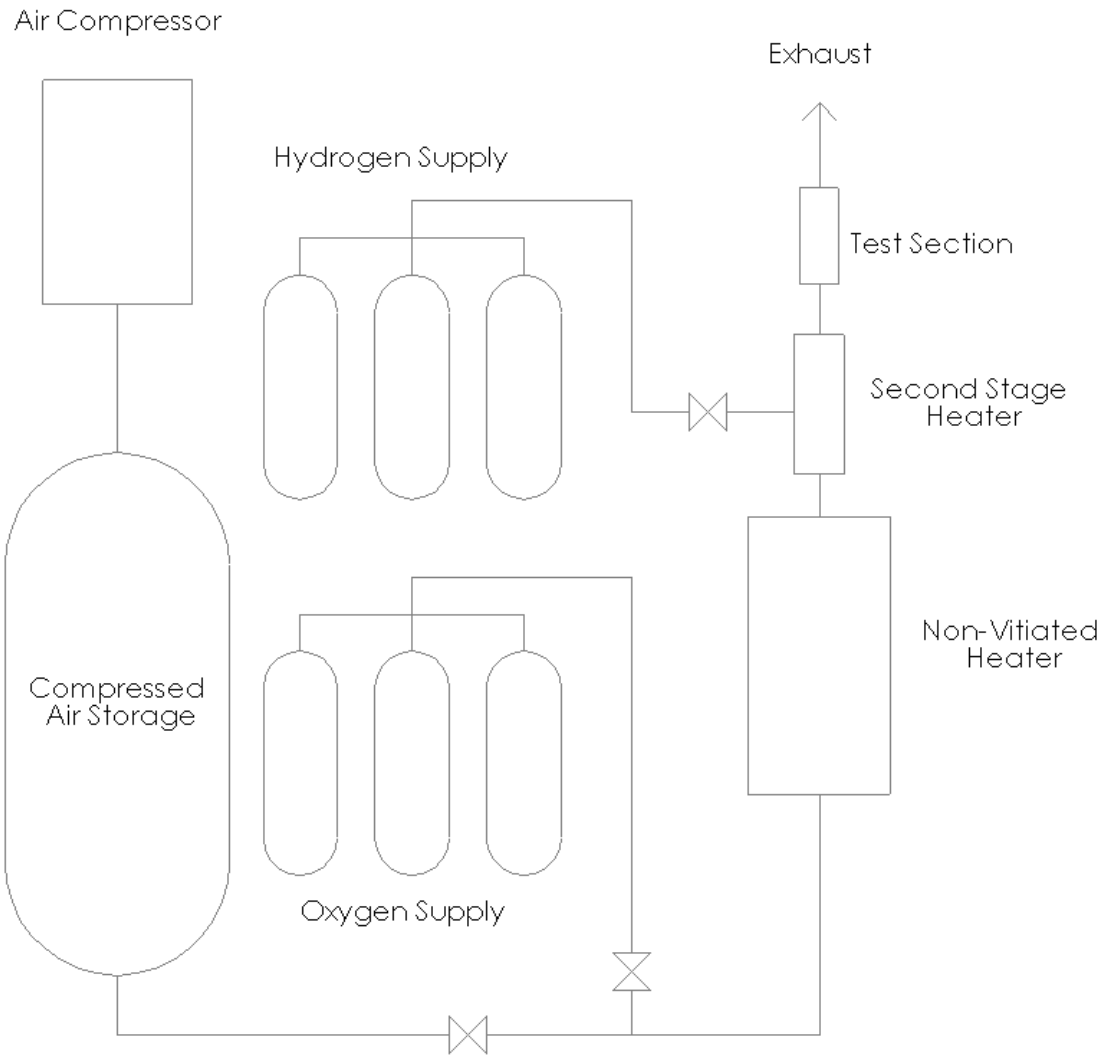

Figure 2-1. Heater facility diagram with optional second stage heater. Second stage heater requires hydrogen or some other fuel and oxygen replenishment.

Table 2-1. List of materials considered and their properties used for material selection

Material	Type	Thermal conductivity [W/m*K] @ 373K	Electrical resistivity [Ω-cm]	Melting point [K]	85% MP [K]	Max service temp. [K]
Stainless steel	304	16.2	7.20E-05	1728	1469	1198
Stainless steel	309	15.6	7.80E-05	1728	1469	1368
Stainless steel	310	14.2	7.80E-05	1728	1469	1423
Stainless steel	316	16.3	7.40E-05	1673	1422	1198
Nickel	200	70.2	9.60E-06	1719	1461	1646
Nickel	220	59.0	8.00E-06	1723	1465	1205
Monel	400	14.9	1.03E-04	1846	1569	Unknown
Inconel	600	14.9	1.03E-04	1686	1433	Unknown
Fecralloy	N/A	16.0	1.39E-04	1773	1507	1673
Nichrome	N/A	13.4	1.08E-04	1673	1422	1523

Matweb.com

Insulation Sizing

Continuous operation minimization of the loss of heat requires insulation of all hot parts. The insulation was sized using simulation data, computational analysis, and experimental data from the prototype. The insulation materials chosen for the heater facility were Zircar alumina-silica type AXL for use as solid semi cylinders and Zircar Type ASB-2300 blanket insulation; both have a maximum service temperature of 1500K. The solid material was chosen because its operating temperatures exceed that of the steel used, it is easily machined, relatively inexpensive, and has high thermal and electrical resistances. The blanket was chosen for portions of the heater where rigid insulation would be difficult to manufacture and install.

A semi-composite insulation structure is used in the current design. This semi-composite structure is comprised of an air gap between the hot tubes and the insulation cylinder mentioned to take advantage of the high thermal resistance of air. This setup requires the use of several ceramic spacers that maintain proper displacement between the insulating cylinders and the hot tubes and aid in the structural support of the hot tubes, which begin to lose rigidity at the high operating temperatures. The spacers also allow an easy access point for the placement of thermocouples which are required for safety monitoring of the facility and will be welded to the steel. Finally, the spacers create a barrier between the air gaps of the large cylinders minimizing natural convective flow and enhancing thermal resistance. Figure 2-2 shows these spacers and how they are placed between each tube.

Since the material chosen has nearly identical thermal resistance as used in the Prototype, discussed in the next section, similar heat transfer characteristics are expected for this new facility. This performance includes minimizing heat loss enabling attainment of efficiencies of nearly 90%. In addition, the outer surface temperature stayed below 473K while internal tube temperatures were above 1300K.

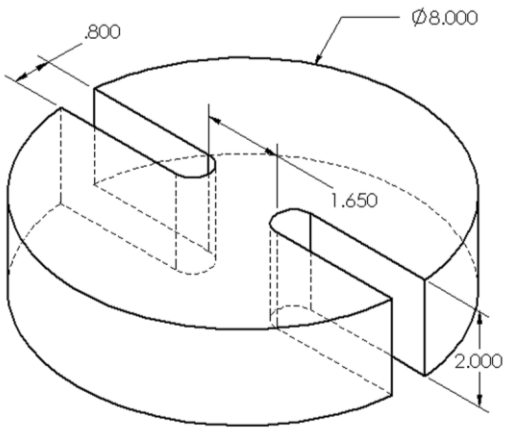

A

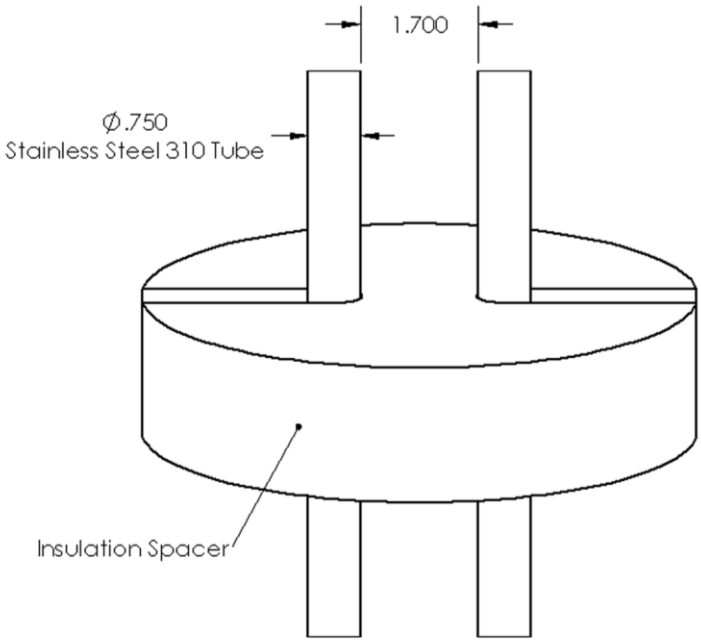

B

Figure 2-2. Insulation spacer required for structural support, insulation displacement, and thermocouple access. Dimensions in inches. A is an isometric view of the spacer. B show how spacer is installed between the tubes.

Insulation Dimensions and Assembly

The cylinders are made of two semi cylinders tied together with metallic brackets as shown in Figure 2-3. This cylinder assembly allows for easy installation and replacement of the insulation. The spacers have been designed to fit in between the two tubes to limit freedom of motion and ensure the two tubes do not make contact causing an electrical short circuit. The slot of the spacer has a generous clearance fit to allow the stainless steel tube to expand freely from thermal expansion thereby preventing stress that would otherwise damage the ceramic.

To monitor temperatures five thermocouples are welded to each tube at selected locations. Insulation assembly takes place after all hardware has been securely fastened and electric connections are tested. Finally after all spacers and cylinders are assembled hangers can be installed to provide additional support. The tube bends, hot collector, branch flanges, and discharge pipe use blanket insulation wrapped in direct contact.

Enclosure

An enclosure for the heater provides safety and encompasses the entire non-vitiated heater. The enclosure consists of a frame and various panels. The panels, made of aluminum, minimize cost and weight and are fastened to the angle iron frame with screws. In addition to providing protection these panels permit access to the components for maintenance. The bottom front and top panels have cutouts to allow for flow of free or forced convection that will remove excess heat from inside the enclosure out through ducts from the top panels. Detailed drawings are found in Appendix B. Figure 2-4 shows the heater facility within the enclosure. With this enclosure the footprint of the heater will be 13.5 feet tall, 4.25 ft wide, and 11ft long.

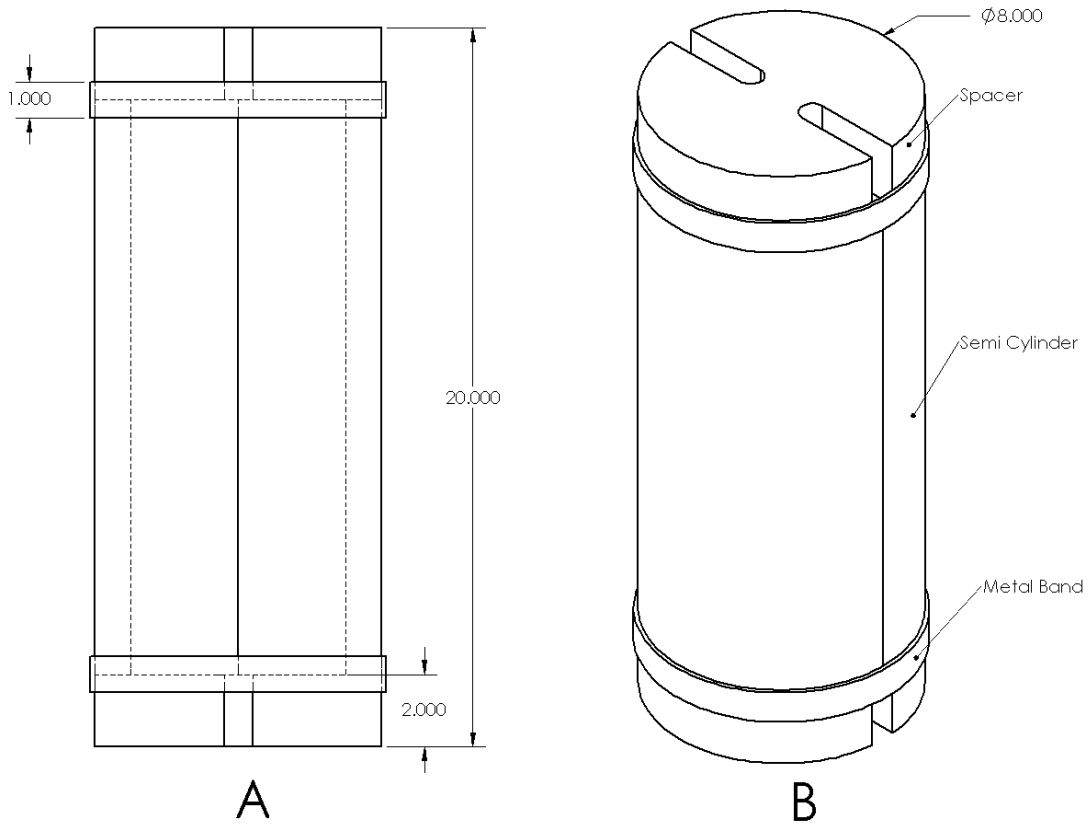

Figure 2-3. Insulation cylinder assembly: Semi cylinders, spacers and metal bands. A is a side view showing hidden lines to view internal profile and proper location of metal bands. B is an isometric view of the insulation assembly.

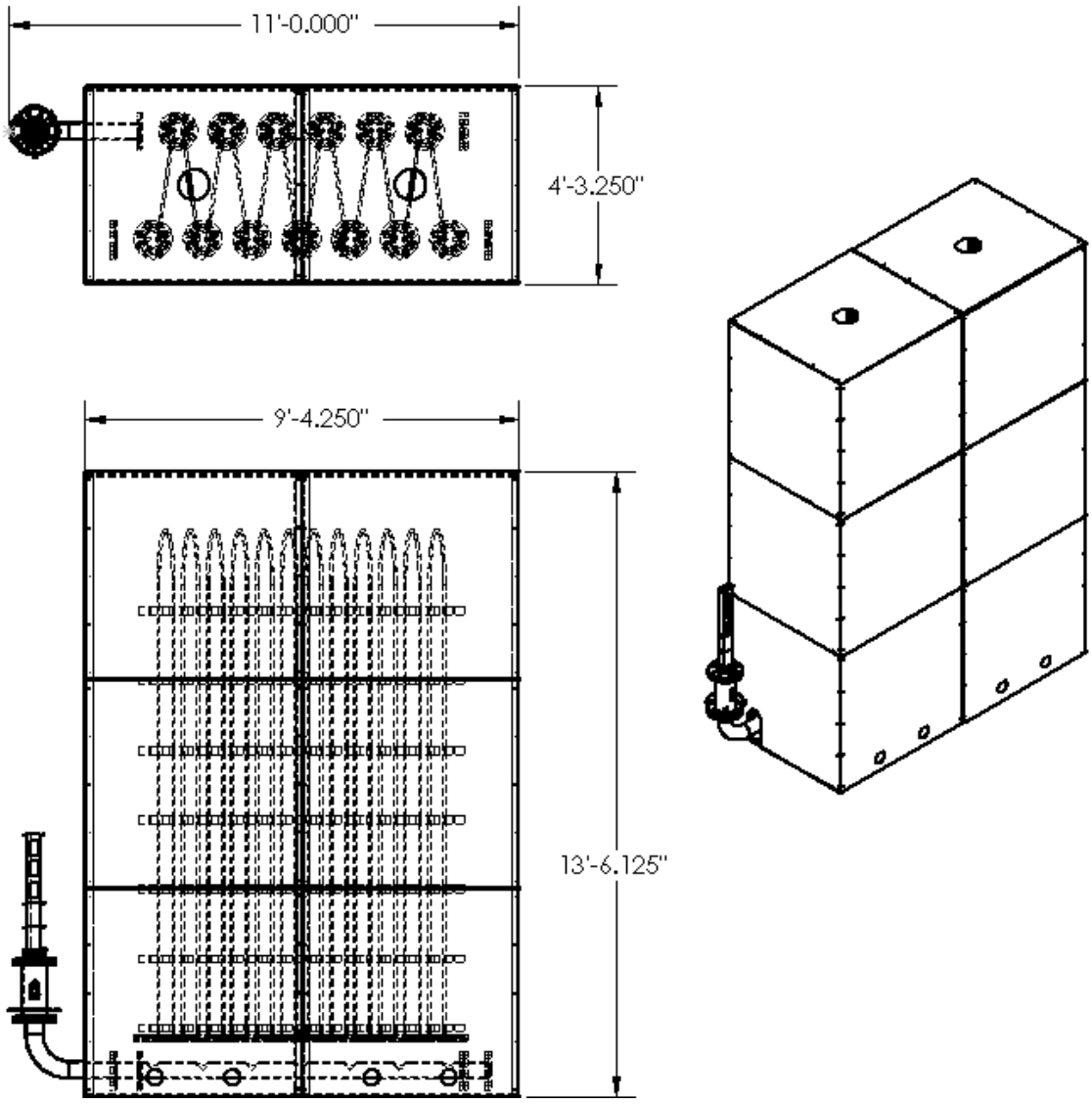

Figure 2-4. Heater facility within enclosure. Hole in the bottom front panels allow for air to enter allowing natural or forced convection to remove heat via ducts through holes in the top panels. Test section must be outside enclosure, optional second stage heater also shown.

CHAPTER 3
PROTOTYPE

Setup

The prototype is a scaled down model of the main facility with a ratio of 1:25 mass flow rate and tube dimensions scaled to maintain equivalent Reynolds numbers. The prototype was used to test the feasibility and performance of such a heater. The entire heater assembly was constructed of stainless steel 310. The heater consists of an electric resistance heating element, inlet and exit flanges, insulation, and mount. Detail drawings of this system and its components are found in Appendix C. A total of six K-type thermocouples were installed to monitor the steel tube temperature and a seventh used to measure the exit air stagnation temperature. Thermocouple locations are measured from the inlet and are given here in percentage of the overall length of 144 inches; 30%, 45%, 60%, 80%, 95% and 100%. Thermocouple locations are clearly marked in Figure 3-1.

Air is supplied from a large storage vessel and controlled via a pressure regulator with Figure 3-2 showing the air flow circuit of the experiment. Flow rates were measured using an inline float flow meter downstream of the regulator. Electric power was supplied by a DCR-A250 transformer whose power rating was determined by the maximum voltage and current that could be produced, where the maximum achievable power was 9.4 kW. From the Reynolds number's relationship to heat transfer characteristics analysis of this heater is compared to the design operating conditions of the main facility where the design operating conditions occurs at a Reynolds number of 93,400.

Insulation Sizing

Insulation was designed and applied to the heater for safety and to improve performance. The insulation used was a Zircar Type ASB-2300 blanket, which has a maximum operating

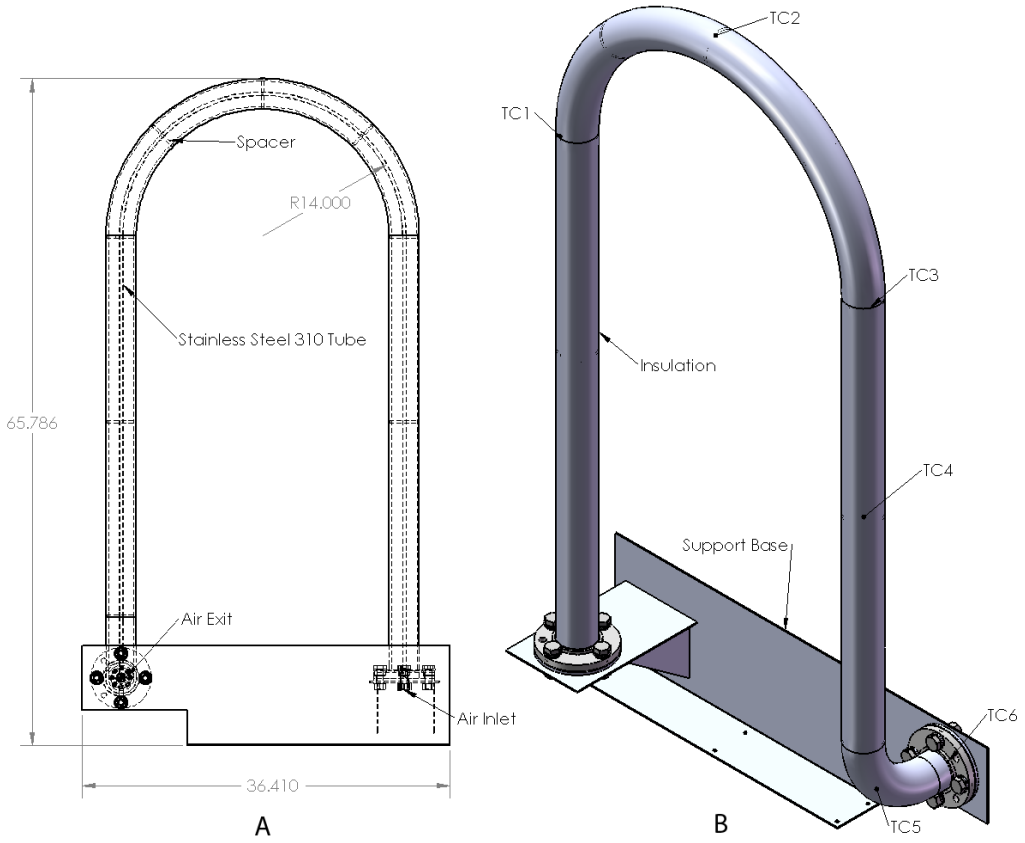

Figure 3-1. Prototype assembly with insulation. A is rear view of the prototype with hidden lines showing spacers and internal structure. B is an isometric view with thermocouple locations.

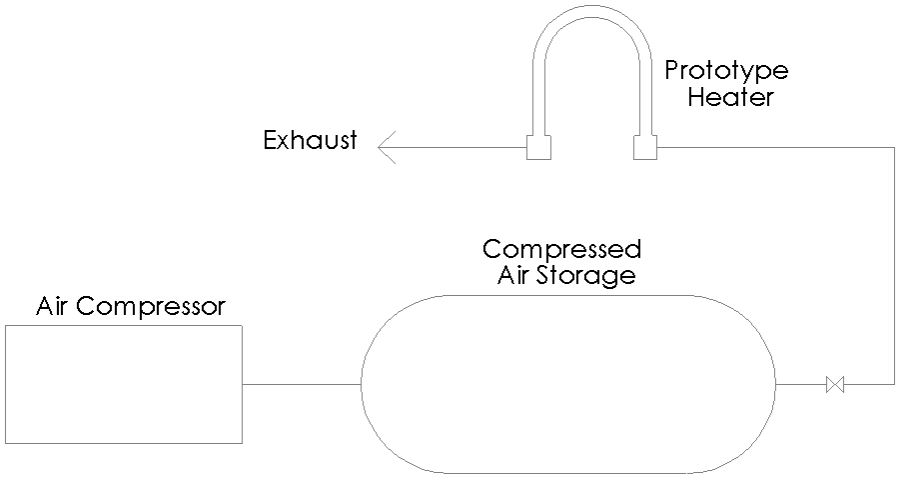

Figure 3-2. Air flow circuit of prototype system. Compressor produces compressed air up to 1.4MPa where a half inch supply line delivered the air to the prototype.

temperature of 1500K, and was lined on the inside of a three inch galvanized steel air-conditioning ducting. The air conditioning duct material was used because it acted as an exoskeleton for the insulation to enable creation of a uniform air gap with blanket material.

Sizing of the insulation was developed from results obtained from computational heat transfer analysis comparing the effects insulation in direct contact to the heater tube with varying thicknesses and composite insulation of different inner diameters and thicknesses. The heat transfer analysis was based on the thermal resistance concept of a multilayer radial medium. Equations are taken from Cengel.[14] The steady state heat conduction equation is the following

$$Q = \frac{\Delta T}{R_{Total}}$$

$$R_{Total} = \sum_i R_i = R_{Insulation} + R_{NC}$$

where R_{Total} is the total resistance of the medium, Q is the rate of heat transfer, and ΔT is the difference of the gas temperature inside the cylinder and the ambient temperature. Thermal contact resistances were neglected as a conservative approach in all heat transfer calculations. The equations governing the resistances are as follows.

$$R_{NC} = \frac{1}{h_{NC} A_{NC}}$$

$$R_{Insulation} = \frac{\ln(OD/ID)}{2\pi L \cdot k_{Insulation}}$$

and for the composite insulation

$$R_{Inuslation} = \frac{\ln(ID/TD)}{2\pi L \cdot k_{Air}} + \frac{\ln(OD/ID)}{2\pi L \cdot k_{Insulation}}$$

$$h = \frac{Nu \cdot k}{L_c}$$

$$A = 2\pi r \cdot L$$

where OD and ID are the inner and outer diameters of the insulation and TD is the outer diameter of the heating tube. L is the length of the insulation where in this analysis a unit length scale is used, h is the convection heat transfer coefficient, k is the thermal conductivity of a material, L is

the length of the cylinder, A is the area corresponding to the surface boundary in contact with the fluid with r the outer radius of the insulation. Nu is the Nusselt number of the fluid, and L_c is the characteristic length of the geometry, in this case the diameter. The Nusselt number is dependent on the motion of the fluid and the geometry associated with it. The Nusselt number in this case is based on natural convection around a cylindrical body, and is defined as follows

$$Nu_{NC} = 0.825 + \frac{0.387\left(G_r \cdot \Pr\right)^{\frac{1}{6}}}{\left(1+\left(\frac{0.492}{\Pr}\right)^{\frac{9}{16}}\right)^{\frac{8}{27}}}$$

$$G_r = \frac{g\left(1-\frac{T_{\inf}}{T_{surface}}\right)L_c^{\,3}}{\nu^2}$$

This Nu number equation is valid when the diameter of the cylinder meets the following criteria

$$D \geq \frac{35L}{G_r^{\frac{1}{4}}}$$

Here G_r is the Grashof number, g is gravity, υ is the kinematic viscosity of the fluid, and Pr is the Prandtl number, which for standard air has the value of 0.73.

Heat transfer analysis results of the insulation are given in Figure 3-3. The composite gapped insulation provides significantly better performance over that insulation that is in contact with the tube. As the gap or inner diameter of the insulation increased to 2.5 inches the effect of insulation thickness became negligible. Therefore insulation with inner diameter of 2.5 inches and thickness of 0.25 inch was used due to a limitation of a 3inch OD from heater geometry and negligible gain arises from any increase in ID or thickness.

Spacers made of hard insulation were used to ensure the air gap between the insulation and the tube was maintained and made the entire structure more stable and supportive. The spacers and ducting material act as a supportive frame for the stainless steel tube that becomes less rigid at the high operating temperatures.

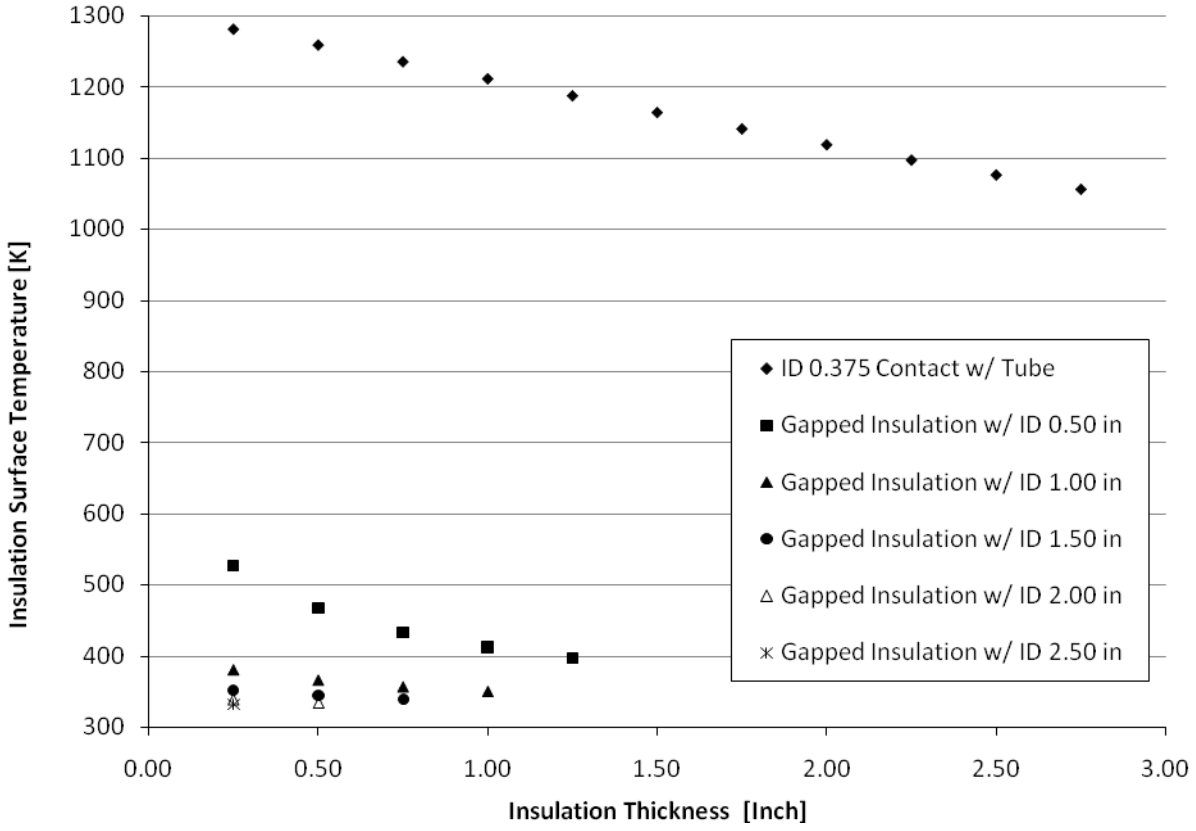

Figure 3-3. Insulation sizing analytical results comparing insulation thickness and composite insulation with varying internal diameter. Heat loss and surface temperature decrease with increasing insulation thickness and internal diameter of insulation. Analysis completed for a tube temperature of 1300K.

Experimental Results and Conclusions

A range of Reynolds numbers was tested from 18,860 to 130,076. From the theoretical analysis, under the condition of 100% efficiency for a mass flow rate of 0.0208kg/s, corresponding to Re = 93,400, the power required is 25.8 W. With the power supply used the desired temperature could be attained at only Re = 70,000 based on the supply stagnation temperature of 300K. Tests achieving the desired temperature were successfully completed for Re up to 42,030 due to inefficiencies of the system.

All tests showed the temperature of the air increased rapidly permitting attainment of the design operating temperatures in minutes (Figure 3-4). Similarly, it was found that the temperature of the fluid and heater cooled more rapidly thereby enabling quick response and control of the system. The maximum measured rate of temperature change was 19K per second. Care was taken in operation not to increase or decrease the temperature of the heater too rapidly in order to prevent thermal stresses. Temperatures along the heater tube were monitored for safety and determine the location of the peak temperature. Contrary to intuition the highest temperature does not occur at the exit because of the high heat transfer from the tube through the exit flange. Figure 3-5 shows the temperature profile from the six thermocouple locations for 5 power inputs and constant flow rate corresponding to a Re of 20,000.

η, the efficiency of the heater is the ratio of heat supplied to the air, defined by the difference from the inlet and exit energy of the air ($E = mC_pT_0$), to the power inputted to the heating element, defined by voltage (V) multiplied by current (A) shown here

$$\eta = \frac{m\left(C_pT_{0f} - C_pT_{0i}\right)}{V \cdot A}$$

where m is the air mass flow rate, C_p is the specific heat capacity of air, and T_{0f} and T_{0i} is the inlet and exit stagnation temperatures, respectively. The prototype shows a peak in efficiency of

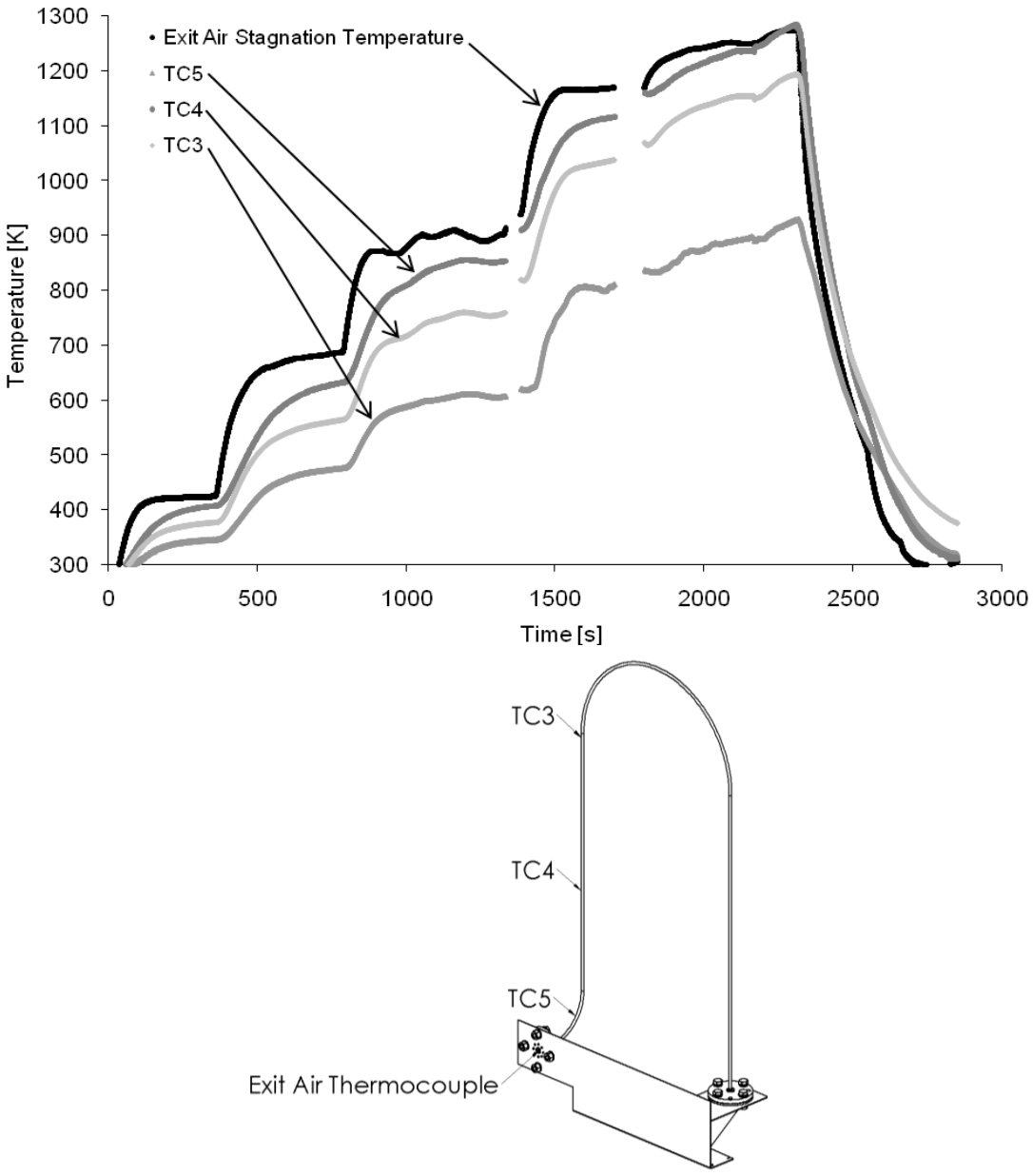

Figure 3-4. Temperature response of prototype heater. Experimental data showing the rate of temperature increase and maximum temperature obtained along with monitored tube temperatures. Power input began at 1.0kW and ended at 9.4W with initial and final air mass flow rate of 6.94g/s and 4.71g/s respectively. Flow rates decrease due to a decrease in air density from the increasing air temperature. The large plateaus are not necessary for the operation of the heater but were used to obtain steady state condition used to determine the efficiency of the system. Discontinuities exist due to removal of unnecessary data. The bottom shows the location of the thermocouples used to measure the plotted temperatures.

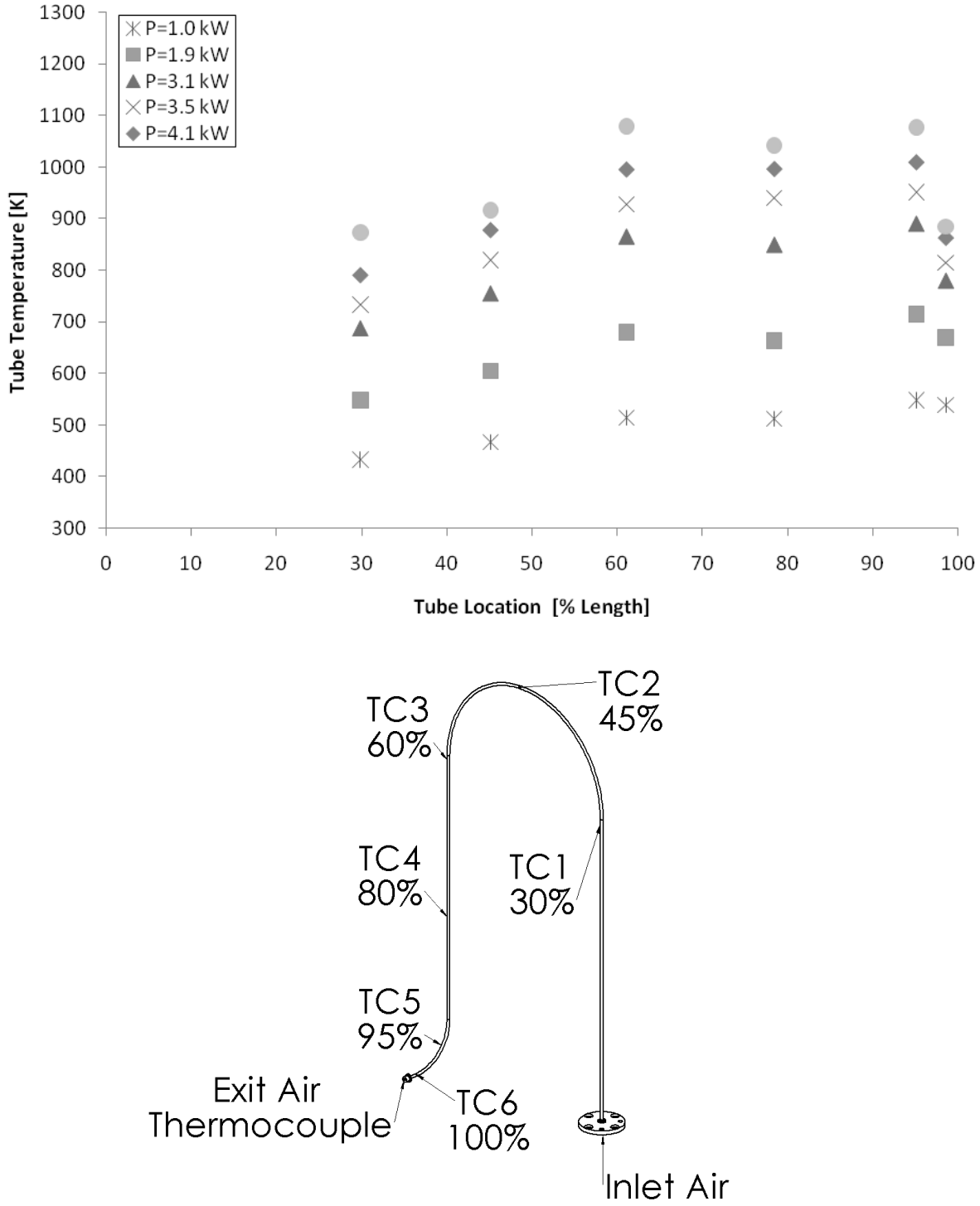

Figure 3-5. Prototype heater tube temperature distribution. Monitored steady-state tube temperatures for flow with Re = 20,000 at five different power inputs. Total length of the tube is 144 inches; location is given in percentage of this length with 100% corresponding to the exit. Peak temperature does not occur at the exit due to high heat loss from exit flange. Bottom shows the specific location of the thermocouples on the heater element.

90% at a Reynolds number of 85,000. Considering the efficiency's dependence on both Reynolds number and exit air temperature the efficiency at design condition has been estimated to be 80%. This could be done since the magnitude and rate of change of efficiency is dependent on the Reynolds number in addition to a linear dependence on exit air temperature as seen in Figure 3-6. The efficiency increases with increasing Reynolds number to 85,000 then begins to decrease showing there is an optimum operating range of Reynolds numbers, and this facility has been designed to operate in this range. Figure 3-7 shows the required power to mass flow rate ratio required to obtain specific values of the exit air stagnation temperature. This means significantly more power for the same flow rate is required to increase the air stagnation temperature at high temperatures than it does at low temperature.

In conclusion this heater is easily controlled and operated, and is feasible for use in a large scale non-vitiated facility for the given design condition provided sufficient power is available. The quick response of the system enables experiments that require fast transient conditions.

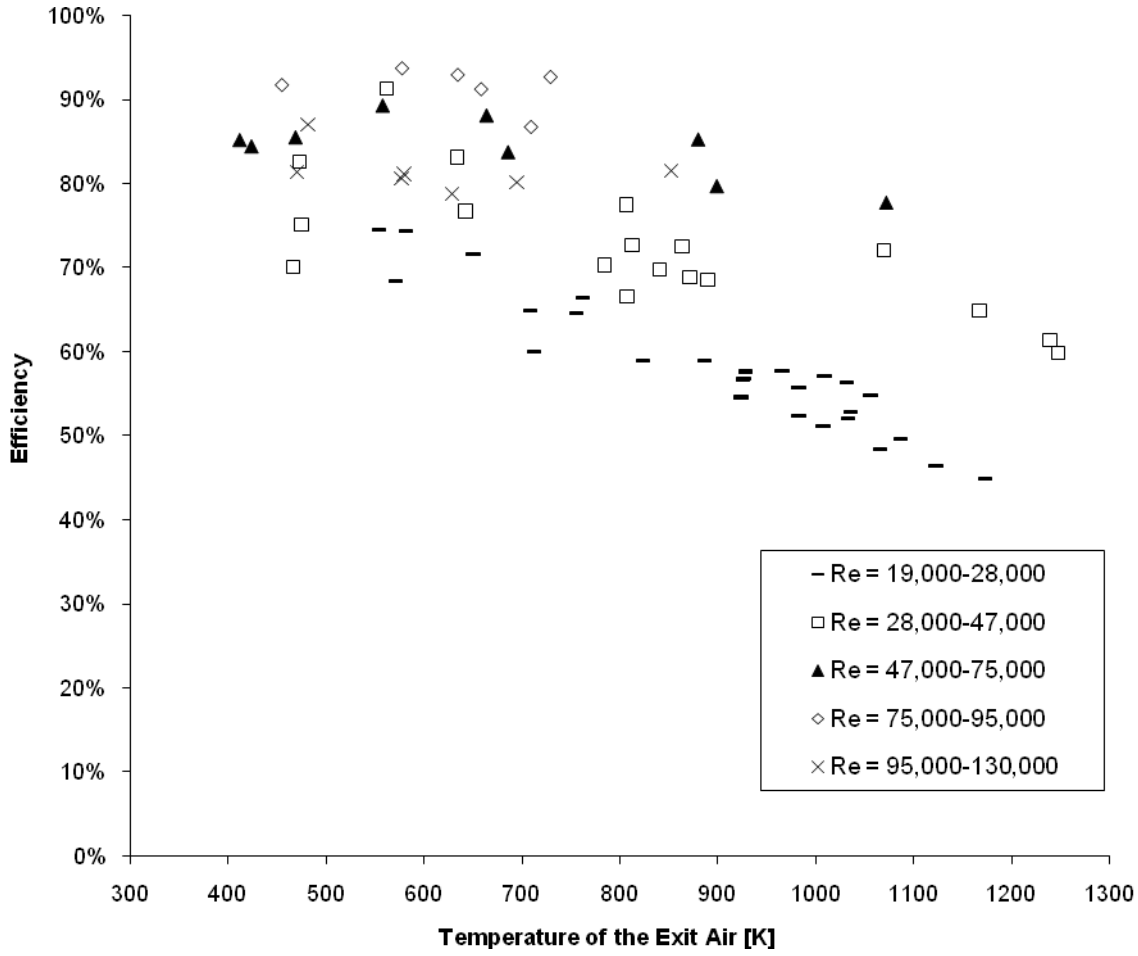

Figure 3-6. Prototype efficiency plot. Shows efficiency's dependence on Reynolds number and exit air temperature. It can be seen that efficiency decreases with increasing desired exit air stagnation temperature however the rate of decrease is dependent on the Reynolds number of the flow. The rate of change decreases with Reynolds number and the magnitude of the efficiency increase to a maximum at a Reynolds number of 85,000.

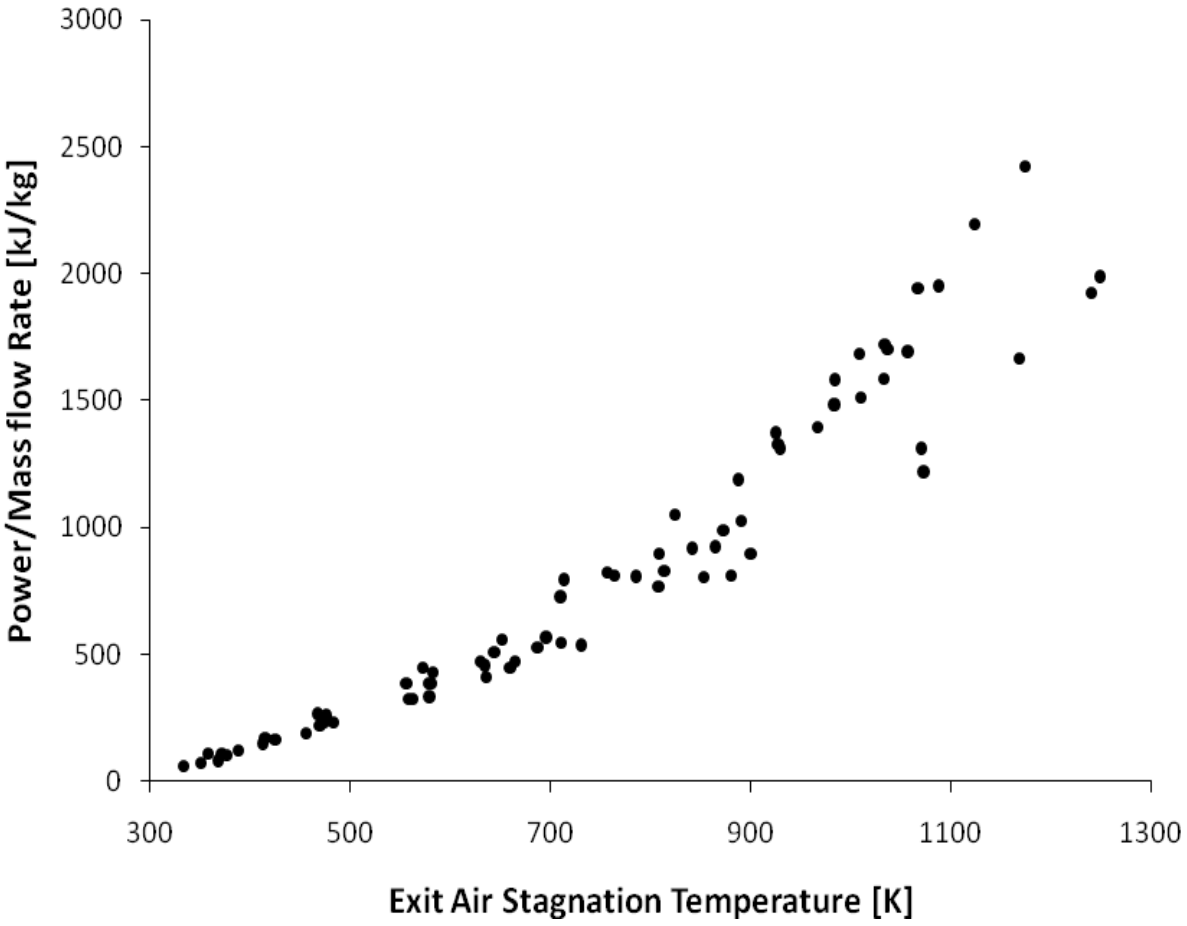

Figure 3-7. Specific heat input required for exit air stagnation temperature. Plot show the relationship between power input and mass flow rates to the exit air stagnation temperature. The data has a band that spreads as the exit air temperature increases which results from the varying Reynolds number of the flow.

CHAPTER 4
SECOND STAGE HEATER DESIGN

The second stage heater is an additional, although optional, component and its use creates vitiated air flow, via hydrogen combustion, to send to the test section. The main purpose of its inclusion is to enhance the temperature capabilities of the non-vitiated system as well as to provide the ability of back-to-back testing under same day conditions using both vitiated and non-vitiated flow through a test section for comparison on the effects of the vitiated flow. This is useful in determining correlations from data already obtained from vitiated tests to how the data relates to real conditions. The heater design comprising of a stainless steel 310 cylinder with appropriate flanges for assembly, high temperature Zircar ceramic insulation, flame holder, parallel series of four fuel injectors, and a plasma torch. Figure 4-1 shows the heater and test section assembly to the non vitiated heater and Figure 4-2 is a detail of the heater assembly. Detailed part and assembly drawings of the heater are found in Appendix D.

Design Parameters

The second stage heater utilizes hydrogen as the working fluid. This fuel was chosen due to its high energy content giving the highest possible temperatures, and minimal combustion products. Although this system is designed for hydrogen, other fuels may be used as is or with minor modifications. One such modification would be the type of injector used, due to a change in required flow rate and mixing characteristics.

The design specification was to provide test air stagnation temperatures of 1800K to cover the entire range of the non-vitiated heater and enable tests of up Mach 6. Several factors were considered in this design, such as proper material selection and geometry sizing and design. A secondary objective was to minimize the size of this heater for ease of installation and removal and to reduce cost.

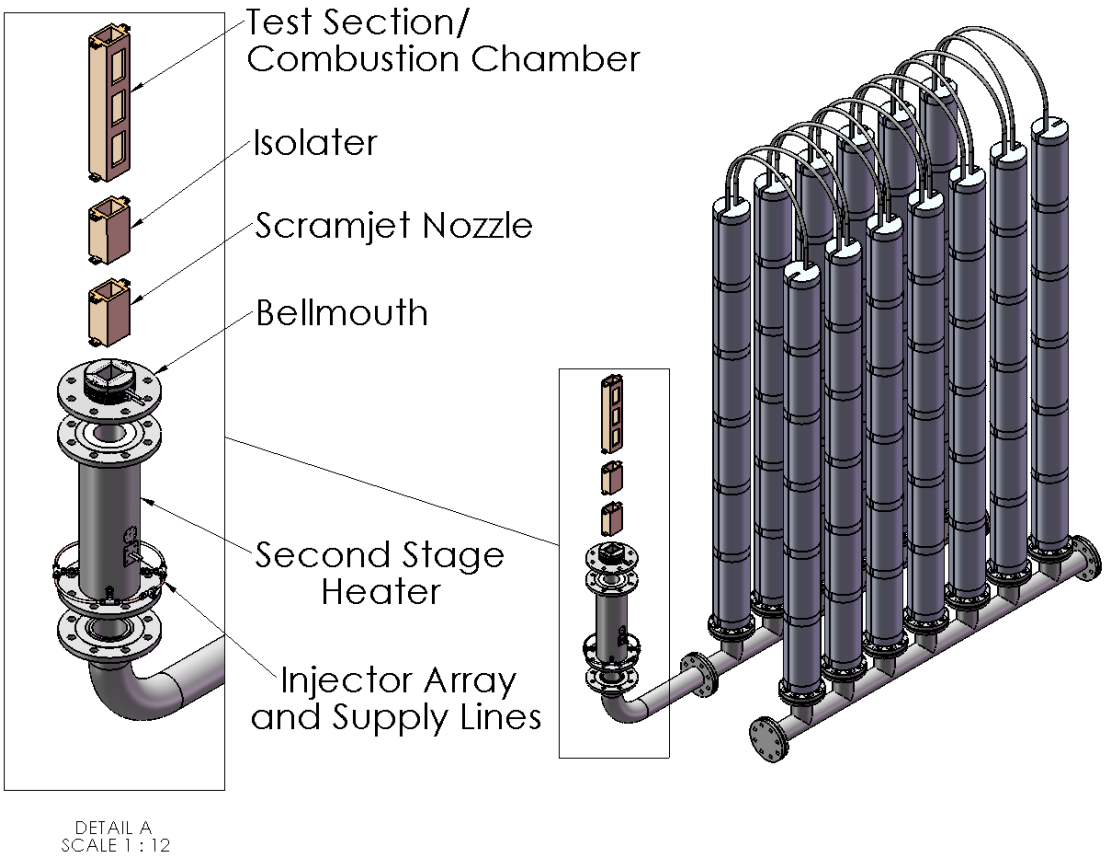

Figure 4-1. Second stage heater assembly to non-vitiated heater. Exploded assembly of the second stage heater, bellmouth, and scramjet test section.

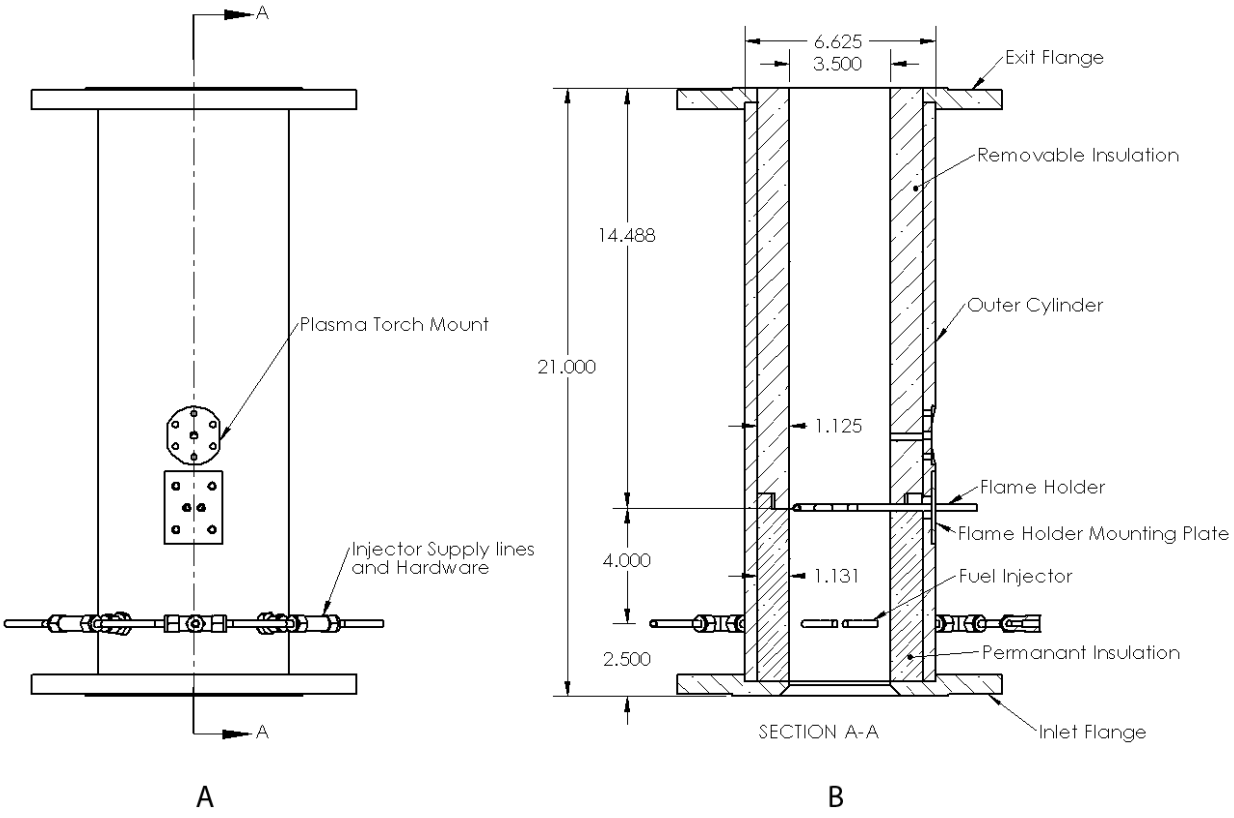

Figure 4-2. Second stage heater assembly drawing. A shows the second stage heater assembly without plasma torch. B is a section view showing internal components and layout.

Heater Design

Sizing of the heater length and positioning of the injectors and flame holder was based on the combustion and mixing characteristics of the fuel air mixture. Proper time for fuel air mixing and complete combustion determined the distance between the injectors and the flame holder and the flame holder and the exit, respectively. Temperatures are monitored on the exterior and interior portions of the heater via the installation of thermocouples. This is required to control temperature of the test conditions and maintain all the components at safe temperatures.

Plasma Torch

Ignition of the fuel is by means of a plasma torch. This was chosen because, unlike spark plugs and other ignition sources, which must be in the flow, the torch can project plasma into the combustion chamber. This prevents igniter contact with the hot fluid, preventing damage that would occur during continuous exposure to the hot gas for long periods of time.

A DC powered torch was chosen as the igniter because of its capacity to produce a continuous stream of plasma whole using low flow rates of either air or nitrogen as the working fluids. For a given flow rate of fuel the DC torch produces a higher maximum mean intensity of the radical hydroxyl (OH) while using less power in comparison to an AC powered torch. A higher maximum mean intensity of OH means the plasma has created a greater number of OH radicals which are required for chain branching reactions to produce and continue combustion. The AC torch is limited to bursts of plasma at specific frequencies and requires a higher flow rate of only air to produce characteristics similar to that of a DC torch.[15]

Cylinder and Insulation Sizing

The sizing of the cylinder and the insulation had to be completed simultaneously due to the dimensional dependence one has on the other. Insulation of this heater is not only necessary to minimize heat loss but also to protect the heater components from melting. An internal insulating

cylinder made of Zircar Alumina Type ALC is used with its outer walls in contact with the inner walls of the steel cylinder housing. The insulation has a maximum service temperature of 1825K and is sized to have an inner diameter smaller than that of the supply pipe in order to throttle the fluid, decreasing the static temperature of the fluid, and to minimize throttling required downstream at the bellmouth. Sizing was based on a compromise between the outer cylinder diameter influencing flange design and pipe size availability, maximum steel operating temperature, and heat loss.

The heat transfer analysis is based on the following computational analysis and associated assumptions. All calculations were made in the radial coordinate system with a conservative assumption of an inner cylinder uniform static temperature of 1800K. Two models for insulation were used, a standard single cylinder and a composite insulation that utilized an air gap. Forced Turbulent Convection was modeled inside the chamber, conduction for the insulation and steel material, and natural convection on the outer surface temperature of the steel cylinder.

The heat transfer analysis was conducted similarly to the method used in the sizing of the prototype insulation with the addition of forced convective heat transfer. The basic equations governing the analysis are

$$Q = \frac{\Delta T}{R_{Total}}$$

$$R_{Gas} = \frac{1}{h_{Gas} \cdot A_{Gas}} \qquad R_{NC} = \frac{1}{h_{NC} \cdot A_{NC}} \qquad R_{SS} = \frac{\ln(r_3 / r_2)}{2\pi L \cdot k_{SS}}$$

$$R_{Insulation} = \frac{\ln(r_2 / r_1)}{2\pi L \cdot k_{Insulation}}$$

and in the case of the composite insulation

$$R_{Inuslation} = \frac{\ln(r_{1A} / r_1)}{2\pi L \cdot k_{Insulation}} + \frac{\ln(r_{1B} / r_1)}{2\pi L \cdot k_{Air}} + \frac{\ln(r_2 / r_{1B})}{2\pi L \cdot k_{Insulation}}$$

The Nusselt number required for the determination of the convective heat transfer coefficient of the internal forced convection is obtained from

$$Nu_{Turbulent\_Gas} = 0.027\,\mathrm{Re}^{\frac{4}{5}}\,\mathrm{Pr}^{\frac{1}{3}}$$

which corresponds to flows with Re>10,000. The Nusselt number that corresponds to natural convection for large cylinders is defined as

$$Nu_{NC} = 0.825 + \frac{0.387\left(G_r \cdot \mathrm{Pr}\right)^{\frac{1}{6}}}{\left(1+\left(\frac{0.492}{\mathrm{Pr}}\right)^{\frac{9}{16}}\right)^{\frac{8}{27}}}$$

equations are from Cengal.[14]

Sizing was chosen giving a maximum temperature of 900K for the stainless steel cylinder corresponding to a factor of safety of 1.6 with respect to maximum service temperature. In addition to the insulation, metal tubing is coiled around the cylinder to water cool the steel allowing the use of higher stagnation temperatures when required, as well as additional safety. With this addition the maximum steel temperature will be within 10K of the maximum water temperature and the total heat loss will increase by a factor of 1.65. The insulation (Figure 4-3) was designed to be assembled in two pieces, a removable section and a permanent section. The reason for this was to enable removal of the upper section to gain access to the flame holder for easy installation and removal.

Fuel Injectors

The hydrogen fuel injectors were designed to achieve air stagnation temperatures up to 1800K. The design considerations include air flow rate, maximum supply pressure, mixing performance, and fuel mass flow requirement. From combustion and stoichiometric fuel analysis, for the design air mass flow rate of 250g/s, hydrogen mass flow rates up to 6.04g/s are required. Combustion analysis was based on the following reaction

$$H_2 + \frac{1}{2}O_2 + Air \rightarrow H_2O + Air$$

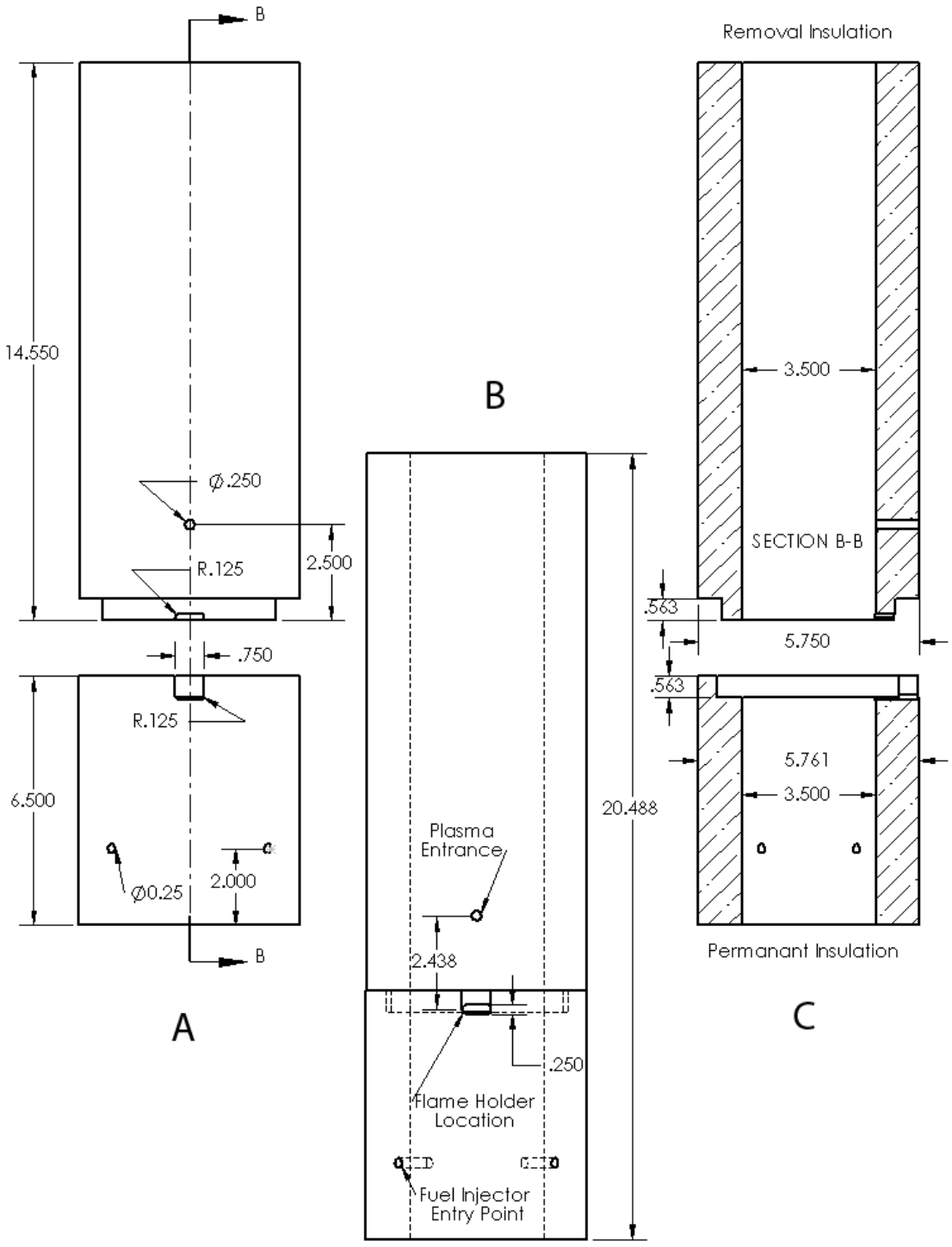

Figure 4-3. Insulation assembly detail drawing. Shows complex geometry required for assembly and insertion of flame holder, injectors, and plasma. A is an exploded view of the insulation assembly. B shows the assembled insulation. C is a section view of insulation featuring insulation thickness and coupling geometry.

Figure 4-4 shows the relationship of the hydrogen mass flow rate required to achieve specific exit air stagnation temperatures for various inlet air temperatures. Figure 4-5 compares the vitiation that occurs by heating air to 1400 to1800K during operation of the second stage heater with and without simultaneous use of the non-vitiated heater. Vitiation is decreased by 15% with simultaneous use of the non-vitiated heater. Combustion analysis required fluid properties of air at elevated temperatures, including Prandtl number, thermal conductivity, and viscosity which were obtained from Ibele.[16] Combustion analysis as well as lean and rich flammability limits of hydrogen was obtained from Turns.[17] Oxygen replenishment is needed due to the amount of oxygen required to fully burn the fuel and ensure the air composition has the proper oxygen percentage. This replenishment/enrichment occurs in the air supply line upstream of the heaters.

To supply the fuel a total of four injectors, detailed in Figure 4-6, were decided upon with each injector having five nozzles. Three of the orifices are oriented to inject the fuel vertically while two are offset from the vertical by an angle of 45 degrees to provide improved mixing in comparison to the case where all five nozzles are oriented vertically. The performance of this design has been verified with the use of COSMOS CFD software (Figures 4-7 and 4-8) for various required flow rates. Figure 4-8 specifically compares the performance of the injector with all the nozzles oriented vertically with that of the chosen design. Simulation conditions for of all figures involve 250g/s of supply air plus the additional mass flow rate of oxygen mass. The figure legend shows the hydrogen mass fraction in the flow and the scale chosen such that the lowest (0.00404) and highest (0.06875) values correspond to the lean and rich flame limits[17] of hydrogen, respectively, thus visualizing the possible flame regions. The horizontal planar cuts shown are at half inch intervals.

The nozzle diameter was sized to ensure sonic flow of the hydrogen gas over a large range of design requirements with reasonable required pressures to produce the maximum needed mass

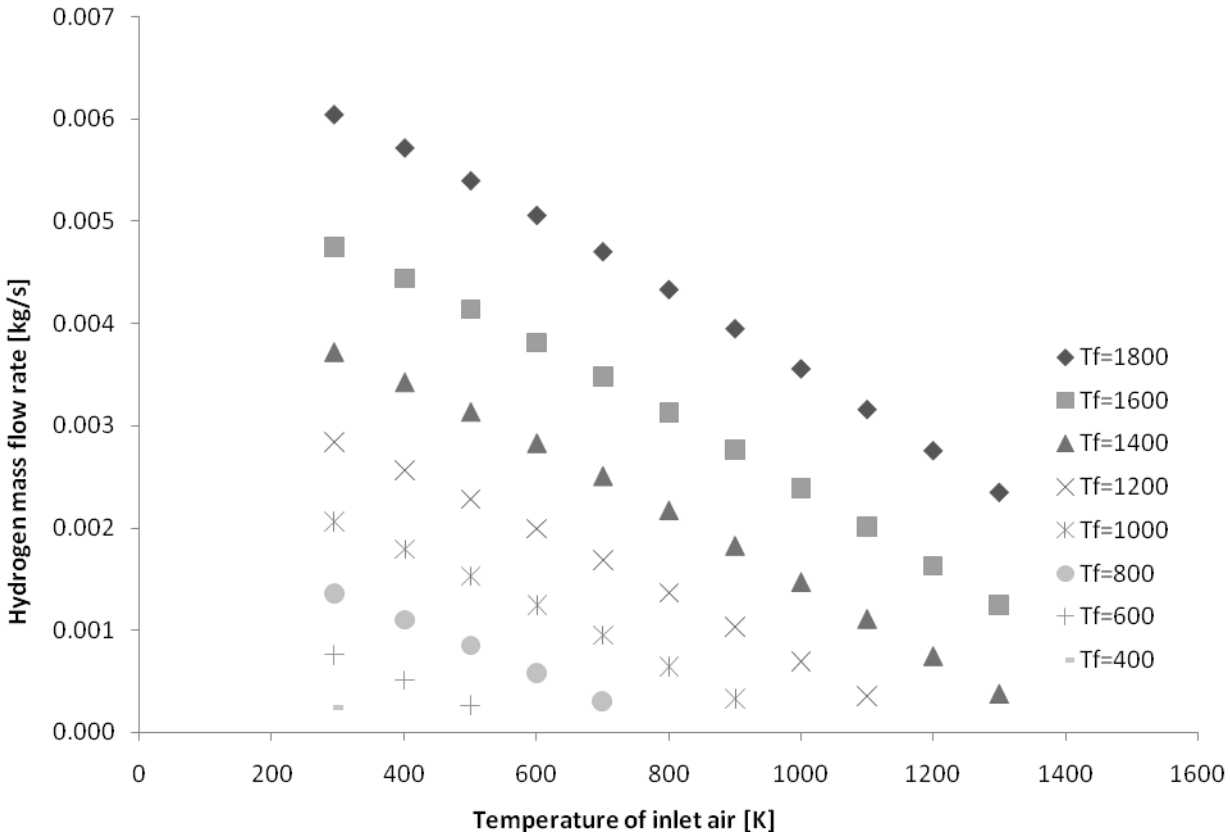

Figure 4-4. Hydrogen mass flow rate required to heat 250g/s of supply air to a specific exit air stagnation temperature with varying input temperartures. Plot shows analytic results with oxygen replenishment and shows a significant decrease in hydrogen fuel required can be achieved with simulataneous use of the non-vitiated with the second stage heater.

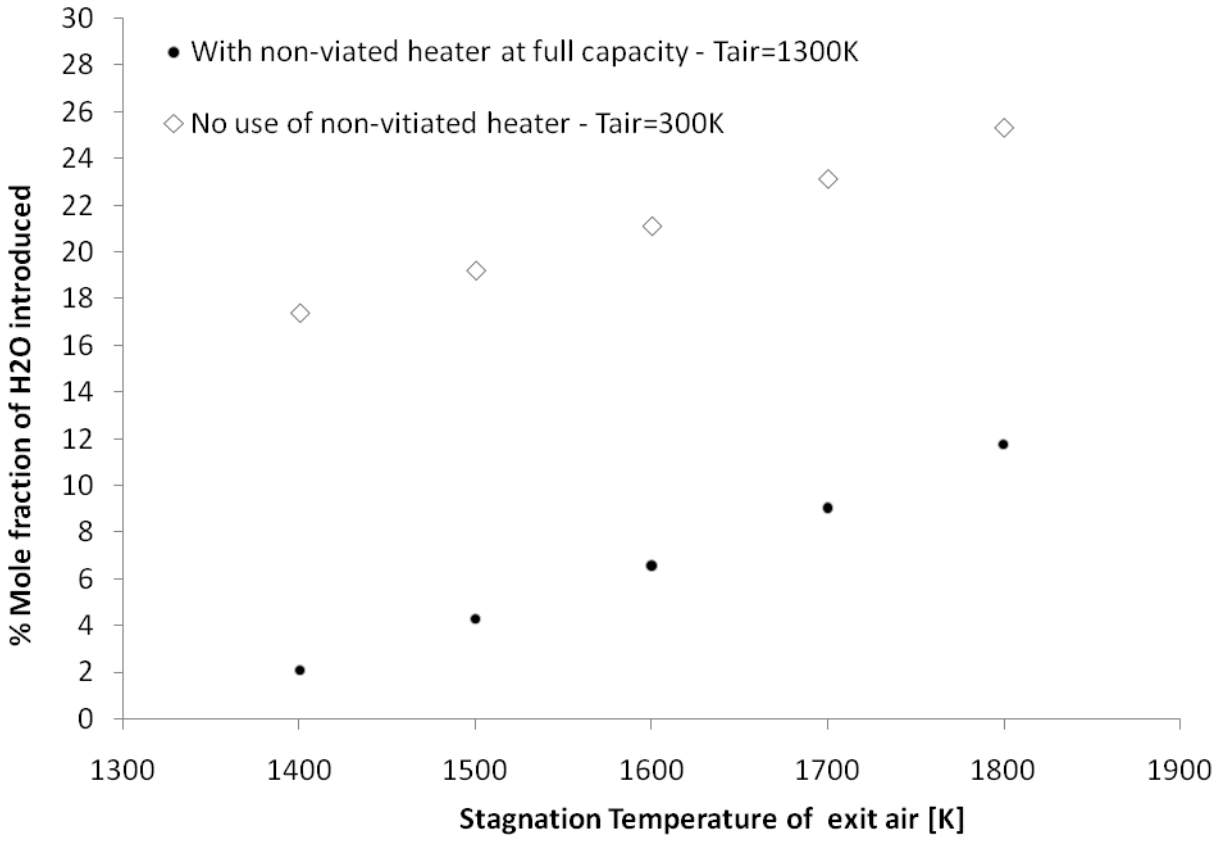

Figure 4-5. Vitiation characteristics of the second stage heater. Analytical comparison of the vitiation introduced by measure of % mole fraction of water from heating air to 1400 to 1800K without the use of non-vitiated heater and inlet temperature of 300K and with non-vitiated heater at full capacity with inlet temperature of 1300K. The chart shows there is 15% less vitiation for the same temperature while using both heaters simultaneously.

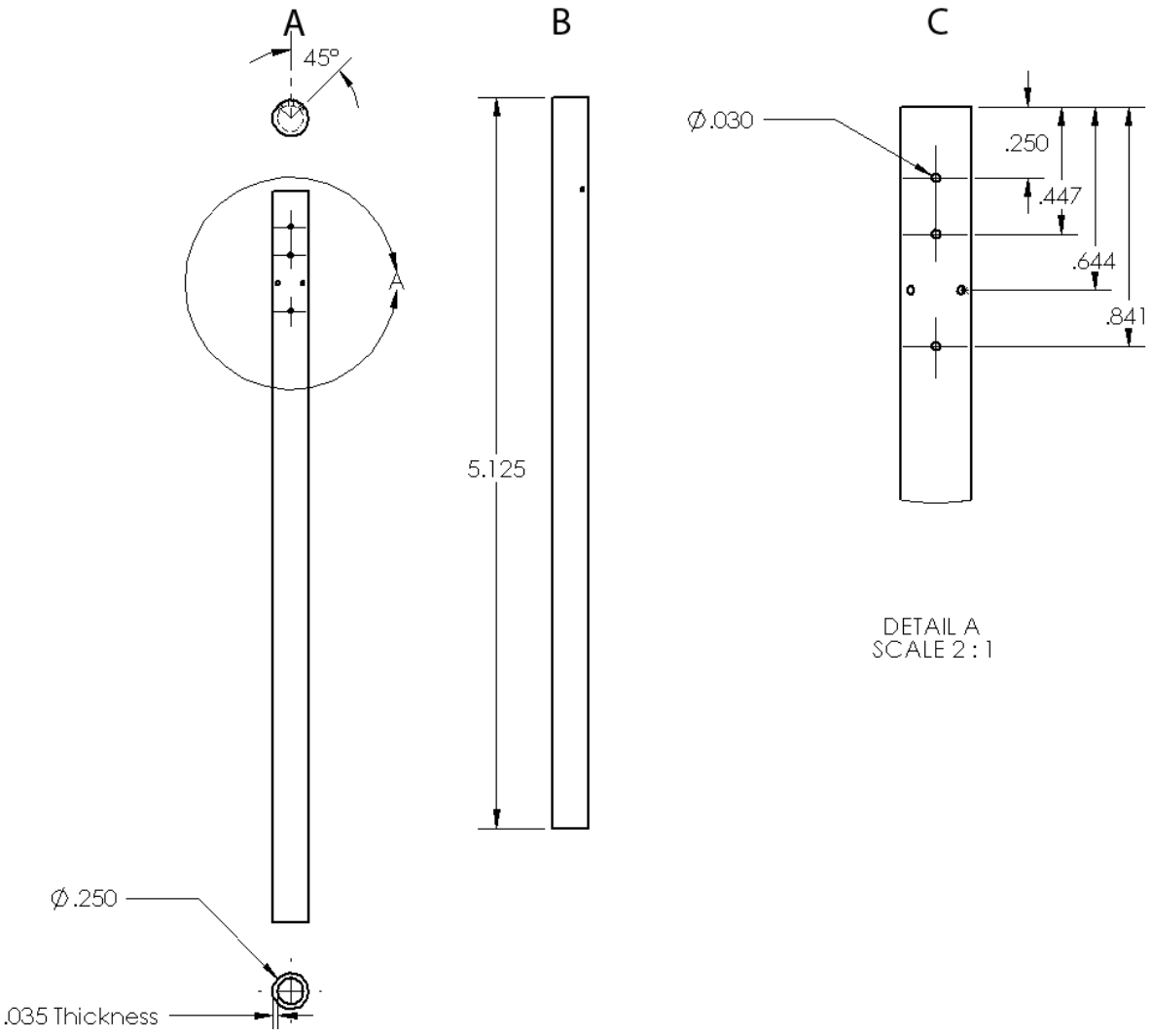

Figure 4-6. Fuel injector detail drawing. A shows top view with injector end views showing injector dimensions and nozzle orientation. B shows side view of the injector. C is a detail section showing nozzle size and layout.

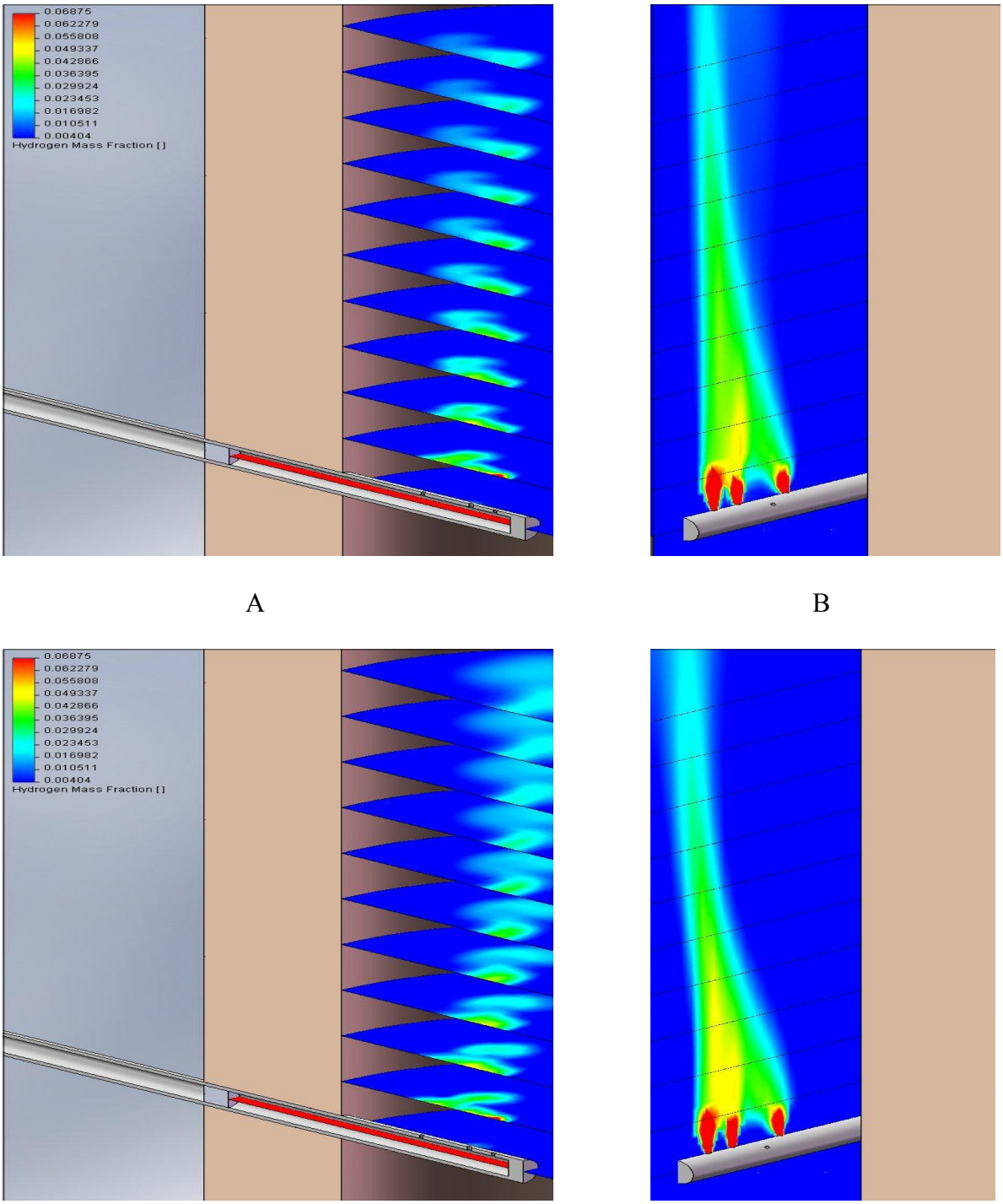

Figure 4-7. Hydrogen mixing characteristics of two flow rates. Mixing for hydrogen mass flow rates of 1.24g/s in A and B and 3.23g/s in C and D with flow rates corresponding to temperature increases of 300K and 700K respectively. A and C show horizontal slices of the mixing profile at half inch intervals. B and D show a vertical slice of the injector centerline.

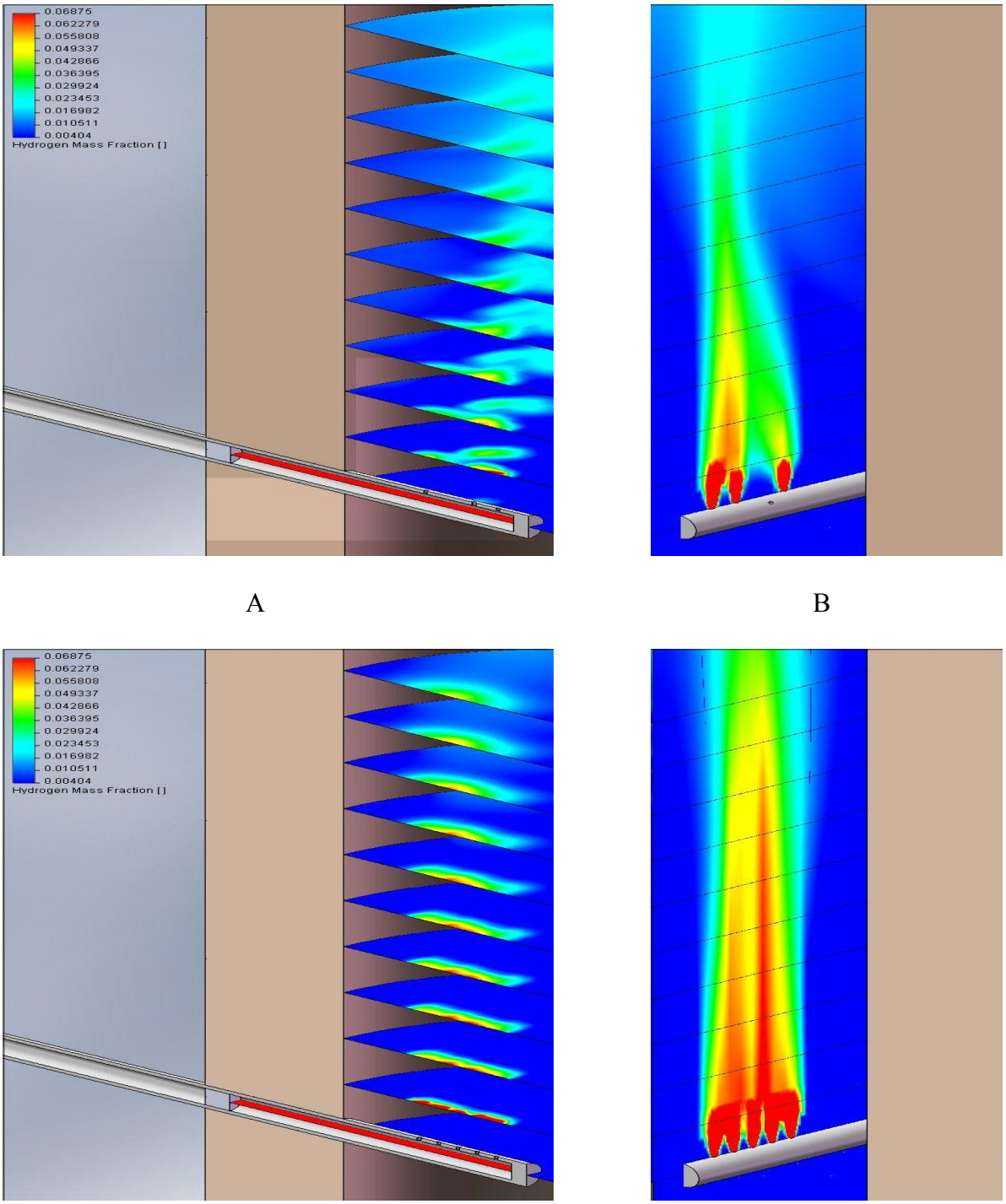

Figure 4-8. Fuel injector design mixing comparison. Hydrogen mass flow rate of 6.04 g/s for a temperature increase of 1500K. Injector design A and B is compared to design with all nozzles oriented vertically C and D. Mixing of the chosen injector design is faster and more distributed.

flow rate. Operating at the sonic condition enables easy control of the flow rates due to the mass flow rate dependence only in the difference of combustion chamber pressure and the hydrogen injector pressure.

Flame Holder

Flame holders are used to stabilize a flame at a specific location. The flame holder location was chosen to be 4 inches downstream of the fuel injectors and was designed to distribute the flame by maximizing the surface area of the tubing, where the flame is stabilized, to provide even heating of the fluid and thus more uniform fluid properties. Figure 4-9 shows how a flame is stabilized and becomes evenly distributed over a water cooled coil. The flame holder (Figure 4-10) is constructed from ¼" stainless steel 310 tubing and be water cooled because it is in direct contact with the flame where temperatures will exceed the melting point of the flame holder material. The use of an external pump is required to provide the necessary water flow rate and sufficient cooling.

Flanges

The inlet and exit flanges were required to have the same mounting patterns since the bellmouth requires that it be mountable to both the second stage heater as well as the non-vitiated heater. The inlet flange was designed to create a footing for the insulation whereas the exit flange required an inner diameter equal to the inner diameter of the steel cylinder to allow installation and removal of the insulation (Figure 4-11).

Bellmouth

The bellmouth is necessary to couple the test section to either the non-vitiated or the second stage heater. This component controls the final throttling of the fluid into the test section. The bellmouth has complex geometry making it difficult to manufacture from solid stock. The solution was to design several relatively simple pieces that would then be welded together to

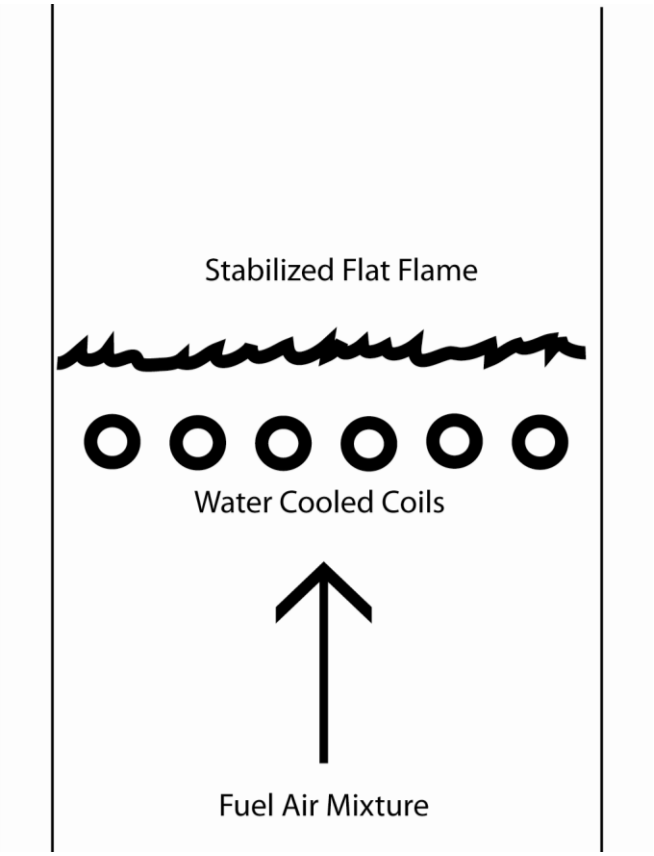

Figure 4-9. Flame distribution and stabilization over water cooled coils. Similar to that of the design used.

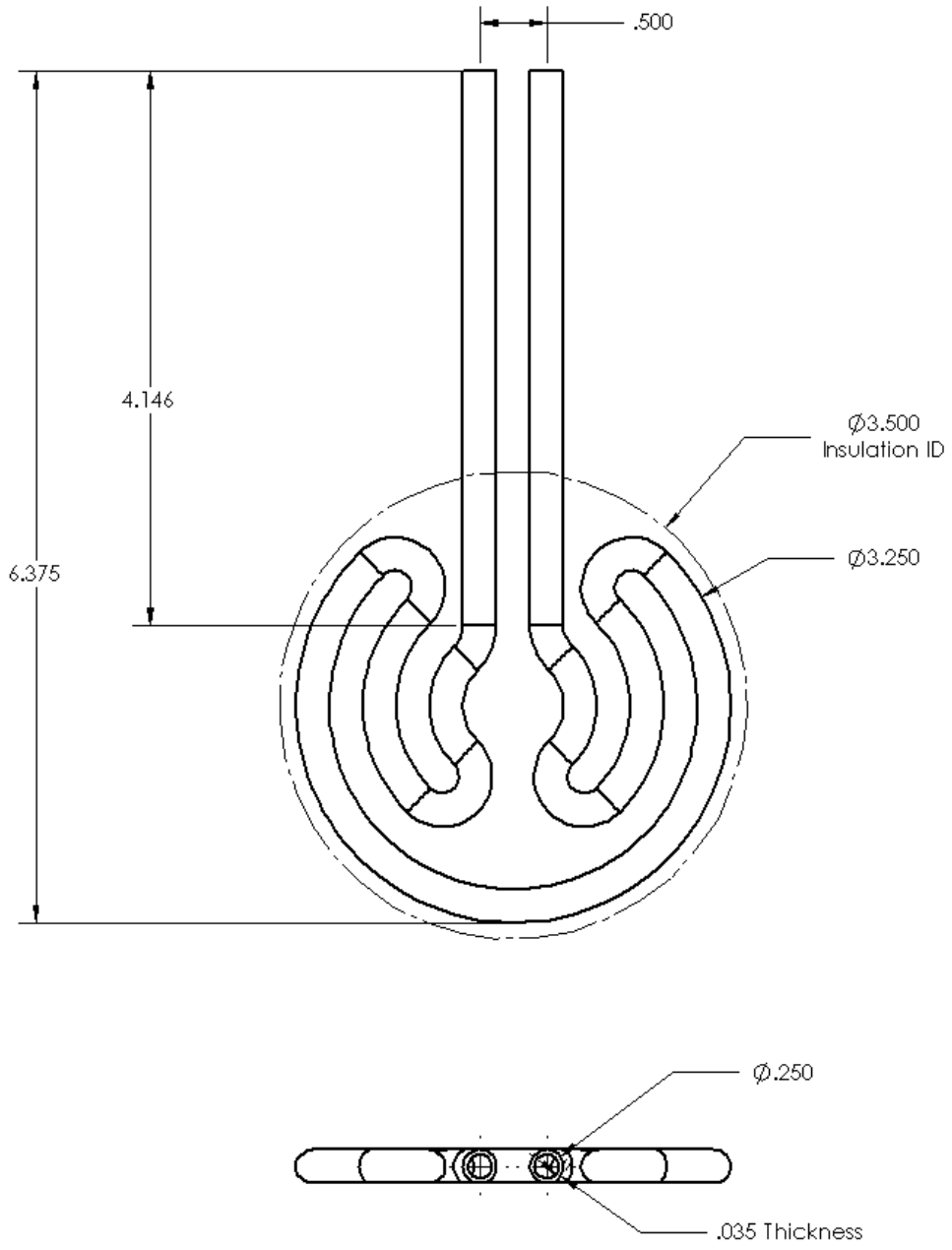

Figure 4-10. Flame holder detail drawing. Top view shows complex geometry to achieve maximum flame surface area. Water inlet and exit ports shown on bottom with tube dimensions.

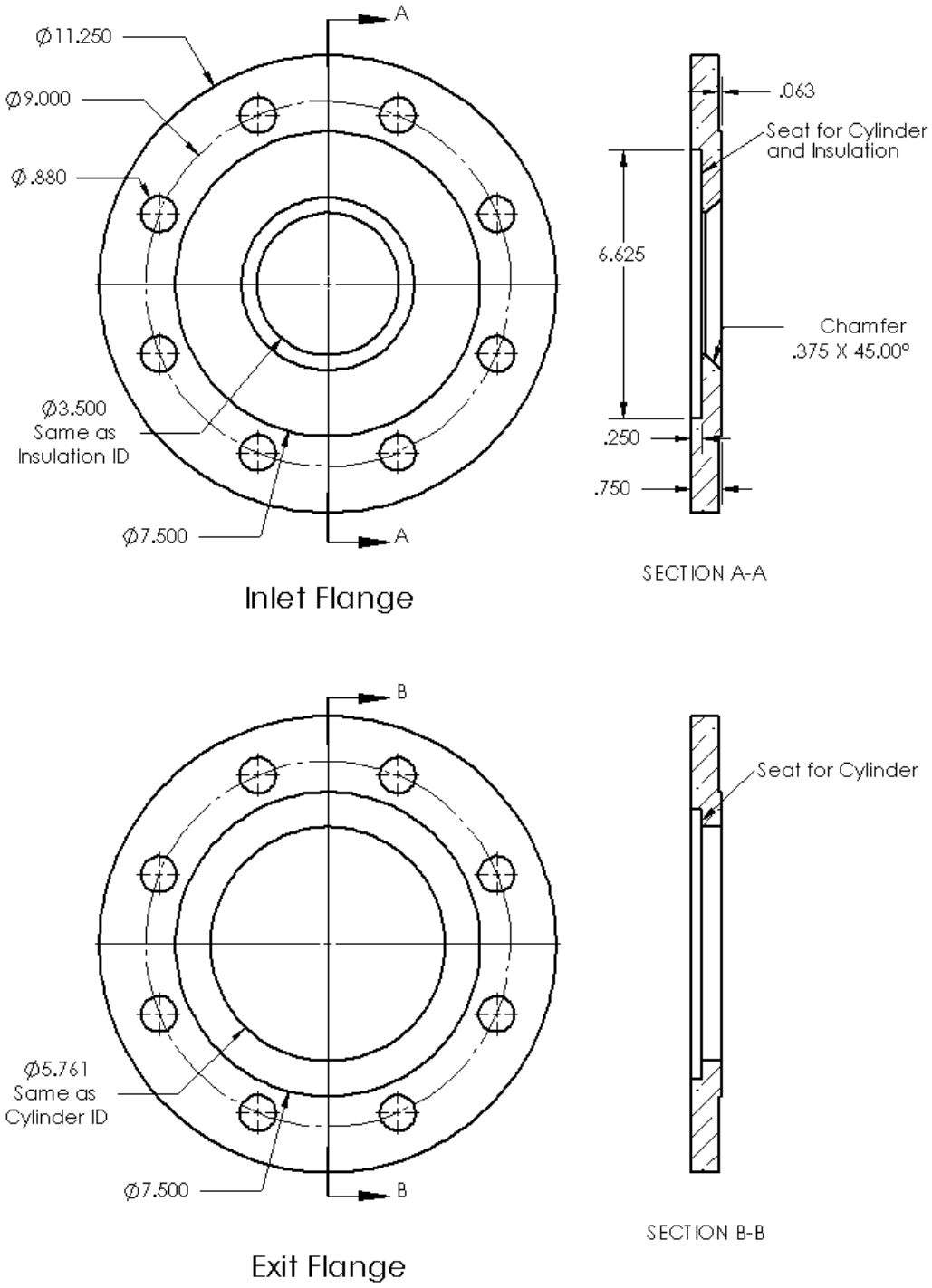

Figure 4-11. Second stage heater inlet and exit flanges. Common dimensions not shown twice.

form the bellmouth. Two models have been developed, the first to adapt to the current test section used and a second for a larger test section that will be manufactured.

Temperature control is important due to the high stagnation temperature to which the bellmouth (Figure 4-12) is exposed to. To prevent overheating the internal components are insulated with moldable insulation to a thickness of ¼" and be water cooled. There are three grooves for placement of the water cooling piping in the bell mouth. An optional configuration has a spiral groove with varying depth to match the inner profile of the bellmouth so that a tube can be coiled around the bellmouth without discontinuities. Insulation grooves (Figure 4-13), are necessary so that the moldable insulation, installed after assembly, has a place to seat and be held in place. The insulation will be molded to provide a smooth transition from the second stage heater insulation to the test section. Detailed drawings of the bellmouth are found in Appendix E.

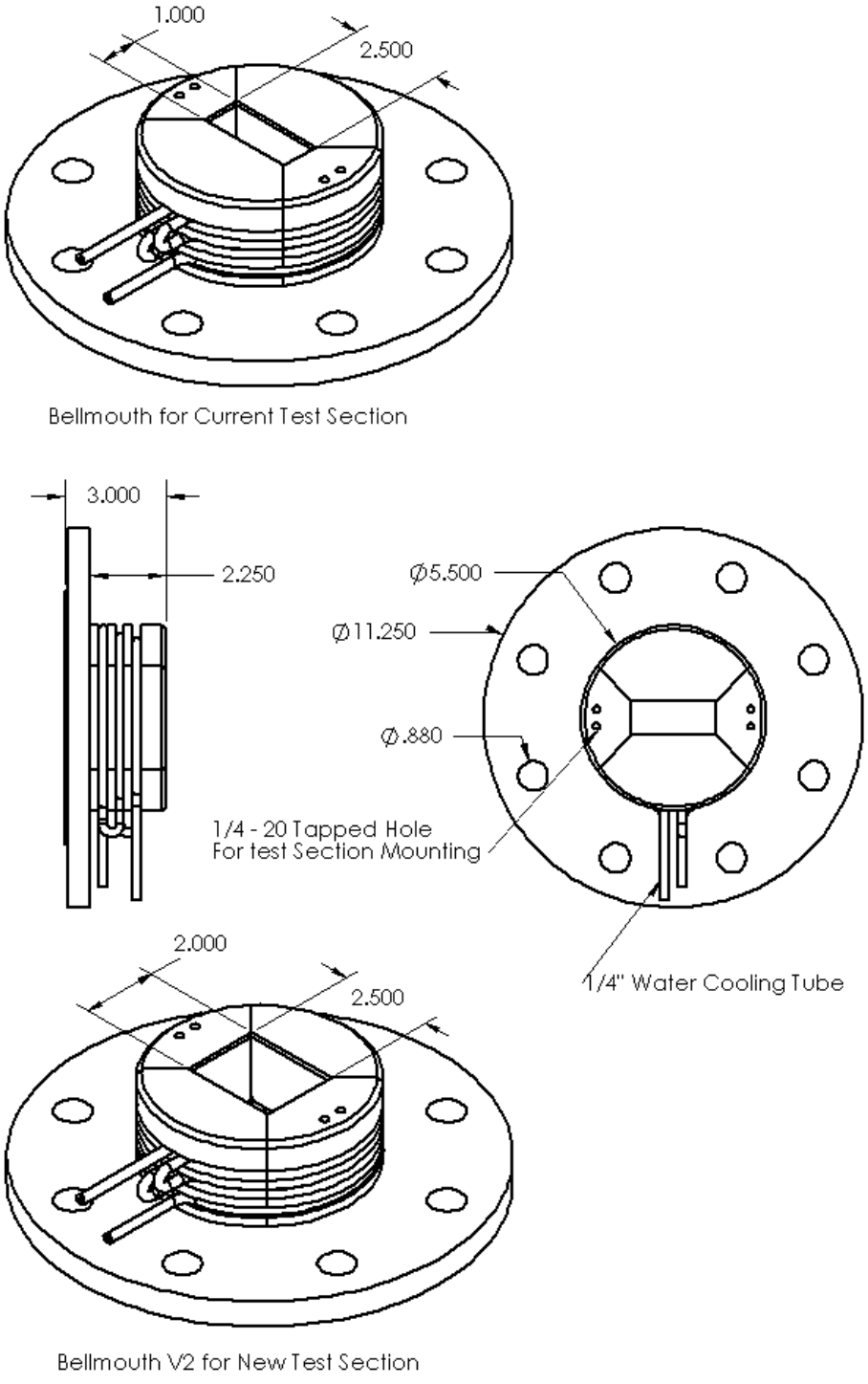

Figure 4-12. Bellmouth assembly views. Isometric views of the two bellmouth assemblies with side and top views detailing the common features of both adapters.

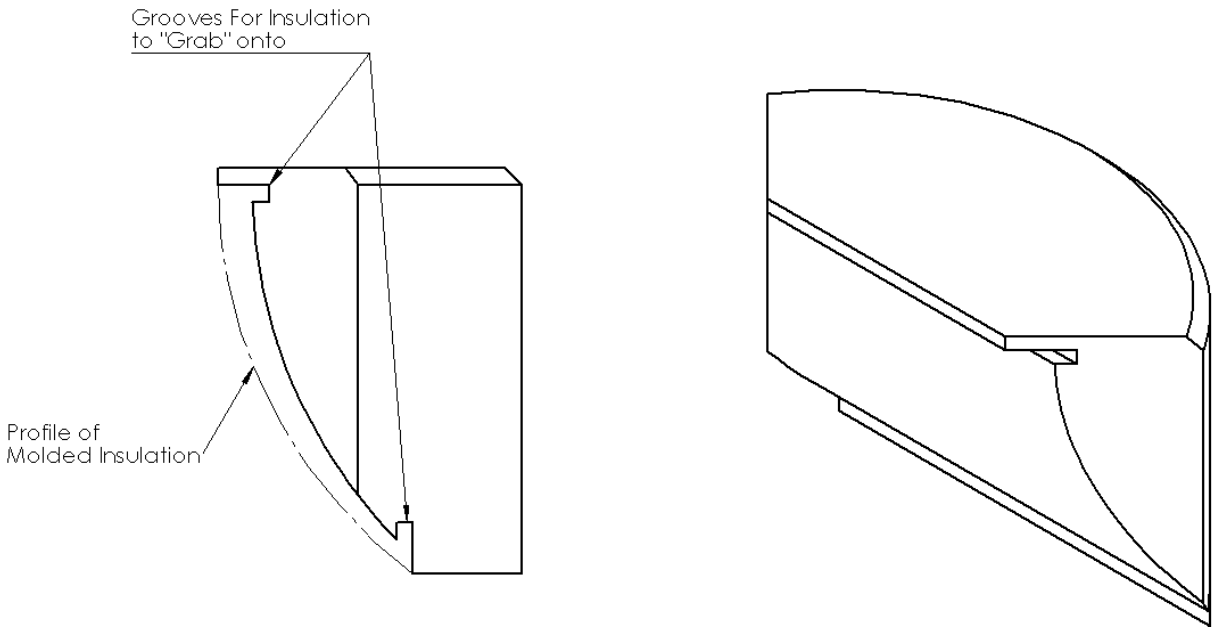

Figure 4-13. Bellmouth quarter section showing geometry and grooves for insulation. Side view shows the desired profile of the insulation.

CHAPTER 5
CONCLUSIONS

This work found that this design of a non-vitiated heater ground test facility is feasible and practical for use in supersonic combustion testing. The facility is required to produce air stagnation temperatures of 1300K. A prototype was built and tested over a range of Reynolds number showed that the heater is capable of heating air to this temperature under continuous operation. Specifically, the desired results were obtained at a Reynolds number of 42,000. The heater is very effective at heating air quickly and efficiently. The rapid response of the heater to heat up or cool down allows experiments requiring fast transient test conditions to be performed. Efficiencies of the heater ranged from 50 to 90% and were found to depend on the Reynolds number of the air. The peak efficiency occurred at a Reynolds number of 85,000 and therefore the heater facility has been designed to operate in this range.

A second stage heater was designed to supplement the non-vitiating heater. With this addition vitiated air and non-vitiated air tests could be performed and compared to develop correlations between both types of experimental results which can be used to better interpret data obtained under vitiated conditions. This heater enhances the non-vitiated heater providing the capacity to obtain Mach numbers up to 6 independently or with minimal vitiation when the two systems are operated simultaneously.

APPENDIX A
NON-VITIATED HEATER DRAWINGS

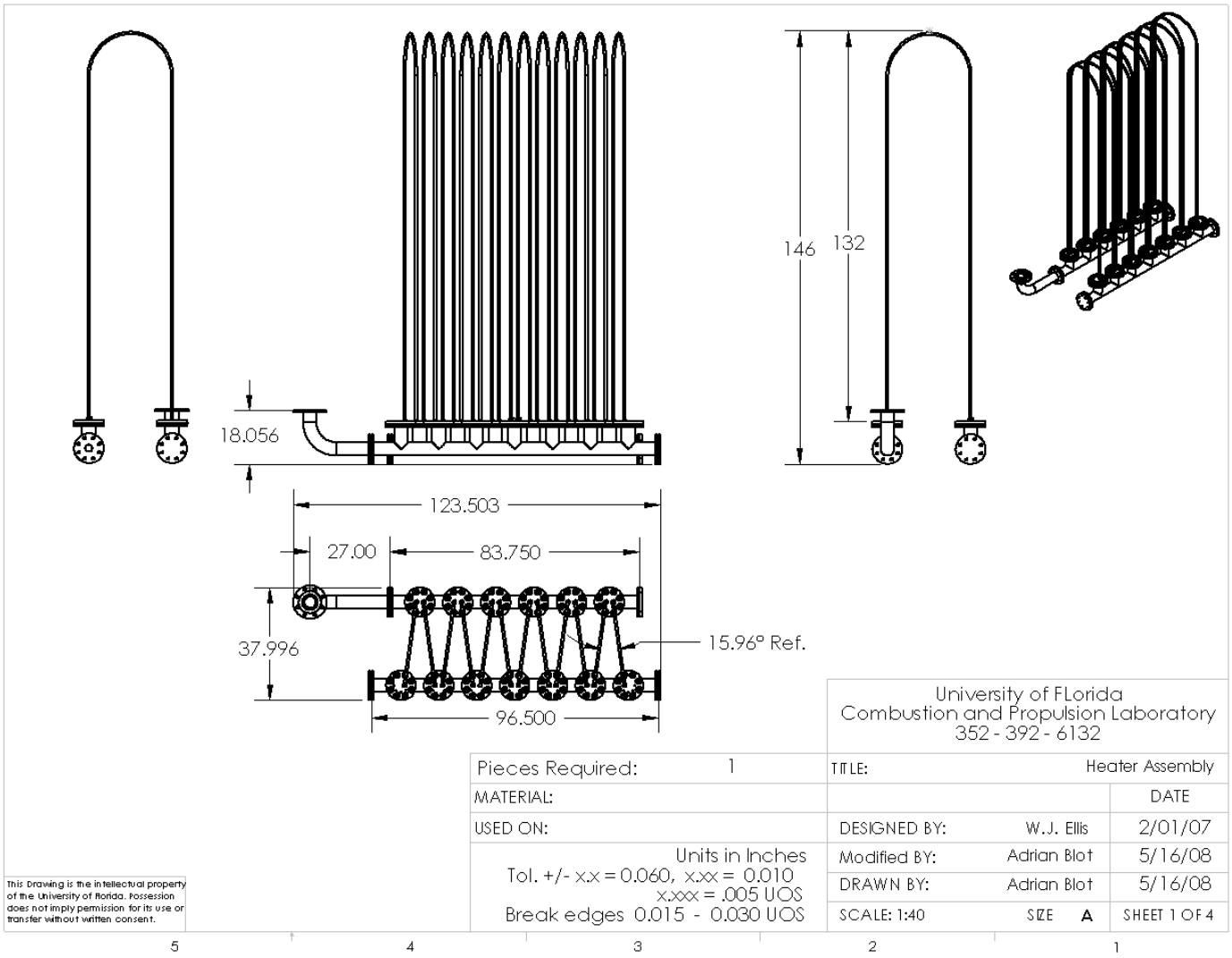

Figure A-1. Non-vitiated heater layout

ITEM NO.	PART NUMBER	QTY.
1	Cold Collector	1
2	Collector Branch	13
3	Collector Flange	18
4	Collector Branch Flange Gasket	13
5	Cold Collector Single Tube Flange Entrance	1
6	Cold Collector Double Tube Flange	5
7	Cold Collector Single Tube Flange Exit	1
8	Cold Collector Supply Flange	1
9	Collector Flange End Cap	2
10	Hot Collector	1
11	Hot Collector Double Tube Flange	6
12	Swagelok SS-1210-6-12W 0.75in	2
13	Tube	12
14	Tube Bushing	22
15	Ceramic Inserts	104
16	Hot Collector Discharge Pipe	1
17	Hot Collector Discharge Elbow	1
18	Hot Collector Discharge Nipple	1
19	Discharge Exit Flange	1

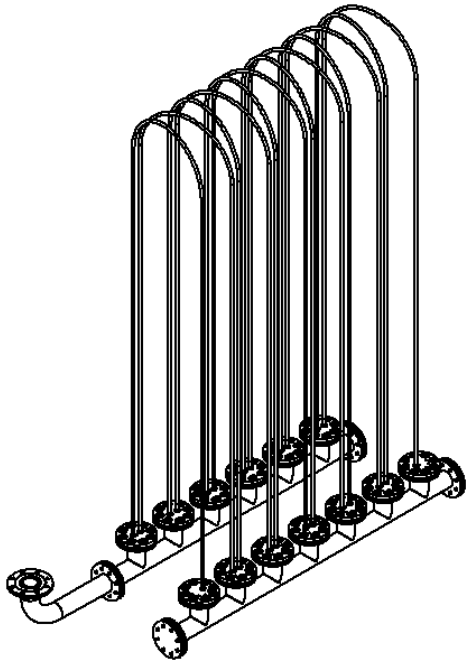

BOM FOR COMPLETE LIST AND QUANTITY OF PARTS

University of FLorida
Combustion and Propulsion Laboratory
352 - 392 - 6132

Pieces Required:	TITLE:		Heater Assembly
MATERIAL:			DATE
USED ON:	DESIGNED BY:	W.J. Ellis	2/01/07
Units in Inches Tol. +/- x.x = 0.060, x.xx = 0.010 x.xxx = .005 UOS Break edges 0.015 - 0.030 UOS	Modified BY:	Adrian Blot	5/16/08
	DRAWN BY:	Adrian Blot	5/16/08
	SCALE: 1:32	SIZE A	SHEET 2 OF 4

5 4 3 2 1

Figure A-2. Non-vitiated heater bill of materials of all parts

ITEM NO.	PART NUMBER	QTY.
1	Weldment, Cold Collector	1
2	Collector Branch Flange Gasket	13
3	Cold Collector Single Tube Flange Entrance	1
4	Cold Collector Double Tube Flange	5
5	Cold Collector Single Tube Flange Exit	1
6	Cold Collector Supply Flange	1
7	Collector Flange End Cap	2
8	Weldment, Hot Collector	1
9	Hot Collector Double Tube Flange	6
10	Swagelok SS-1210-6-12W 0.75in	2
11	Weldment, Tube	10
12	Weldment, Tube V2	2
13	Ceramic Inserts	104
14	Weldment, Hot Collector Discharge Pipe	1

BOM For Assembly

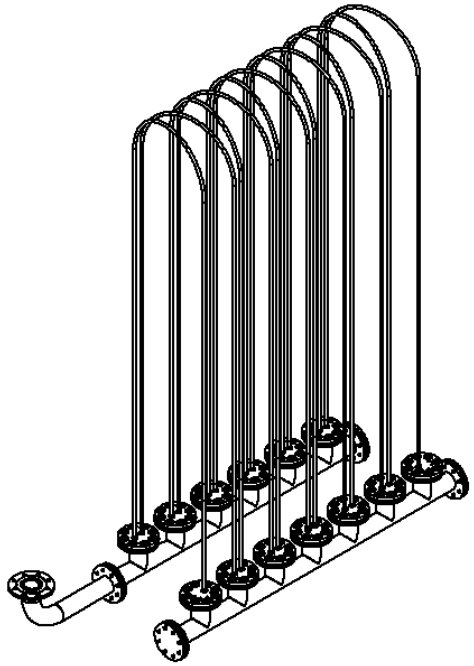

University of FLorida
Combustion and Propulsion Laboratory
352 - 392 - 6132

Pieces Required:	TITLE:		Heater Assembly
MATERIAL:			DATE
USED ON:	DESIGNED BY:	W.J. Ellis	2/01/07
Units in Inches Tol. +/- x.x = 0.060, x.xx = 0.010 x.xxx = .005 UOS Break edges 0.015 - 0.030 UOS	Modified BY:	Adrian Blot	5/16/08
	DRAWN BY:	Adrian Blot	5/16/08
	SCALE: 1:32	SIZE A	SHEET 3 OF 4

5 4 3 2 1

Figure A-3. Non-vitiated heater bill of materials for assembly

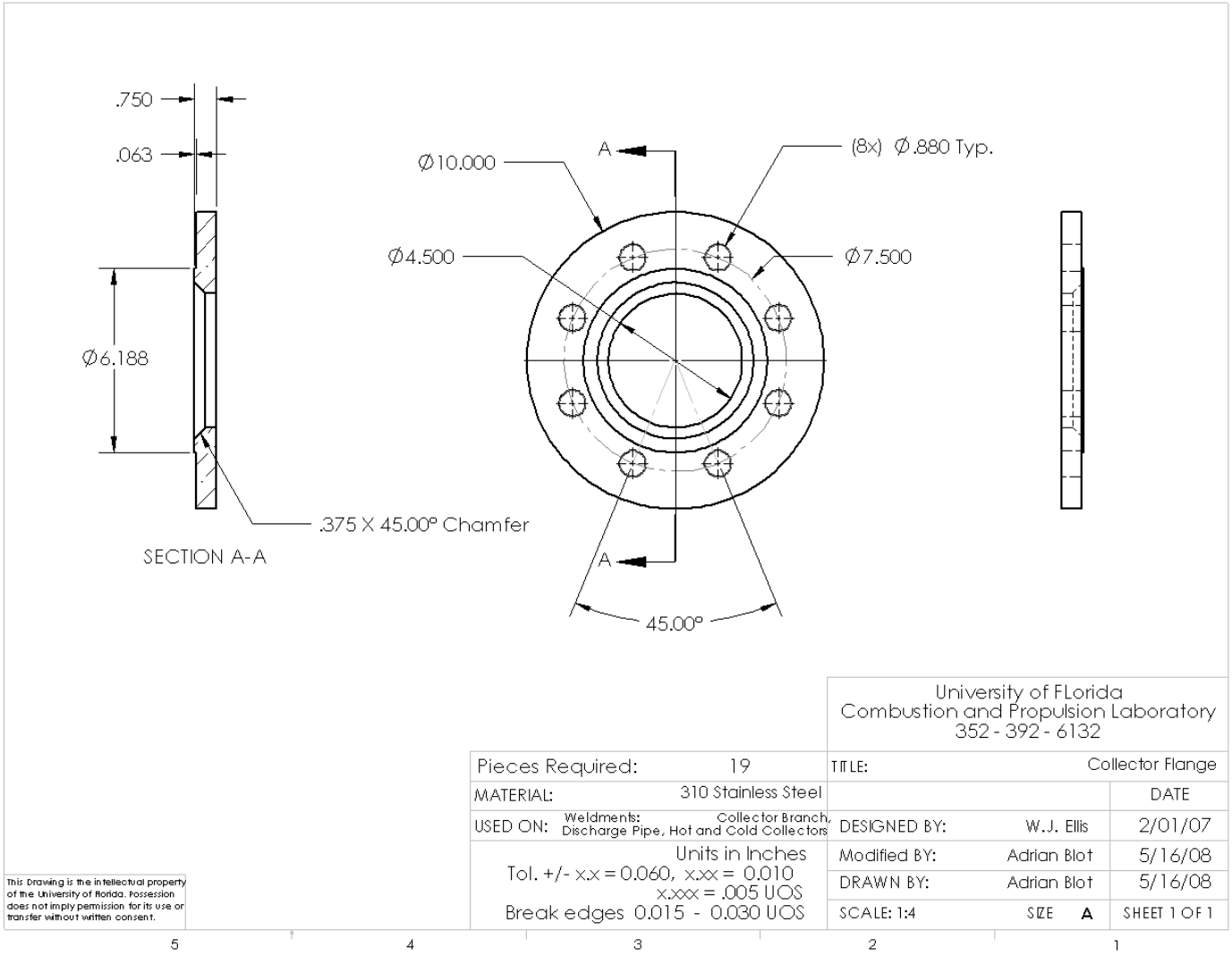

Figure A-4. Collector flange mechanical drawing

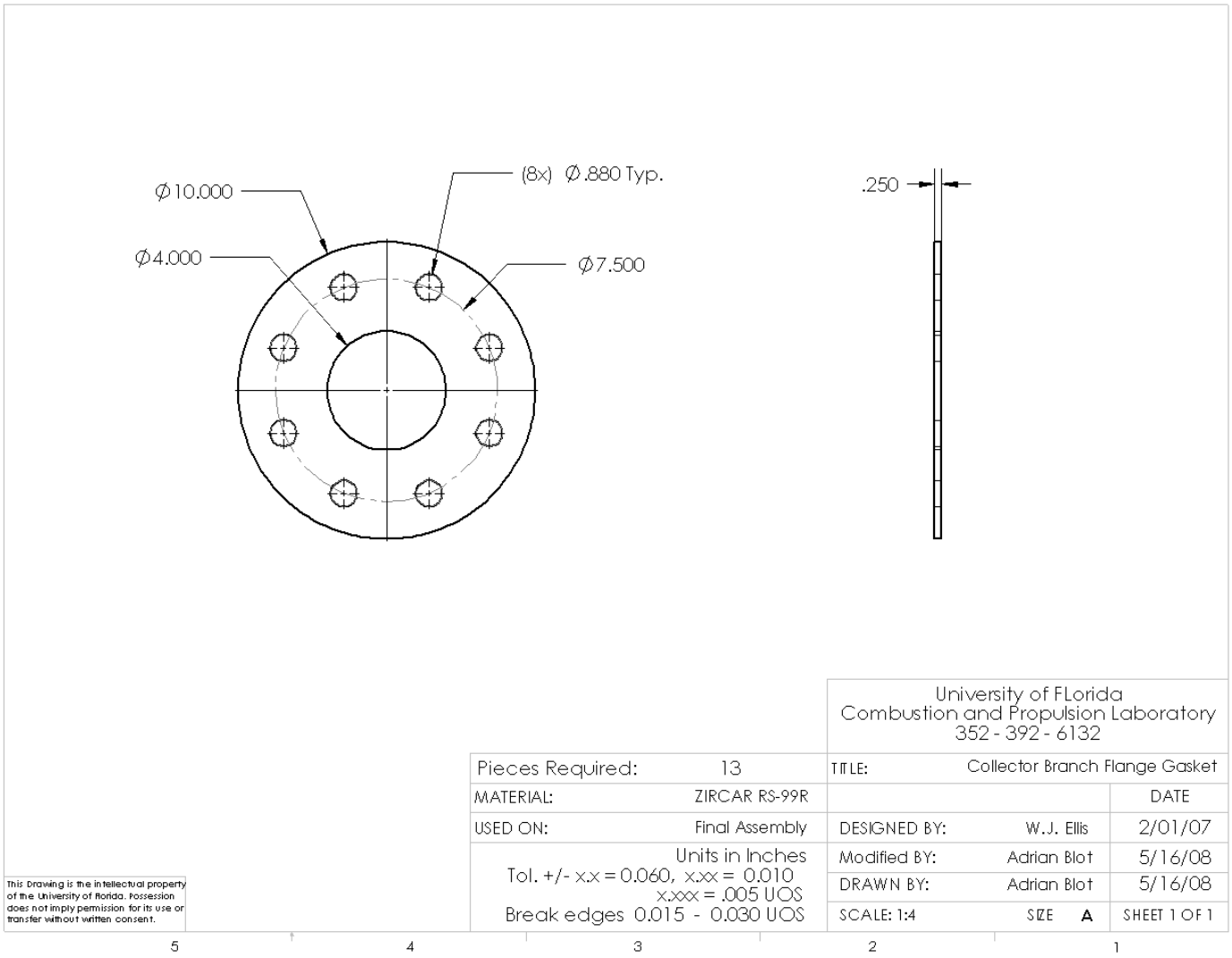

Figure A-5. Collector branch flange gasket mechanical drawing

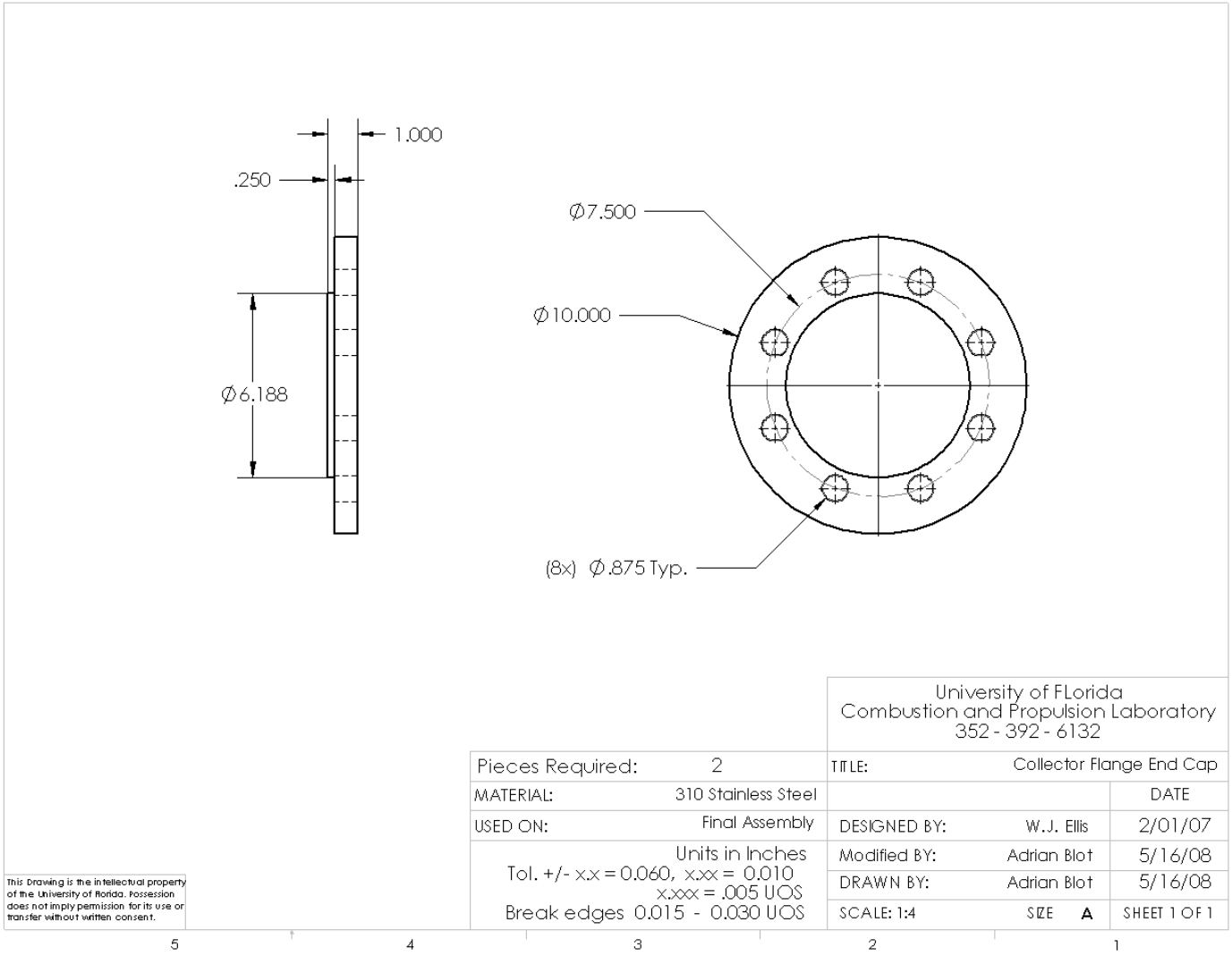

Figure A-6. Collector flange end cap mechanical drawing

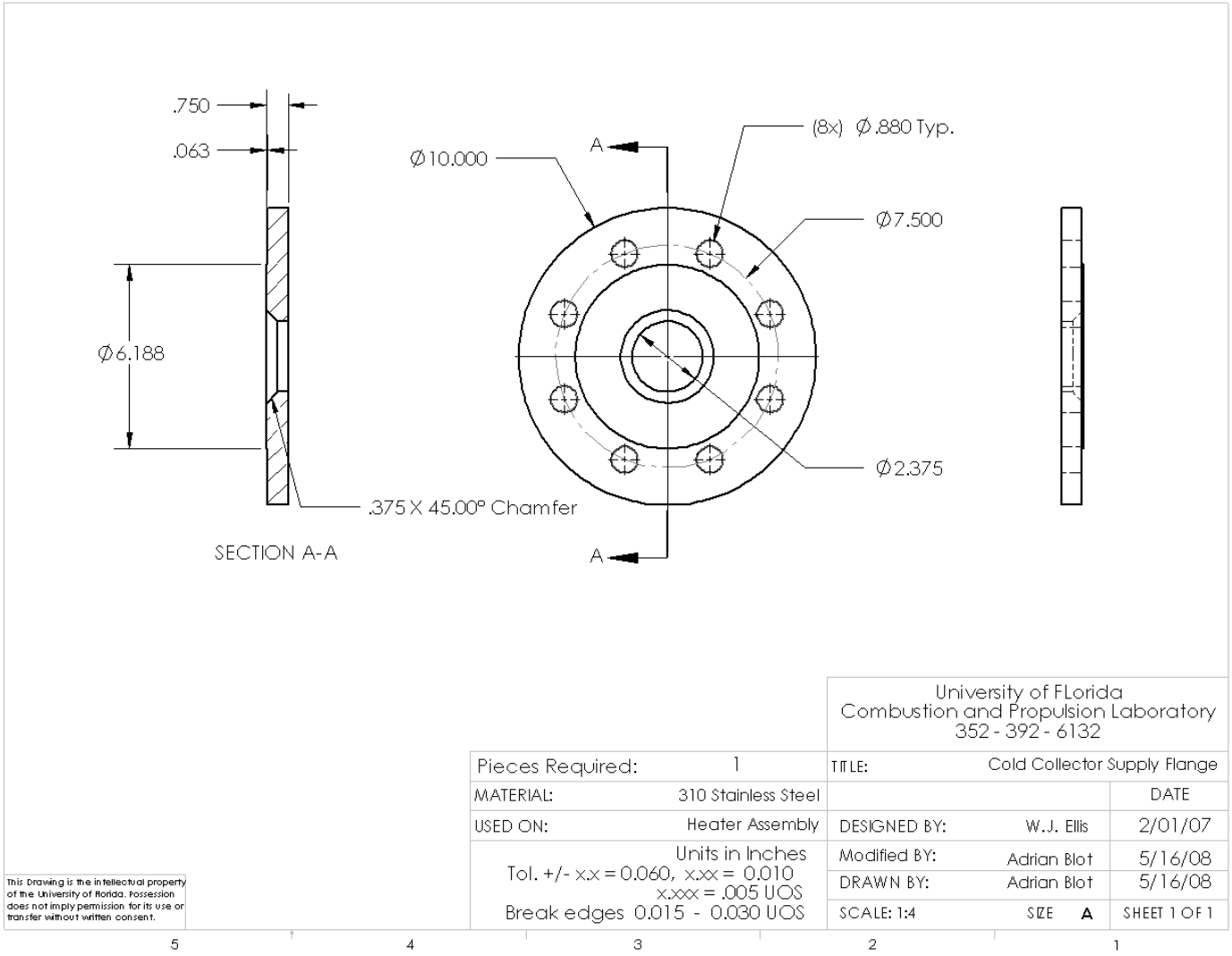

Figure A-7. Cold Collector supply flange mechanical drawing

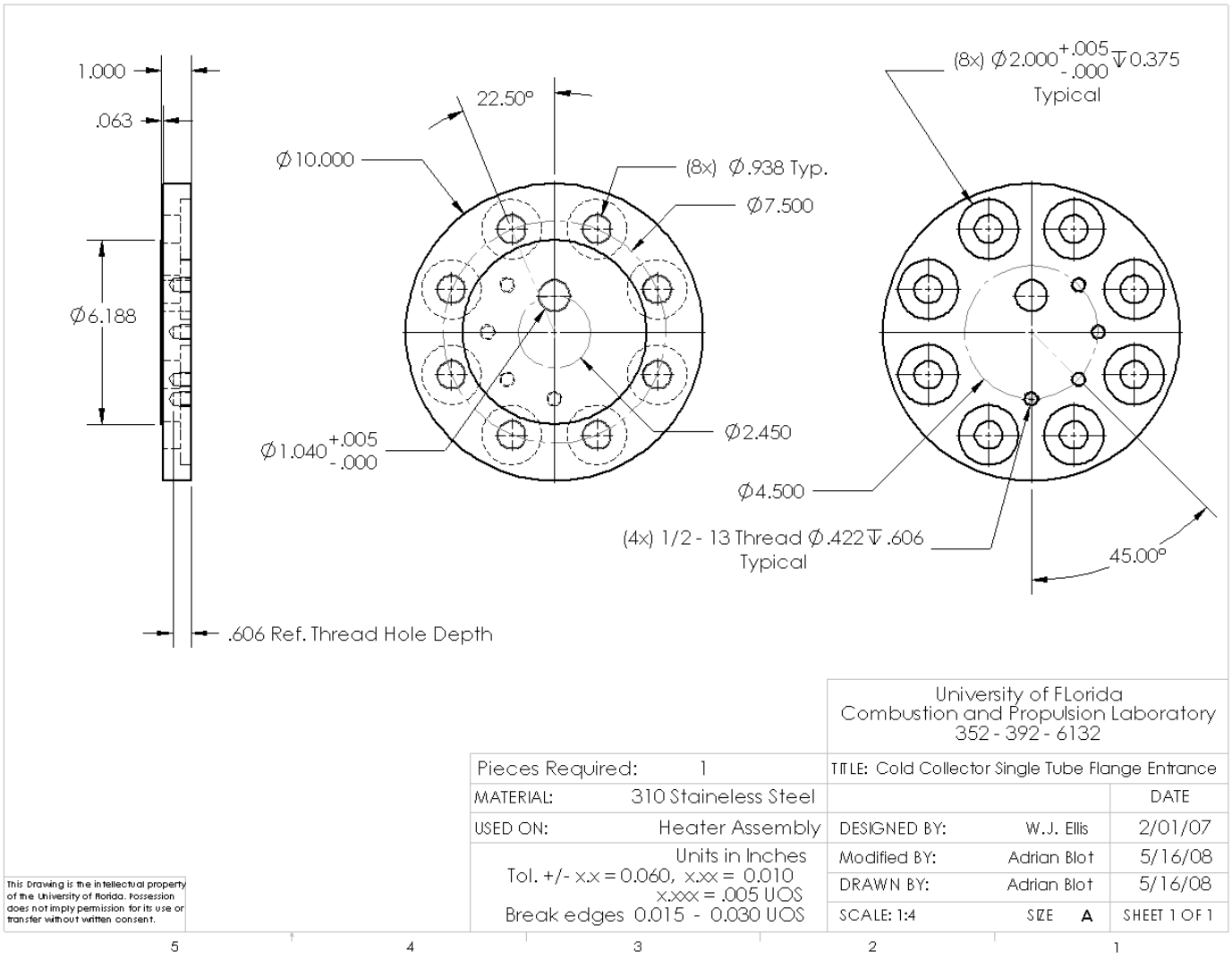

Figure A-8. Cold collector single tube entrance flange mechanical drawing

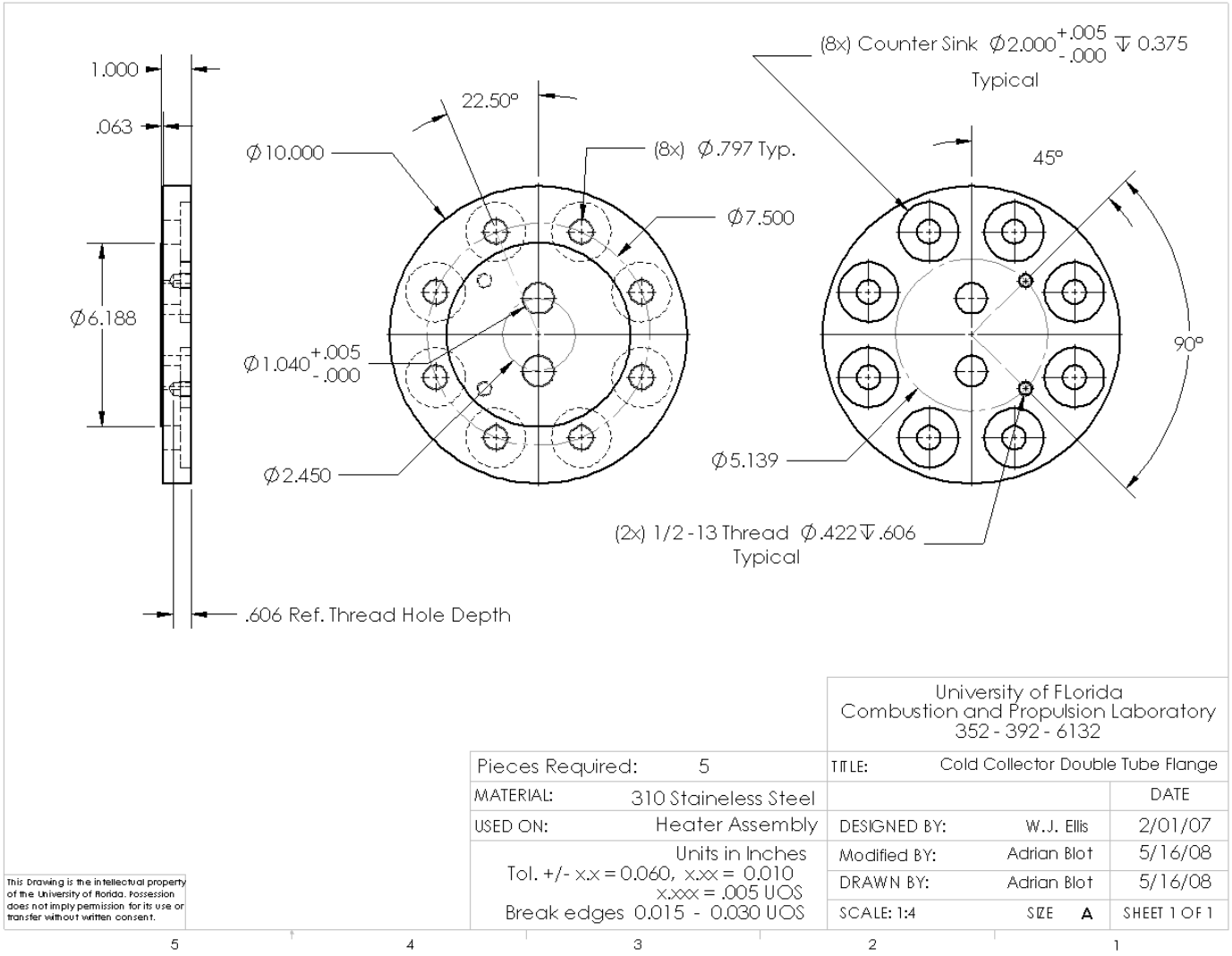

Figure A-9. Cold collector double tube flange mechanical drawing

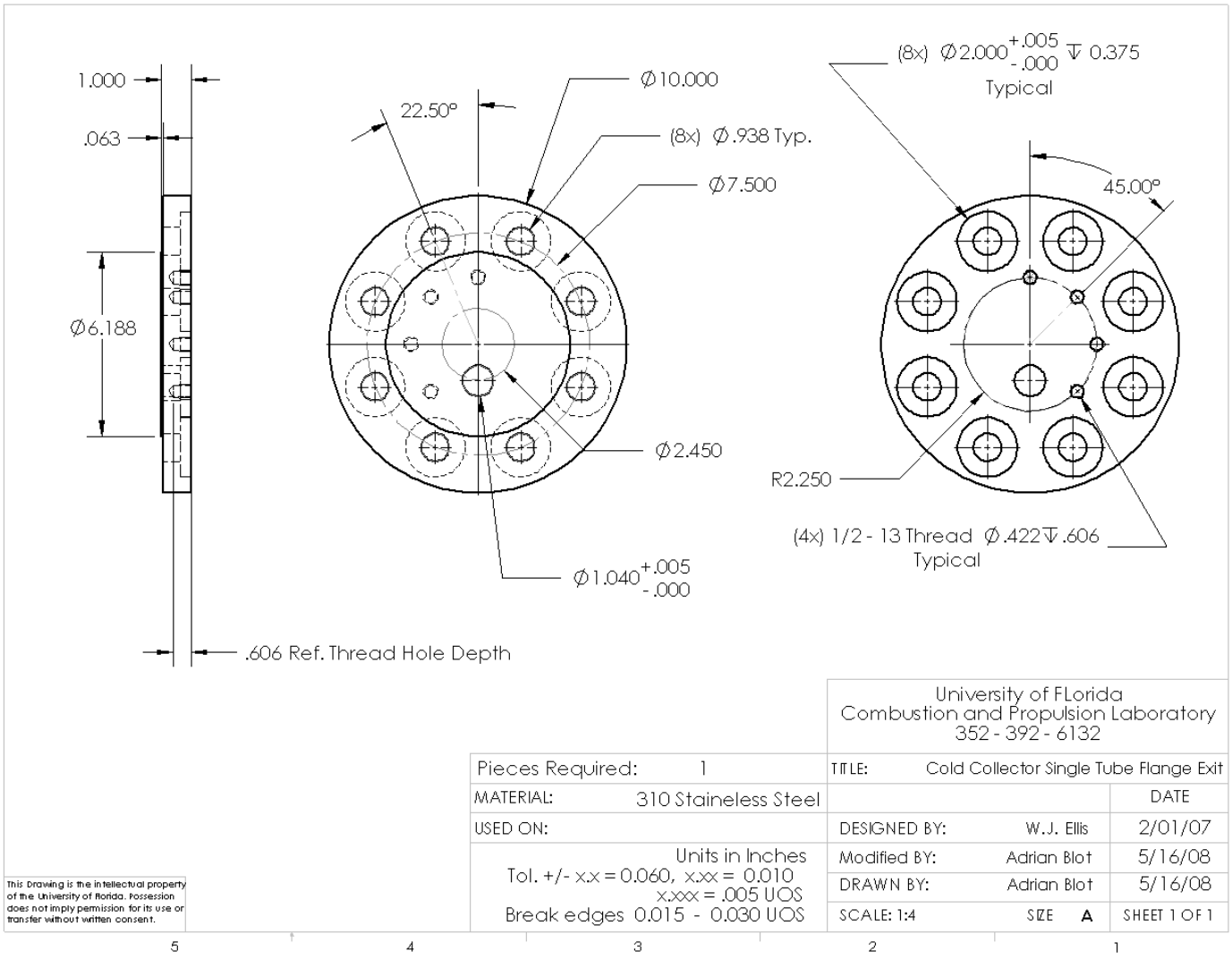

Figure A-10. Cold collector single tube exit flange mechanical drawing

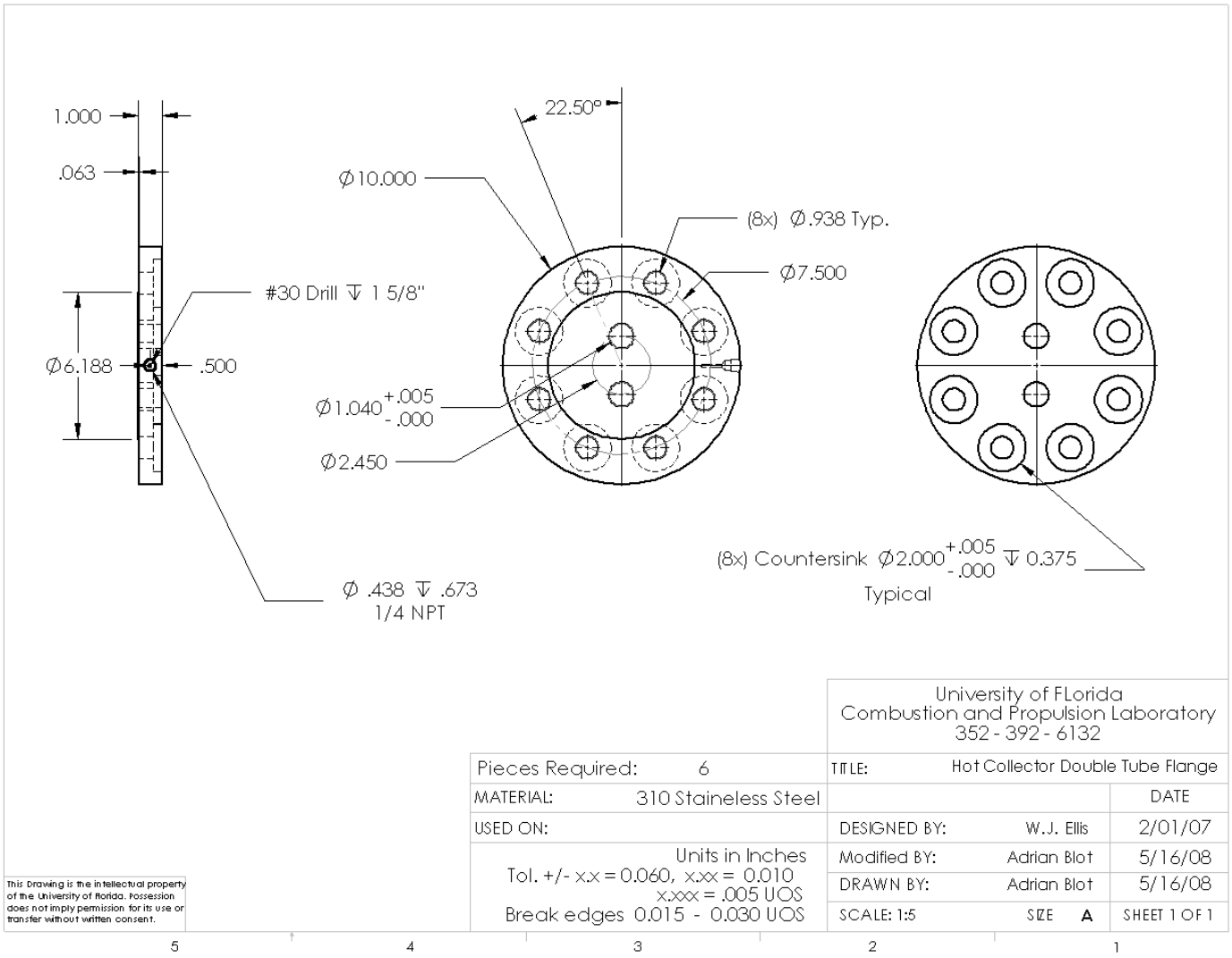

Figure A-11. Hot collector double tube flange mechanical drawing

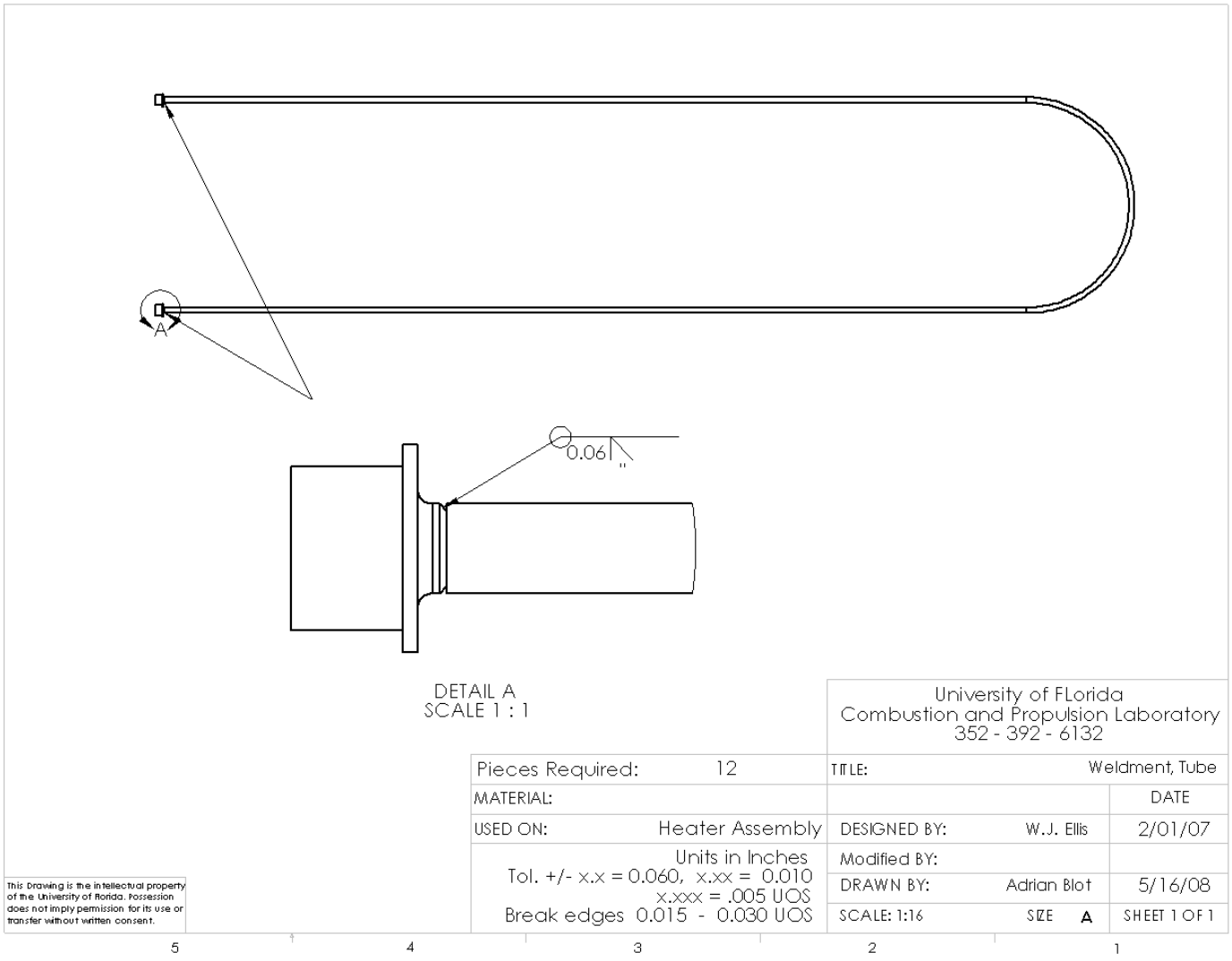

Figure A-12. Tube weldment mechanical drawing

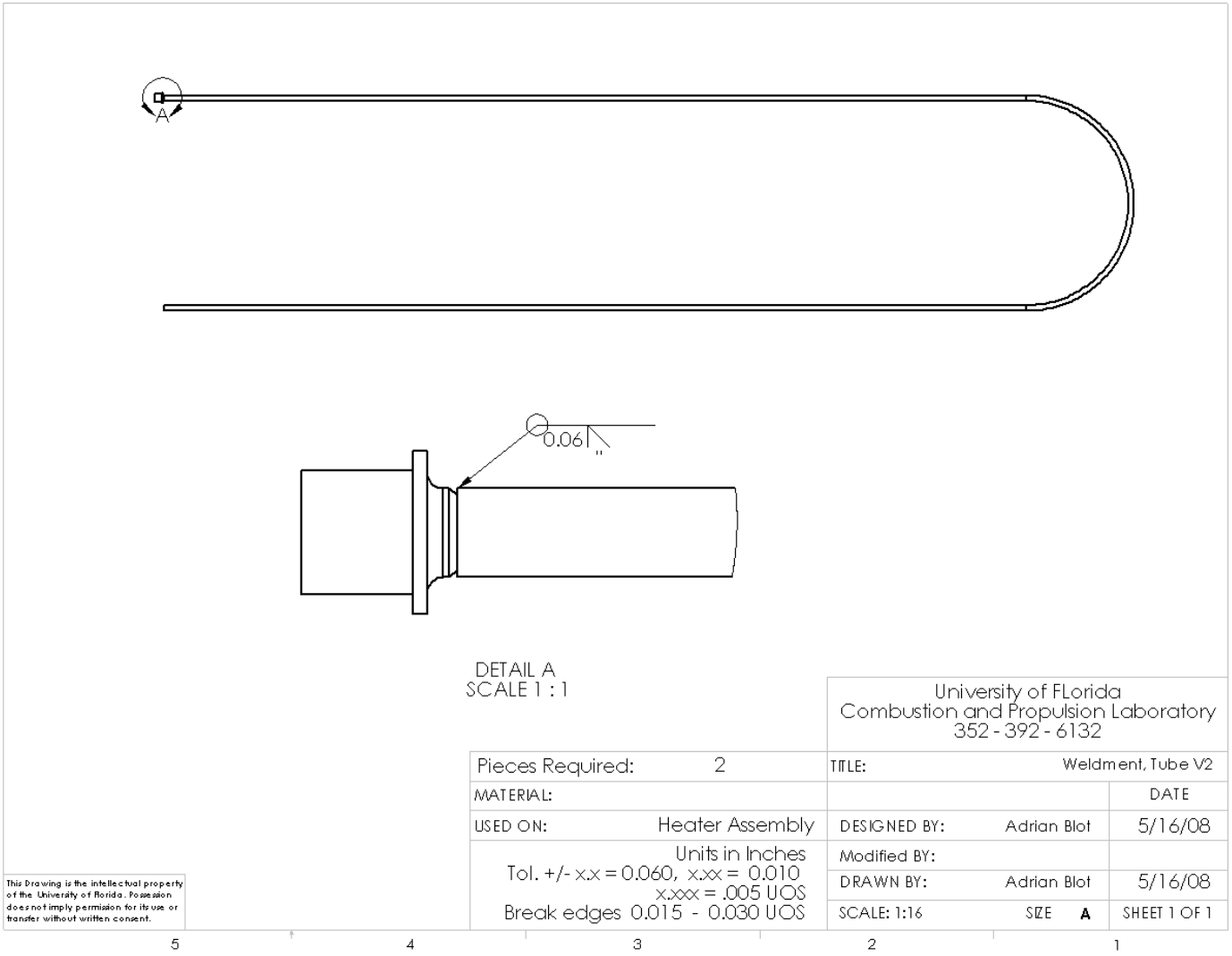

Figure A-13. Disconnect tube weldment mechanical drawing

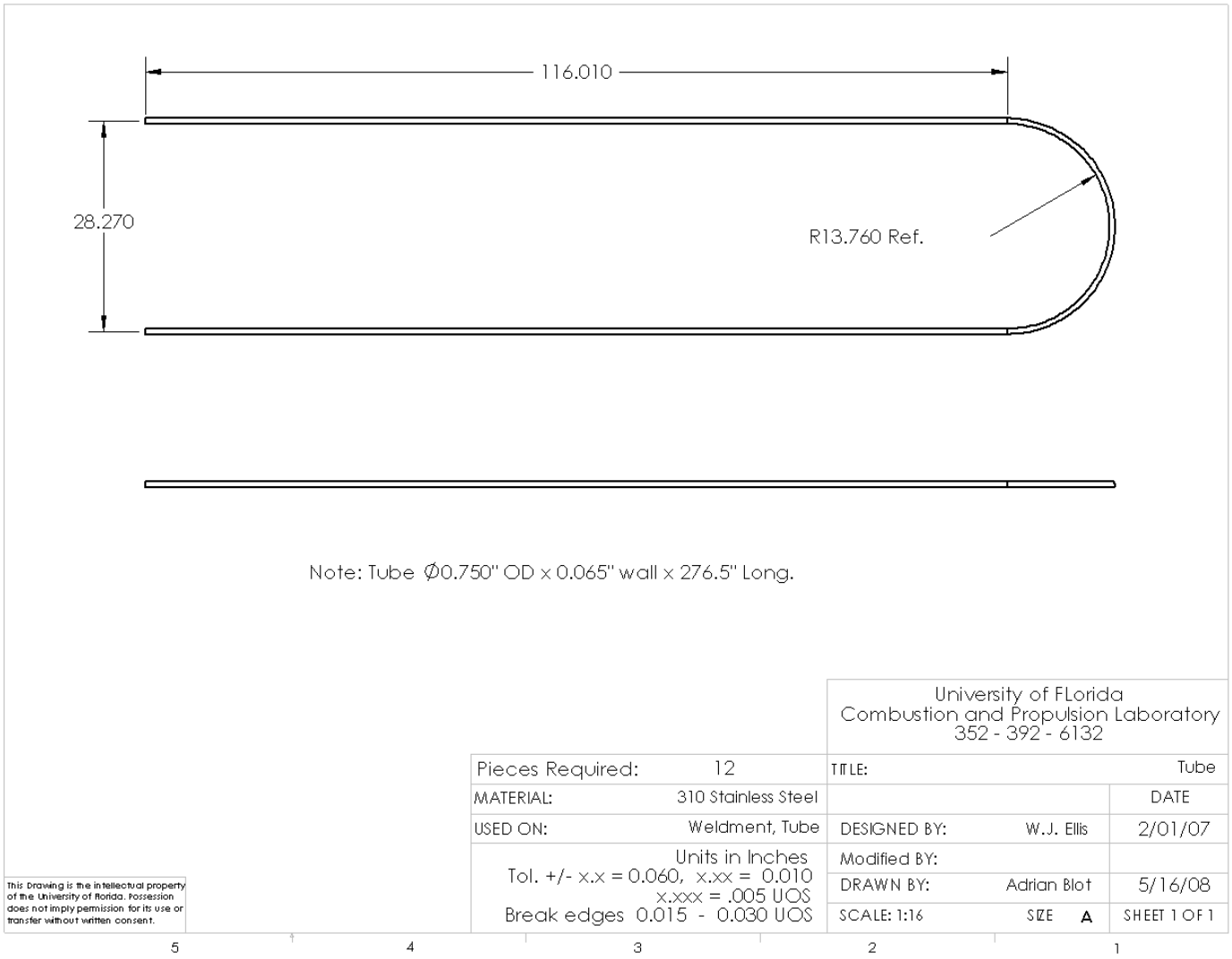

Figure A-14. Tube mechanical drawing

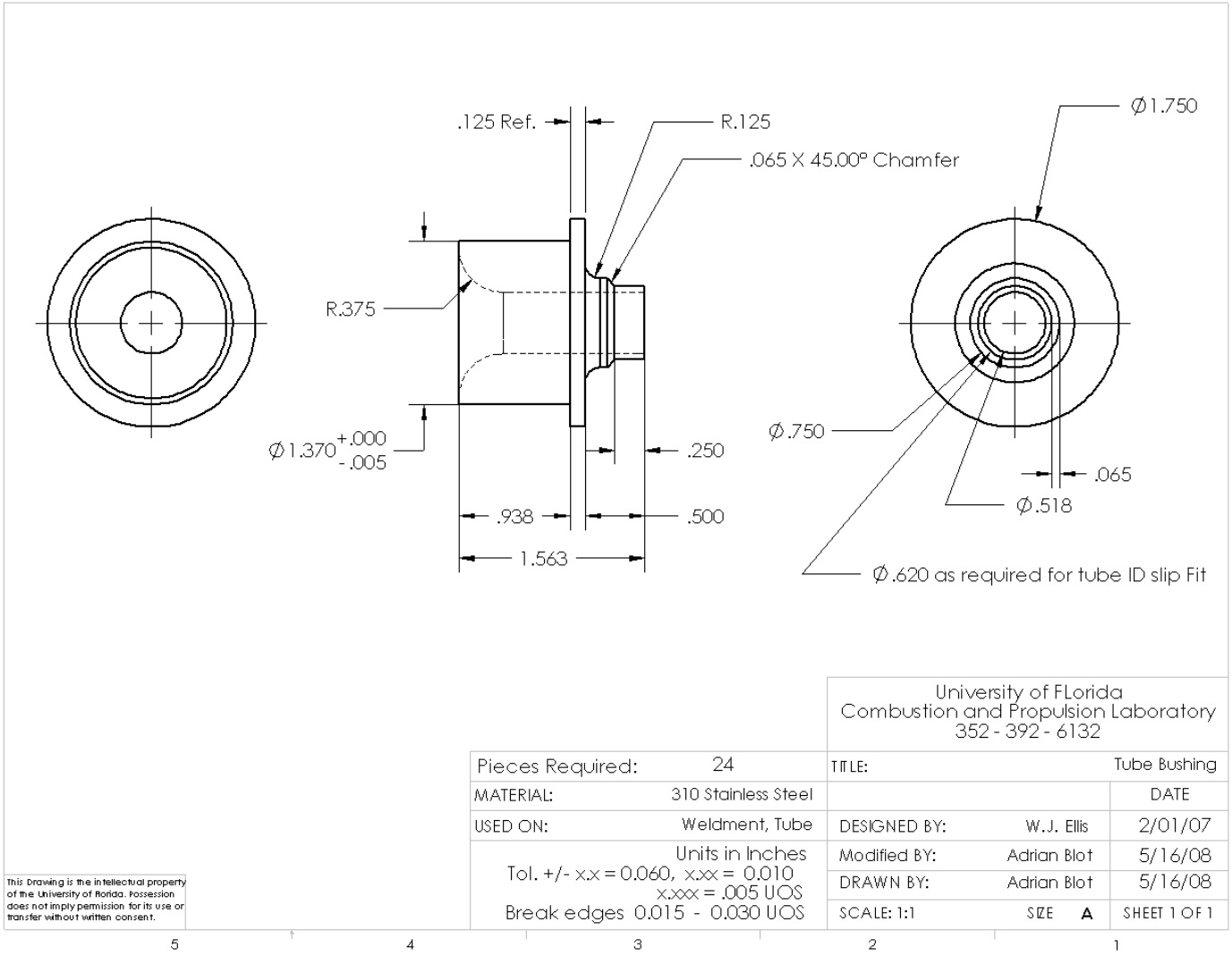

Figure A-15. Tube bushing mechanical drawing

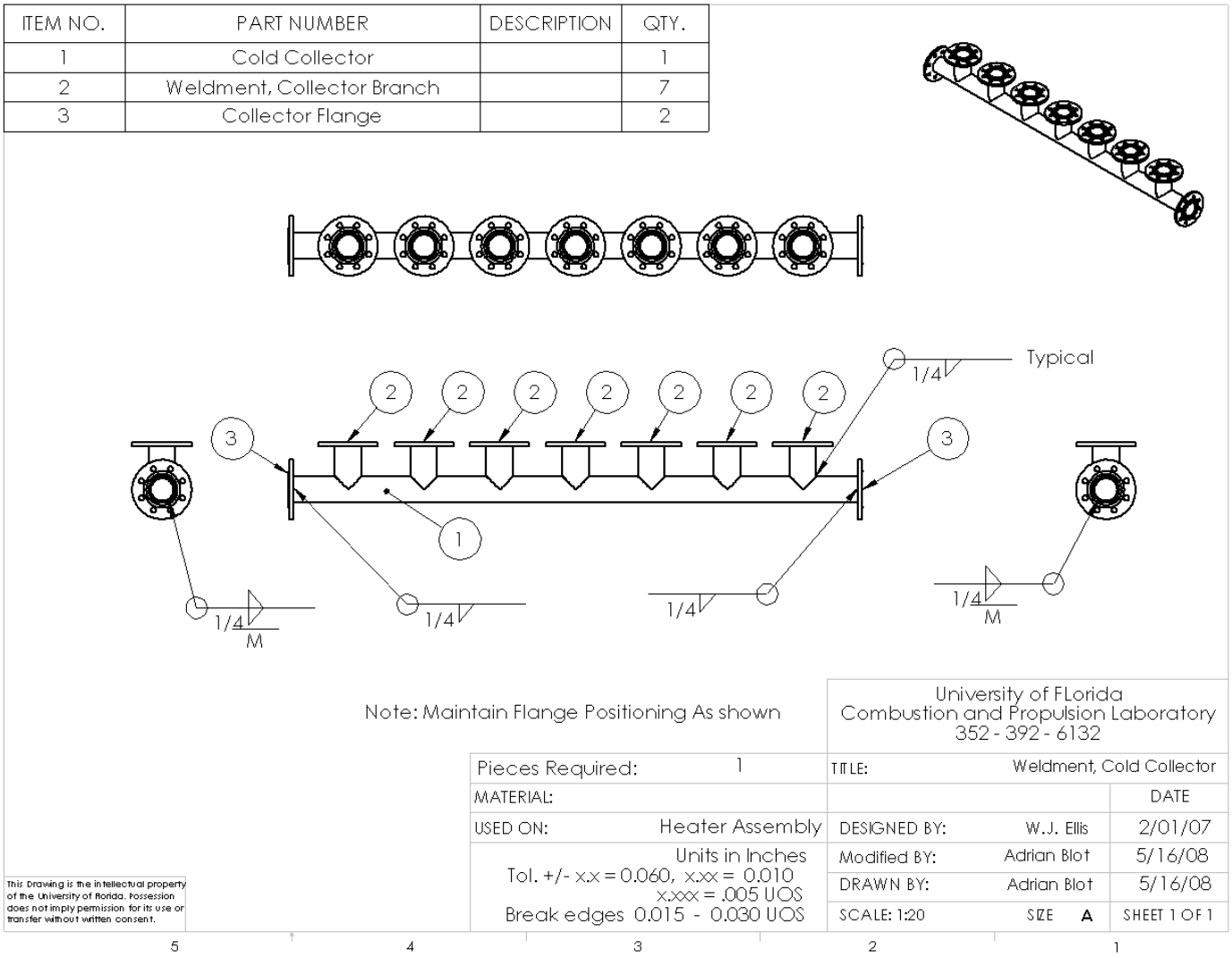

Figure A-16. Cold collector weldment mechanical drawing

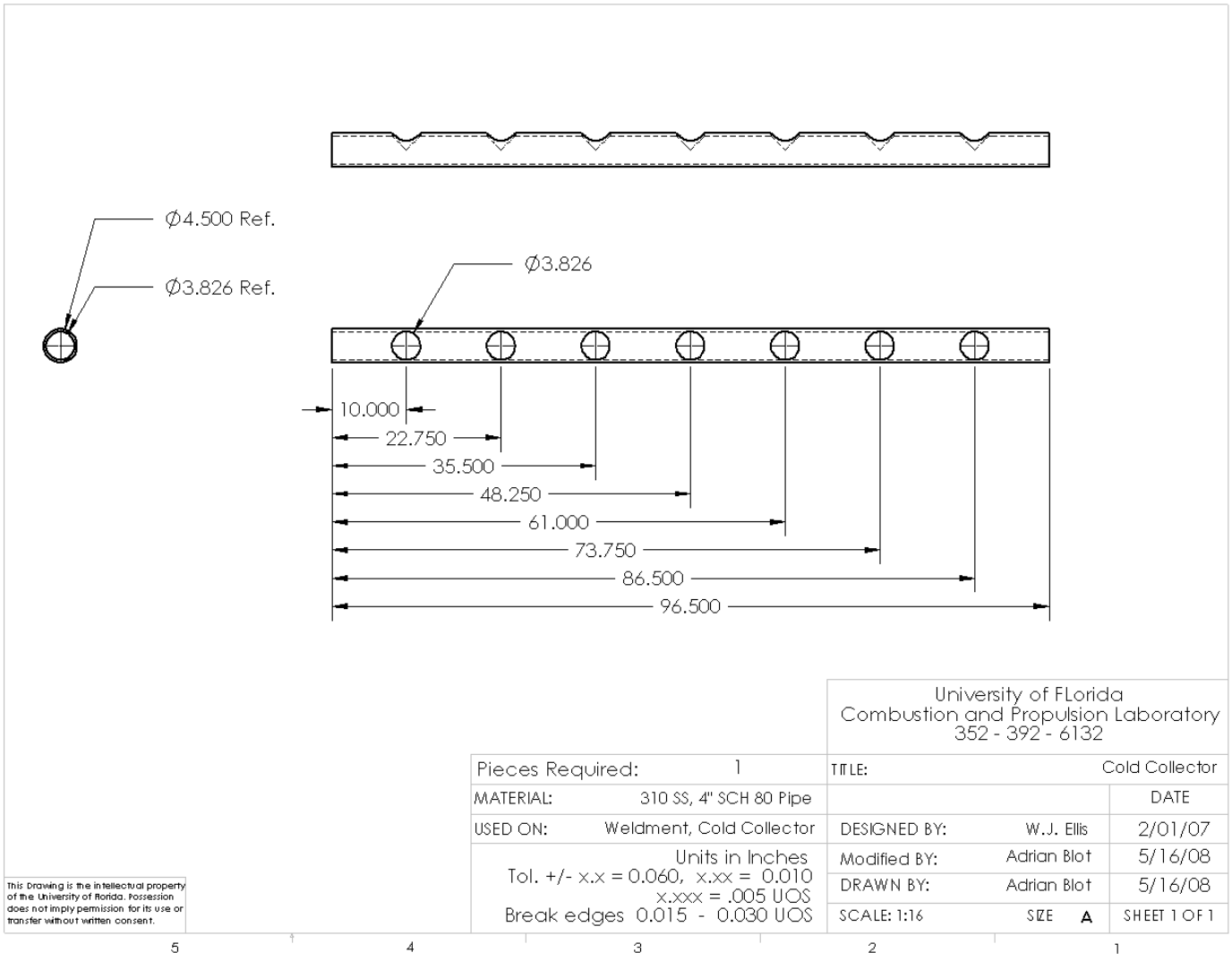

Figure A-17. Cold collector mechanical drawing

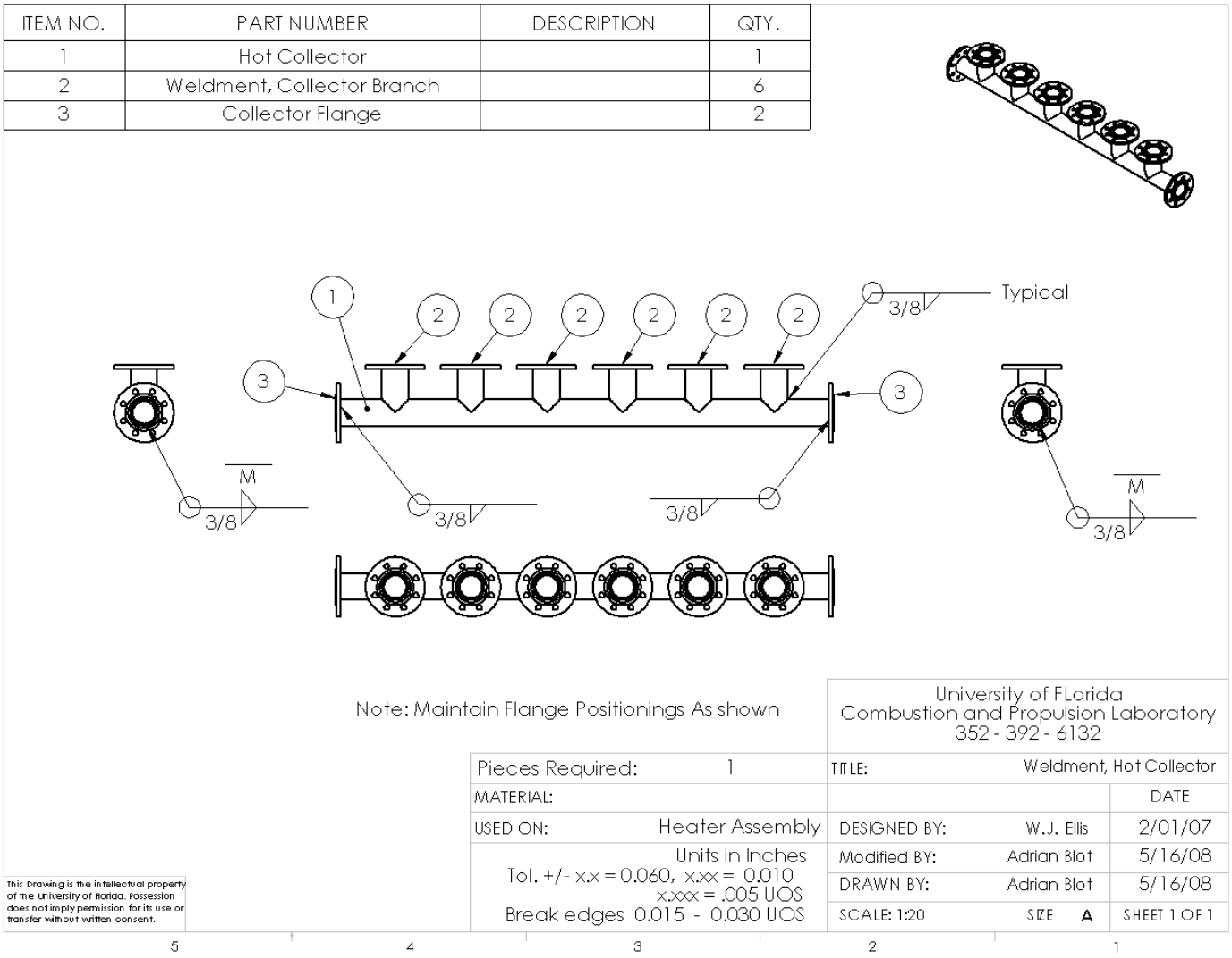

Figure A-18. Hot collector weldment mechanical drawing

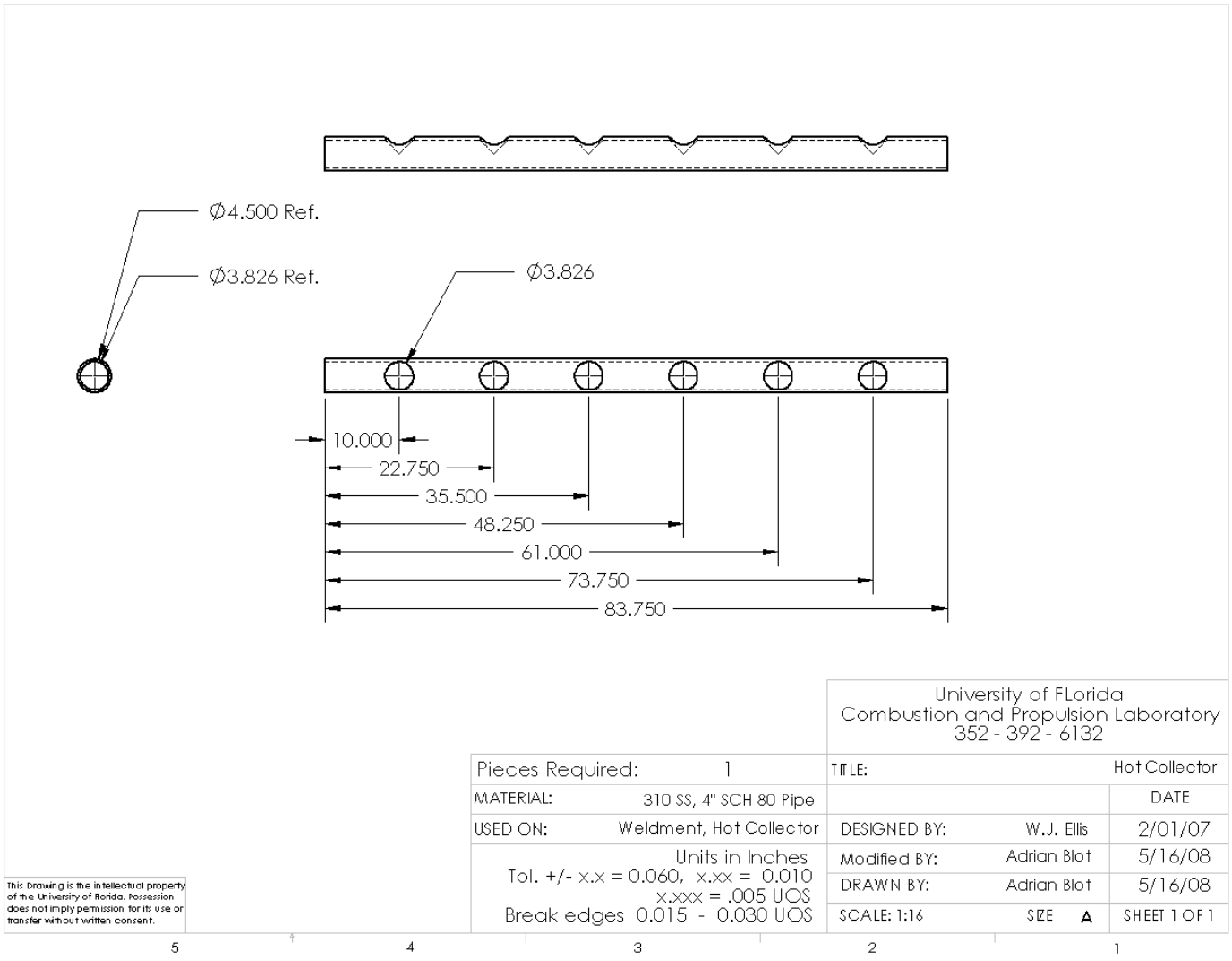

Figure A-19. Hot collector mechanical drawing

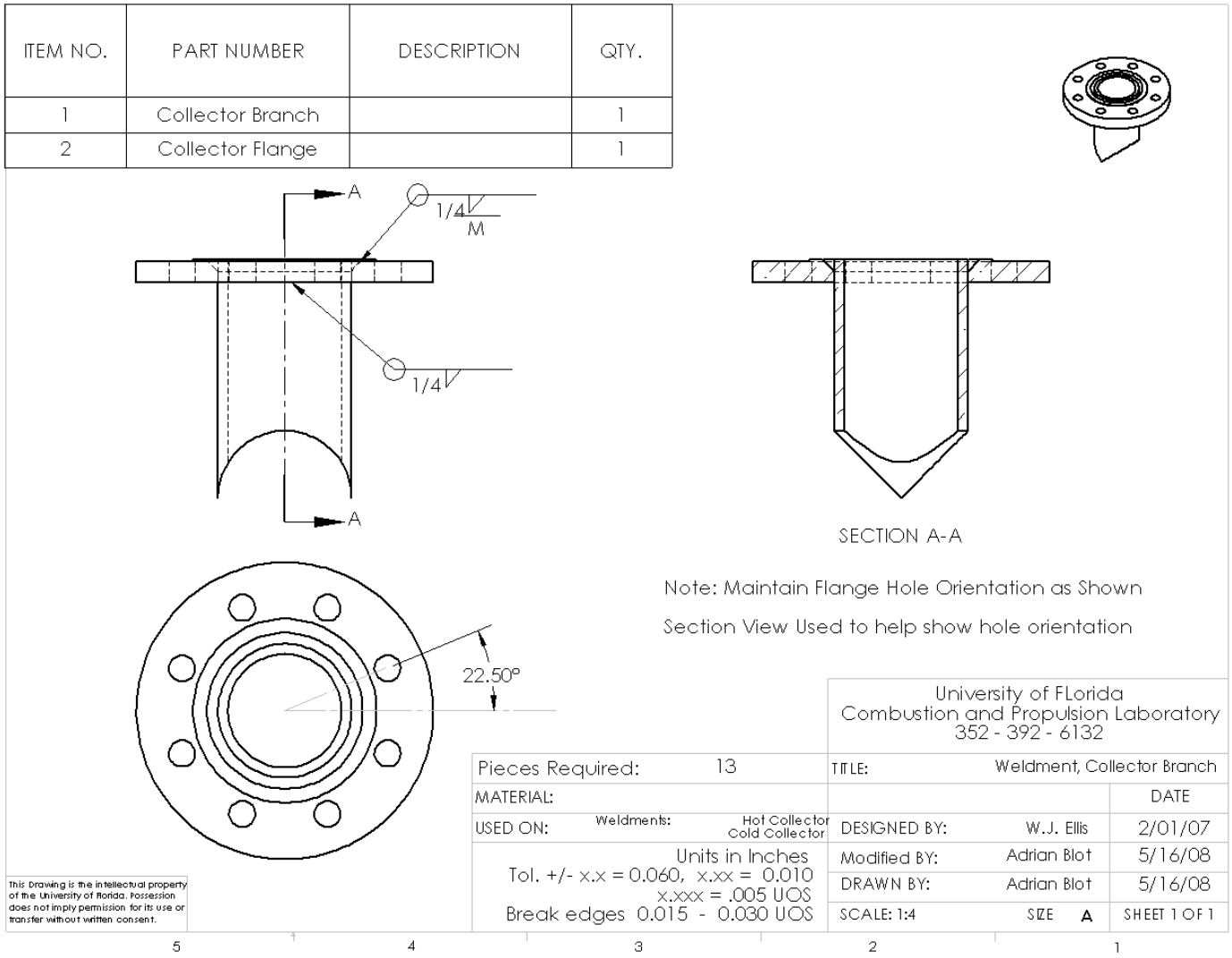

Figure A-20. Collector branch weldment mechanical drawing

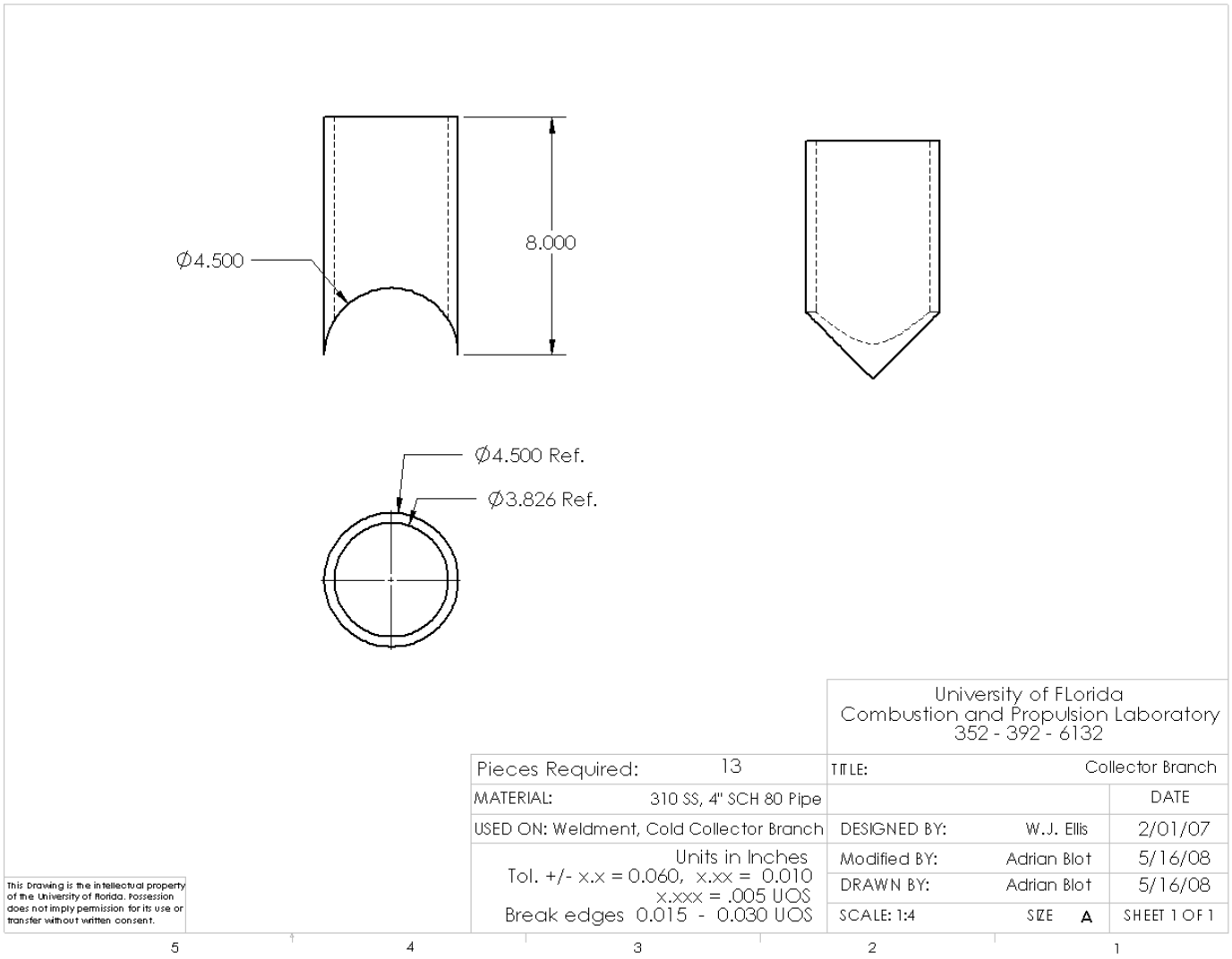

Figure A-21. Collector branch mechanical drawing

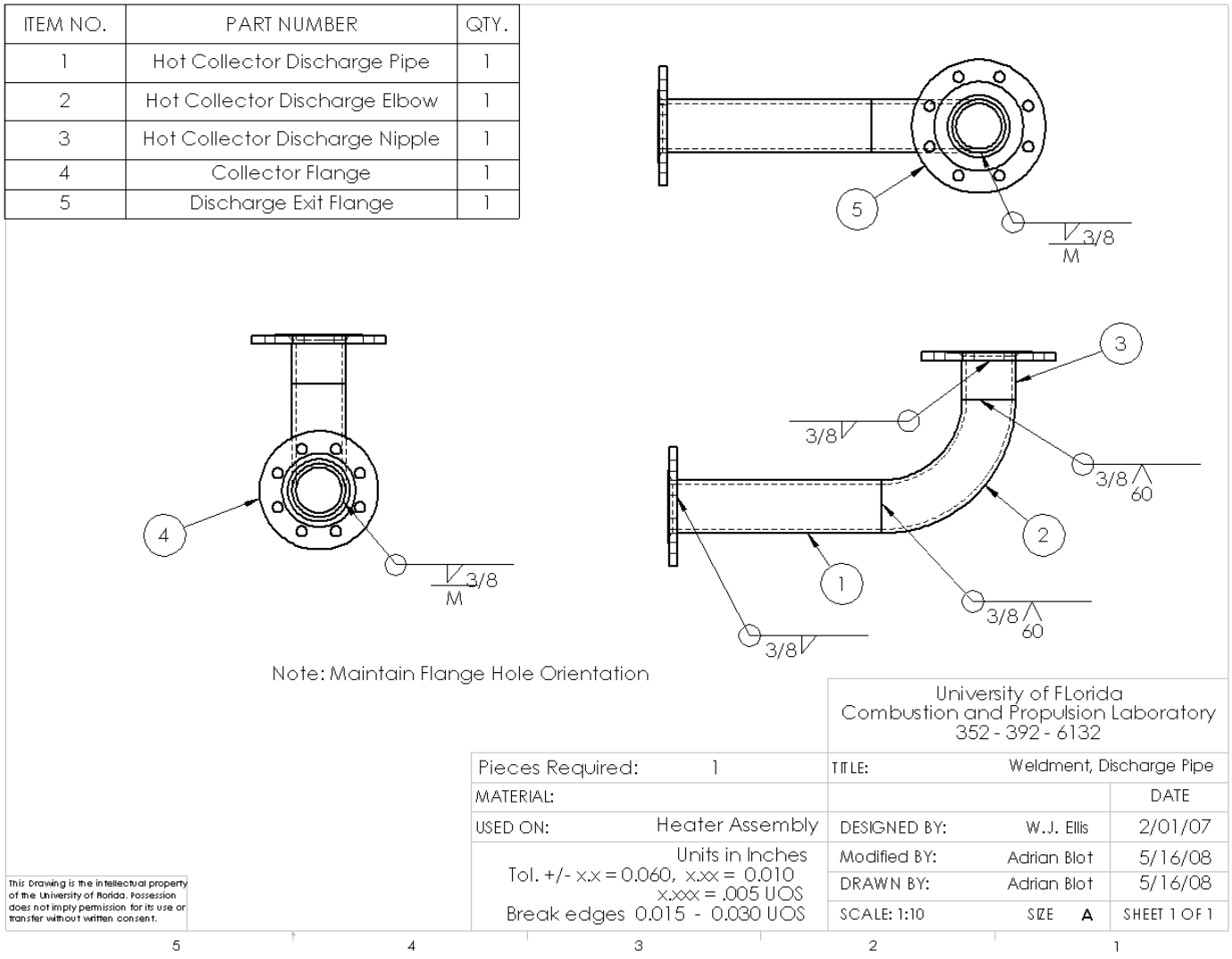

Figure A-22. Discharge pipe weldment mechanical drawing

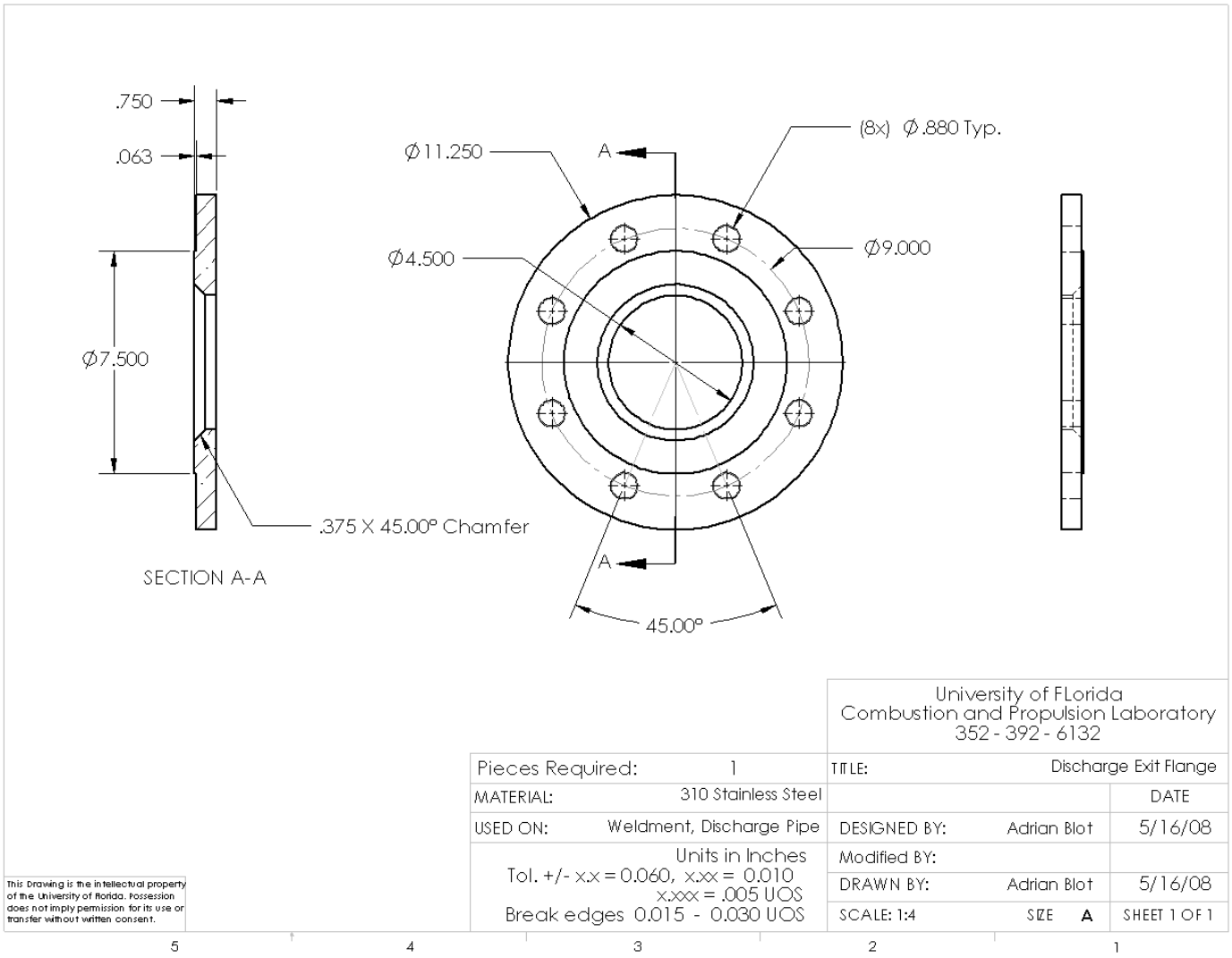

Figure A-23. Discharge exit flange mechanical drawing

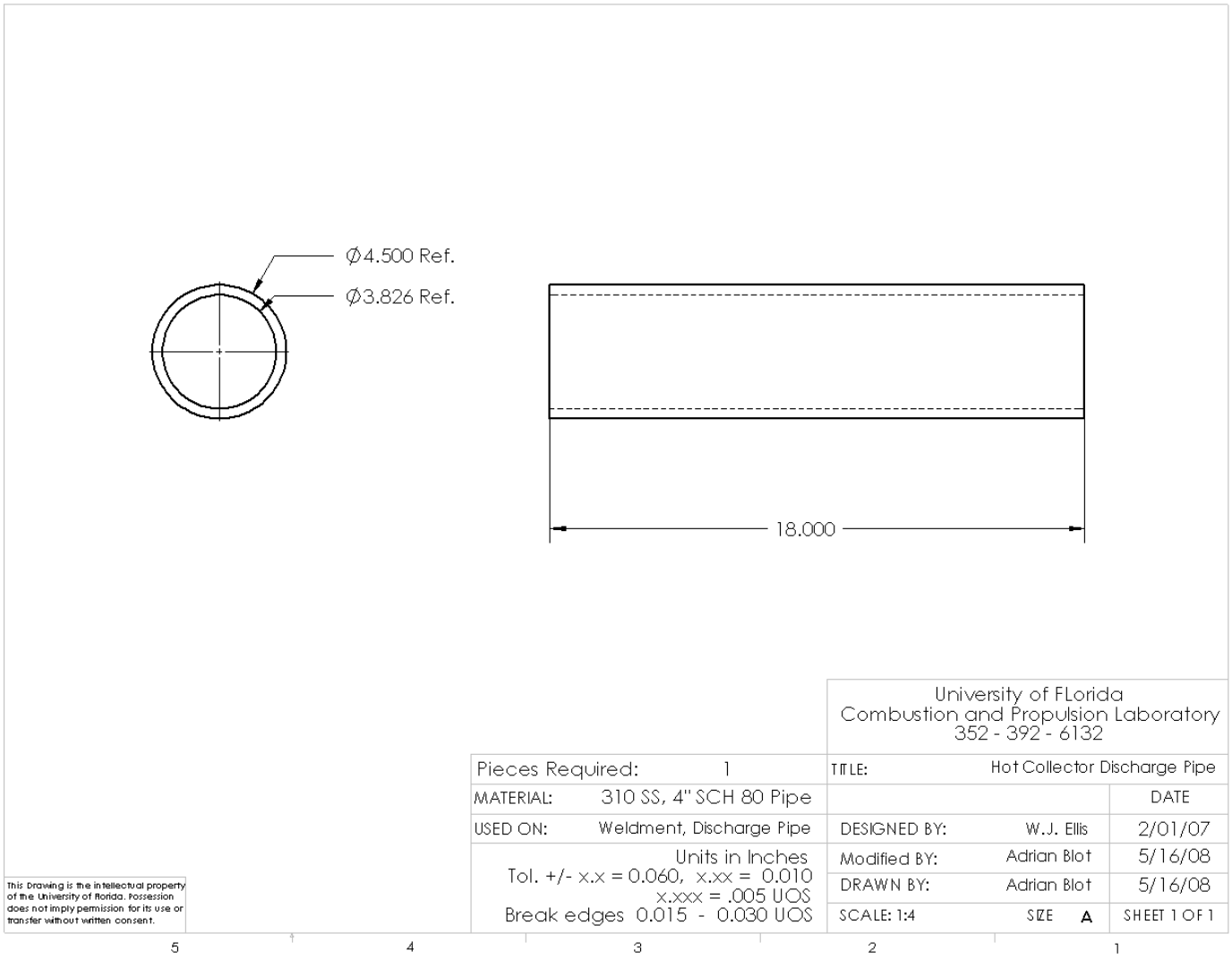

Figure A-24. Hot collector discharge pipe mechanical drawing

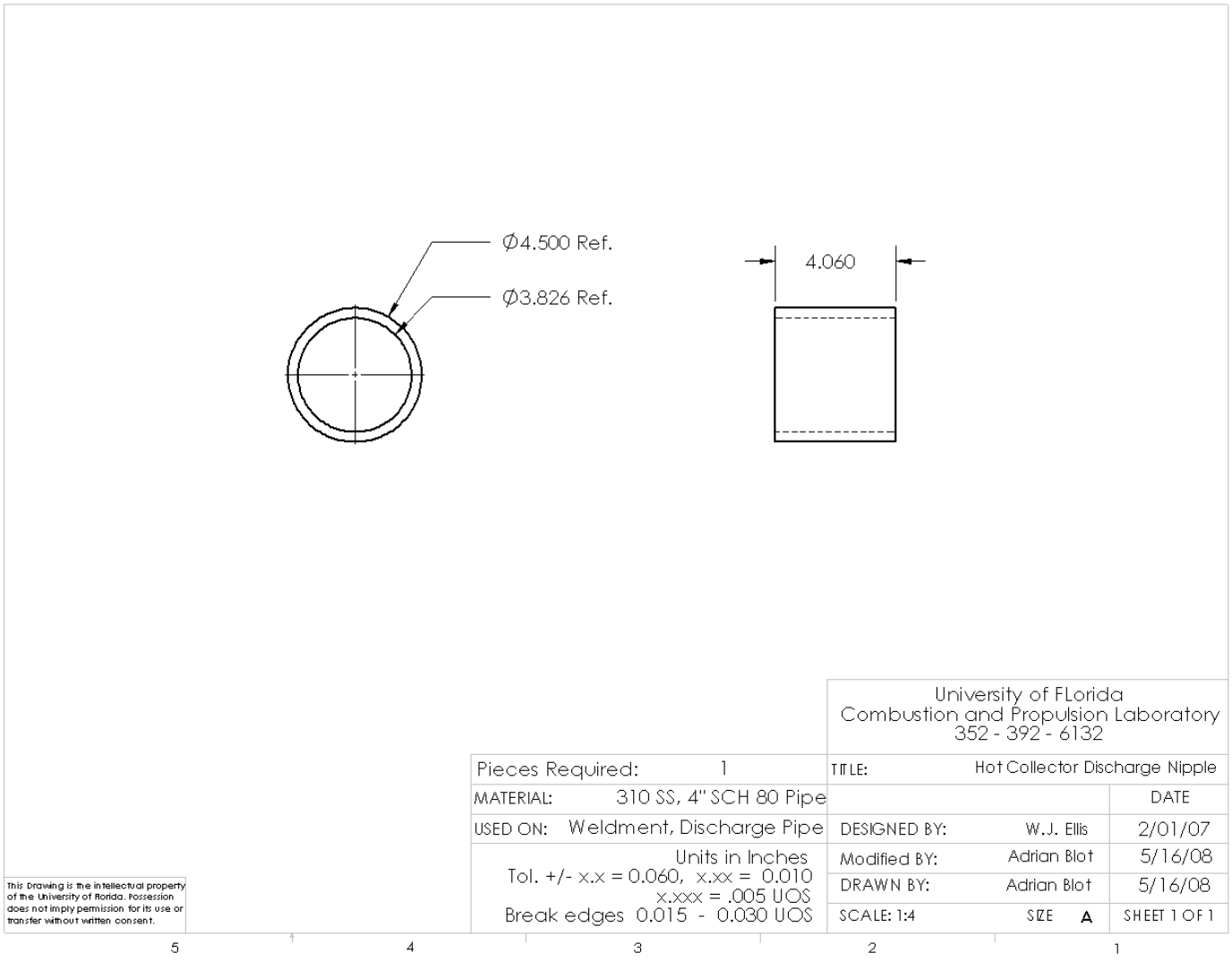

Figure A-25. Hot collector discharge nipple mechanical drawing

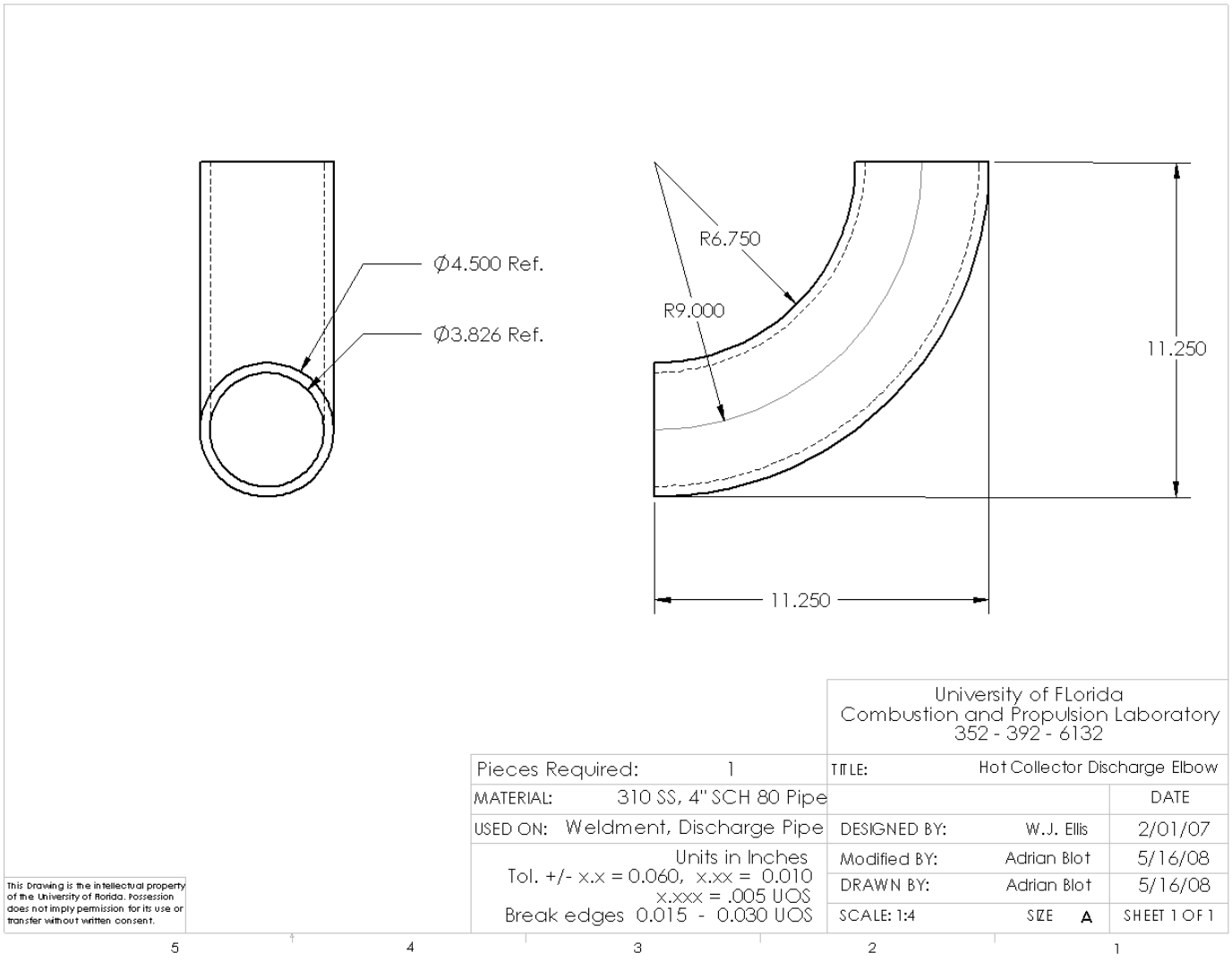

Figure A-26. Hot collector discharge elbow mechanical drawing

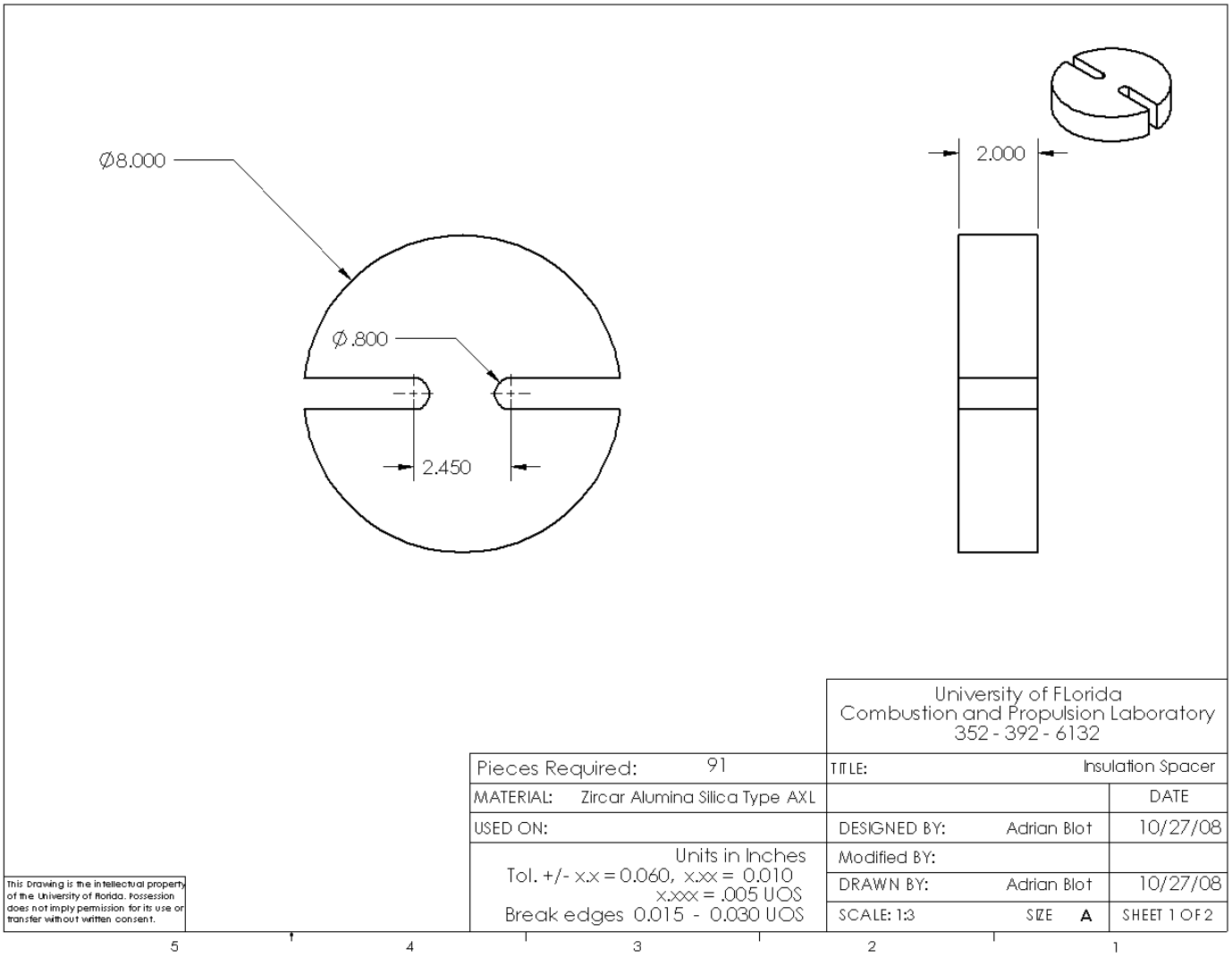

Figure A-27. Insulation spacer mechanical drawing

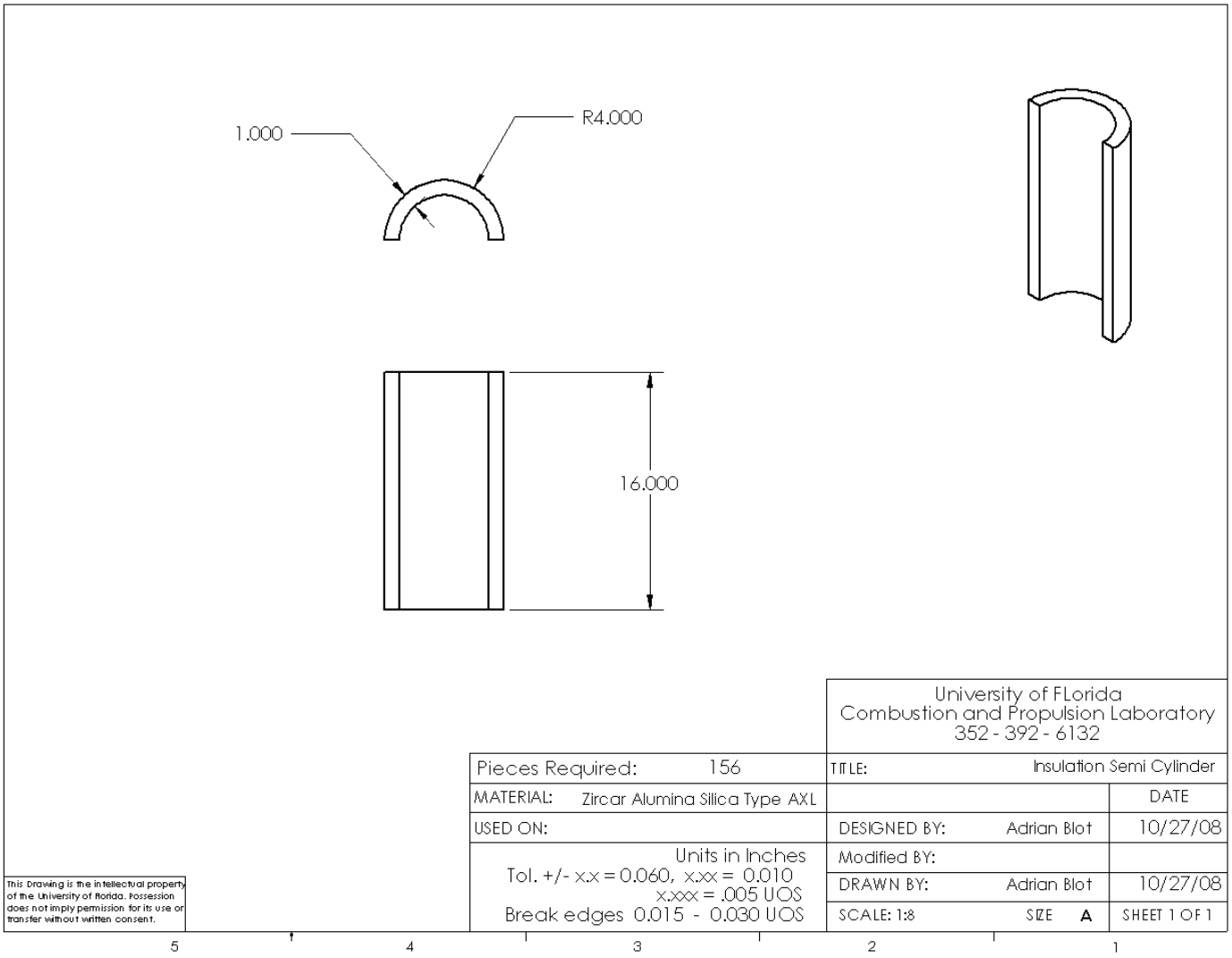

Figure A-28. Semi cylinder insulation mechanical drawing

APPENDIX B
HEATER ENCLOSURE DRAWINGS

ITEM NO.	PART NUMBER	QTY.
1	AngleB<As Machined>	4
2	AngleD<As Machined>	4
3	AngleA	8
4	AngleC	8
5	Top Panel	2
6	Side Panel	4
7	Bottom Side Panel	2
8	Front Panel	8
9	Bottom Front Panel	4

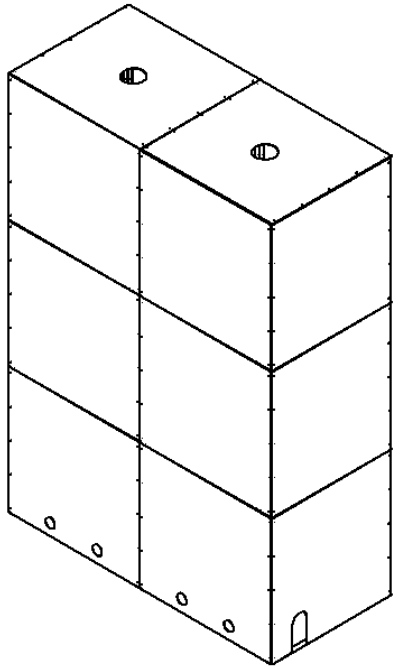

BOM for Complete List of Parts

University of FLorida
Combustion and Propulsion Laboratory
352 - 392 - 6132

Pieces Required:	TITLE:		Case Assembly
MATERIAL:			DATE
USED ON:	DESIGNED BY:	Adrian Blot	6/17/08
Units in Inches Tol. +/- x.x = 0.060, x.xx = 0.010 x.xxx = .005 UOS Break edges 0.015 - 0.030 UOS	Modified BY:		
	DRAWN BY:	Adrian Blot	6/17/08
	SCALE: 1:64	SIZE A	SHEET 2 OF 2

5 4 3 2 1

Figure B-1. Enclosure bill of materials for all parts

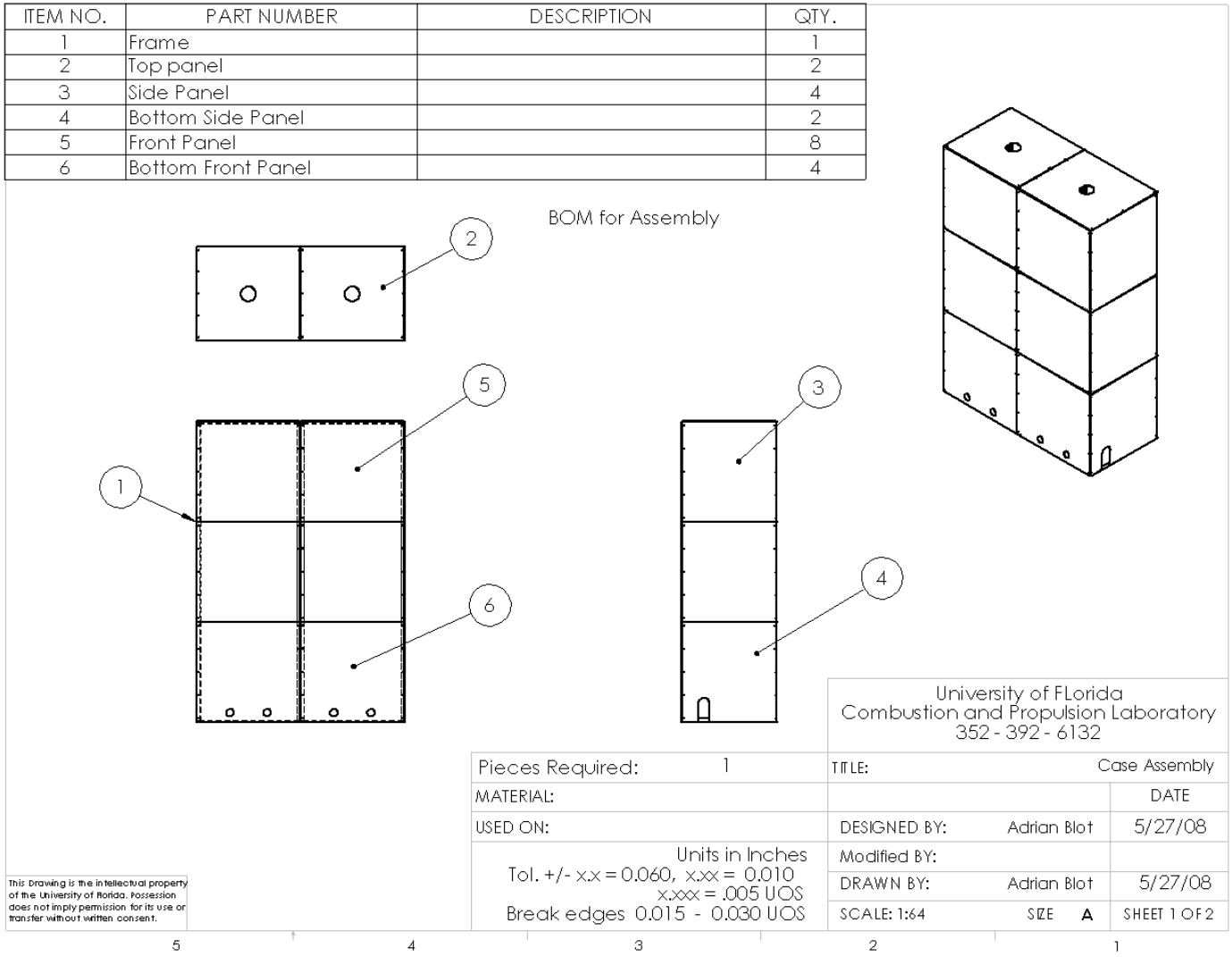

Figure B-2. Enclosure assembly mechanical drawing

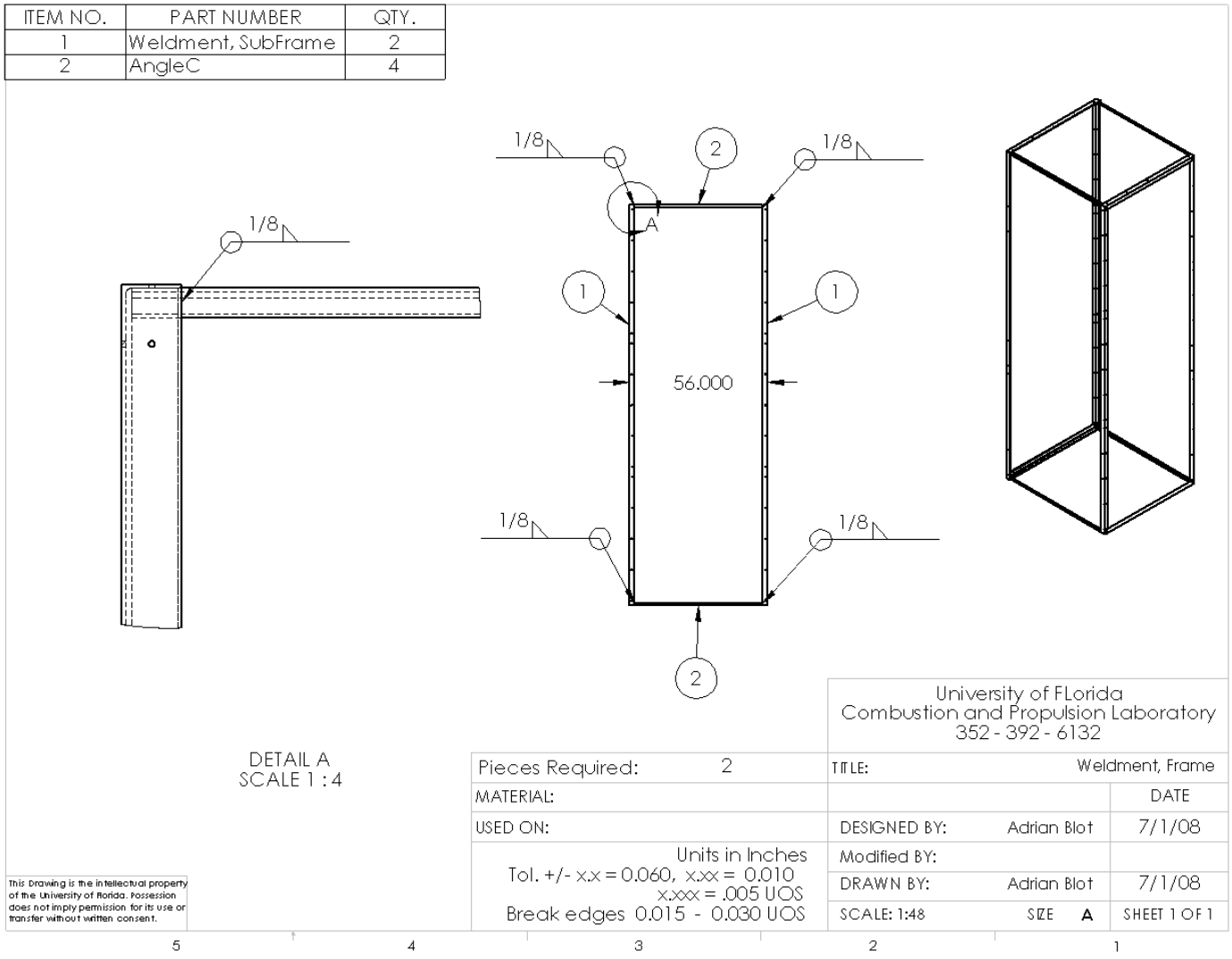

Figure B-3. Frame weldment mechanical drawing

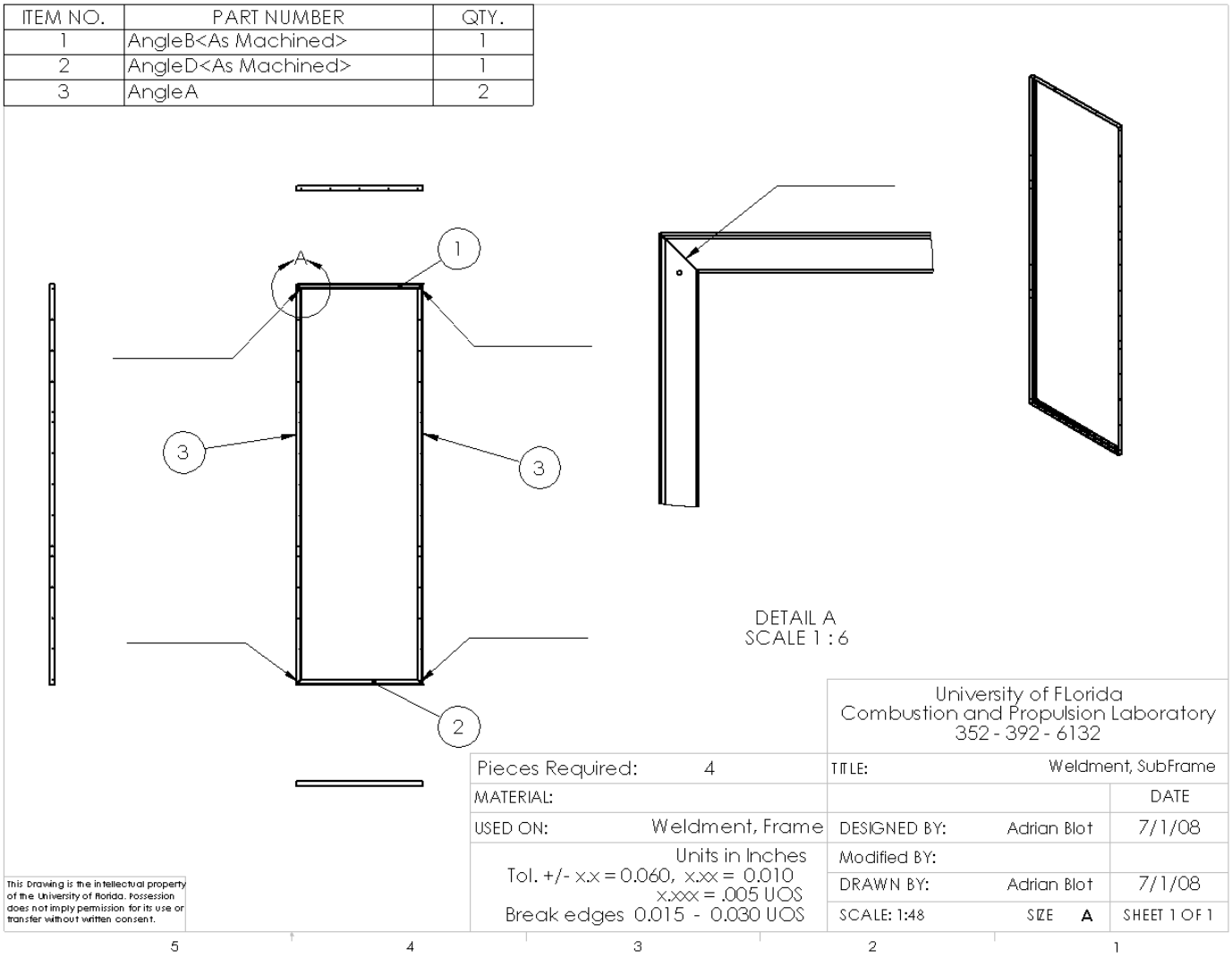

Figure B-4. Subframe weldment mechanical drawing

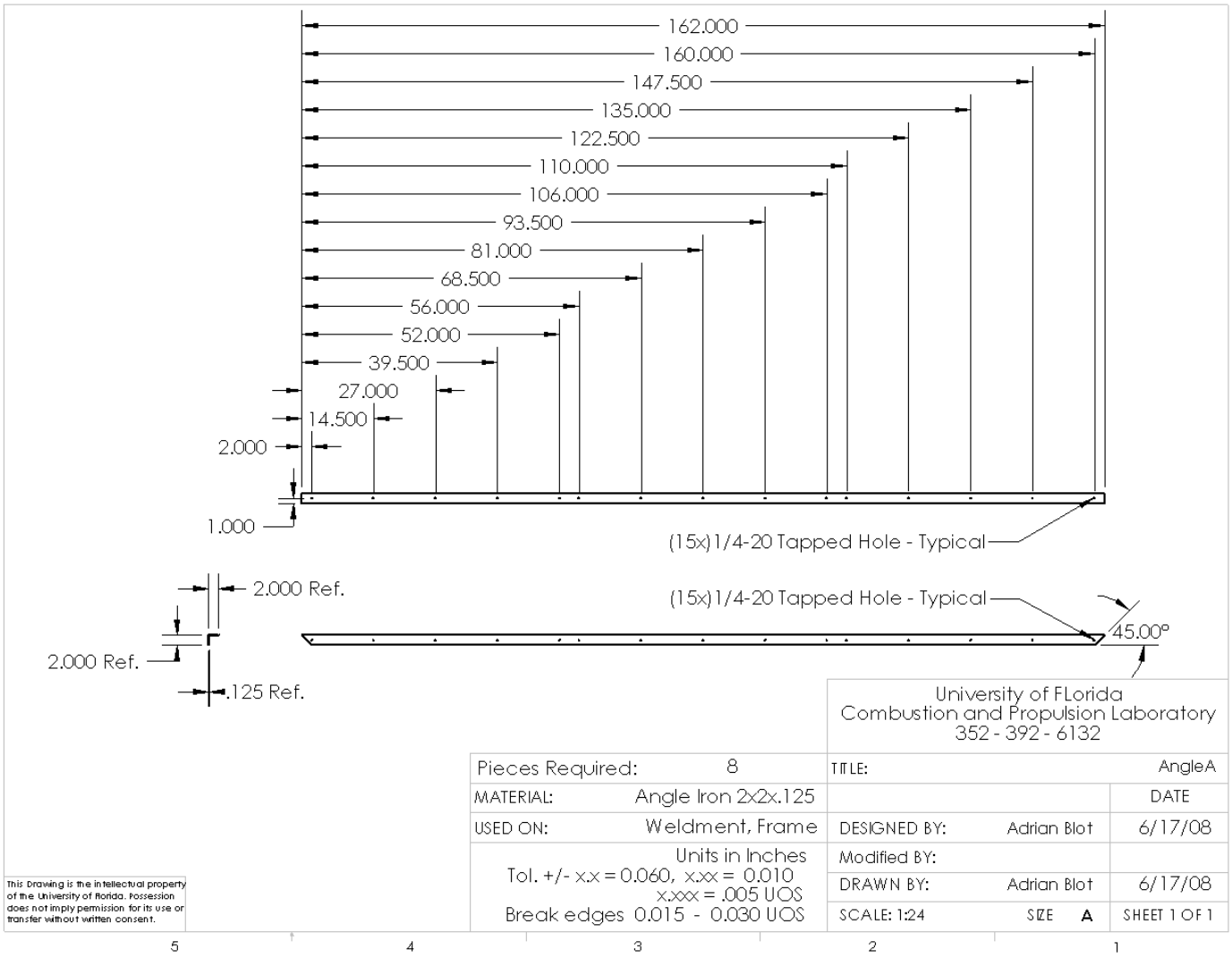

Figure B-5. Angle iron A mechanical drawing

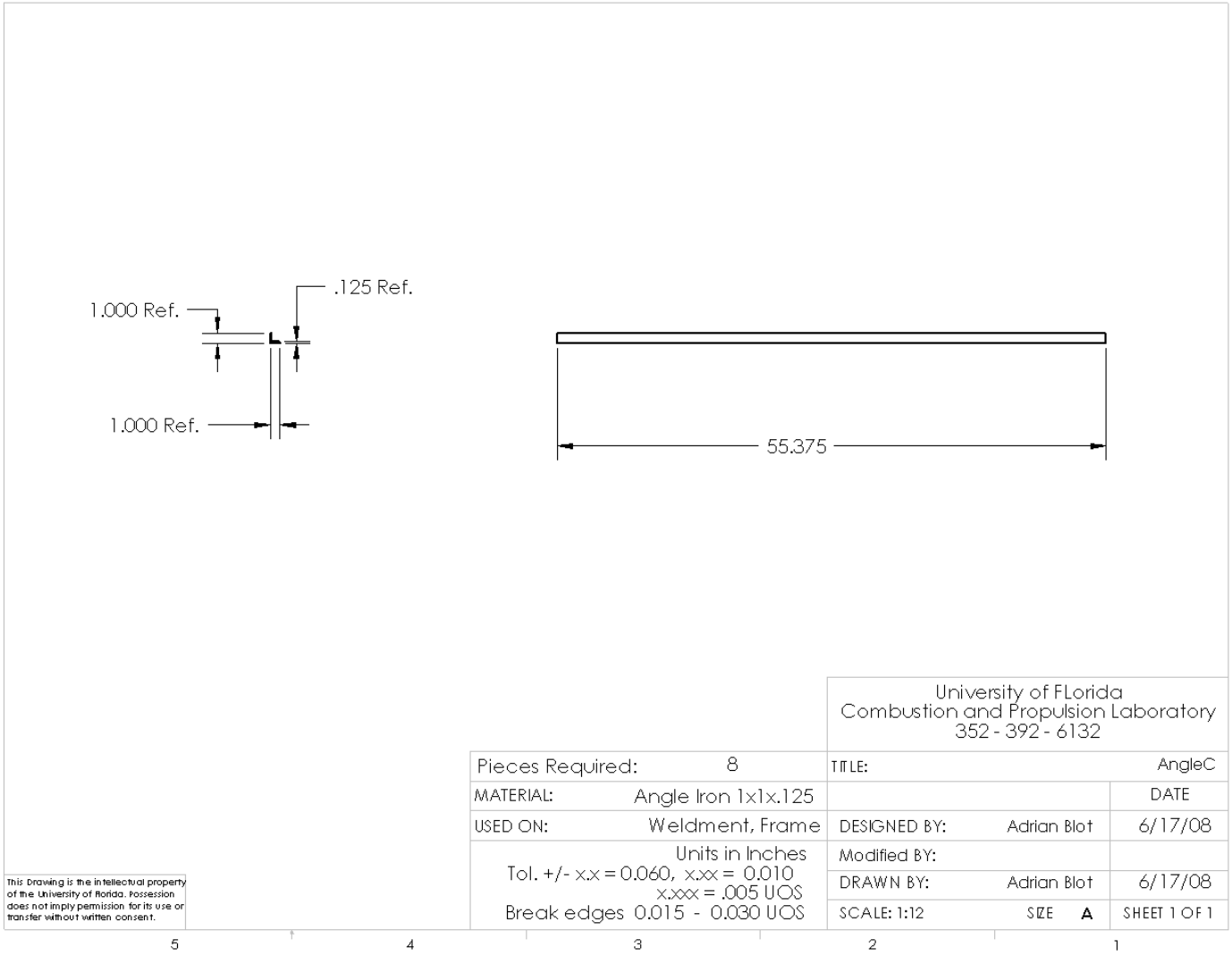

Figure B-6. Angle iron C mechanical drawing

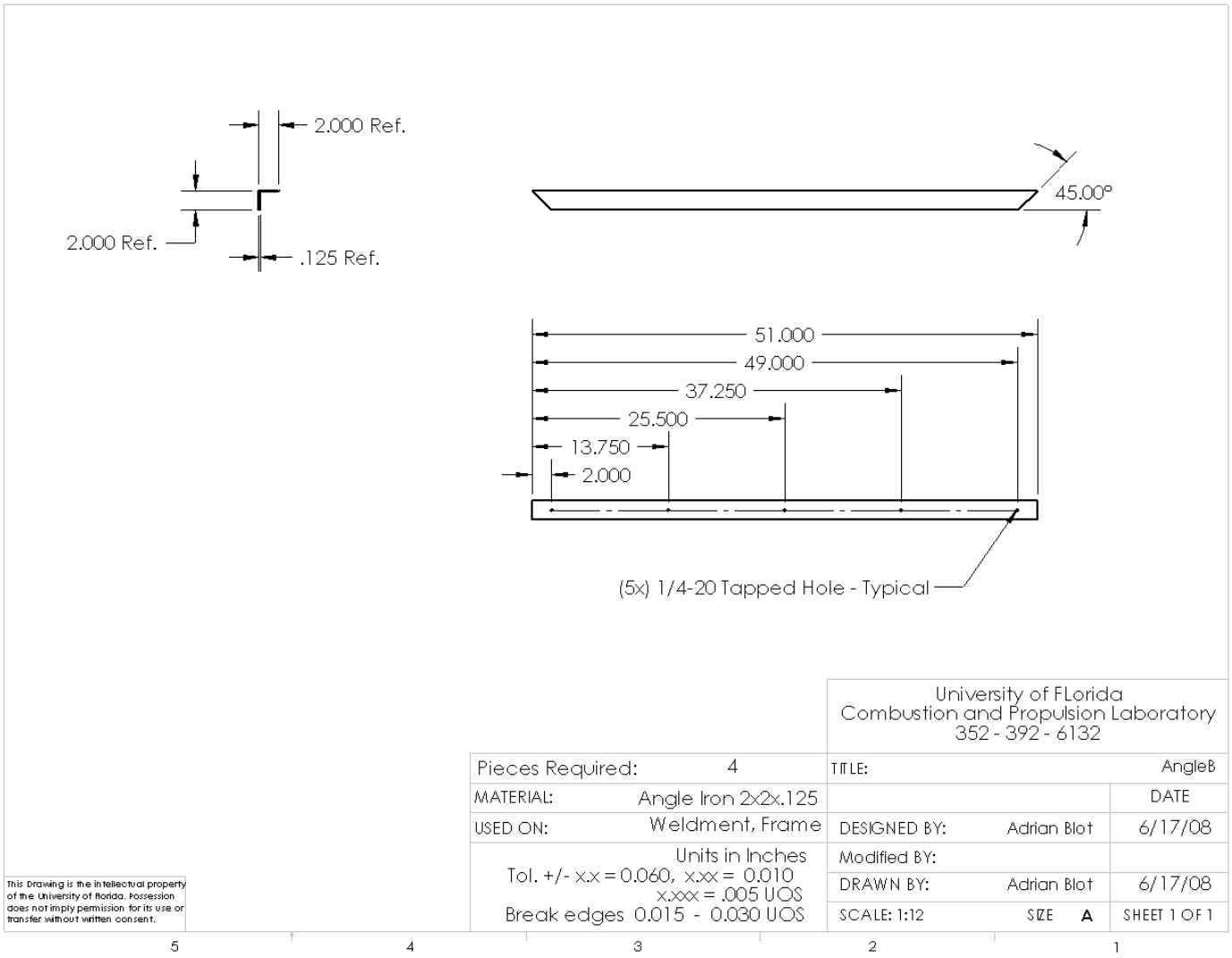

Figure B-7. Angle iron B mechanical drawing

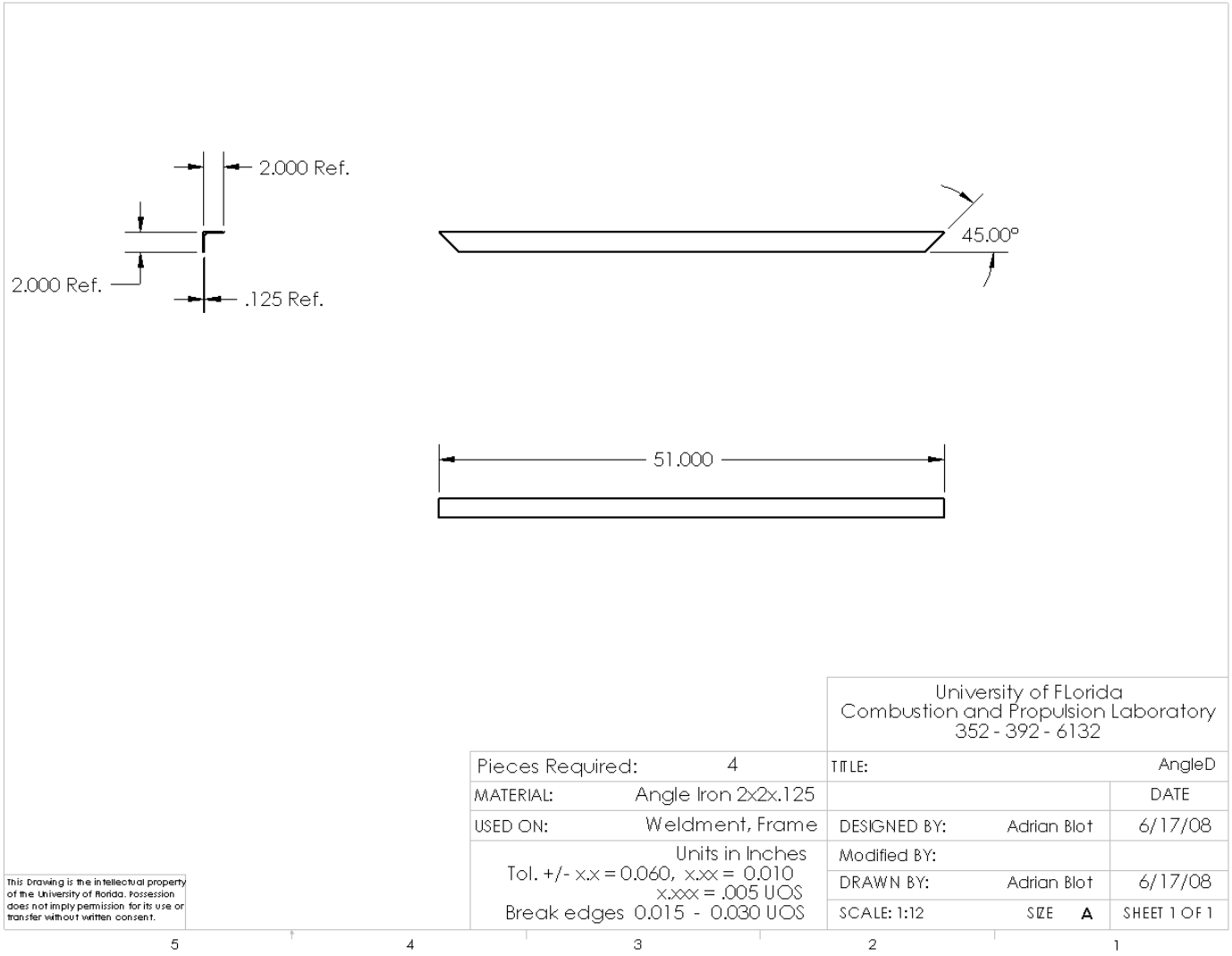

Figure B-8. Angle iron D mechanical drawing

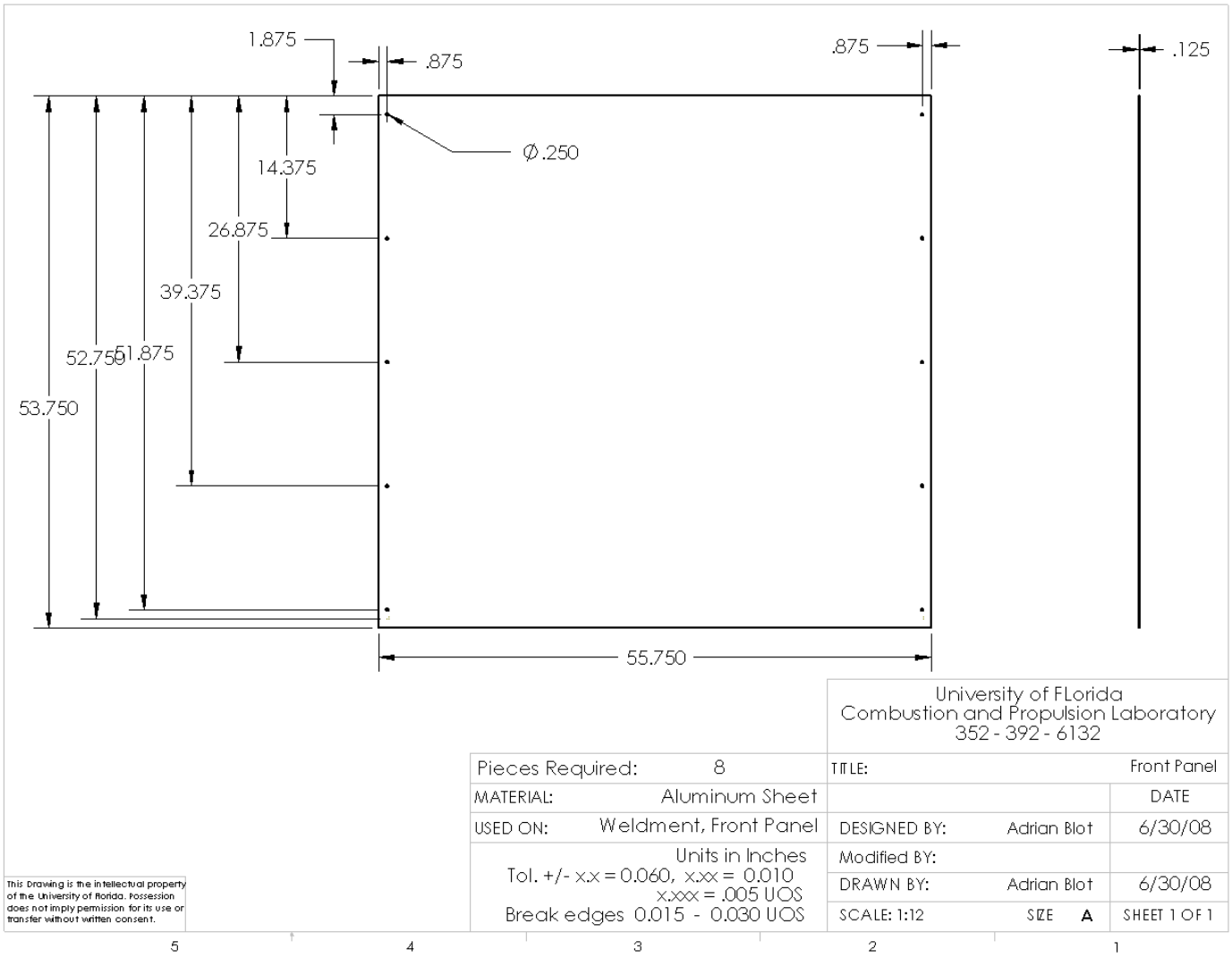

Figure B-9. Front panel mechanical drawing

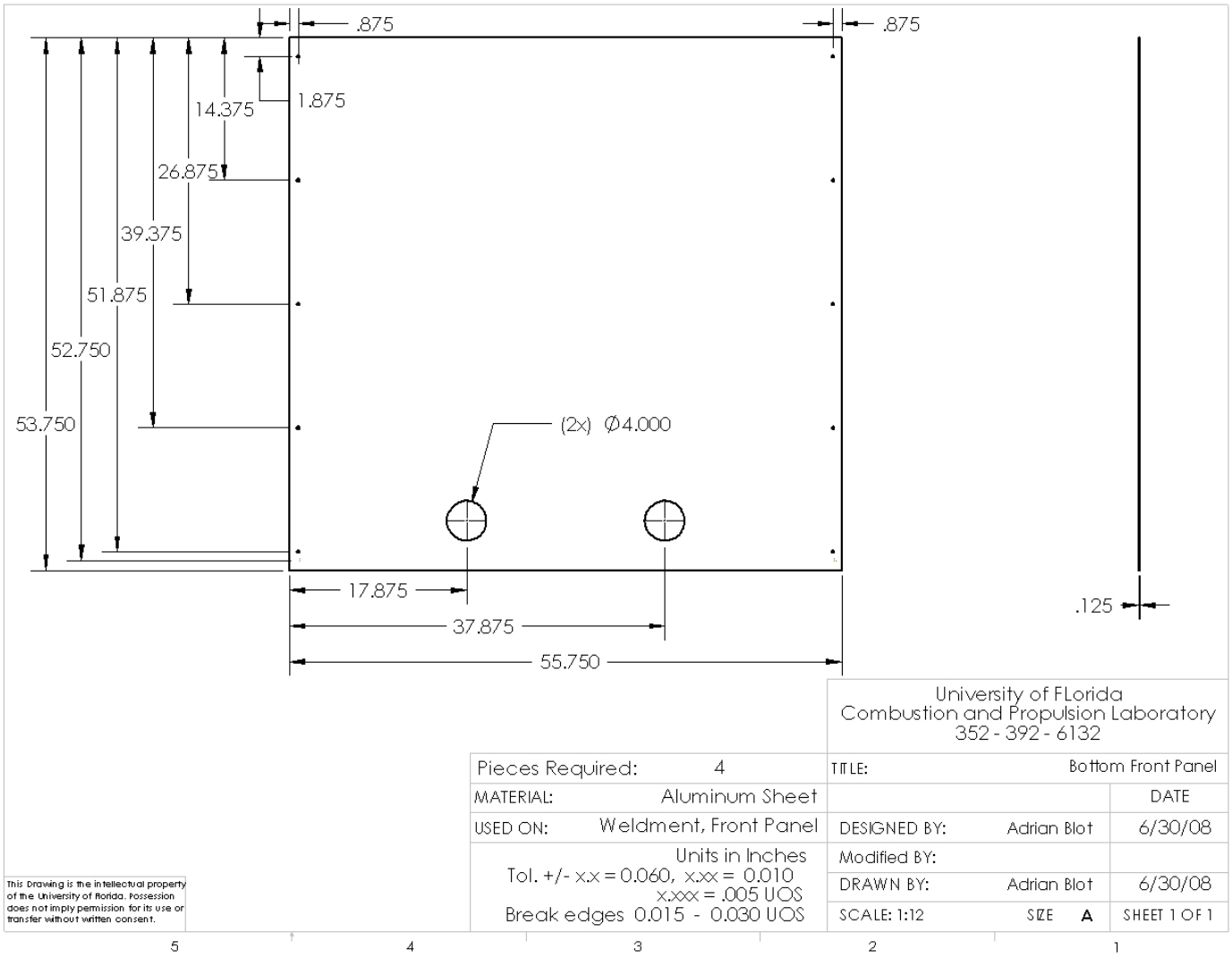

Figure B-10. Bottom front panel mechanical drawing

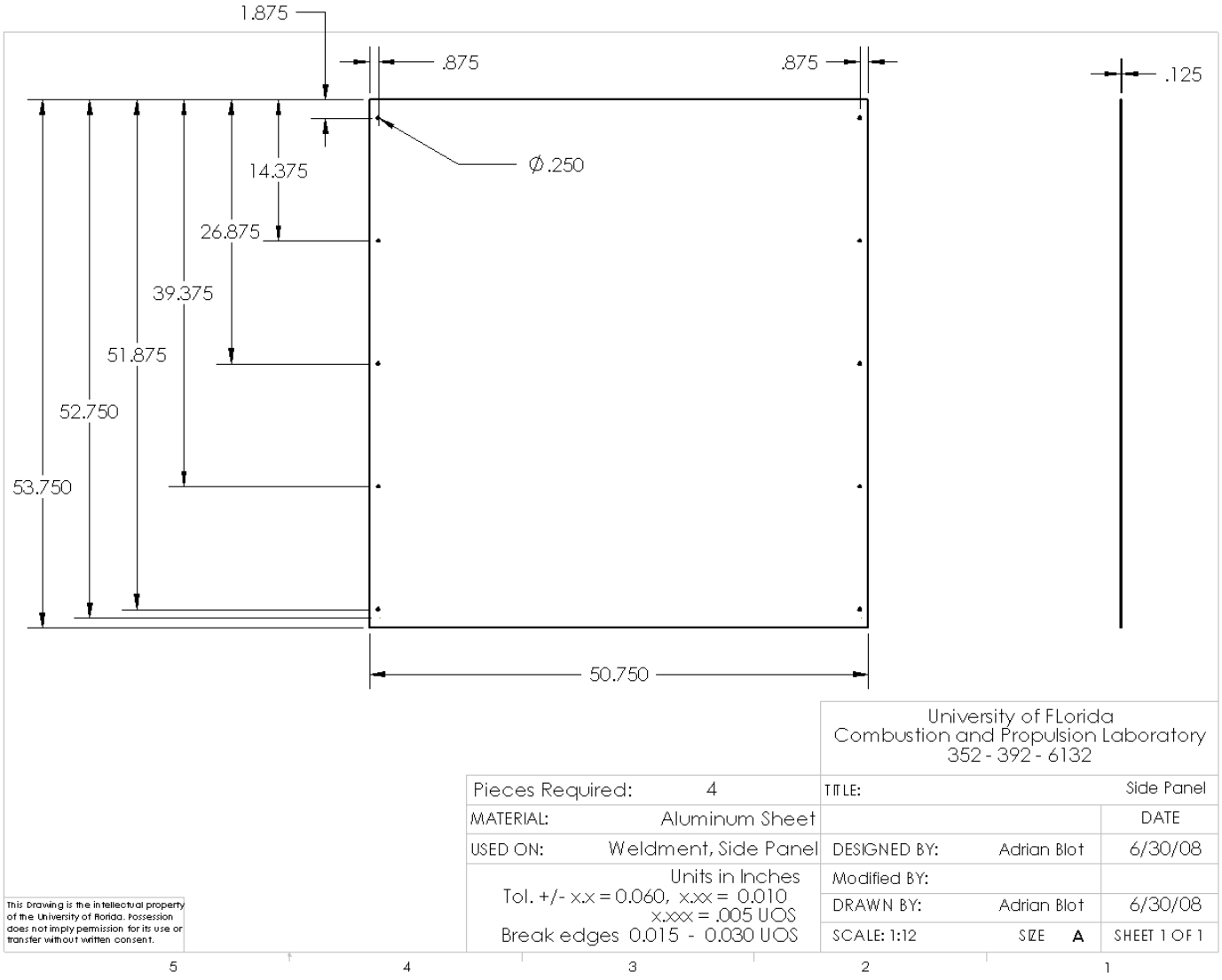

Figure B-11. Side panel mechanical drawing

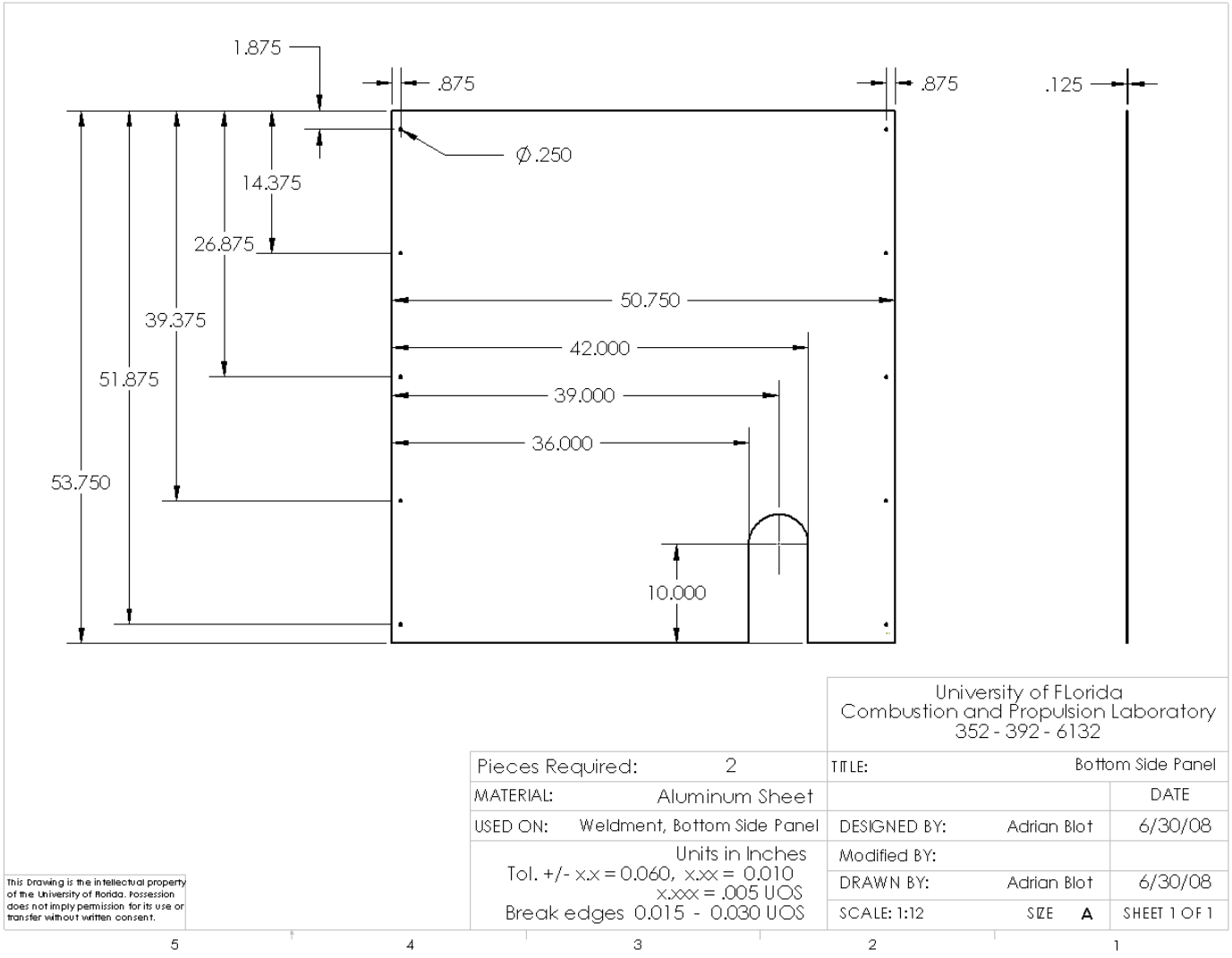

Figure B-12. Bottom side panel mechanical drawing

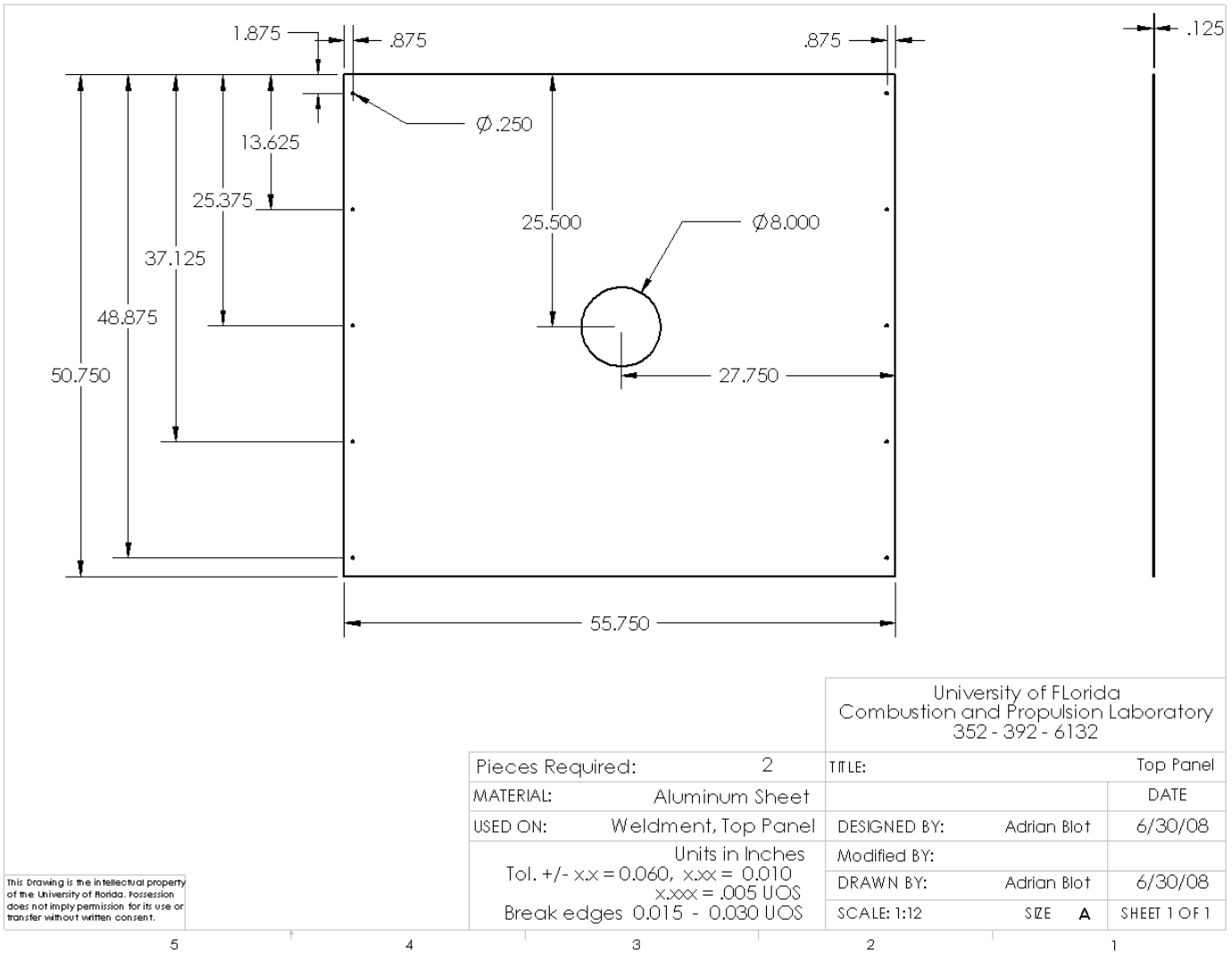

Figure B-13. Top panel mechanical drawing

APPENDIX C
PROTOTYPE HEATER DRAWINGS

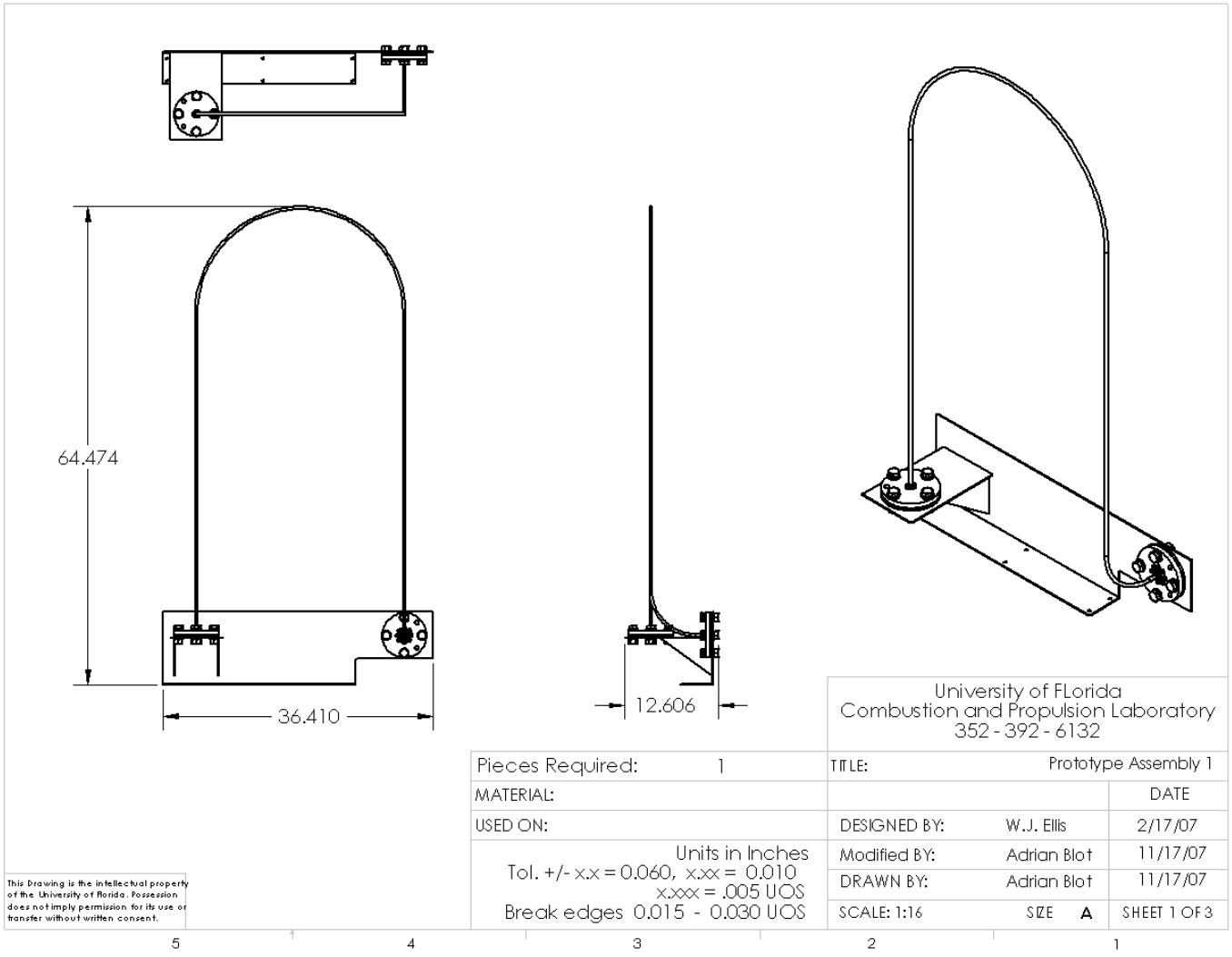

Figure C-1. Prototype assembly layout

ITEM NO.	PART NUMBER	QTY.
1	Support Base	1
2	Inlet Flange Base	1
3	Brace	2
4	Threaded Insert	1
5	Tube	1
6	Flange	1
7	Flange	1
8	Tube Exit Bushing	1
9	Tube Inlet Bushing	1
10	Inlet Flange Gasket	1
11	Outlet Flange Gasket	1
12	Flange Inserts	8
13	HHNUT 0.6250-11-D-C	8
14	FW 0.625	16
15	HHSBOLT 0.6250-11x2x1.25-C	8

BOM for Complete list of Parts

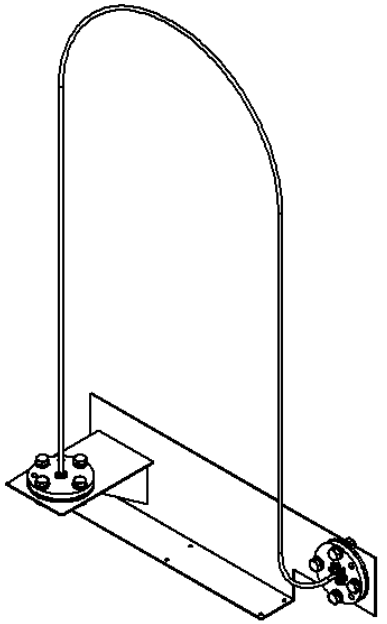

University of FLorida
Combustion and Propulsion Laboratory
352 - 392 - 6132

Pieces Required:	TITLE:		Prototype Assembly
MATERIAL:			DATE
USED ON:	DESIGNED BY:	W.J. Ellis	2/17/07
Units in Inches Tol. +/- x.x = 0.060, x.xx = 0.010 x.xxx = .005 UOS Break edges 0.015 - 0.030 UOS	Modified BY:	Adrian Blot	11/17/07
	DRAWN BY:	Adrian Blot	11/17/07
	SCALE: 1:16	SIZE A	SHEET 2 OF 3

5 4 3 2 1

Figure C-2. Prototype bill of material of all parts

ITEM NO.	PART NUMBER	QTY.
1	Weldment, Support Base	1
2	Tube Weldment	1
3	Inlet Flange Gasket	1
4	Outlet Flange Gasket	1
5	Flange Inserts	8
6	HHNUT 0.6250-11-D-C	8
7	FW 0.625	16
8	HHSBOLT 0.6250-11x2x1.25-C	8

BOM for Assembly

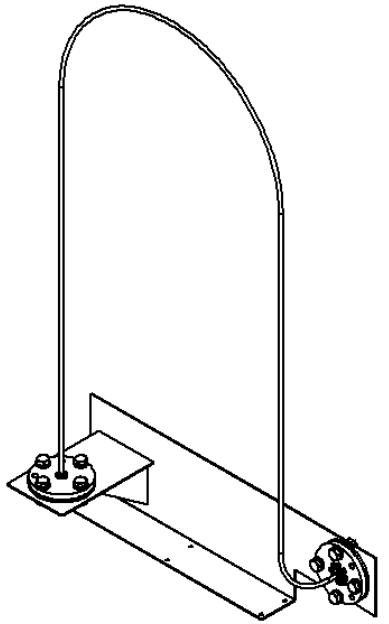

University of FLorida
Combustion and Propulsion Laboratory
352 - 392 - 6132

Pieces Required:	TITLE:		Prototype Assembly
MATERIAL:			DATE
USED ON:	DESIGNED BY:	W.J. Ellis	2/17/07
Units in Inches Tol. +/- x.x = 0.060, x.xx = 0.010 x.xxx = .005 UOS Break edges 0.015 - 0.030 UOS	Modified BY:	Adrian Blot	11/17/07
	DRAWN BY:	Adrian Blot	11/17/07
	SCALE: 1:16	SIZE A	SHEET 3 OF 3

5 4 3 2 1

Figure C-3. Prototype bill of material for assembly

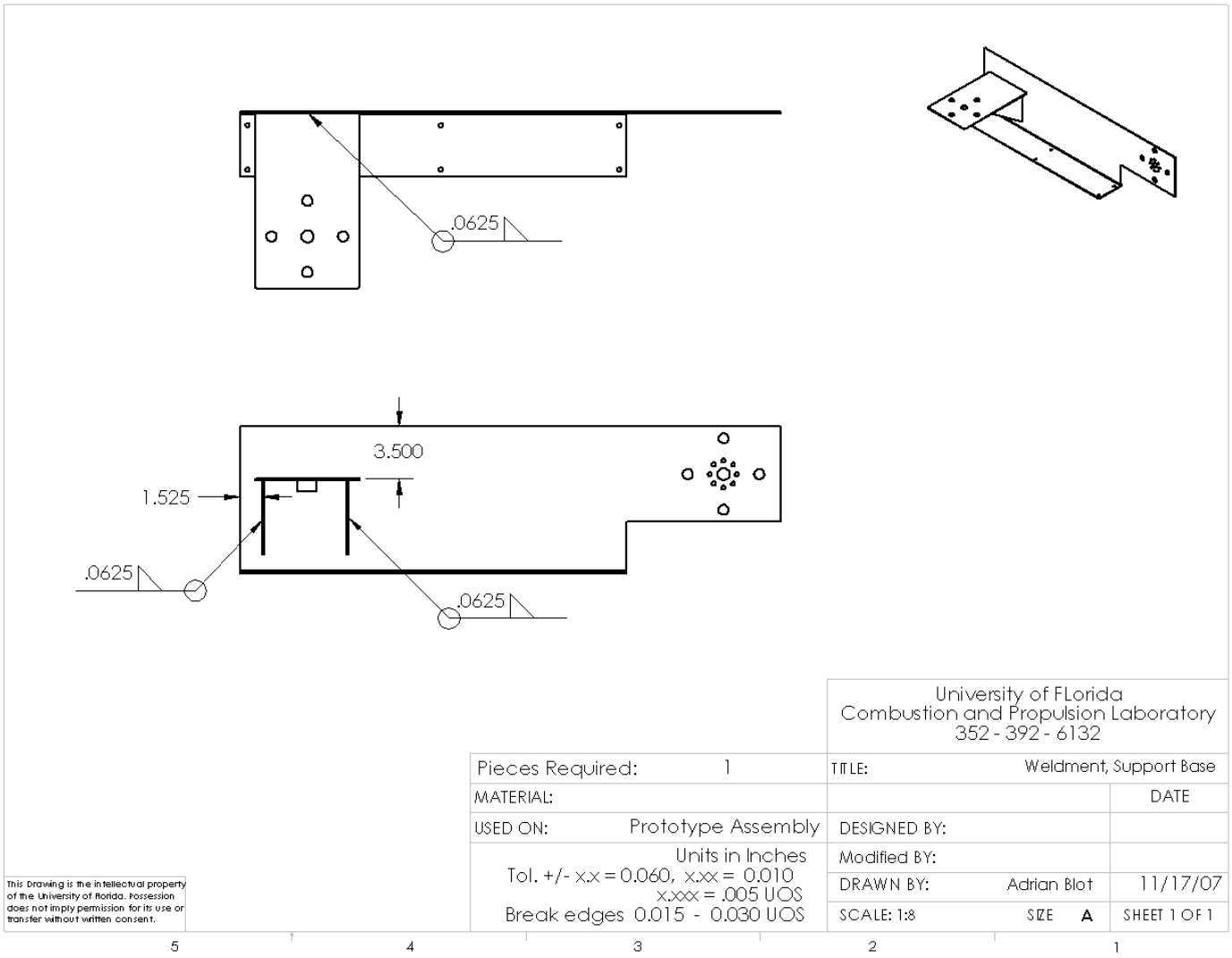

Figure C-4. Support base weldment mechanical drawing

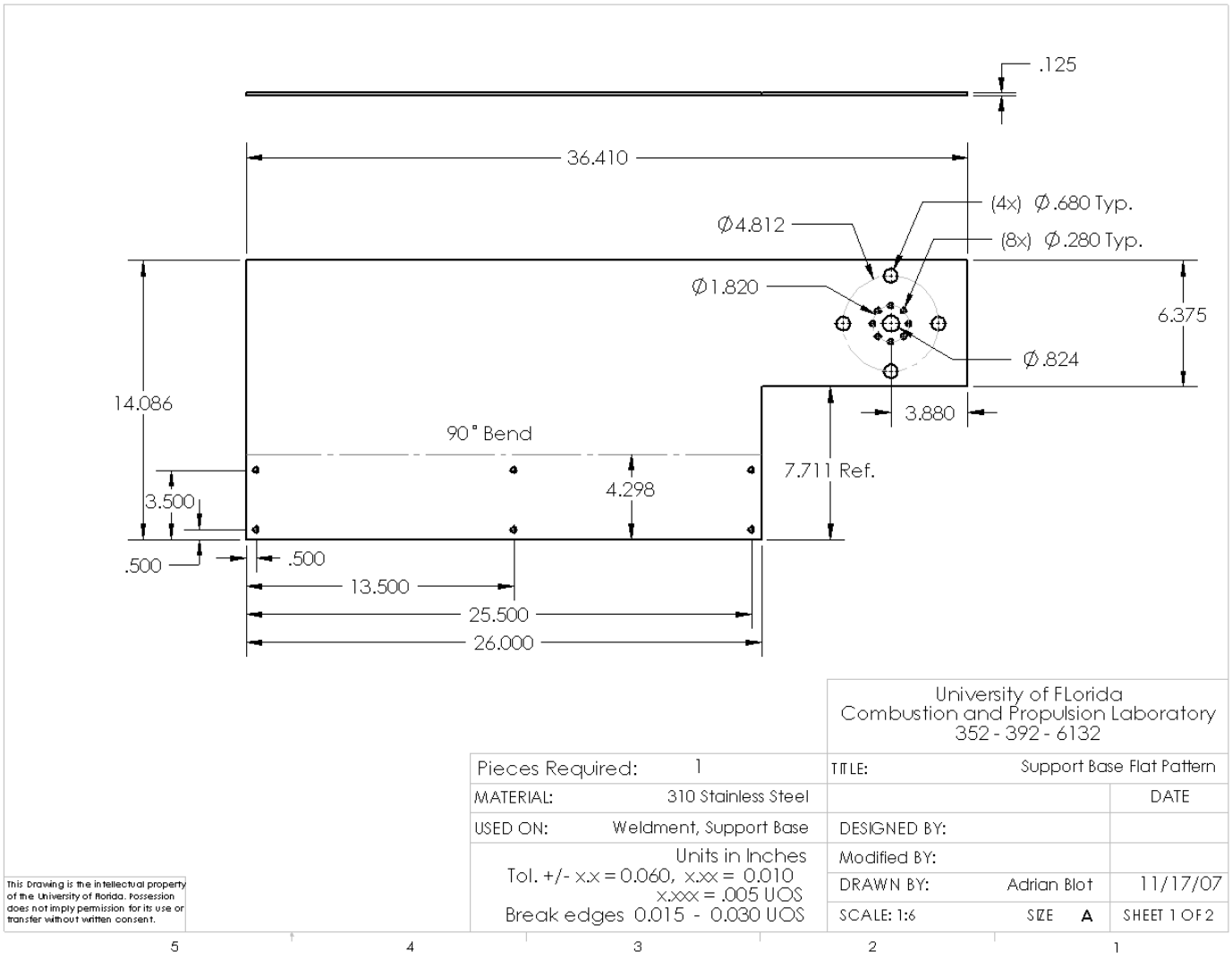

Figure C-5. Support base flat pattern sheet metal mechanical drawing

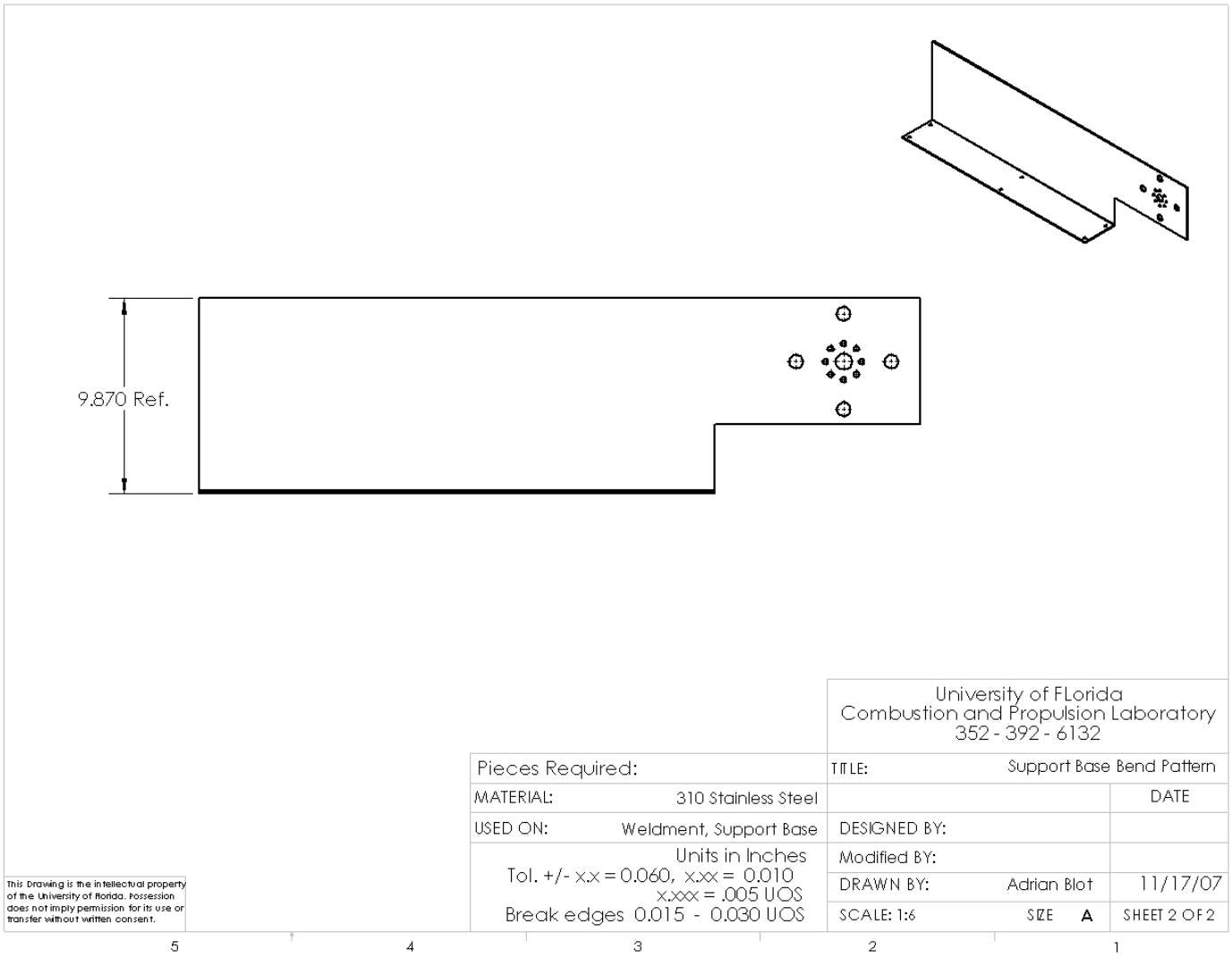

Figure C-6. Support base bend pattern sheet metal mechanical drawing

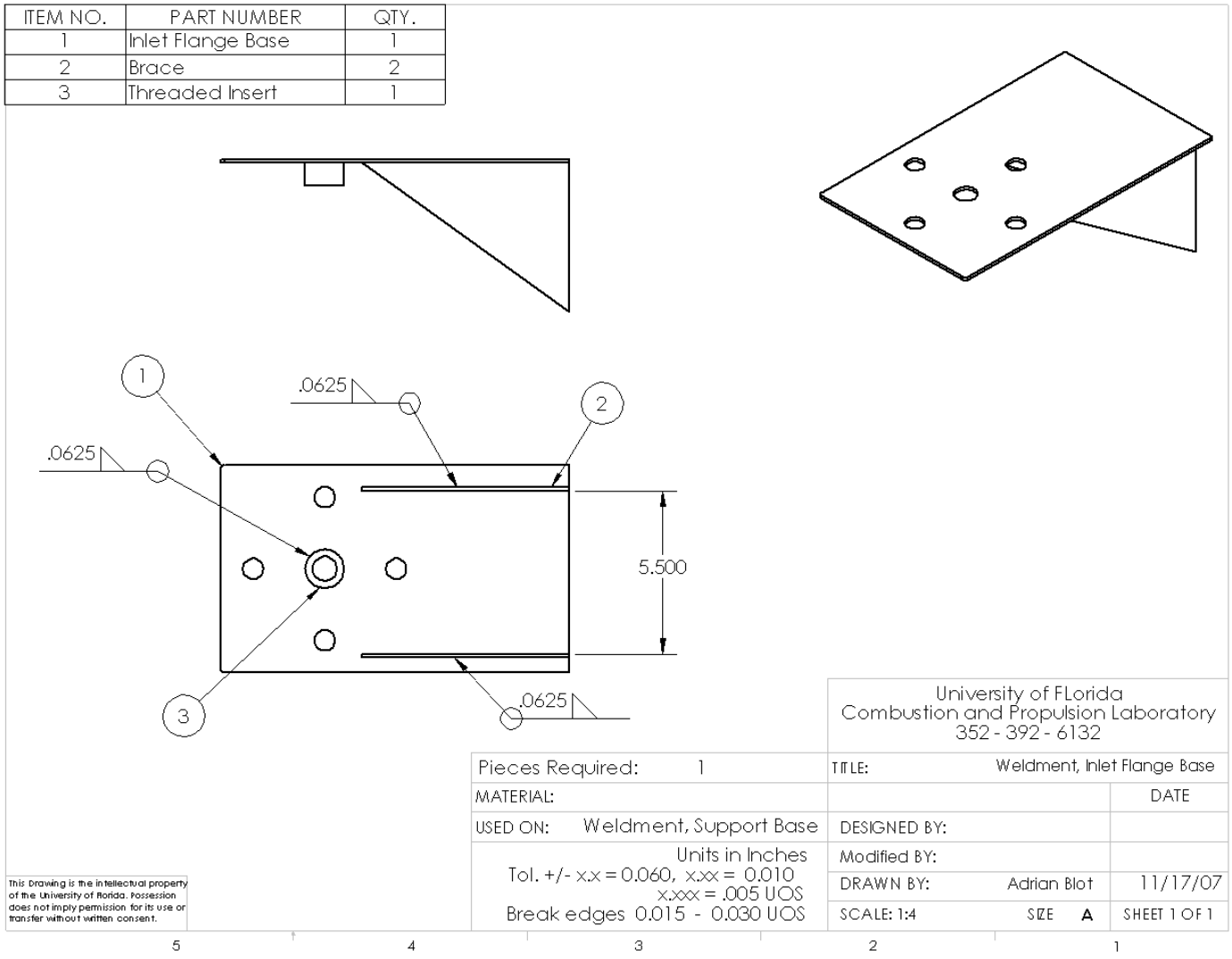

Figure C-7. Inlet flange base weldment mechanical drawing

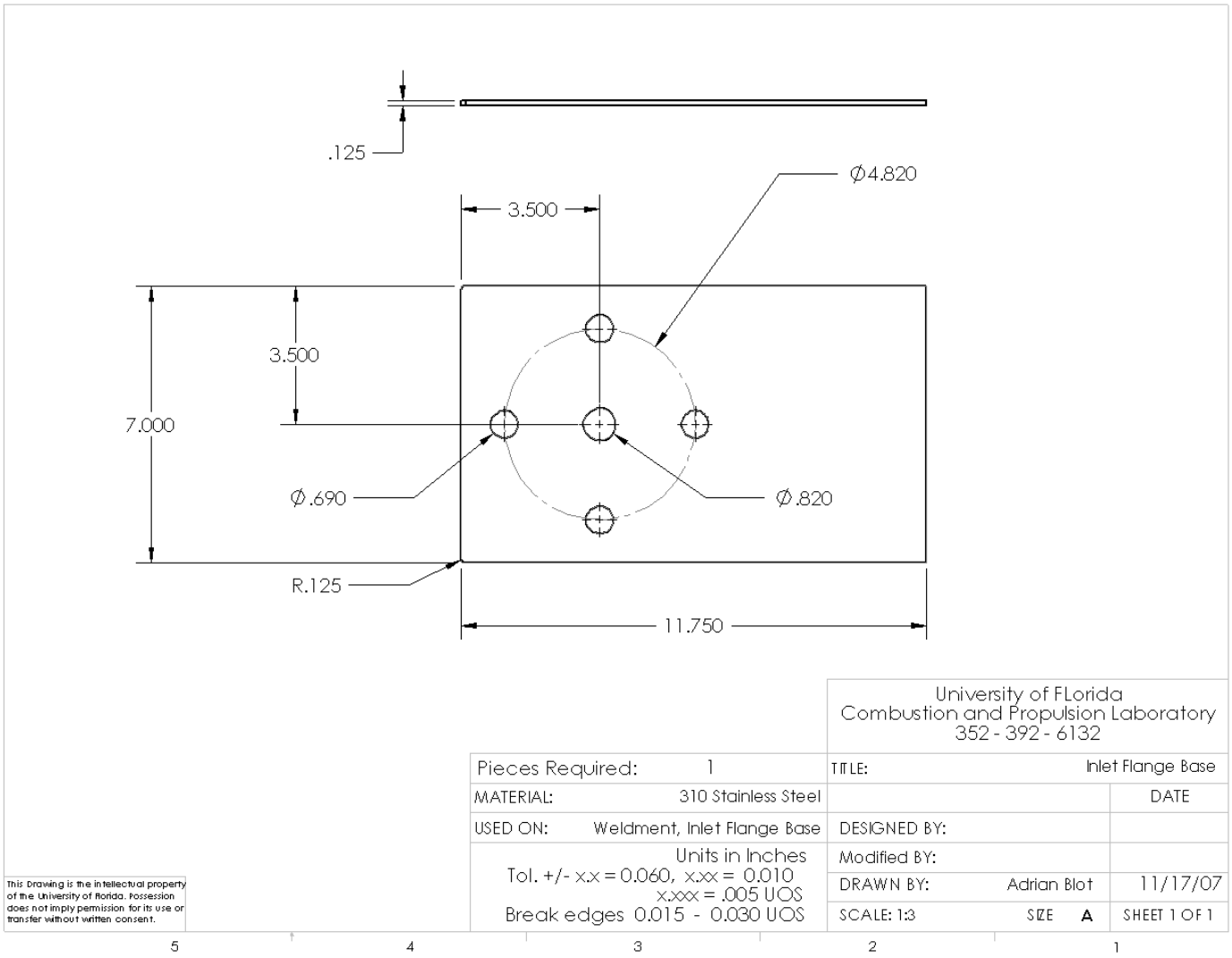

Figure C-8. Inlet flange base sheet metal mechanical drawing

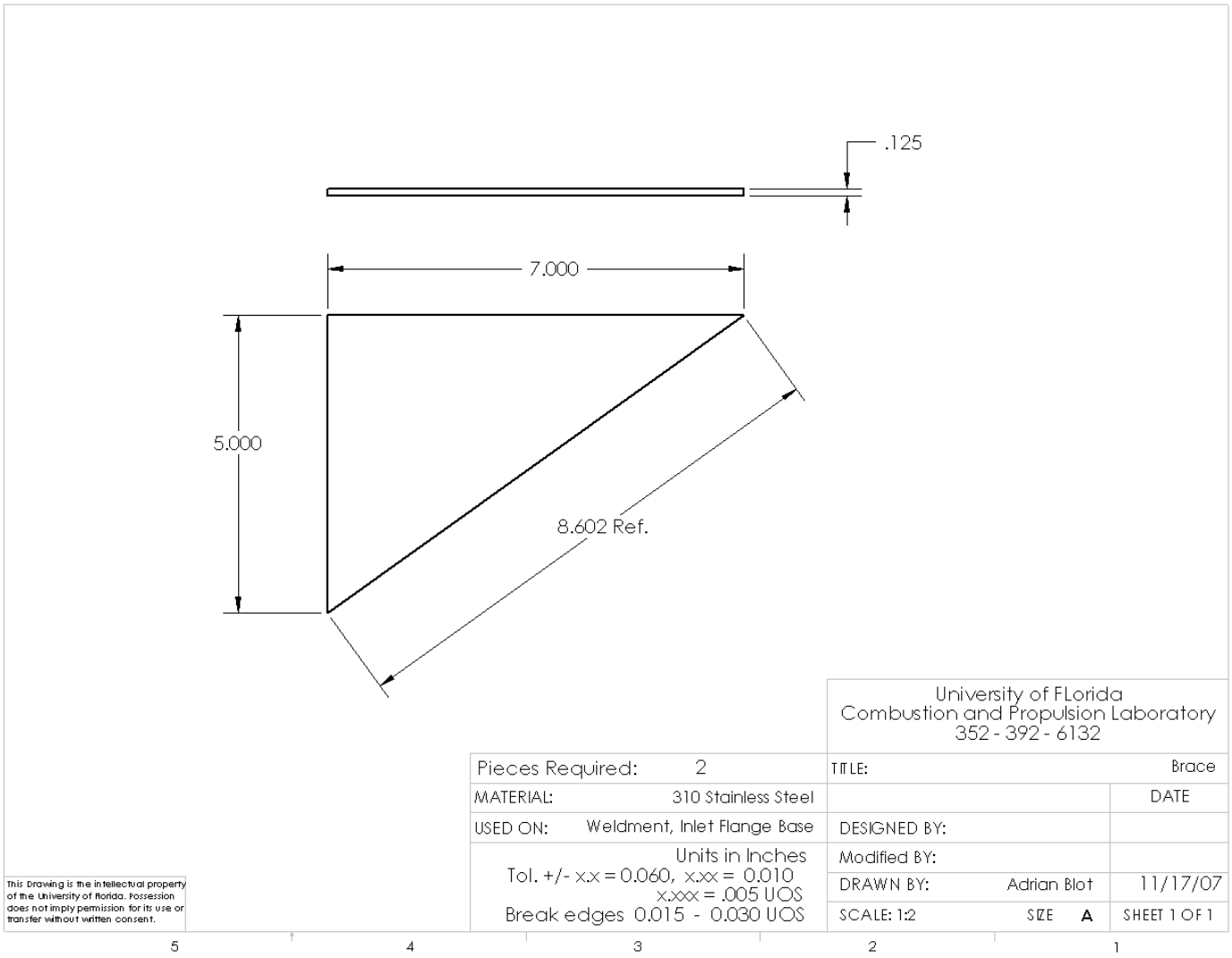

Figure C-9. Brace sheet metal mechanical drawing

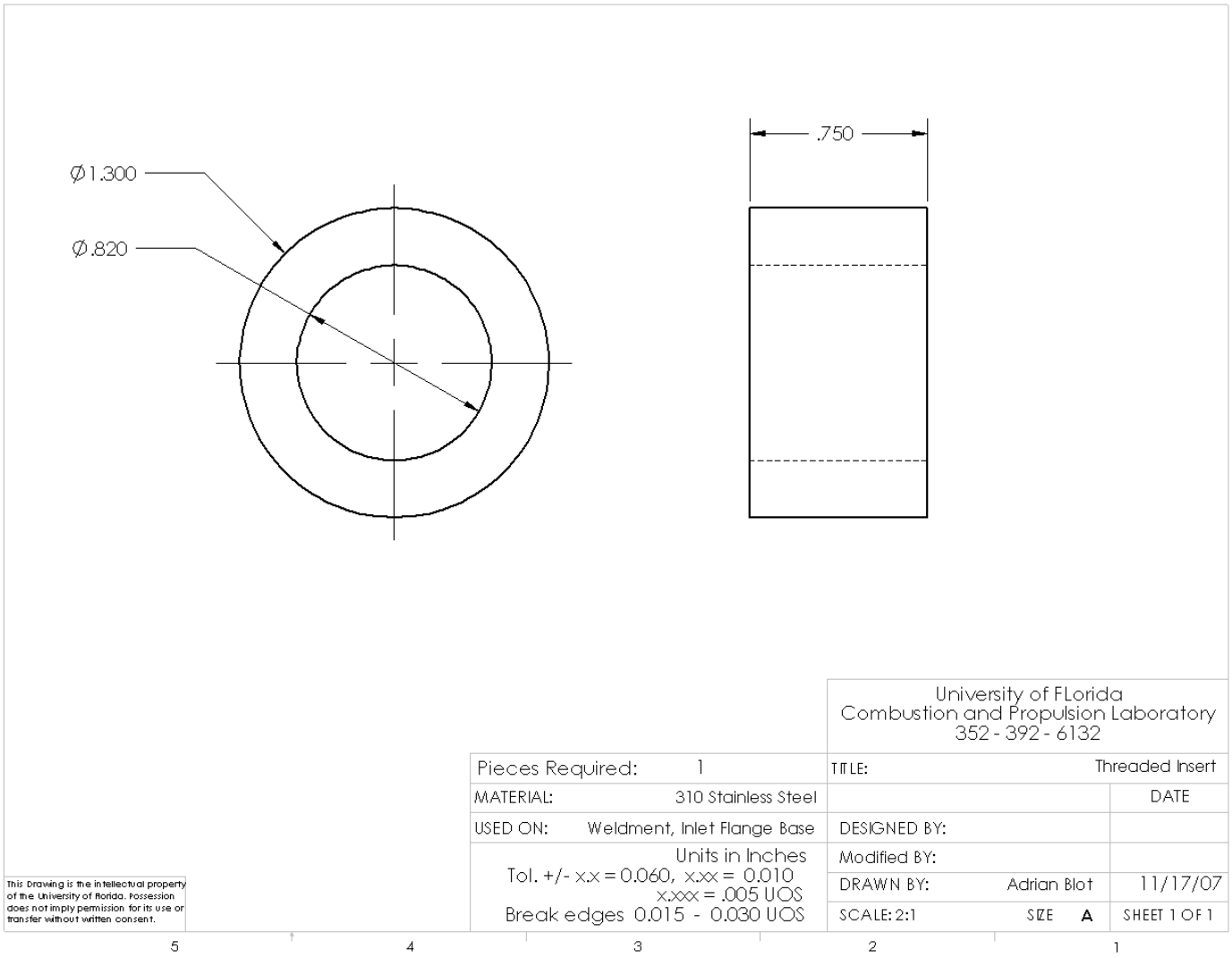

Figure C-10. Threaded insert mechanical drawing

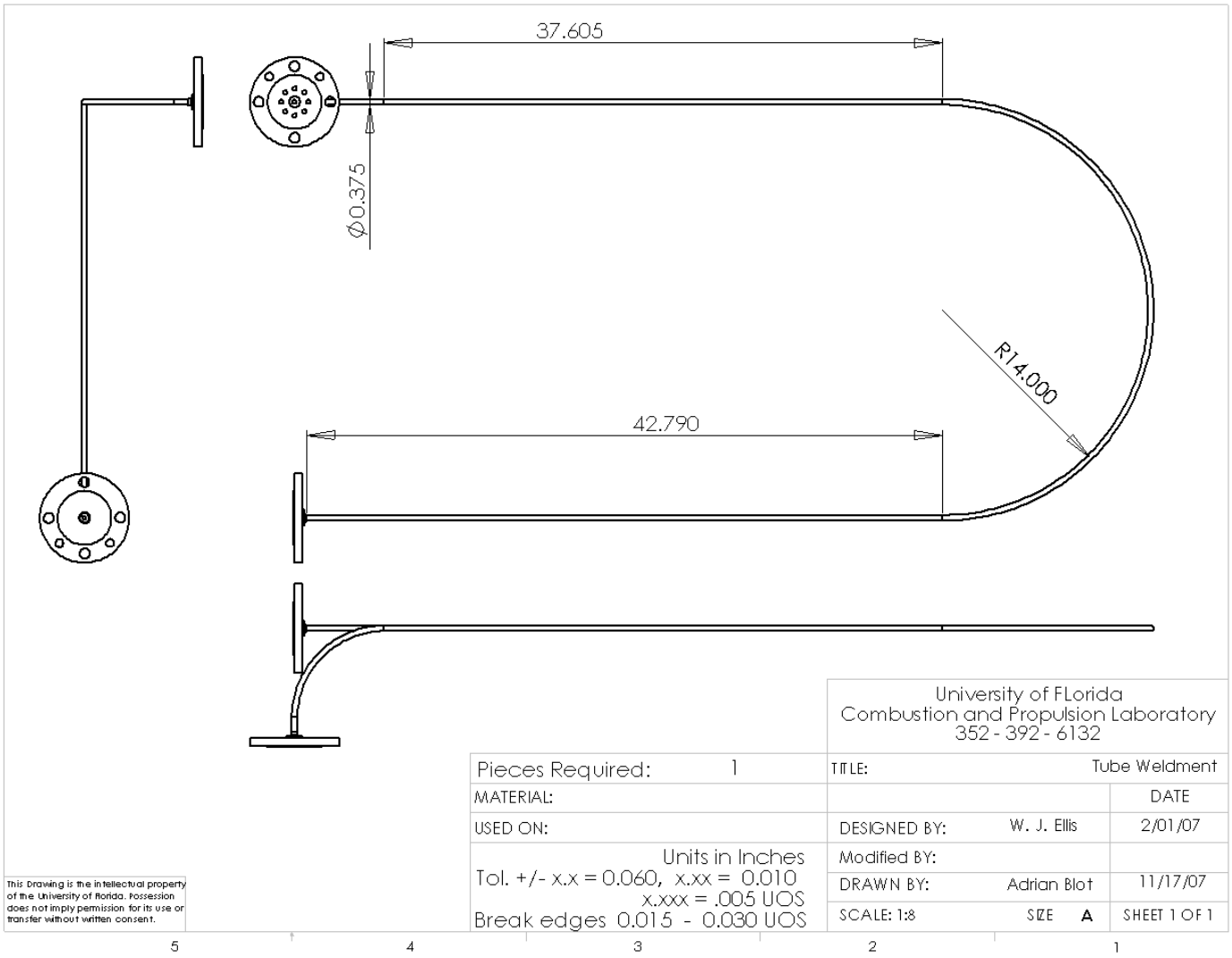

Figure C-11. Prototype tube weldment mechanical drawing

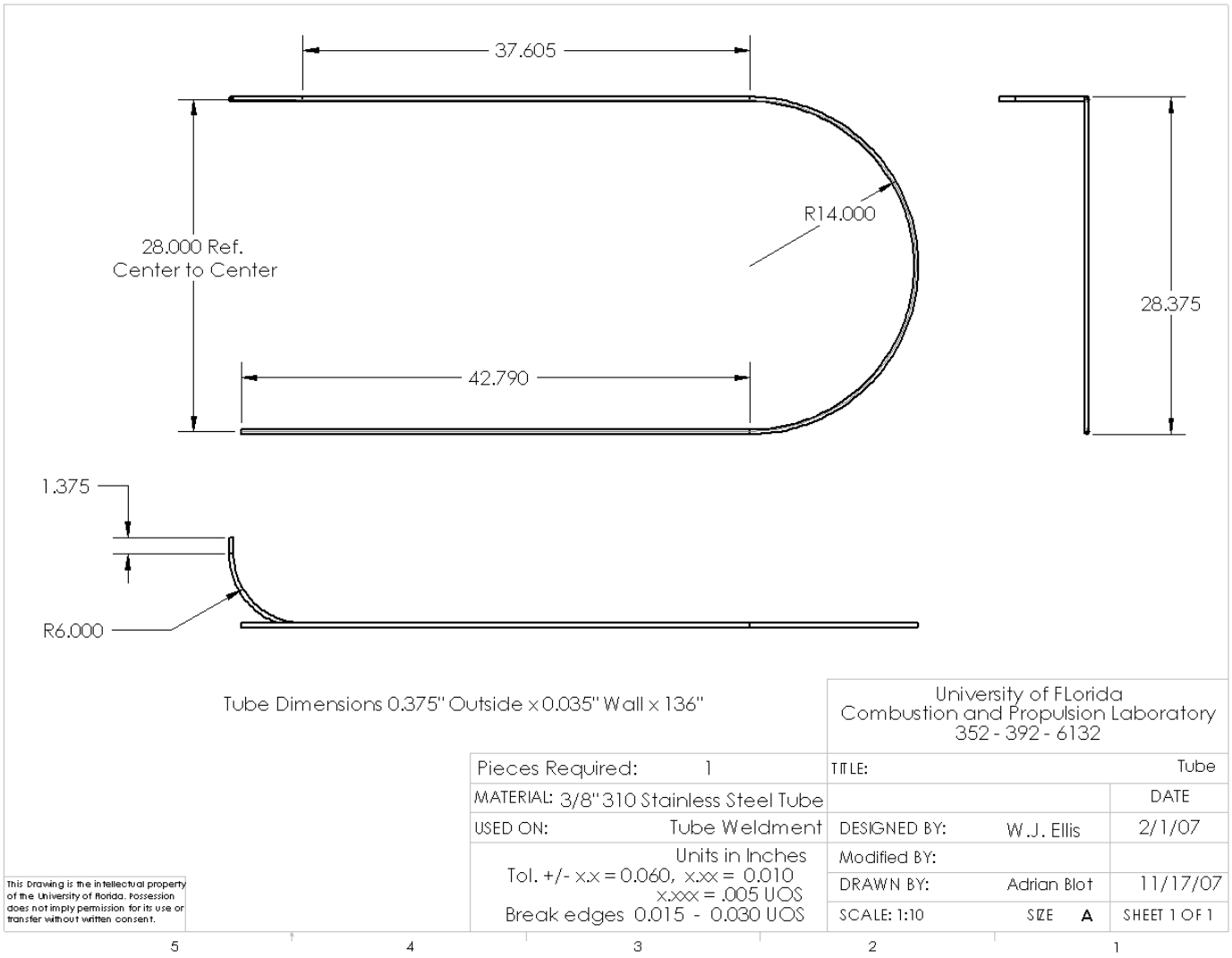

Figure C-12. Prototype tube mechanical drawing

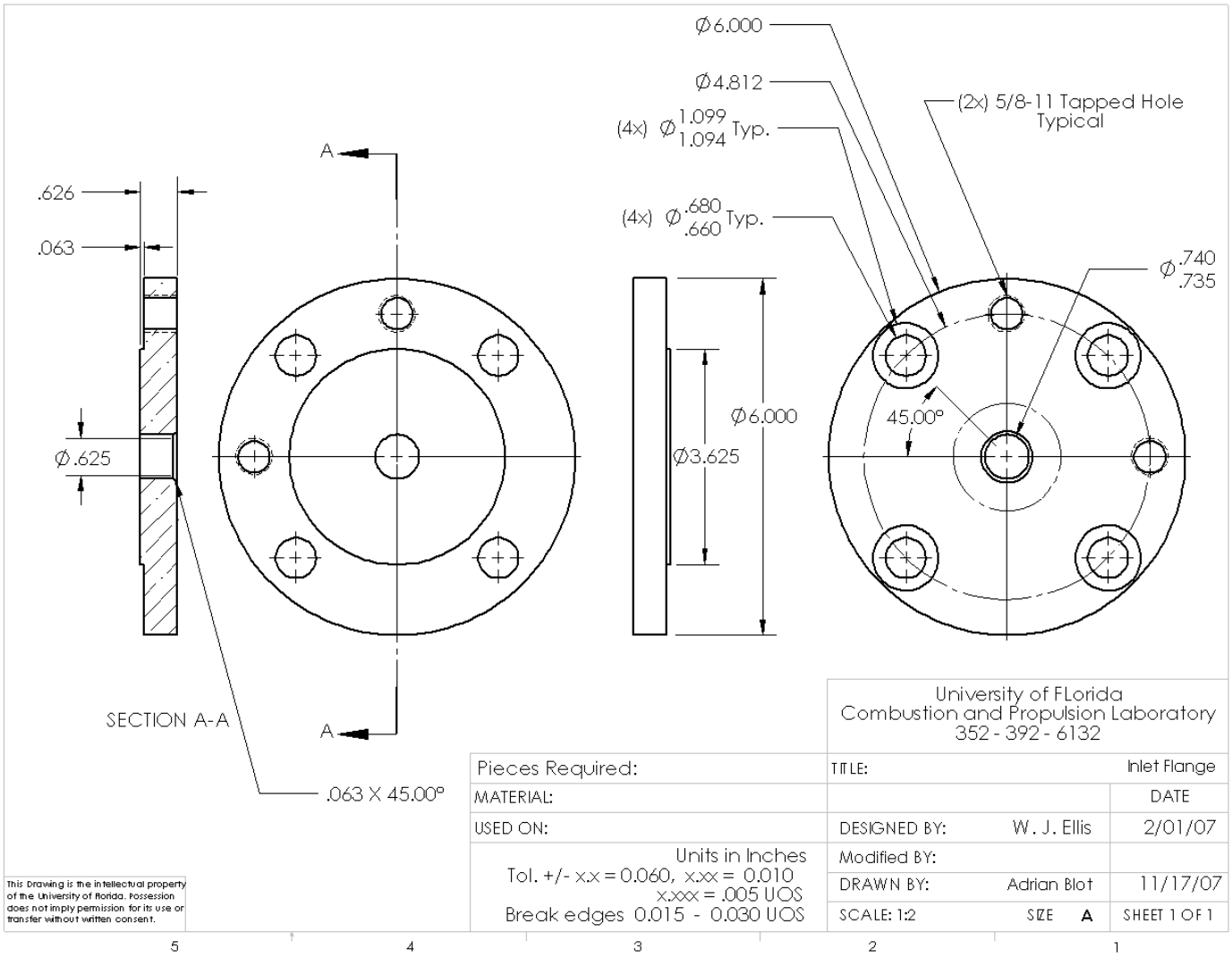

Figure C-13. Inlet flange mechanical drawing

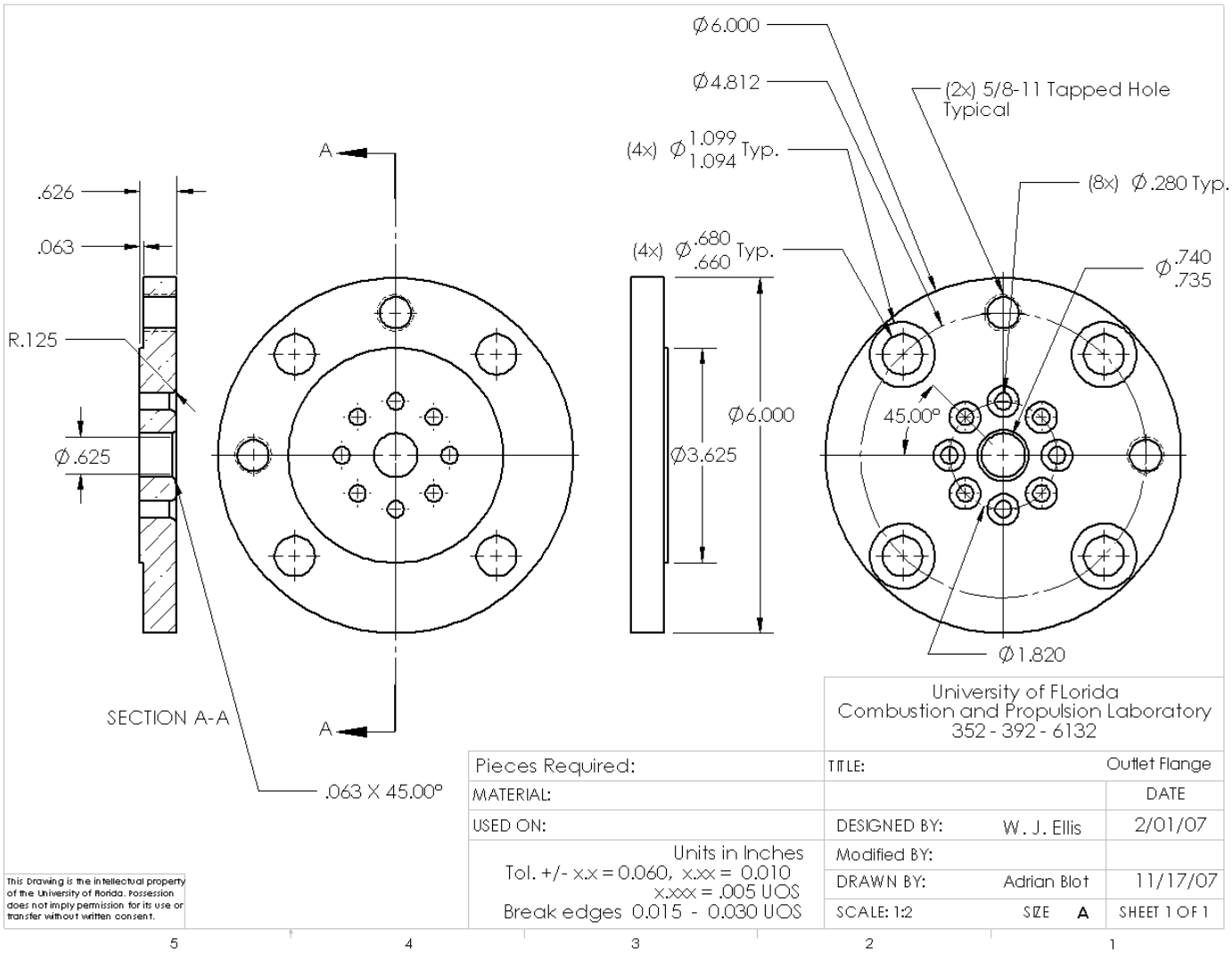

Figure C-14. Outlet flange mechanical drawing

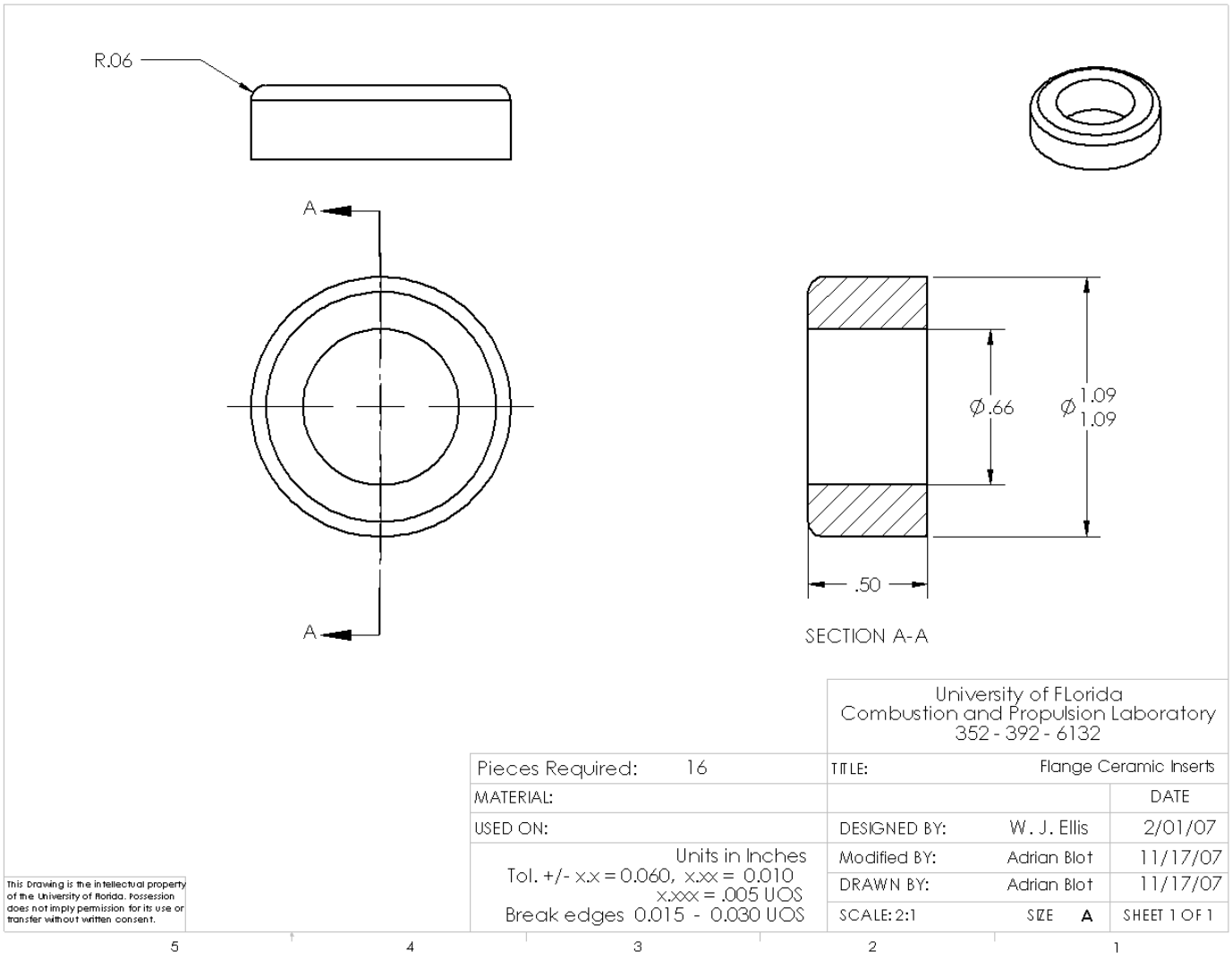

Figure C-15. Flange ceramic insert mechanical drawing

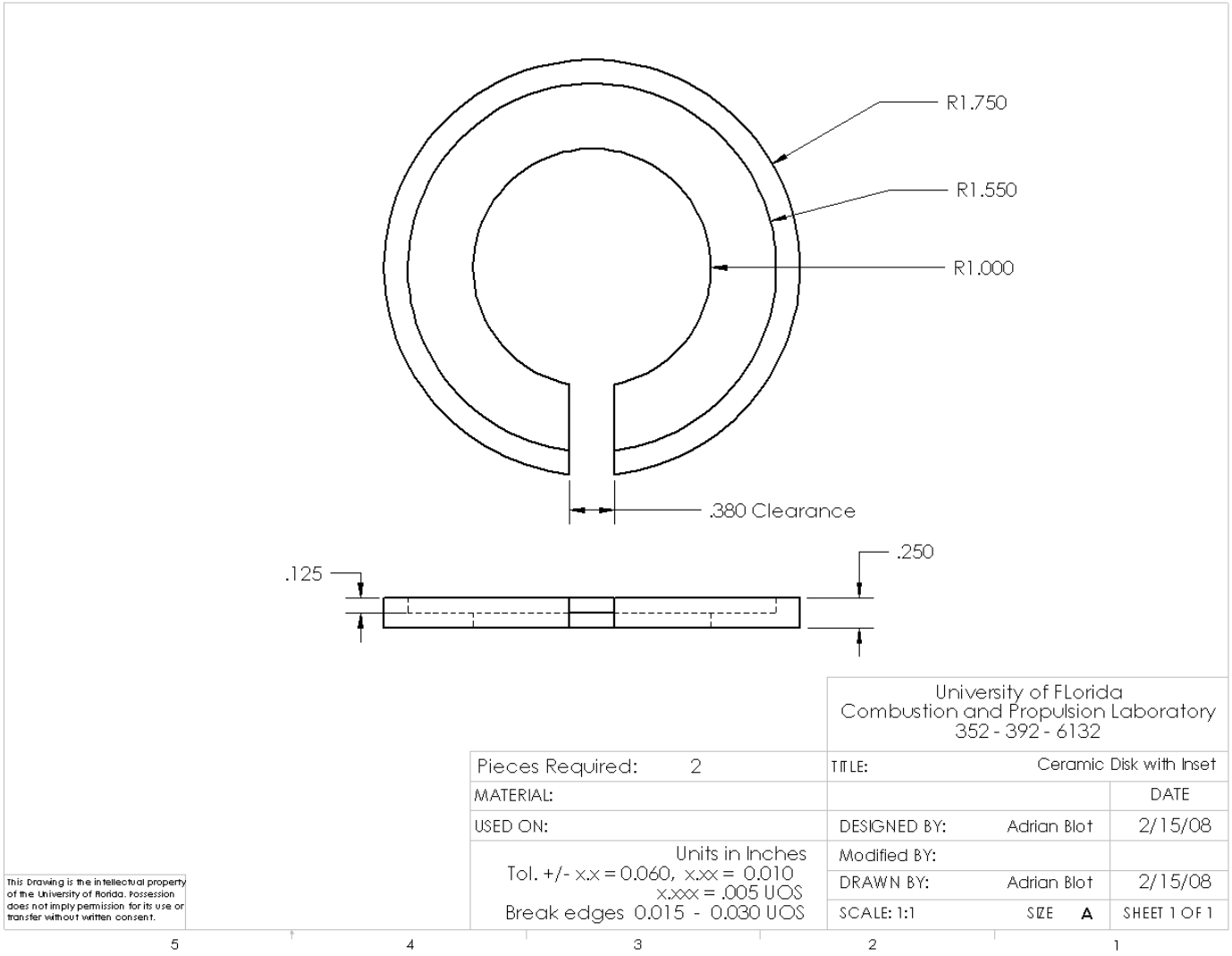

Figure C-16. Ceramic disk with inset mechanical drawing

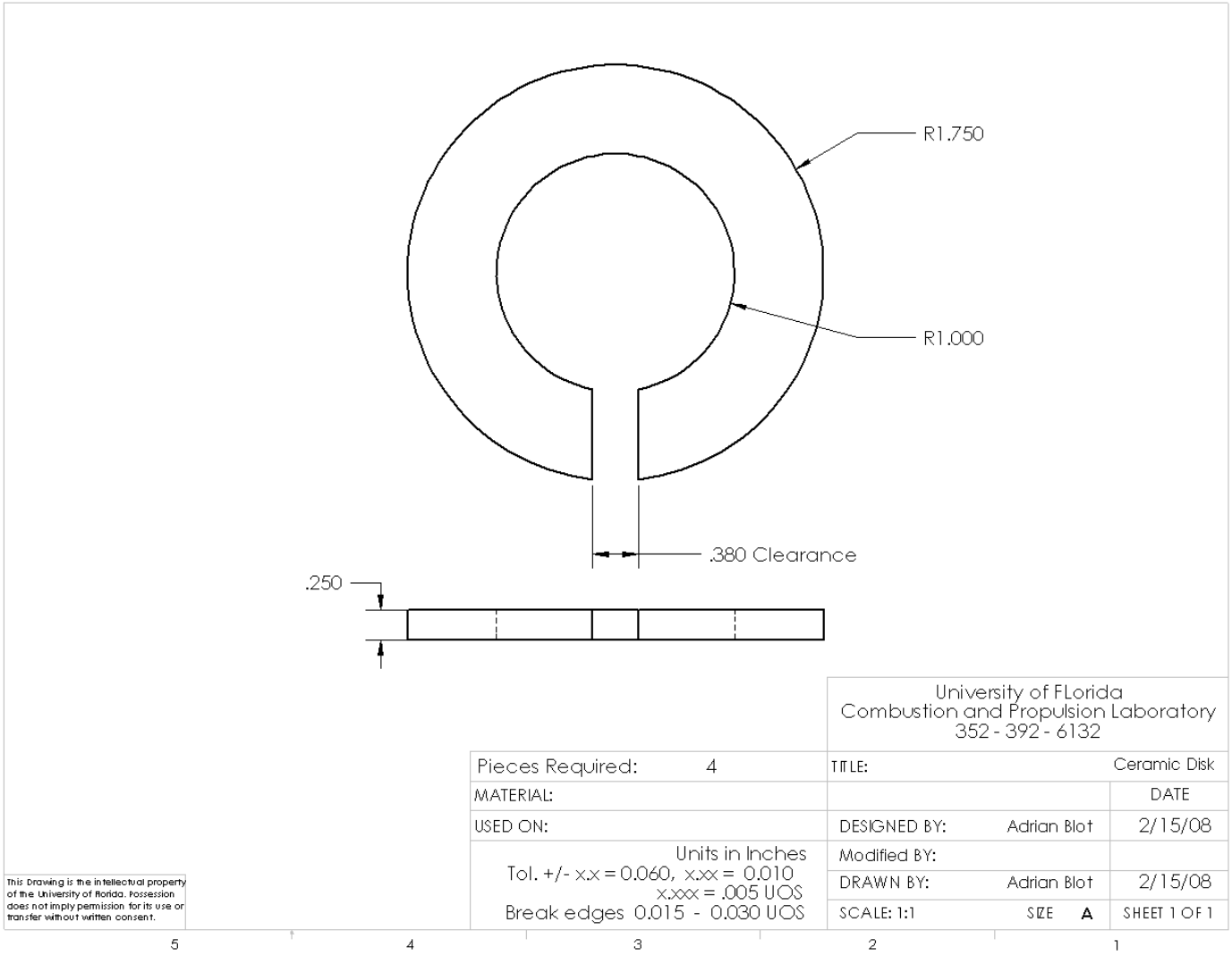

Figure C-17. Ceramic disk mechanical drawing

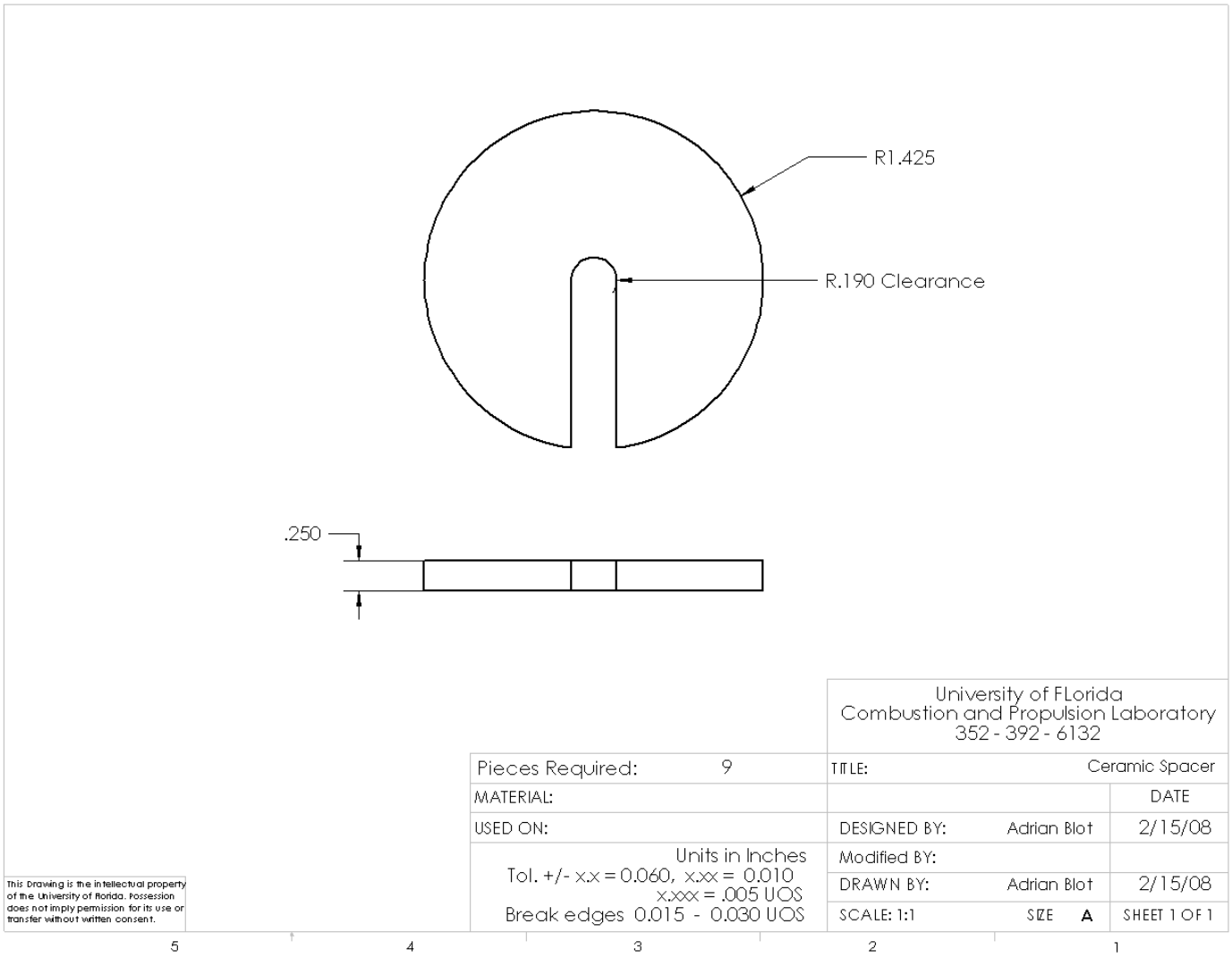

Figure C-18. Ceramic spacer mechanical drawing

APPENDIX D
SECOND STAGE HEATER DRAWINGS

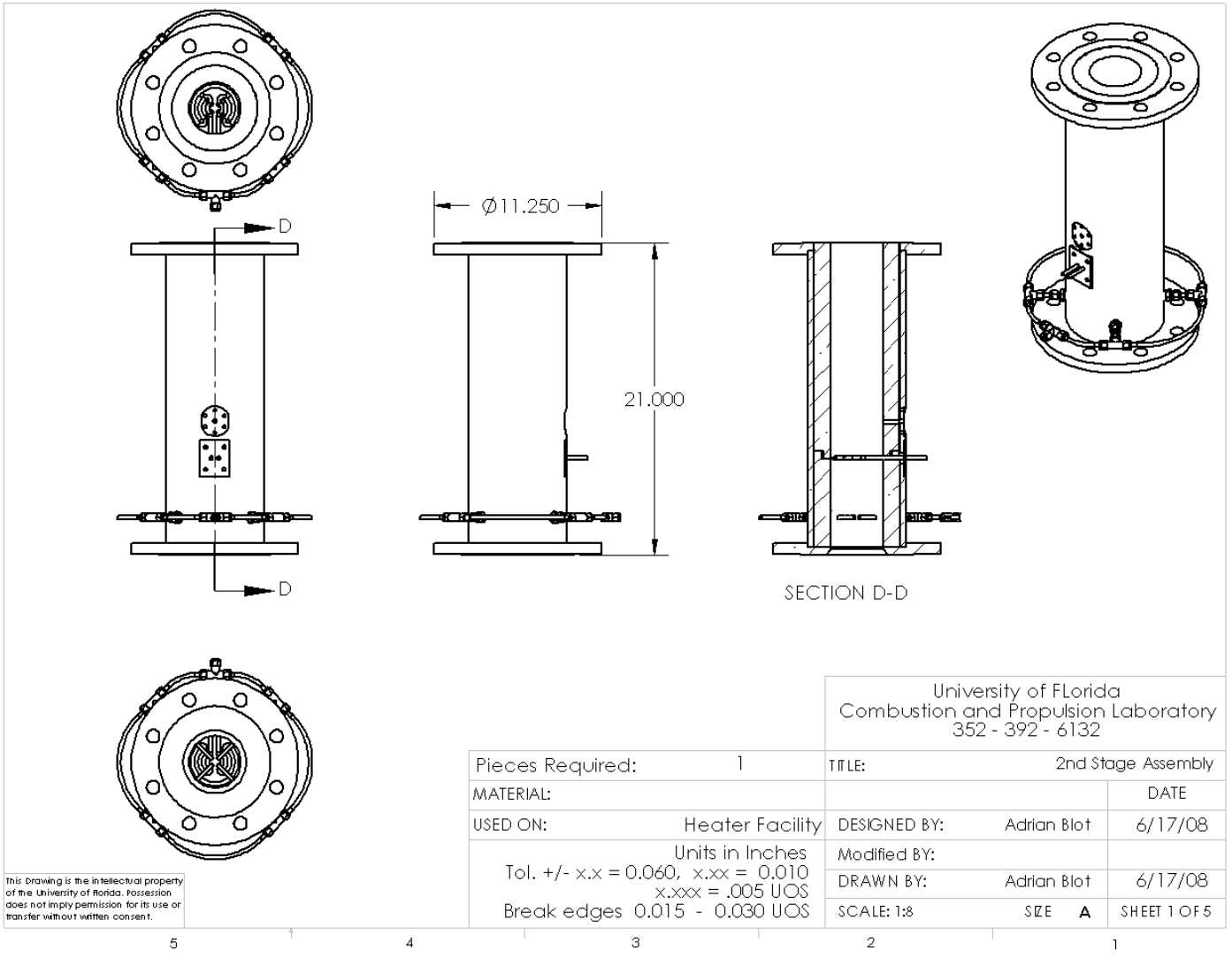

Figure D-1. Second stage layout

ITEM NO.	PART NUMBER	QTY.
1	2nd Stage Pipe	1
2	2nd Stage Inlet Flange	1
3	2nd Stage Exit Flange	1
4	FlameHolder	1
5	2nd Stage Permanant Insulation	1
6	2nd Stage Removable Insulation	1
7	Flame Holder Plate	1
8	Swagelok S-400-1-6BT	4
9	Fuel Injector	4
10	Swagelok S-400-3	5

BOM of Complete List of Parts

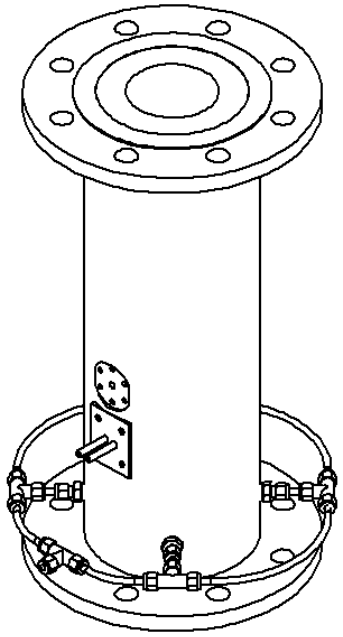

University of FLorida
Combustion and Propulsion Laboratory
352 - 392 - 6132

Pieces Required:	TITLE:	2nd Stage Assembly	
MATERIAL:			DATE
USED ON:	DESIGNED BY:	Adrian Blot	6/17/08
Units in Inches Tol. +/- x.x = 0.060, x.xx = 0.010 x.xxx = .005 UOS Break edges 0.015 - 0.030 UOS	Modified BY:		
	DRAWN BY:	Adrian Blot	6/17/08
	SCALE: 1:5	SIZE A	SHEET 2 OF 5

5 4 3 2 1

Figure D-2. Second stage bill of material of all parts

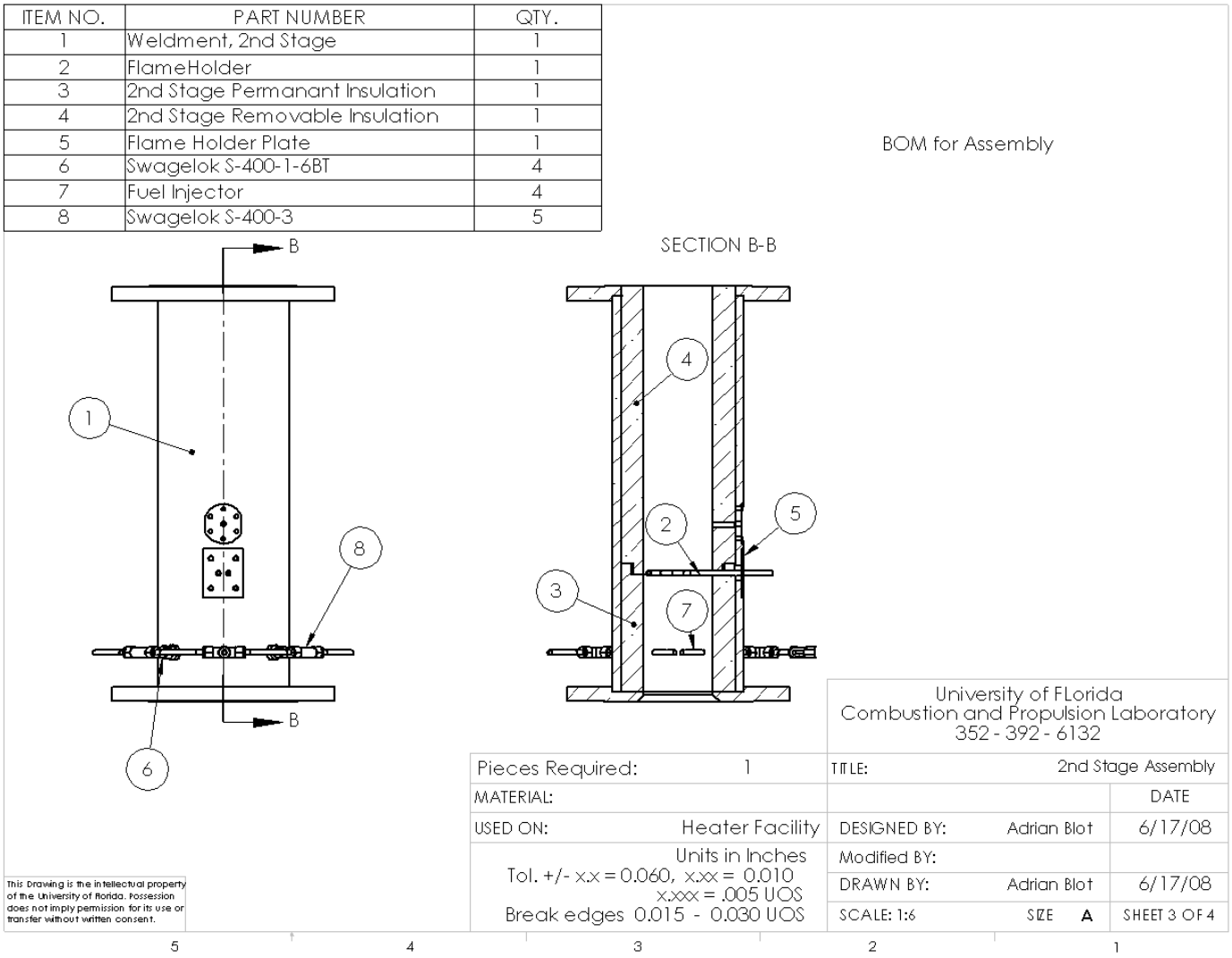

Figure D-3. Second stage bill of material for assembly

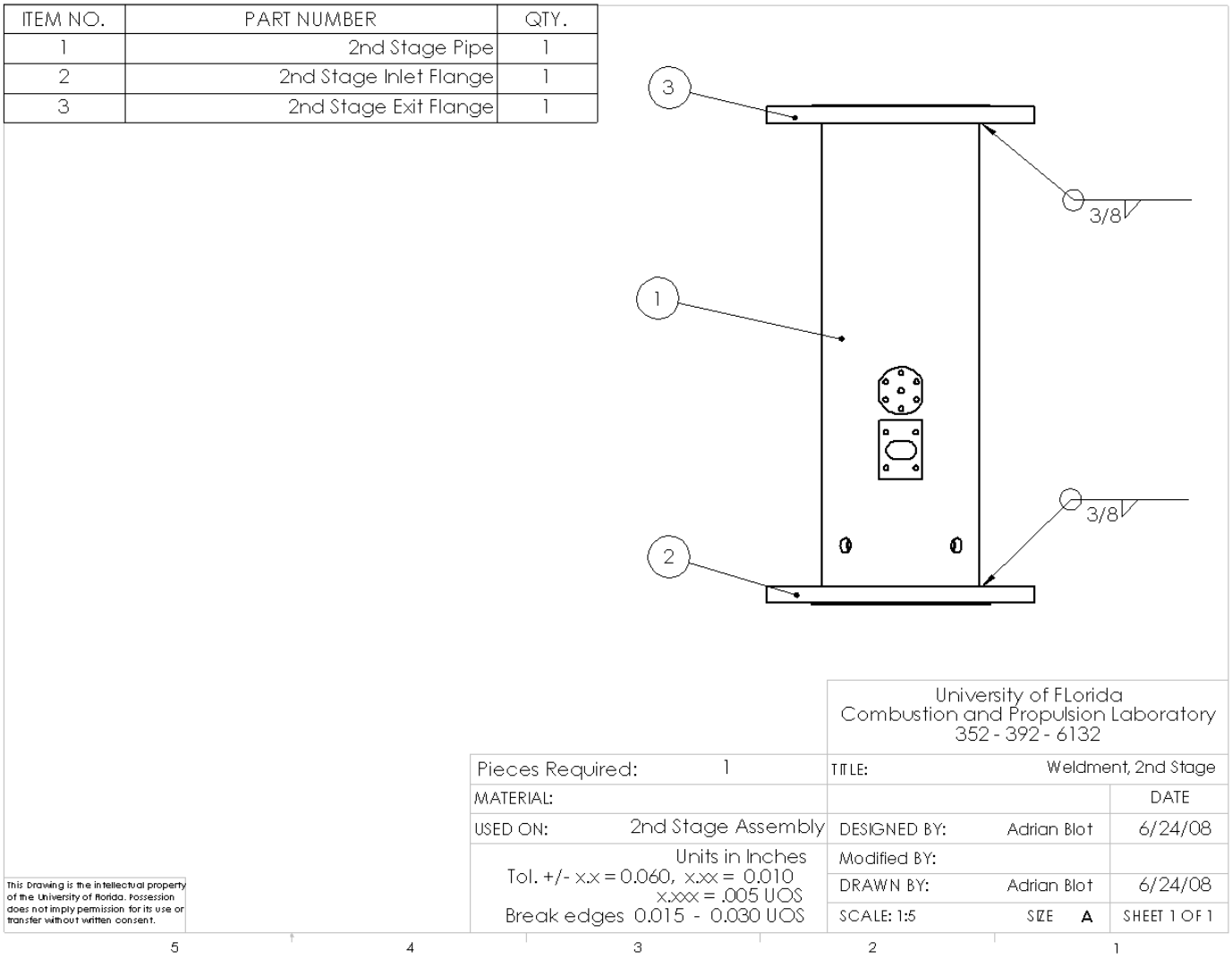

Figure D-4. Second stage weldment mechanical drawing

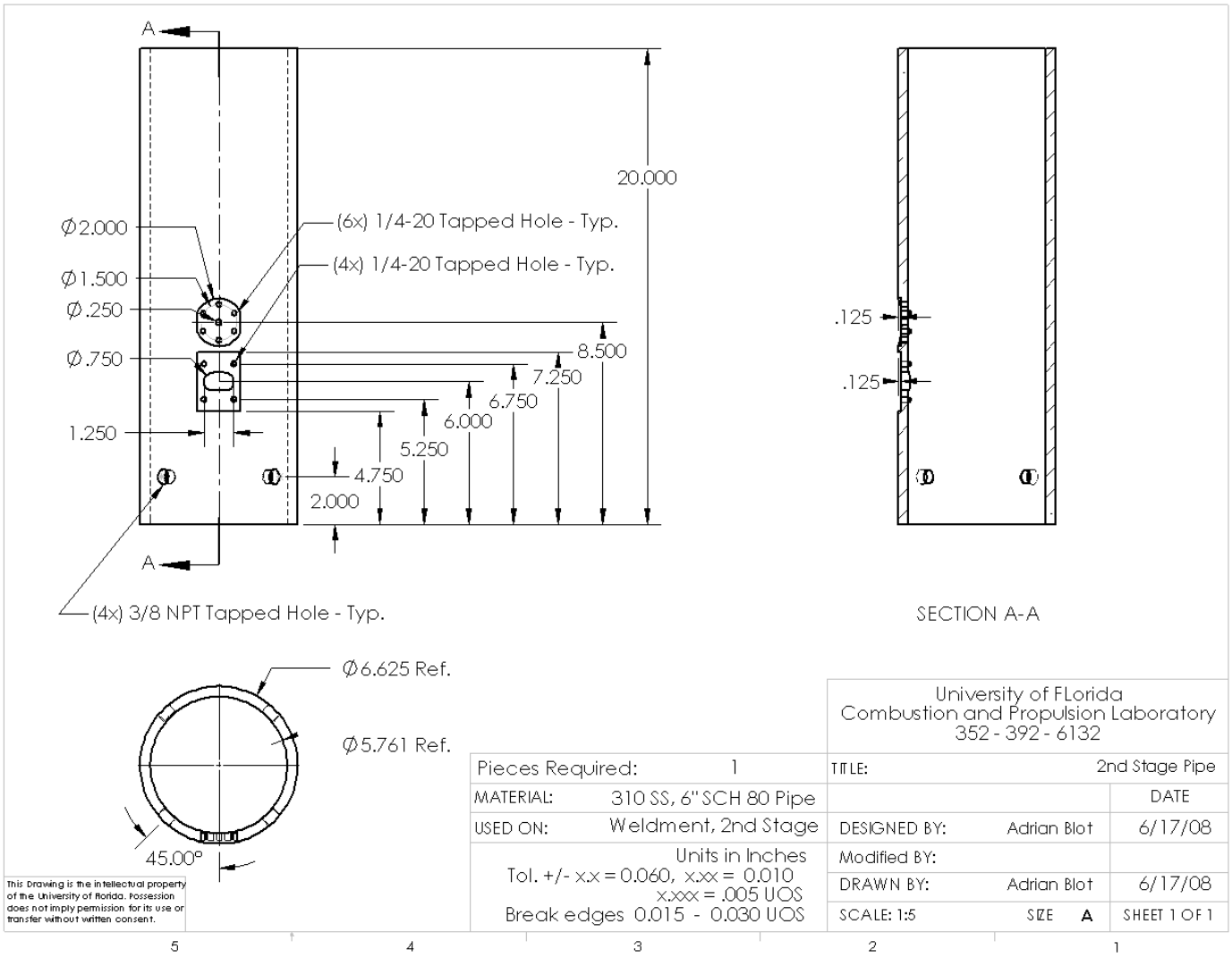

Figure D-5. Steel outer cylinder mechanical drawing

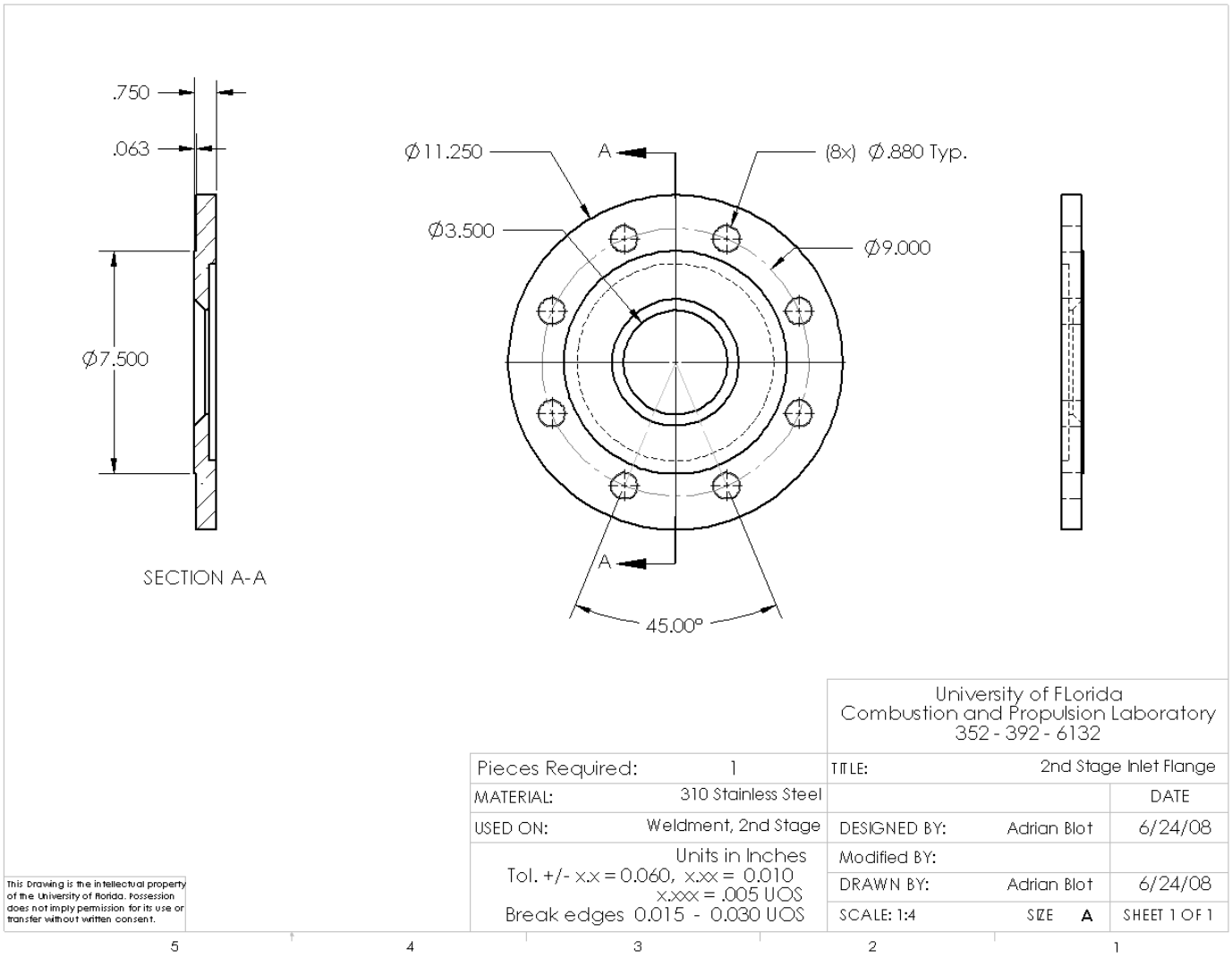

Figure D-6. Second Stage inlet flange mechanical drawing

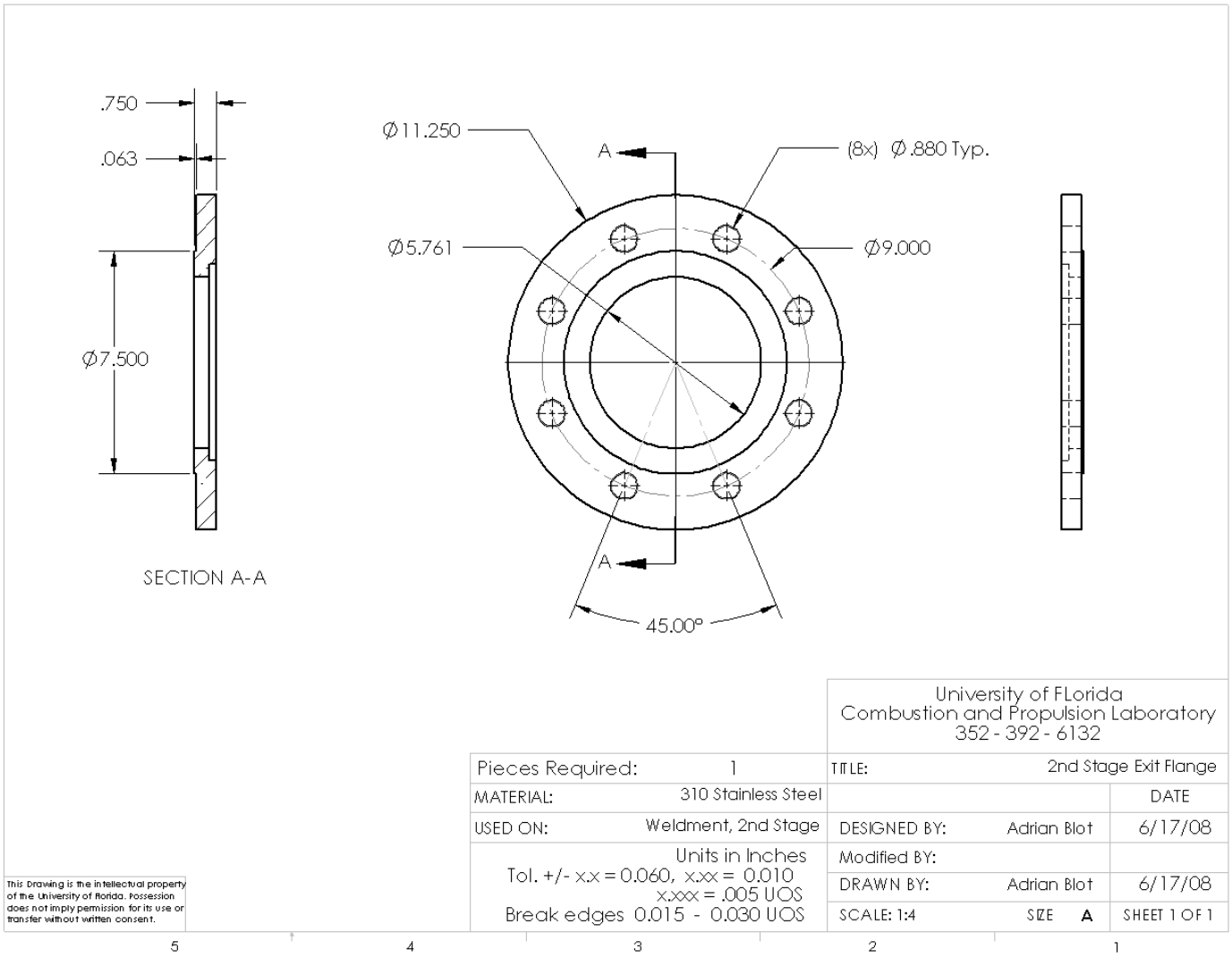

Figure D-7. Second stage exit flange mechanical drawing

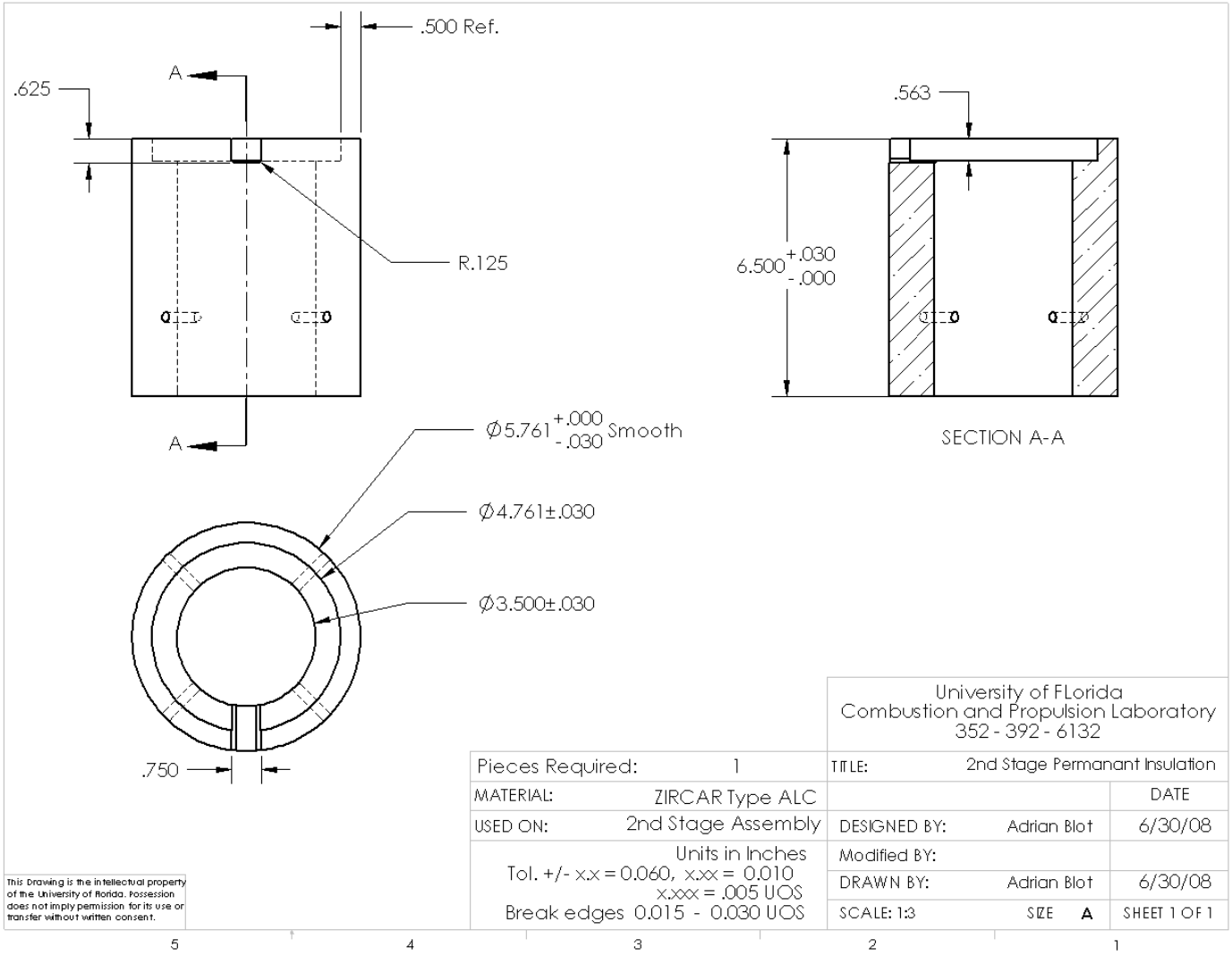

Figure D-8. Permanent insulation mechanical drawing

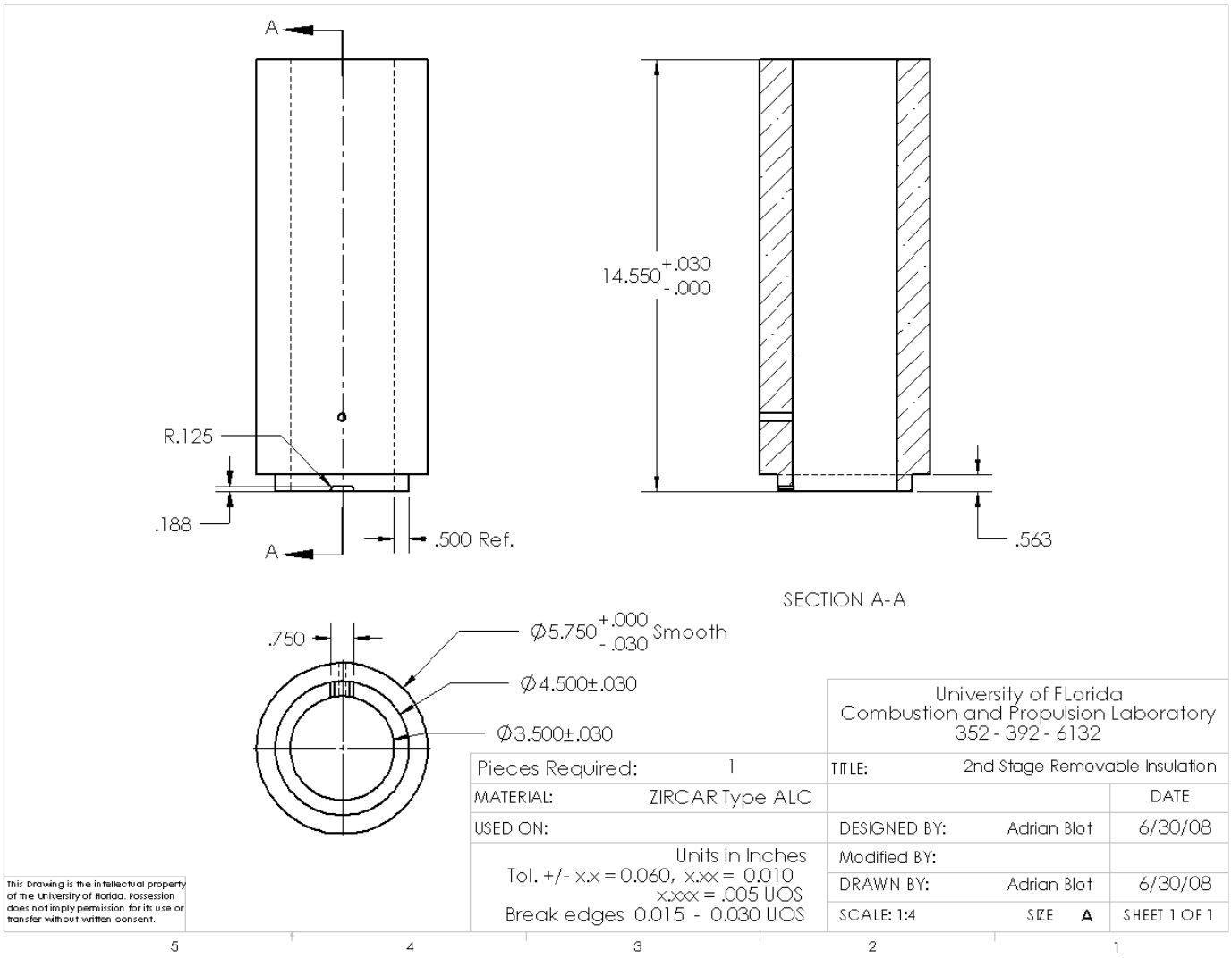

Figure D-9. Removable insulation mechanical drawing

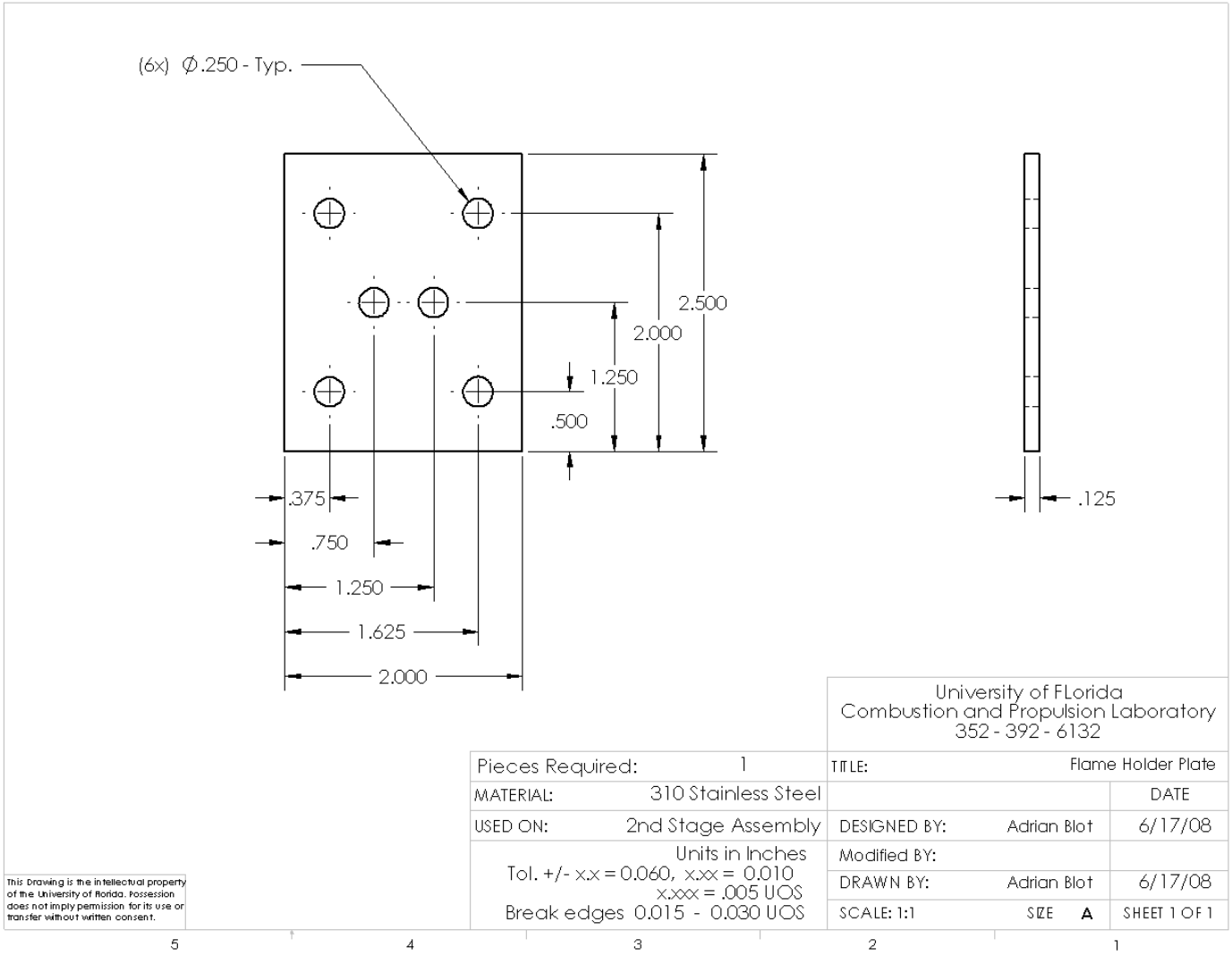

Figure D-10. Flame holder plate mechanical drawing

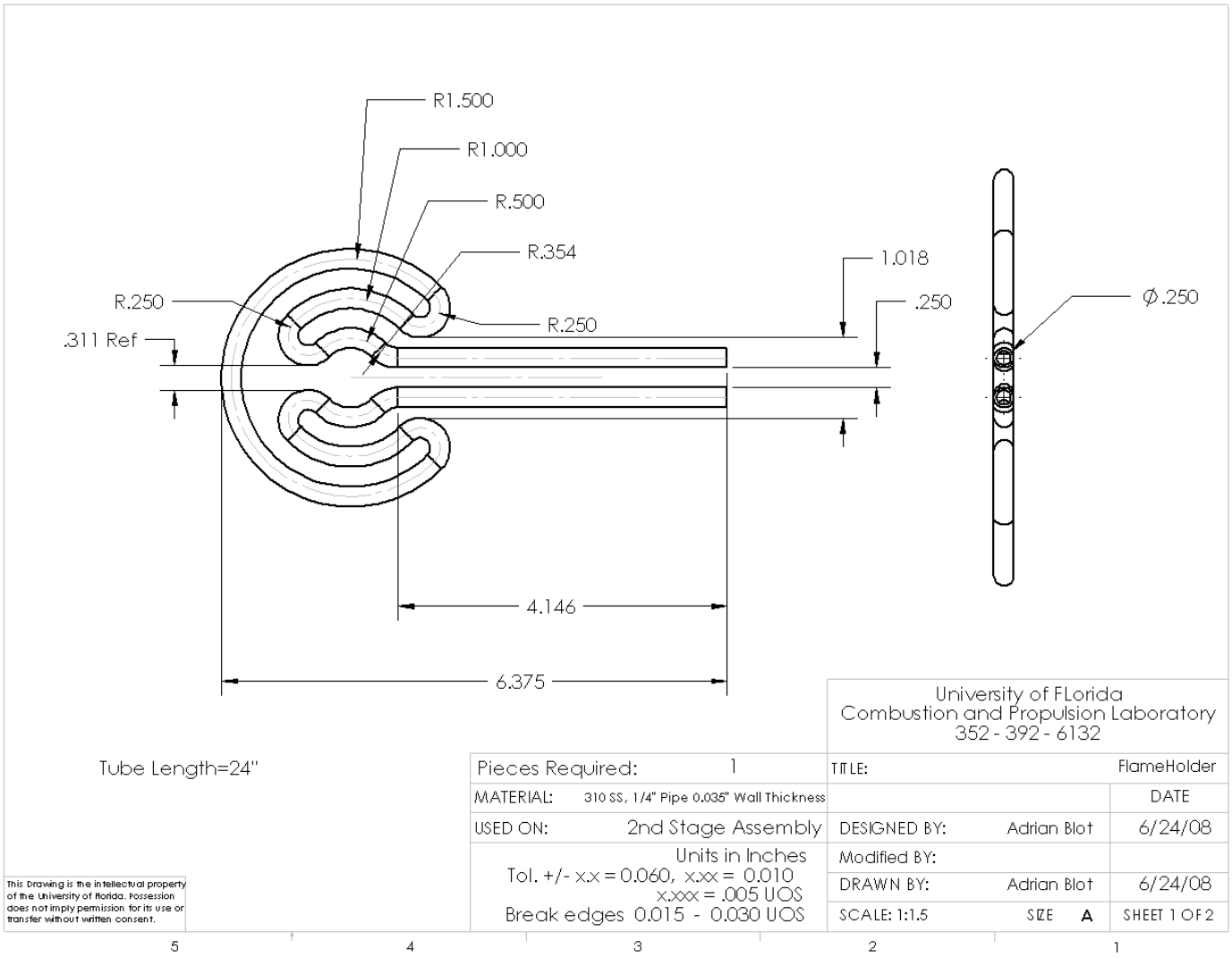

Figure D-11. Flame holder mechanical drawing

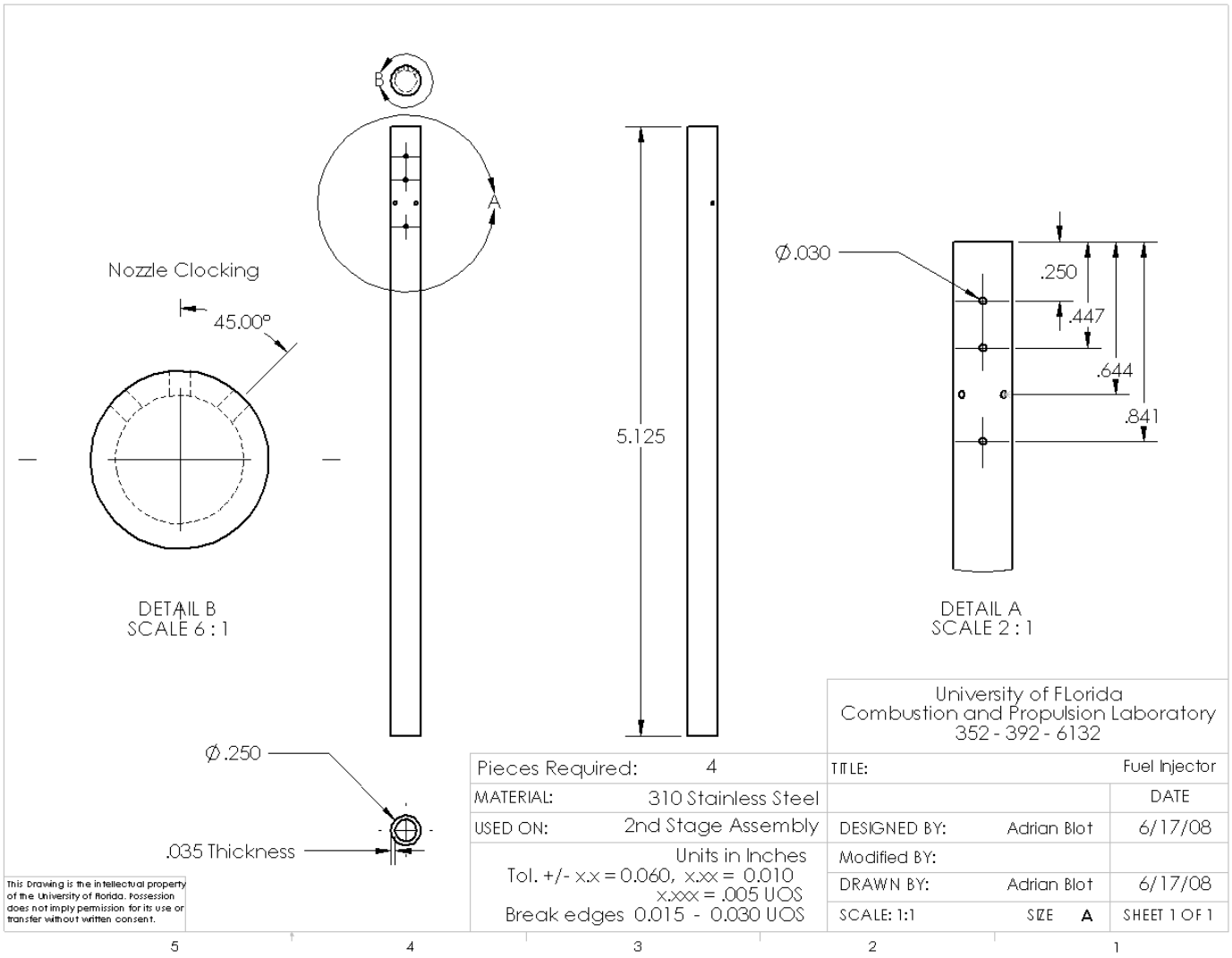

Figure D-12. Hydrogen fuel injector mechanical drawing

APPENDIX E
BELLMOUTH DRAWINGS

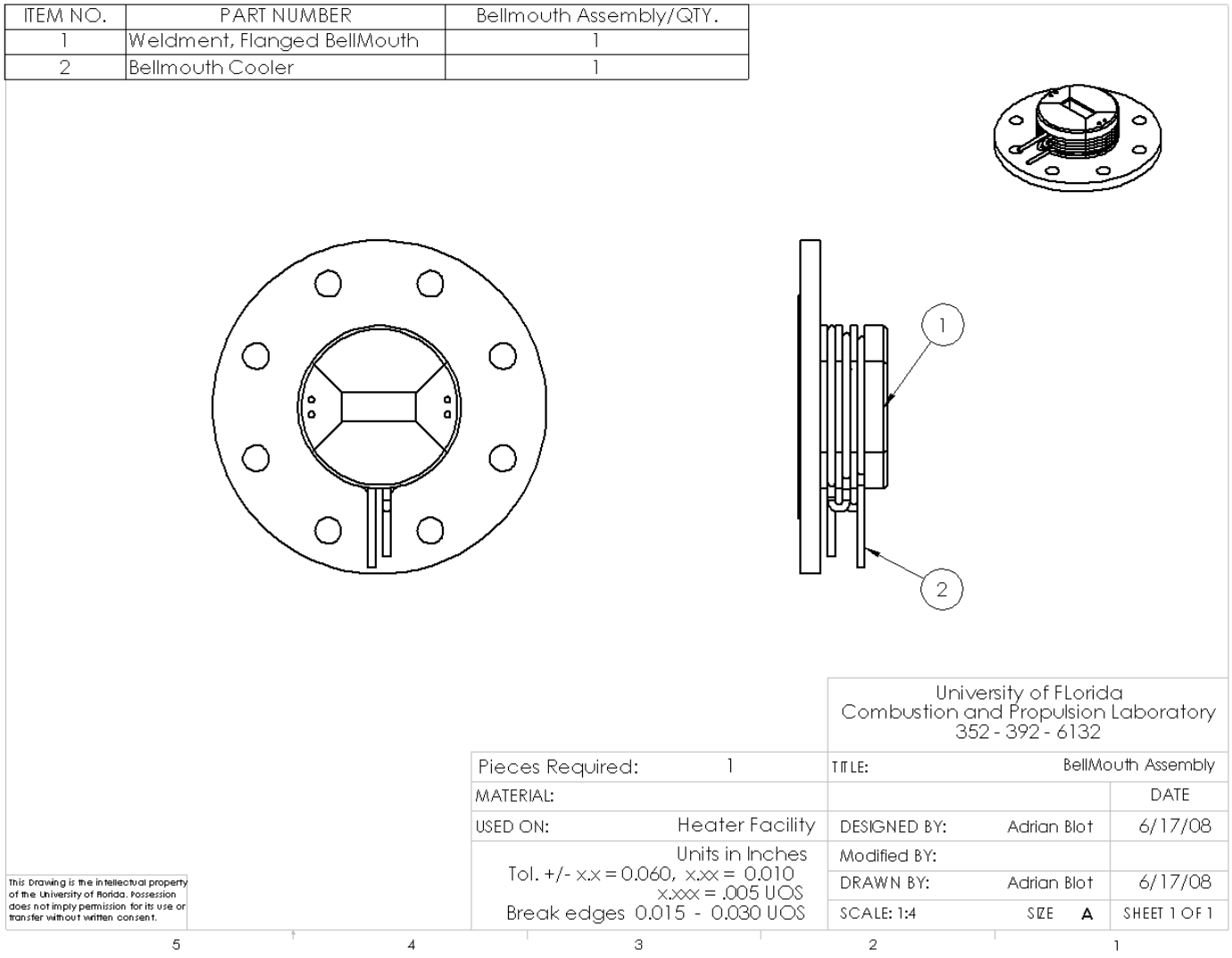

Figure E-1. Bellmouth assembly for currently used test section

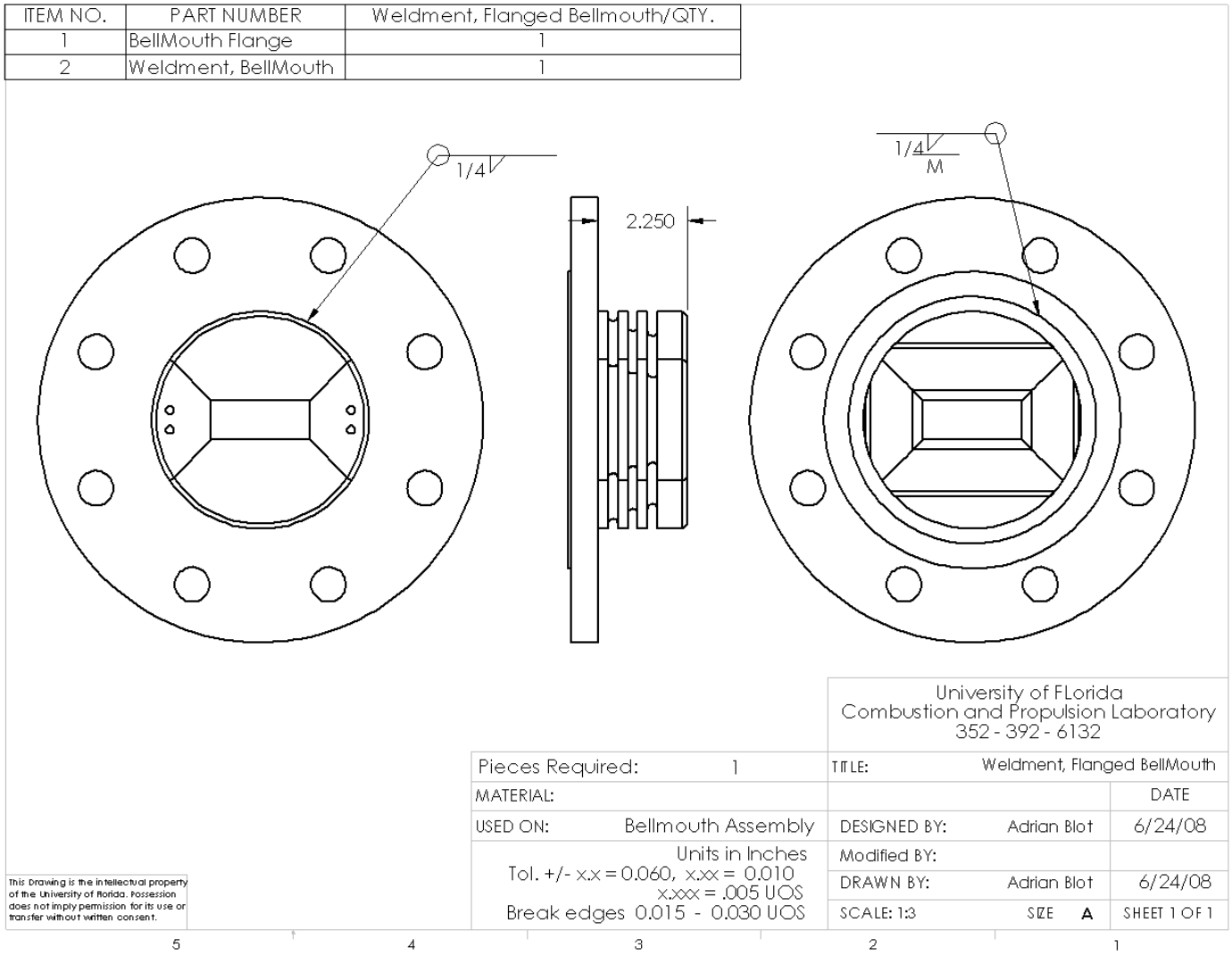

Figure E-2. Bellmouth weldment drawing for currently used test section

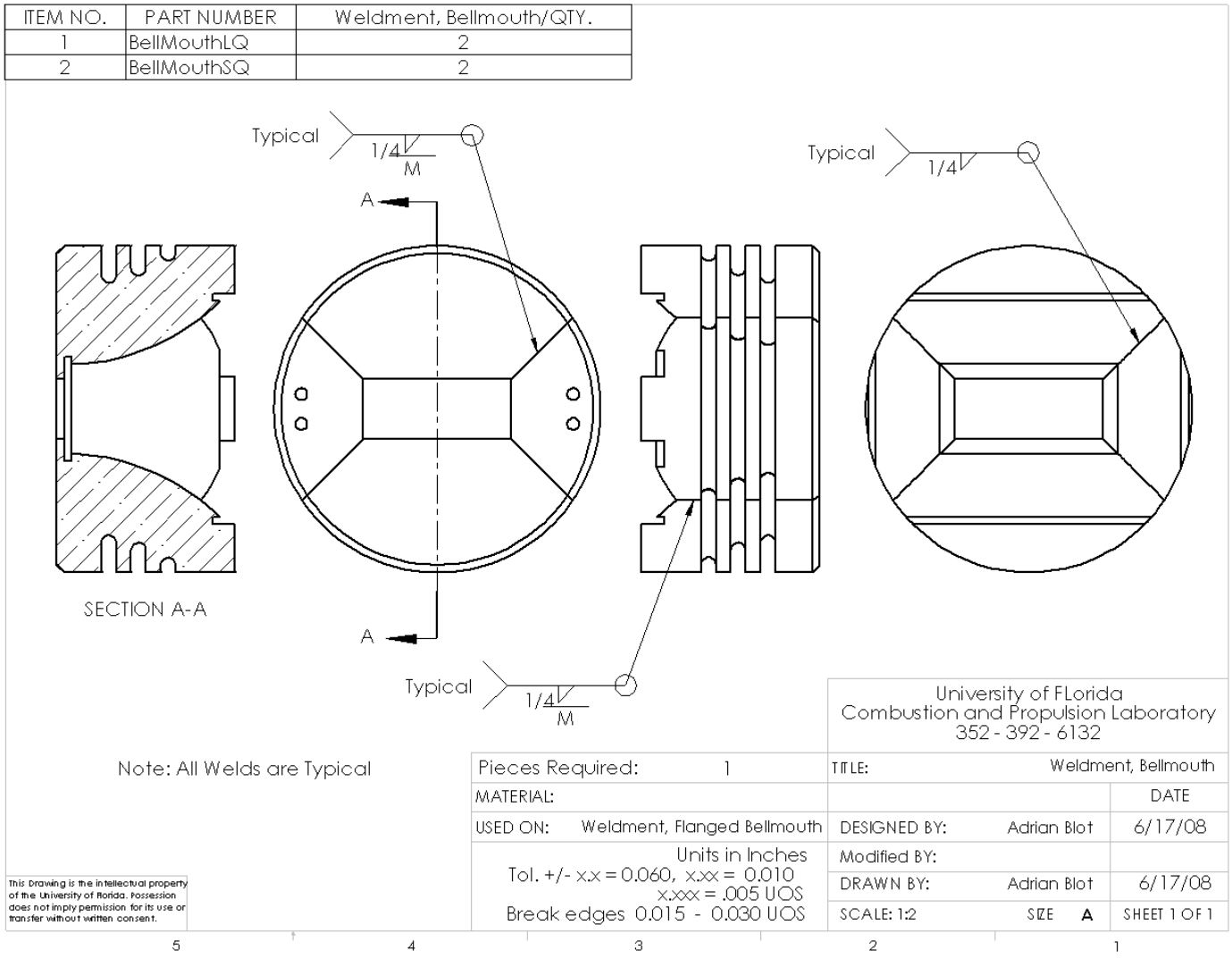

Figure E-3. Weldment drawing of bellmouth sections for currently used test section

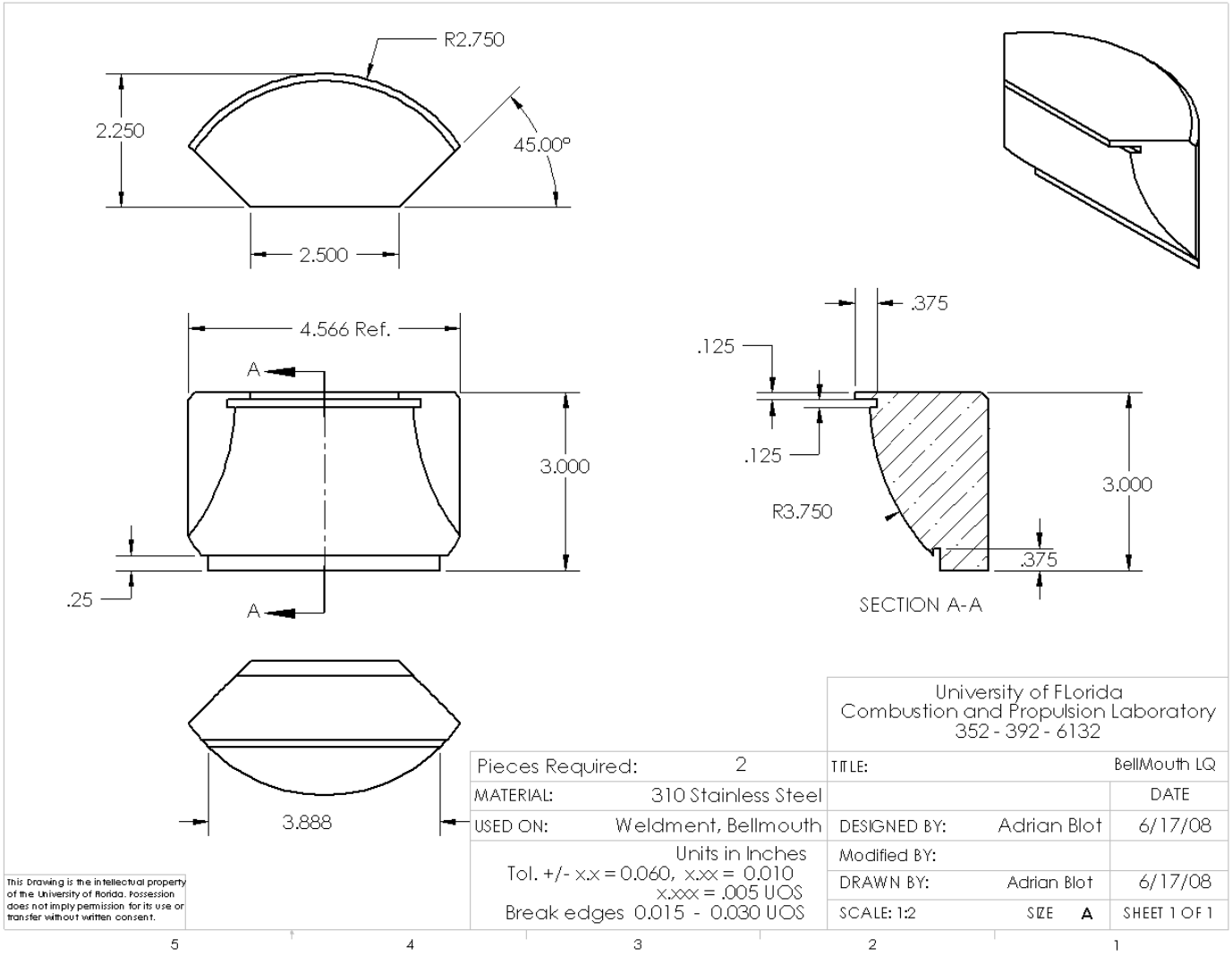

Figure E-4. Large quarter section of bellmouth for currently used test section mechanical drawing

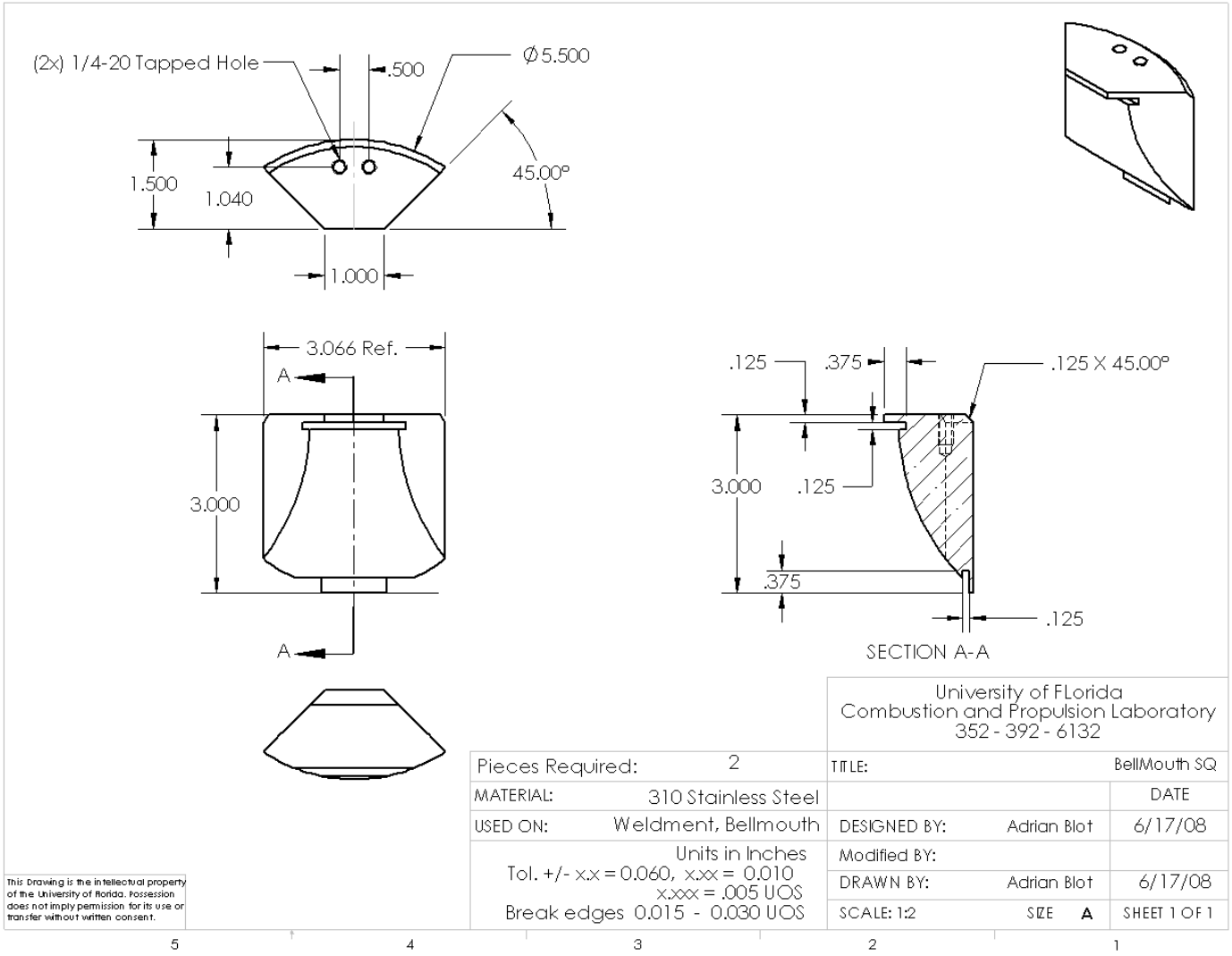

Figure E-5. Small quarter section of bellmouth for currently used test section mechanical drawing

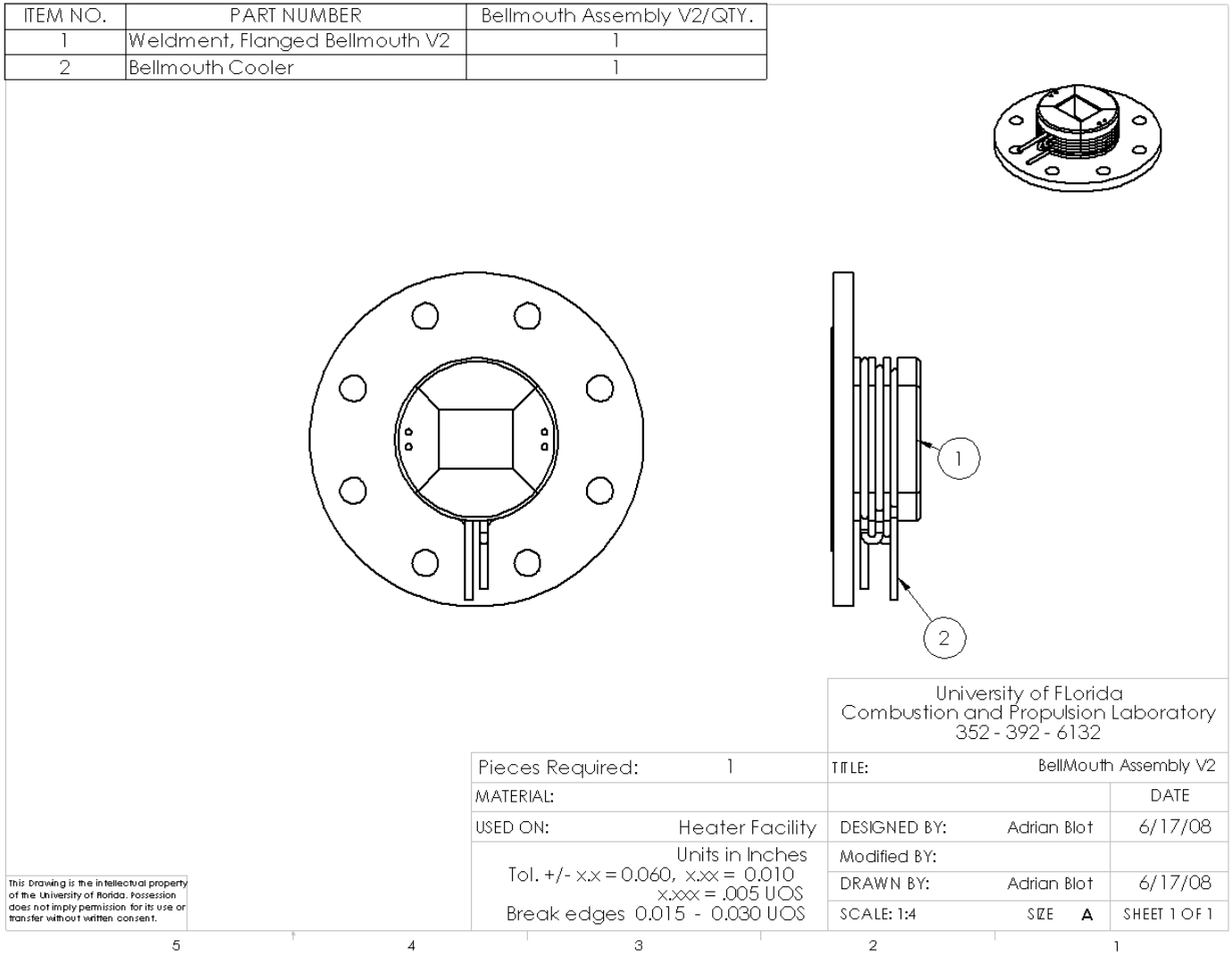

Figure E-6. Bellmouth assembly for new test section

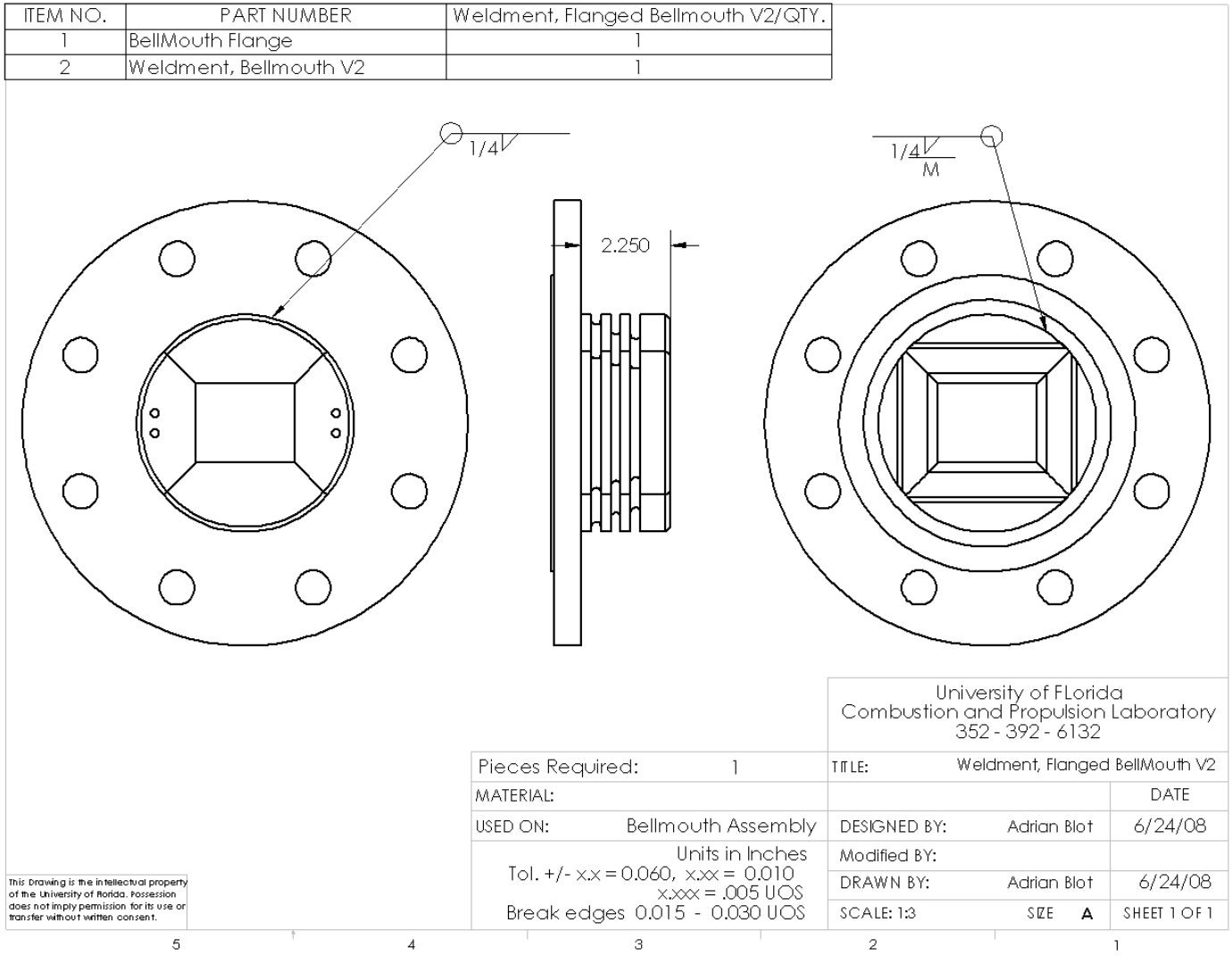

Figure E-7. Bellmouth weldment drawing for new test section

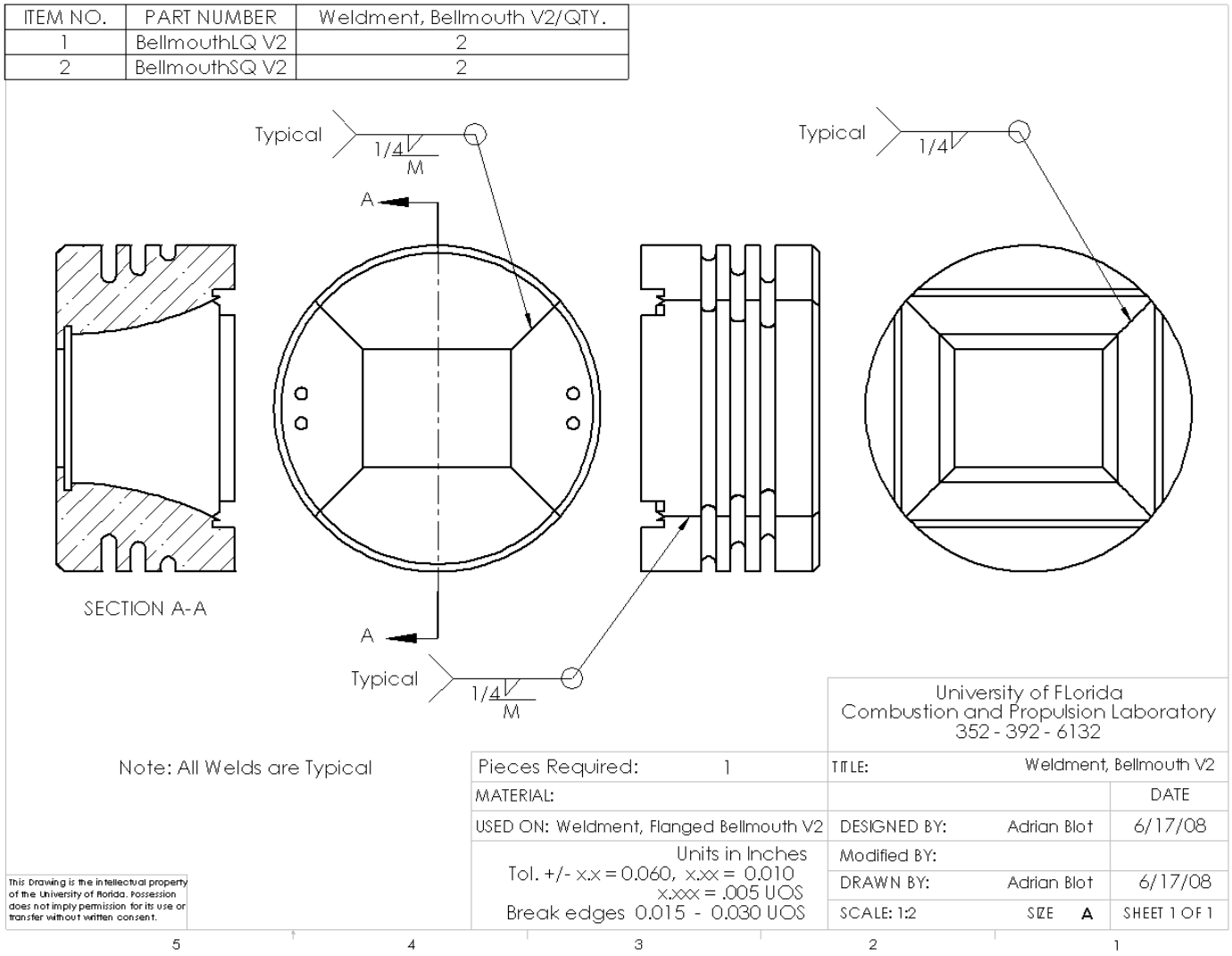

Figure E-8. Weldment drawing of bellmouth sections for new test section

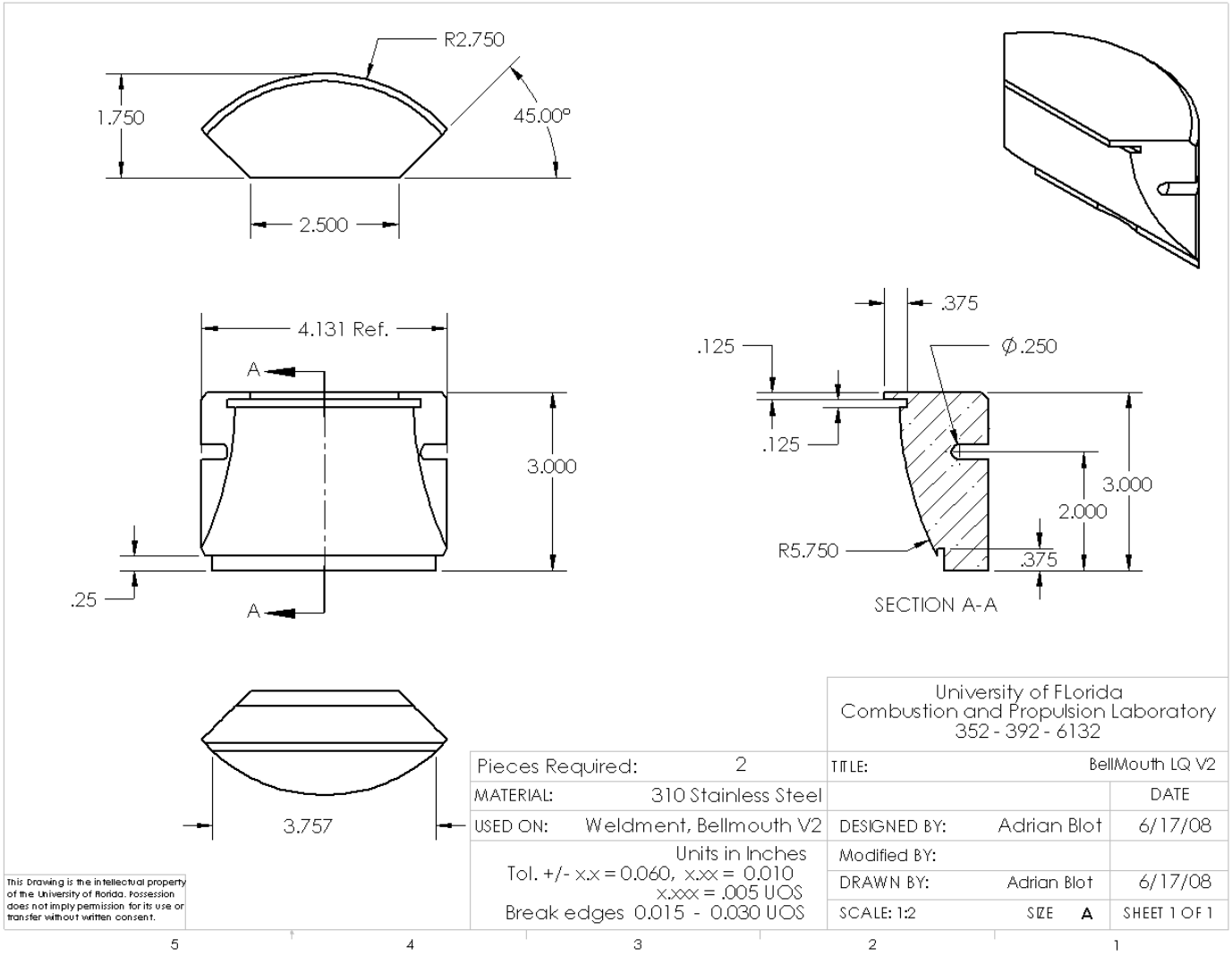

Figure E-9. Large quarter section of bellmouth for new test section mechanical drawing

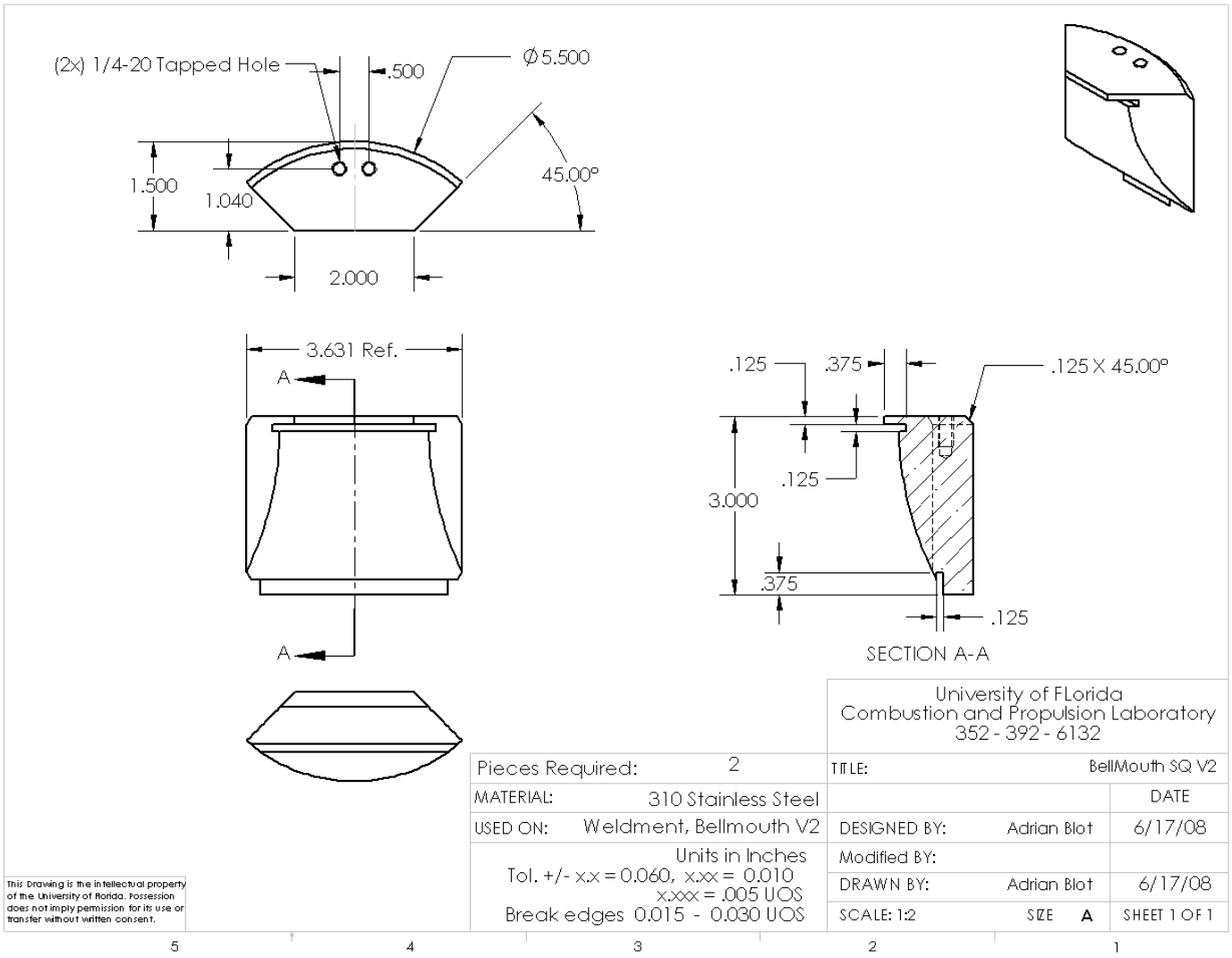

Figure E-10. Small quarter section of bellmouth for new test section mechanical drawing

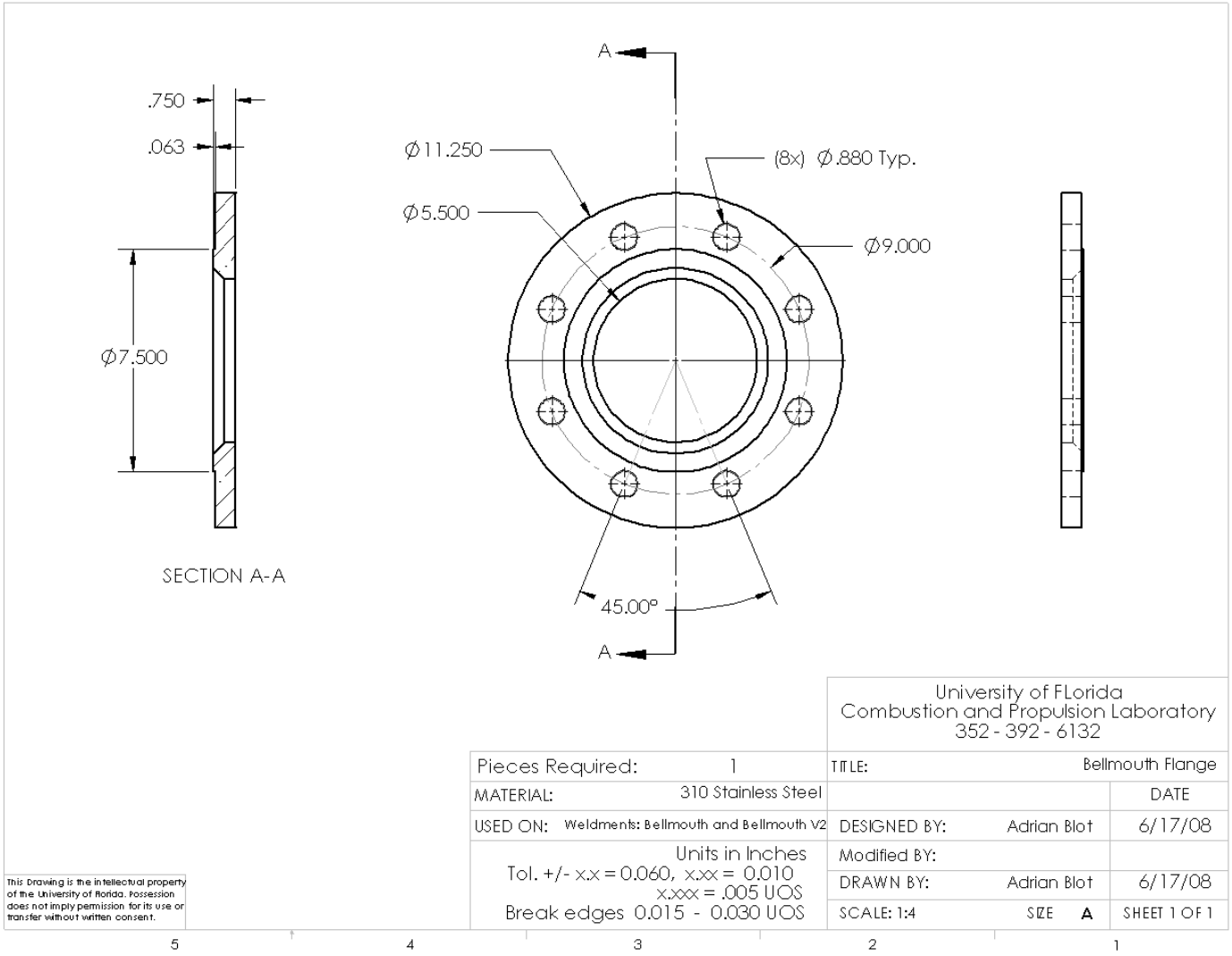

Figure E-11. Bellmouth flange mechanical drawing

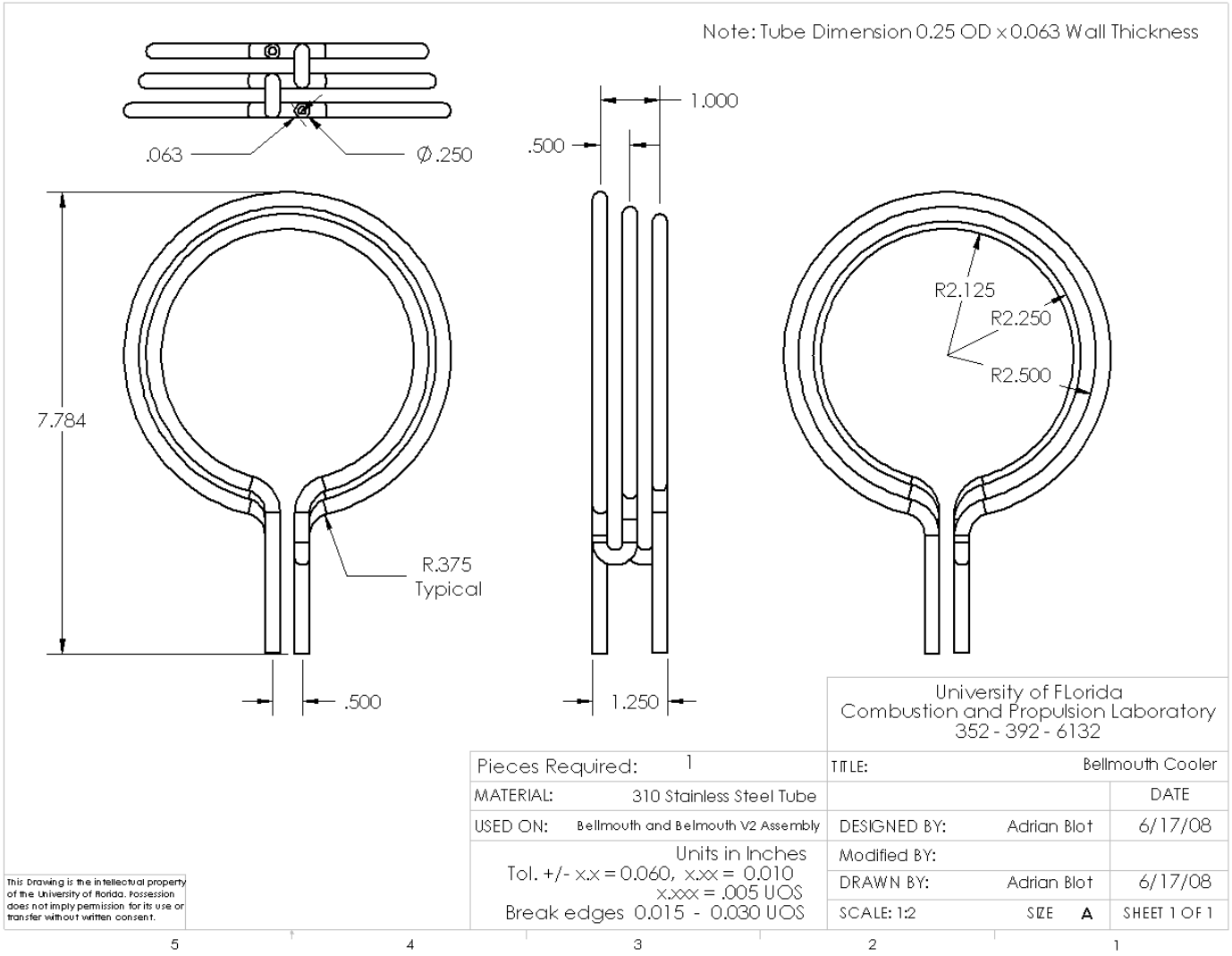

Figure E-12. General mechanical drawing of bellmouth cooling coil

LIST OF REFERENCES

1. Bushnell, D. M., “Hypersonic Ground Test Requirements”, AIAA Journal, vol. 198, 2002, pp 1-15.

2. Lu, F. K. and Marren, D. E., “Principles of Hypersonic Test Facility Development”, AIAA Journal, vol. 198, 2002, pp 17-27.

3. Andreadis, D., “Scramjet Engines Enabling the Seamless Integration of Air & Space Operations”, 2006, Retrieved December 11, 2007 from PWR Engineering: Data and Resources Web Site: http://www.pwrengineering.com/data.htm

4. Russo, G., De Filippis, F., Borrelli, S., Marini, M., and Carista, S., “The SCIROCCO 70-MW Plasma Wind Tunnel: A New Hypersonic Capability”, AIAA Journal, vol. 198, 2002, pp 315-351.

5. Rigney, S.J. and Garrard, G.D., “Aerodynamic and Propulsion Test Unit”, AIAA Journal, vol. 198, 2002, pp 353-373.

6. Woike, M. R. and Willis, B. P., “NASA Glenn Research Center’s Hypersonic Tunnel Facility”, AIAA Journal, vol. 198, 2002, pp 427-439.

7. Chue, R. S. M., Tsai, C.-Y, Bakos, R. J. and Erdos, J. I., “NASA’s HYPULSE Facility at GASL – A Dual Mode Dual Driver Reflected-Shock/Expansion Tunnel”, AIAA Journal, vol. 198, 2002, pp 29-71.

8. Smith, D.M., Felderman, E. J., and Shope, F.L., “Arc-Heated Facilities”, AIAA Journal, vol. 198, 2002.

9. Hodge, J.S. and Harvin, S.F., “NASA Langley Research Center 8-ft HTT”, AIAA Journal, vol. 198, 2002, pp 405-425.

10. Olivier, H., Zonglin, J., Yu, H. R., and Lu, F. K., “Detonation-Driven Shock Tubes and Tunnels”, AIAA Journal, vol. 198, 2002, pp 135-203.

11. Itoh, K., “Characteristics of the HIEST and its Applicability for Hypersonic Aerothermodynamic and Scramjet Research”, AIAA Journal, vol. 198, 2002, pp 239-253.

12. Kislykh, V. V., “Piston Gasdynamic Units with Multicascade Compression”, AIAA Journal, vol. 198, 2002, pp 255-277.

13. Hennemann, K. and Beck, W. H., “Aerothermodynamics Research”, AIAA Journal, vol. 198, 2002, pp 205-237.

14. Cengel, Y., Heat and Mass Transfer, 3rd ed., McGraw Hill, New York, 2007.

15. Jacobsen, L. S., “Plasma assisted Ignition in Scramjets”, Journal of Propulsion and Power, 2008.

16. Ibele, W.E., “Prandtl number measurements and Thermal Conductivity, Viscosity Prediction for air, Helium, and Air-Helium Mixtures”, University of Minnesota, 1963.

17. Turns, Stephen R., An Introduction to Combustion Concepts and Applications, McGraw Hill, New York, 2006.

BIOGRAPHICAL SKETCH

Adrian Blot was born in Ris Orangis, France in 1984, but grew up in Florida and Virginia. In 2003 Adrian began attendance at the New York Institute of Technology in Old Westbury, NY. He enjoyed the city life of the Big Apple and after 4 years obtained a Bachelor of Science in mechanical engineering with concentration in aerospace engineering and graduated summa cum laude. While there he was also involved in an SAE club geared to the design and production of a mini Baja vehicle for competition. Adrian began work on a Master of Science degree in aerospace engineering in 2007 at the University of Florida where he joined the Combustion Lab Group. After graduation Adrian plans to find an engineering position in the western United States and looks forward to the future challenges that await him.